DESIGN, SYNTHESIS AND SUPRAMOLECULAR PROPERTIES OF HIGHLY FUNCTIONALIZED DONOR-σ-ACCEPTOR MOLECULES

By

LING YUAN

A DISSERTATION PRESENTED TO THE GRADUATE SCHOOL
OF THE UNIVERSITY OF FLORIDA IN PARTIAL FULFILLMENT
OF THE REQUIREMENTS FOR THE DEGREE OF
DOCTOR OF PHILOSOPHY

UNIVERSITY OF FLORIDA

2008

To my parents
To my husband and our daughter

ACKNOWLEDGMENTS

I would like to thank my advisor, Dr. Ronald K. Castellano, for affording me the opportunity to study in his laboratory. The time spent under his direction has been invaluable. I am thankful for his patience, guidance, and encouragement. I am honored to be one of his students and have learned a lot in science, and in character from him. I am and will continue to benefit from all of these throughout my whole life. I would like to thank my lab mates in the Castellano group. Special thanks go to Dr. Andy Lampkins, Dr. Vladimir Gubala, Jennifer Mattler, and Adnan Javed who shared the exciting AAT chemistry with me. I thank Yan Li for his help in the lab and discussions on lactone chemistry. I thank Dr. Roslyn Butler, Dr. Alisha Martin, Pam Cohn, Matt Baker, and Rachel Giessert for their friendship.

I would also like to thank my collaborators, Dr. Kunlun Hong and Dr. Masashi Osa in the Center for Nanophase Materials Sciences (CNMS) at Oak Ridge National Laboratory (ORNL), Dr. Nathanael Stevens in the Particle Engineering Research Center (PERC) at the University of Florida, Dr. Erik Berda, Dr. Ion Ghiviriga, and Dr. Katsu Ogawa in the chemistry department, Dr. Junghun Jang in the Major Analytical Instrumentation center (MAIC) at the University of Florida, for their scientific discussions and assistance in my studies.

I would like to thank my committee members: Prof. Lisa McElwee-White, Prof. Alan Katritzky, Prof. George Christou, and Prof. Joanna Long for being on my committee and for their scientific advice and efforts.

Finally, the foremost and special thanks go to my family. I would like to thank my parents, Yiling Zhong and Zhineng Yuan for their unconditional love and support. I thank my husband, Junliang Zhang for his understanding. The most special thanks go to my little daughter, Helen S. Zhang. She brings so much happiness and many surprises to my life. Her smile is the best gift after all of my hard work.

TABLE OF CONTENTS

page

LIST OF TABLES

LIST OF FIGURES

LIST OF ABBREVIATIONS

AAT	1-aza-admantanetrione
TBI	Through-bond interaction
DMF	Dimethylformamide
DCM	Dichloromethane
DLS	Dynamic light scattering
DSC	Differential scanning calorimetry
TGA	Thermal gravimetric analysis
CPD	Critical point drying
SEM	Scanning electron microscopy
POM	Polarized optical microscopy
XRD	X-ray diffraction
DCC	1,3-Dicyclohexylcarbodiimide
EWG	Electron withdrawing group
HMTA	Hexamethylenetetramine
TFA	Trifluoroacetic acid
PAH	Polycyclic aromatic hydrocarbon

Abstract of Dissertation Presented to the Graduate School
of the University of Florida in Partial Fulfillment of the
Requirements for the Degree of Doctor of Philosophy

DESIGN, SYNTHESIS, AND SUPRAMOLECULAR PROPERTIES OF HIGHLY FUNCTIONALIZED DONOR-σ-ACCEPTOR MOLECULES

By

Ling Yuan

May 2008

Chair: Ronald K. Castellano
Major: Chemistry

1-Aza-adamantanetriones (AATs) constitute an important class of donor-σ-acceptor molecules that show unique electronic and macromolecular properties upon self-assembly. Described are the design, rational syntheses, and characterization of new AAT derivatives to draw structure-property relationships with the materials toward potential applications. AATs bearing expanded aromatic side chains, naphthyl substituents, form organogels at the lowest concentration (critical gelation concentration = 0.2% by weight) to date (in benzene and toluene) that are also thermally robust (T_g = 70 °C). SEM and XRD studies explore the underlying fibrous networks, and organization, in the solid state. In solution, fluorescence emission spectra show intermolecular excimer formation (λ_{max} = 433 nm) upon assembly and implicate π-π stacking interactions as being important for association. Likewise, concentration- and temperature-dependent NMR and IR studies show that intramolecular H-bonding of peripheral amide functional groups likely preorganizes the molecules for self-assembly. Finally, dynamic light scattering (DLS) studies show for the first time how the assembly of functionalized AATs responds reversibly to concentration and temperature in organic solution, where large aggregates are formed at exceedingly low concentrations (< 0.1 mM).

New synthetic methodology is described to prepare differentially-functionalized and even chiral AATs that involves the selective formation and then ring opening of mono-, di-, and trilactones derived from phloroglucinol derivatives. Temperature is the key to controlling the ring-opening reactions and product distributions. In this fashion the first chiral AAT is reported, where the tricyclic core bears three different substituents: an isopropyl ester, an alkyl amide, and an aryl amide. Such molecules appear as new types of chiral tertiary amines that could have potential applications in asymmetric catalysis or chiral recognition. The lactone-based methodology also allows introduction of ether functional groups to the AAT scaffold for the first time. To demonstrate this advance, AATs outfitted with TBS-protected ethylene glycol units have been prepared. Deprotection should afford the first hydrophilic and potentially hydrogelating AATs.

CHAPTER 1
INTRODUCTION

Supramolecular Chemistry

Supramolecular chemistry is defined as the area of chemistry that focuses on the noncovalent interactions of molecules.[1, 2] With the rapid development of this field over recent years, the focus has changed from constructing functional molecules via the formation of direct covalent linkages to creating functional systems by molecular self-assembly.[3-7]

Introduction to Supramolecular Chemistry

Lehn describes supramolecular chemistry as " the design chemistry of the intermolecular bond",[1] and the field finds its inspirational roots in some of the now well-known functional assemblies of nature. The DNA double helix, which forms from two complementary single-stranded polynucleotides, is a familiar example. The strands recognize each other by selective hydrogen bonds between the base pairs and base stacking interactions.[8] Other natural supramolecular assemblies include enzyme–substrate complexes, antibody–antigen complexes, and membrane receptors. The cell membrane itself is another example; it is a highly functionalized and oriented system that plays an essential role in basic biological functions like ion and molecular transport, and signal transduction.[8]

The design of systems that can mimic biological functions remains a challenge to chemists and biochemists.[9, 10] The artificial membrane ion channels based on self-assembled cylindrical β-sheet peptides made by the Ghadiri group[11] represent one of many successful examples. Here cyclic peptide structures comprised of alternating D and L amino acids adopt a flat ring conformation and stack to form a hydrogen-bonded hollow tubular structure. The assembly displays good channel-mediated ion-transport activity. Indeed, supramolecular chemistry is closely related to bioorganic and bioinorganic chemistry.[12]

The principles of supramolecular chemistry have more recently been systematically employed in nanotechnology and materials science,[13, 14] and borrowing Nature's strategies appears as a useful approach to controlling the optical and photophysical properties of functional molecules and ultimately, their performance in devices.[14-16] Numerous supramolecular systems have found practical applications. Liquid crystals are an exemplary class of materials whose unique properties rely on noncovalent interactions. Their applications extend from liquid crystal displays (LCDs) , which appear in everyday life,[17] to various medical areas[18] and chemical analysis.[19] Supramolecular chemistry likewise underlies many technologies involving surfactants,[20] organic semiconductors, conductors,[21] and molecular rectifiers.[22] Organogels, like liquid crystals, form as a consequence of noncovalent interactions and therefore fall within the realm of supramolecular chemistry. Gels appear when organic solvents are immobilized by a three-dimensional network composed of aggregated gelators;[23] their unusual rheological properties and thermoreversibility make them useful materials in diverse fields that include food science, medicine (e.g., drug delivery), cosmetics, and pharmacology.[24]

The chemical structures of the gelators determine the self-assembly of the molecules. In general, gelation is thought to arise from entangled fibers, which become cross-linked by noncovalent interactions and are able to trap solvent molecules. As a consequence, the organogels are often thermally reversible and the gel properties can easily be controlled by changing the temperature, the structures of the interacting functional groups, or by mechanical agitation of the suspension.[25] A challenge that unites synthetic supramolecular systems is understanding how the fundamental structures of the molecular building blocks (e.g., gelators) relates to the properties and potential applications of the self-assembled aggregates.

Self-Assembly

Central to supramolecular chemistry is the concept of self-assembly, defined as "the process by which a supramolecular species forms spontaneously from its components".[7] Liquid crystal formation,[26] the growth of crystals,[27] metal coordination complexes,[28] formation of the DNA double helix, and generation of synthetic lipid bilayers[29] all involve the spontaneous assembly of small components to form larger structures. Various intermolecular interactions mediate the self-assembly of molecules; these, in addition to shape complementarity, are the keys to controlling structure and macromolecular properties. Noncovalent interactions are reversible, and the resultant self-assembled structures are therefore under thermodynamic control and in thermodynamic equilibrium with their molecular components. The idea of "error correction"[7] extends from these principles and is important for both biological and synthetic molecules that may experience numerous possible intermolecular interactions on the way to desired (and often complex) assembly structure. Molecular self-assembly thus stands as one of the most efficient and economical ways to synthesize complex materials.

Many traditional intermolecular interactions come to the fore in the self-assembly of molecules. These include hydrogen bonding, π-π stacking, electrostatic interactions, van der Waals, and hydrophobic interactions. The first two are the most commonly exploited in the design of self-assembled systems.[30-33] π-π Stacking[6] is perhaps best known through its role in stabilizing DNA duplex formation through vertical base-pair interactions. However, such interactions play a prominent role in many synthetic self-assembled systems. Thermotropic liquid crystals (Figure 1-1), for example, are formed from the π-stacking of molecules with a central aromatic core and alkyl chains attached on the periphery. Triphenylbenzene,[34] hexabenzocoronenes (HBCs),[35, 36] and their derivatives are typical examples of discotic liquid

crystal mesogens. The size and shape of the core as well as the length of the side chains help to control the functional properties of these materials,[37] which include one-dimensional charge transport.[37, 38] The conducting properties of discotics are useful for various photovoltaic devices, in particular, solar cells and organic field-effect transistors.[39, 40] The π-stacking interactions of naphthalene, the simplest polycyclic aromatic hydrocarbon (PAH), are exploited in Chapter 2 of this dissertation.

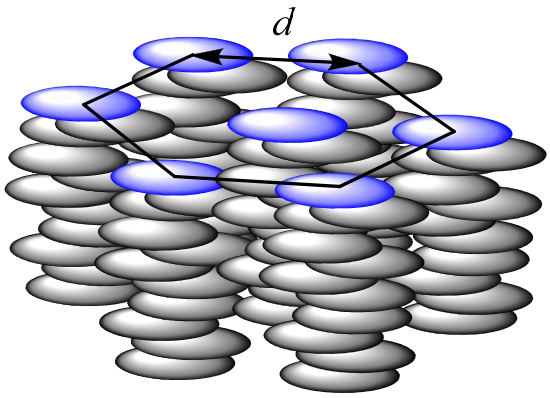

Figure 1-1. Schematic representation of the columnar liquid-crystalline phase formed by the assembly of disk-shaped molecules (*d* = intercolumnar distance).[37]

H-bonding interactions are also commonly used in the design of self-assembled systems.[30-33] These weak, but directional interactions play significant roles in controlling the structure and conformation of most biological supramolecules, like proteins. The Stupp group employs a variety of interactions, including H-bonding, in the self-assembly of peptide-amphiphiles (PAs, Figure 1-2).[41] The molecules assemble in water into cylindrical micelles and fibers; the alkyl chains pack in the center of the micelles (hydrophobic interactions) while the more polar peptide segments associate by H-bonding closer to the aqueous exterior.

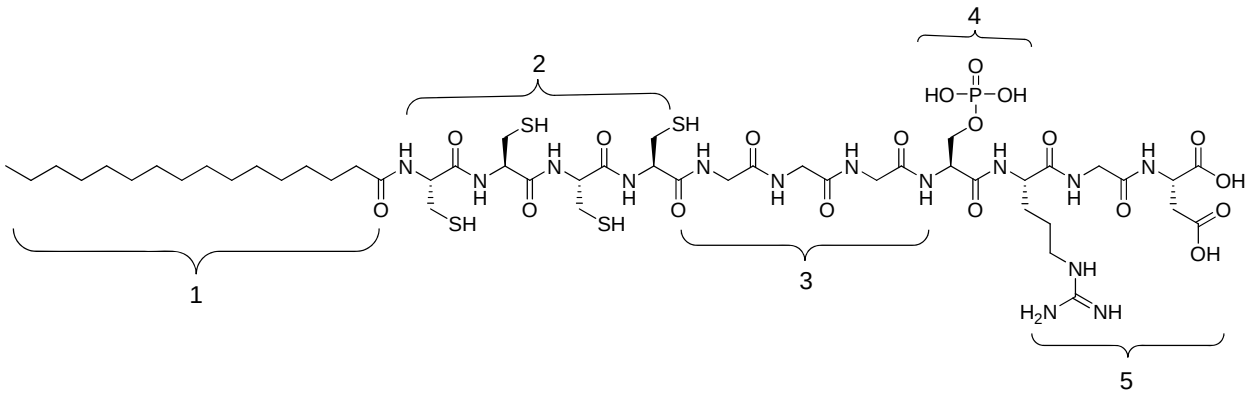

Figure 1-2. Chemical structure of Stupp's peptide amphiphiles, highlighting five key structural features. The long alkyl chain of region 1 conveys hydrophobic character. Region 2 is the peptide main chain which is composed of four consecutive cysteine residues that may form disulfide bonds to crosslink the self-assembled structure when oxidized. Region 3 is a flexible linker region that serves as a hydrophilic head group. Region 4 and 5 feature special molecular recognition functionality.[41]

A "hydrogen-bonding-induced" conformational change from J- to H- aggregates in fluorescent liquid-crystalline perylenebisimides shows how π-π stacking and H-bonding interactions can muturally support self-organization.[42] Recently prepared and highly fluorescent liquid-crystalline perylenebisimide molecules feature amide or ester linkages and are end-capped by phenyl, monododecyloxy phenyl, or tridodecyloxy phenyl units (Figure 1-3). The amide-functionalized series self-organizes to form H- type aggregates regardless of the end-cap in organic solvents like tetrahydrofuran (THF), toluene, and dichloromethane (Figure 1-3a). On the other hand, only the monododecyloxy phenyl end-capped molecule in the ester series shows a tendency to self-organize with a typical J- type aggregation in toluene (Figure 1-3b). The development of this new series of perylenebisimide based liquid-crystalline materials was accomplished using both hydrogen bonding and π-π interactions as well as balancing the rigidity (aromatic core)-flexibility (alkyl chains) ratio of the molecular shape.[42]

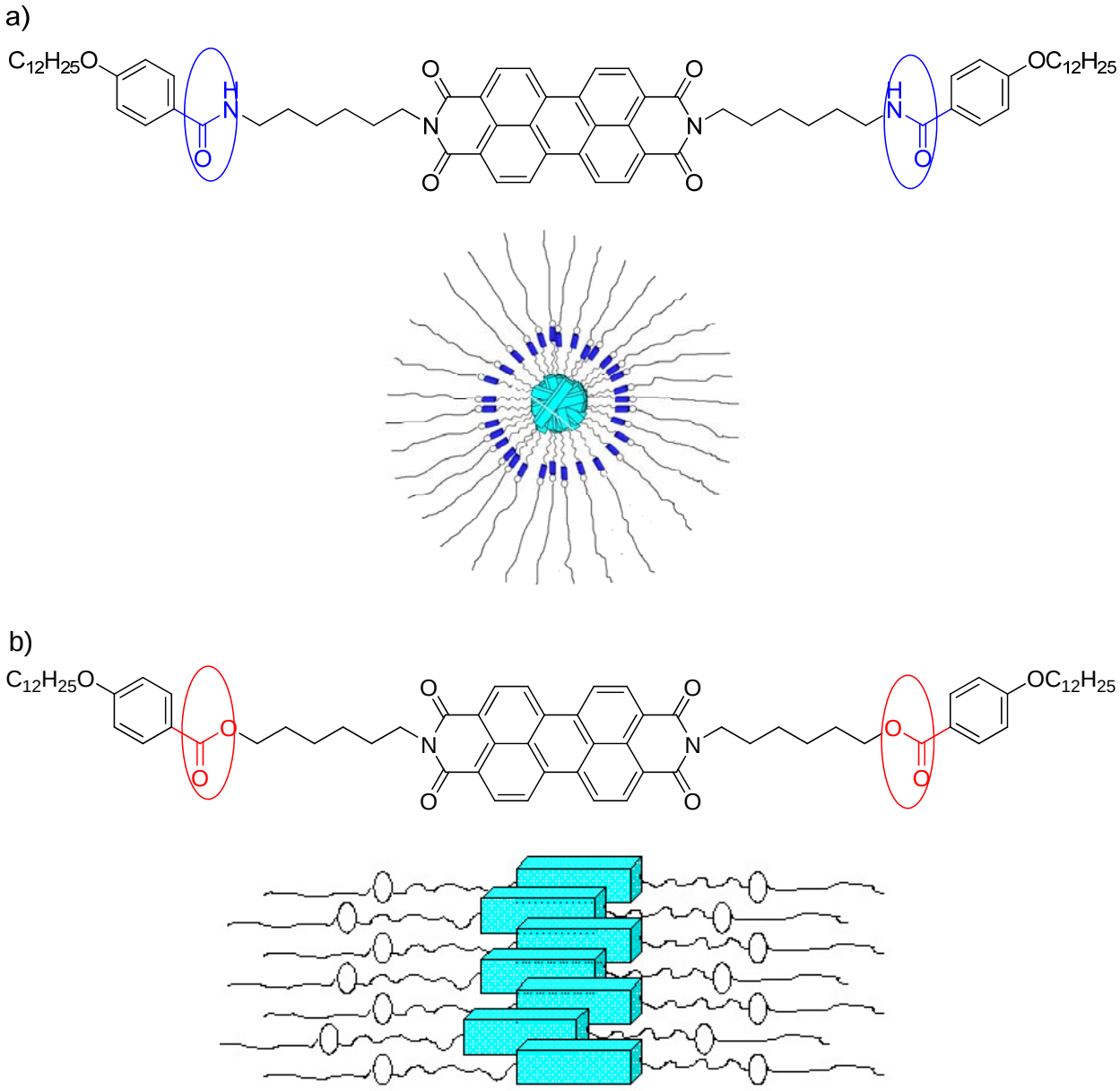

Figure 1-3. Schematic diagram of the packing in (a) H-type aggregates of per6dodecbenzamide perylenebisimide derivative in solution and (b) J-type aggregates of per6dodecbenzester perylenebisimide derivative in solution.[42]

The above examples show how traditional noncovalent interactions like π-stacking and H-bonding can be used to control the structures and properties of self-assembled materials. As supramolecular structures become more complex, numerous interactions are often responsible for self-assembly. Würthner and coworkers have shown, using π-conjugated donor–acceptor

chromophores (e.g. merocyanine dyes, Figure 1-4), how dipolar (electrostatic) interactions can be combined with other noncovalent interactions (like π-stacking) to promote small-molecule self-assembly into gels,[43] liquid crystals,[44] and supramolecular polymers.[43] Similar dipolar interactions are important to the self-assembly of the donor-σ-acceptor molecules discussed in this dissertation.

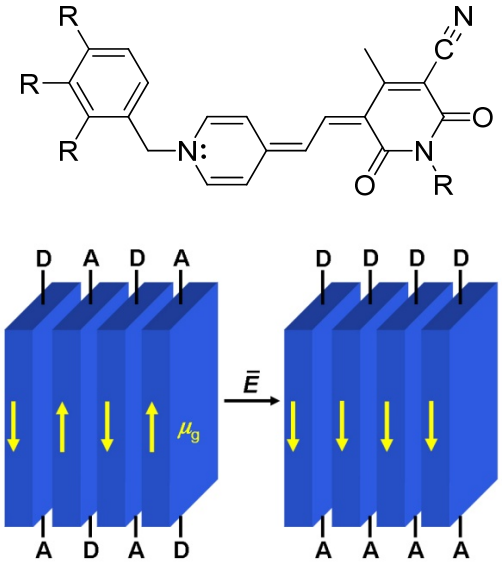

Figure 1-4. The chemical structure of a merocyanine dye and a model for its self-assembly into 1-D stacks that are stabilized by π-stacking and dipolar interactions. The graphic also shows how the molecules might be oriented in an electric field (D = electron donor: A = electron acceptor).[43]

Shape complementarity is important for self-assembly processes; molecules that can fit together well can also optimize the noncovalent interactions between them. Swager and coworkers have used shape, dipole, van der Waals, and π-stacking interactions together to create unidirectional (head-to-tail) liquid-crystalline linear chain polymers (Figure 1-5).[45] Other researchers, like Kato,[46-49] Collet,[50-52] and Tschierske[53, 54] have similarly used interesting molecular shape in their assembly designs.

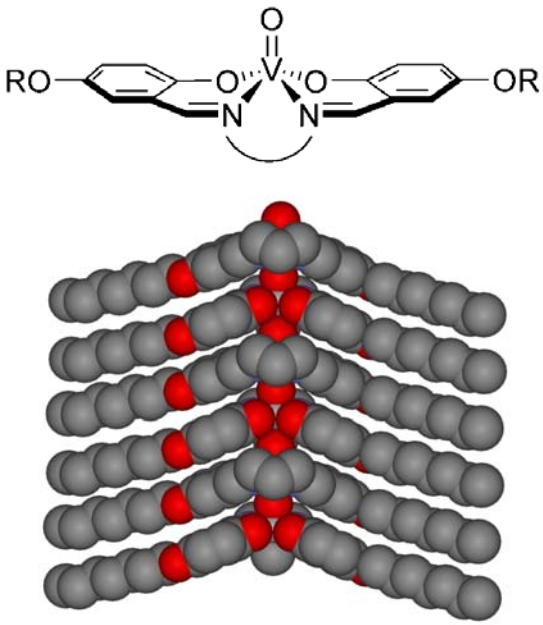

Figure 1-5. Vanadium-oxo linear chain compounds that organize into polar stacks through core-to-core dipolar interactions and π-stacking interactions.[45]

Self-assembly provides access to molecular aggregates and organized matter on size scales well beyond what can be achieved through bond-by-bond construction.[9] The strategy, however, is limited by our ability to predict how assemblies will form, what noncovalent interactions can be used in the process, and what properties will emerge from the equilibrium structures. This dissertation explores these general concepts in the context of new building blocks for supramolecular chemistry, σ-coupled donor-acceptor molecules.

Through-Bond Interactions and σ-Coupled Donor-Acceptor Molecules

Noncovalent interactions play a crucial role in controlling the structures and properties of supramolecular assemblies; identifying new interactions, and studying the molecular structures that feature them, is an important research area. Recently the Castellano group initiated a research program that employs donor-σ-acceptor (D-σ-A) molecules as building blocks in supramolecular architectures. One goal is to study strong σ-coupled donor-acceptor interactions

as complements to traditional noncovalent forces in the directed self-organization of functional molecules.[55, 56]

Through-Bond Interactions

The term 'through-bond interaction' (TBI) was introduced in 1968 by Hoffmann and coworkers to designate the intramolecular interaction between functional groups via intervening σ-bonds.[57, 58] This definition was later expanded to include the experimental results of Heilbronner[59] and the higher-level theory of Dewar and Wasson, researchers who also showed the dependence of such interactions on the geometry of the σ-bridge.[60] Indeed, these types of hyperconjugative interactions are very sensitive to the orientation of the interacting donor and acceptor orbitals with respect to the σ-relay that connects them. Theoretical studies[57, 58, 61, 62] have shown that TBI between two nitrogen lone pairs separated by three σ-bonds will be optimized for the conformation depicted in Figure 1-6, where the interacting groups adopt an antiperiplanar relationship and are parallel to the central carbon-carbon σ-bond. Hudec and Cookson's examples[63, 64] of constrained bi- and tricyclic donor-σ-acceptor (D-σ-A) molecules illustrate this phenomenon nicely.

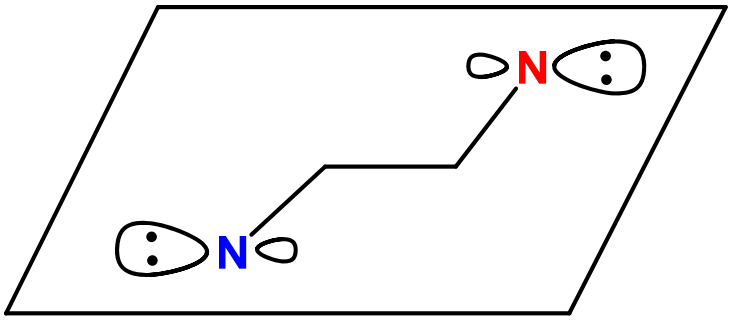

Figure 1-6. A schematic representation of the required orientation for optimal TBI between two nitrogen lone pairs separated by three σ-bonds.[58]

Donor-σ-Acceptor Molecules and Their Traditional Applications

Studies[63-68] have shown that an intramolecular charge transfer (CT) absorption and emission can arise from through-bond interactions between a properly oriented strong electron donor (D) and strong electron acceptor (A)—even if the functional groups are separated by three or more σ-bonds. Verhoeven and coworkers have used this spectroscopic signature to elucidate the stereoelectronic requirements for the donor–acceptor interactions in various cyclic systems. Each molecule in Figure 1-7 contains a nitrogen lone pair as an electron donor and a 1-cyano-1-carbethoxyethylene as an acceptor separated by three σ-bonds.[66, 67] The nitrogen lone pair in the aza-adamantane **1-1** is locked into an equatorial orientation with respect to the six-membered ring, and therefore lies antiparallel to the central C–C bond. A strong CT absorption is observed. Piperidine **1-2** displays no CT absorption although it contains the same donor and acceptor as in **1-1**. The lone pair occupies the axial position as the methyl group preferentially adopts the more stable equatorial conformation and is not suitably aligned for TBI.

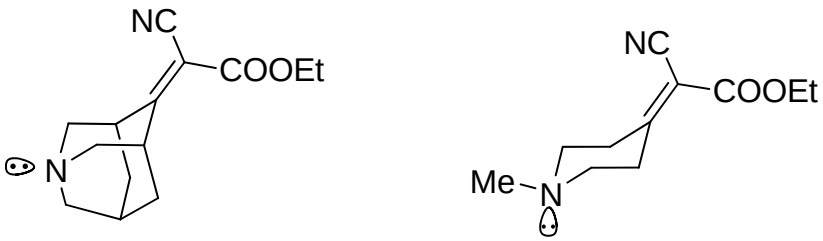

1-1

λ_{CT} = 316 nm
ε = 4900 $M^{-1}cm^{-1}$
(*n*-hexane, 20°C)

1-2

no CT-absorption

Figure 1-7. Verhoeven's molecules that illustrate of the conformational requirements for CT absorption.[66, 67]

Numerous donor-σ-acceptor chromophores have been prepared over the years and studied at the molecular level to model photoinduced charge transfer over fixed distances. The

compounds shown in Figure 1-8 are just two examples.[69] The interesting electron transfer properties of such molecules has gradually filtered into applications[70, 71] that include molecular rectification,[70] nonlinear optics (as NLO chromophores),[71] and electroluminescent (EL) devices,[72] etc. Only recently have σ-bridged donor-accepter molecules been incorporated into polymers, like high molecular weight linear polyesters.[73-75] The use of D-σ-A building blocks for various supramolecular materials, including molecular assemblies, are promising but hitherto virtually unexplored.

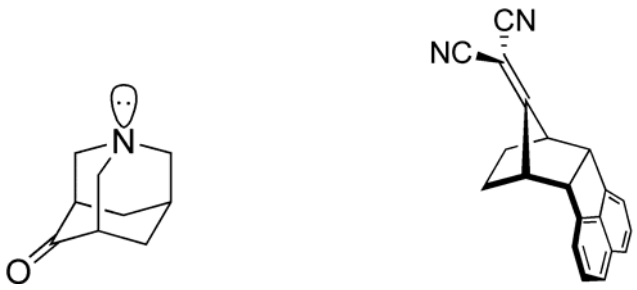

Figure 1-8. Examples of rigid donor-σ-acceptor molecules.[69]

β-Aminoketones

The β-aminoketone fragment is among the simplest that has been studied with respect to donor–acceptor through-bond interactions[76] and appears as a good starting point for the development of new supramolecular building blocks. The donor–acceptor interactions are optimized when the nitrogen lone pair (donor), C_α–C_β bond, and carbonyl π system (acceptor) are in a zig-zag arrangement (Figure 1-9). Three cyclic examples are shown that differ with respect to the permanence of their donor–acceptor interactions. The lone pair of the nitrogen atom in *N*-methylpiperidone **1-3** and tropinone **1-4** is transiently maintained in the optimum configuration for communication with the carbonyl; this configuration is fixed in 1-aza-adamantanone **1-5**.

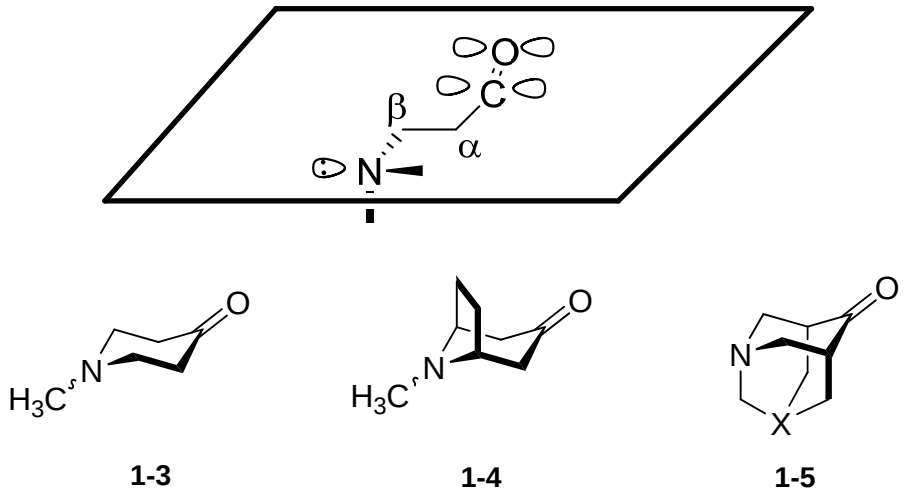

1-3 **1-4** **1-5**

Figure 1-9. Donor-σ-acceptor arrangement in cyclic *β*-aminoketones; *N*-methylpiperidone (**1-3**), tropinone (**1-4**), and 1-aza-adamantanone (**1-5**).[76]

Verhoeven and coworkers, using molecules like **1-2**, have demonstrated the effect of through-bond interactions on nitrogen configuration in such molecules.[68, 77] The Castellano group has focused on functionalized versions of **1-3** and **1-5** (i.e., those bearing groups that facilitate molecular assembly) with respect to their molecular and supramolecular properties. Various 3,5-disubstituted piperidone derivatives were the topic of this author's masters research; the findings are summarized here as they include more recent results.[78] Two representative compounds are shown, **1-8a** and **1-8b** (Figure 1-10), that were synthesized to explore the effects of through-bond interactions on the conformation, nitrogen configuration, and the self-assembly properties of functionalized *β*-aminoketones in the solid state.

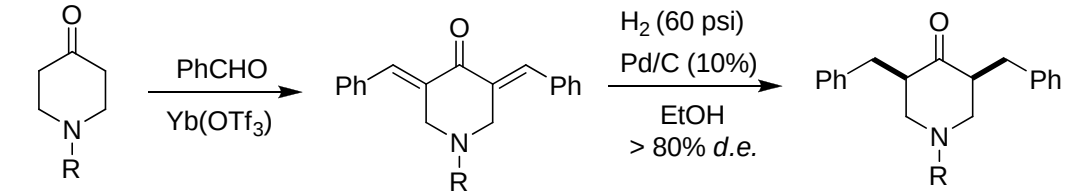

1-6

a R = Ph

1-7

a R = Ph (45%)
b R = CH_3

1-8

a R = Ph (41%)
b R = CH_3 (58%)

Figure 1-10. Synthesis of *cis*-3,5-dibenzyl piperidin-4-ones.

X-ray crystallographic analysis of **1-8a** and **1-8b** reveals that both molecules adopt standard chair conformations with the benzyl groups in the equatorial position. The nitrogen substituent of **1-8b**, a methyl group, occupies the equatorial position with respect to the piperidone ring, a configuration that does not optimize through-bond interactions with the carbonyl acceptor. For compound **1-8a**, however, both the equatorial (**1-8a-eq**) and axial (**1-8a-ax**) nitrogen epimers are accommodated in the crystal lattice in a 2.5:1 ratio (at 173 K) based on refined values of occupancy factors. Detailed structural analysis shows that the packing environments of each epimer are nearly identical. Given that the typical "packing effect" argument does not sufficiently rationalize the significant population of **1-8a-ax**, what does?

The fundamental properties and equilibrium structures of the axial and equatorial epimers of **1-8** and nearly a dozen model compounds were examined using extensive first principles calculations in collaboration with Dr. Bobby Sumpter at Oak Ridge National Laboratory. To summarize the results, **1-8a-ax** is found (at various levels of theory that treat correlation effects well: MP2, CCSD(T), B3LYP, CASSCF, etc.), despite claims for *N*-alkyl and *N*-arylpiperidines and –ones in the literature, to be quite close in energy to **1-8a-eq**. Structure-property studies reveal that the relative stability of the axial epimer increases upon conversion of *N*-CH_3 to *N*-Ph (a better electron donor), substitution of the 3 and 5 positions of the piperidine ring, and introduction of the carbonyl acceptor. Natural bond orbital (NBO) analysis, based on the optimized wavefunctions (at the MP2/6-311G** level) for the **1-8a** epimers, quantify the stability that comes from hyperconjugative interactions for **1-8a-ax**. Molecular orbital plots show the contributions graphically (Figure 1-11 and 1-12). For both isomers, the HOMO plot reveals significant delocalization of the N lone pair into the adjacent C=C π^* orbitals of the phenyl ring.

However, only in **1-8a-ax** is there significant delocalization of the N lone pair into the C–C antibonding orbitals (of the piperidone ring) *and* π* orbital of the carbonyl group.

The work concludes with the idea that through-bond interactions and assembly structure are inextricably linked in the solid-state structures of simple functionalized *β*-aminoketones like **1-8**. The studies also show an inherent stability for the axial epimers of these molecules, previously assumed inaccessible; that the configuration that optimizes donor-acceptor through-bond interactions can be preserved in the solid state bodes well for the use of the systems in solid-state applications.

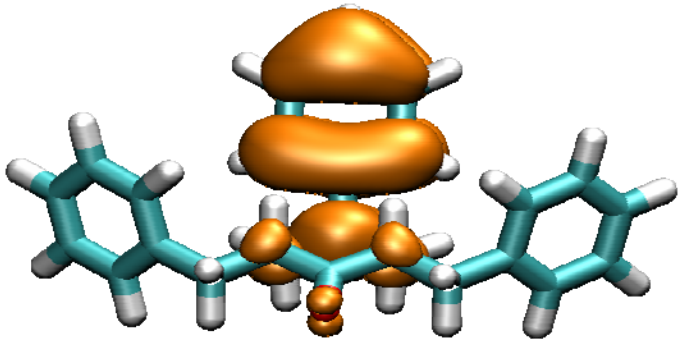

Figure 1-11. Plot of the HOMO for the axial epimer (**1-8a-ax**) which shows delocalization of the nitrogen lone pair onto the phenyl, the adjacent C–C of the piperidione backbone, and the carbonyl.

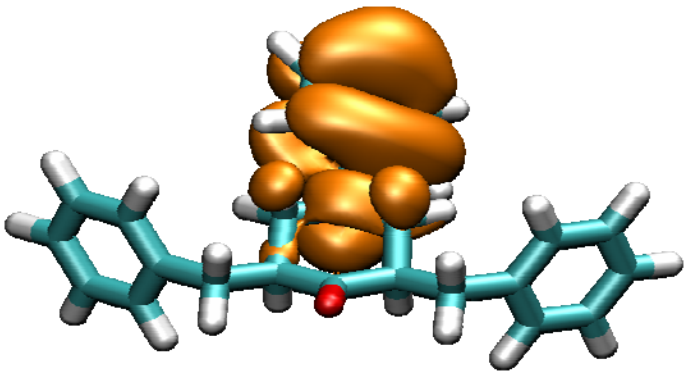

Figure 1-12. Plot of the HOMO for the equatorial epimer (**1-8a-eq**) which shows delocalization of the nitrogen lone pair onto the phenyl, the adjacent C–C of the piperidione backbone.

1-Aza-Adamantanetrione (1-AAT) Platform

Can σ-coupled donor–acceptor interactions be used to influence the self-assembly properties of small molecules in solution from which useful macromolecular properties can emerge? The unique 1-aza-adamantanetrione platform (Figure 1-13) has been used in the Castellano group as a vehicle to explore this question.

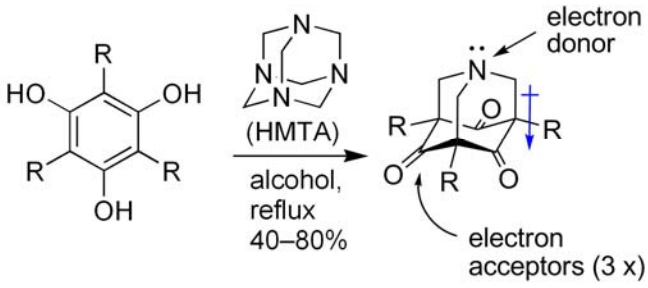

Figure 1-13. Synthesis of the 1-aza-adamantanetrione (AAT) platform.

The AAT platform boasts many features that make it a useful tool to draw structure-property relationships. First, it is efficiently constructed by a single-step cyclization of phloroglucinol derivatives with hexamethylenetetramine (HMTA); a Mannich-type reaction (Figure 1-14).[33, 79-83] Second, three sites exist on the core that can be easily synthetically modified. Next, the enforced shape of the core is suitable for "predictable" assembly, amenable to high-level computation, and optimizes communication between the bridgehead nitrogen lone pair and carbonyl π systems (via three intervening σ-bonds). The AAT also has a sizable ground state dipole moment; together with its shape, directional assembly is conceivable. These small molecules have afforded an excellent opportunity to comprehensively study the fundamental changes in structure, reactivity, and macromolecular properties that can accompany the donor–acceptor arrangement in rigid σ-coupled donor-acceptor molecules.

Recently, definitive evidence for "strong" through-bond interactions in the AATs has been reported.[76] X-ray crystal structures of triester **1-9** and its corresponding mono-reduction product,

alcohol **1-10** (Figure 1-14), have provided some of the best evidence for through-bond interactions at the molecular level. Comparative bond length data from the crystal structures of compounds **1-9**, **1-10**, and various analogues (for example, compounds **1-11**, **1-12**, and **1-13**, Figure 1-15) available in the literature[84-86] is included in Table 1. Analysis of the data shows that somewhat shortened C–N bonds (**a**) and considerably elongated C–C bonds (**b**) result when through-bond interactions are optimized. The bond length alternation is a classically predicted consequence of hyperconjugation.[76, 87, 88] More evidence, such as changes in bond angles, spectroscopic properties (e.g., the presence of the so-called "σ-coupled" transition in the UV-Vis spectra of **1-9** and **1-10**), and reactivity are all consistent with theoretical expectations for well-defined σ-coupled donor-acceptor interactions.

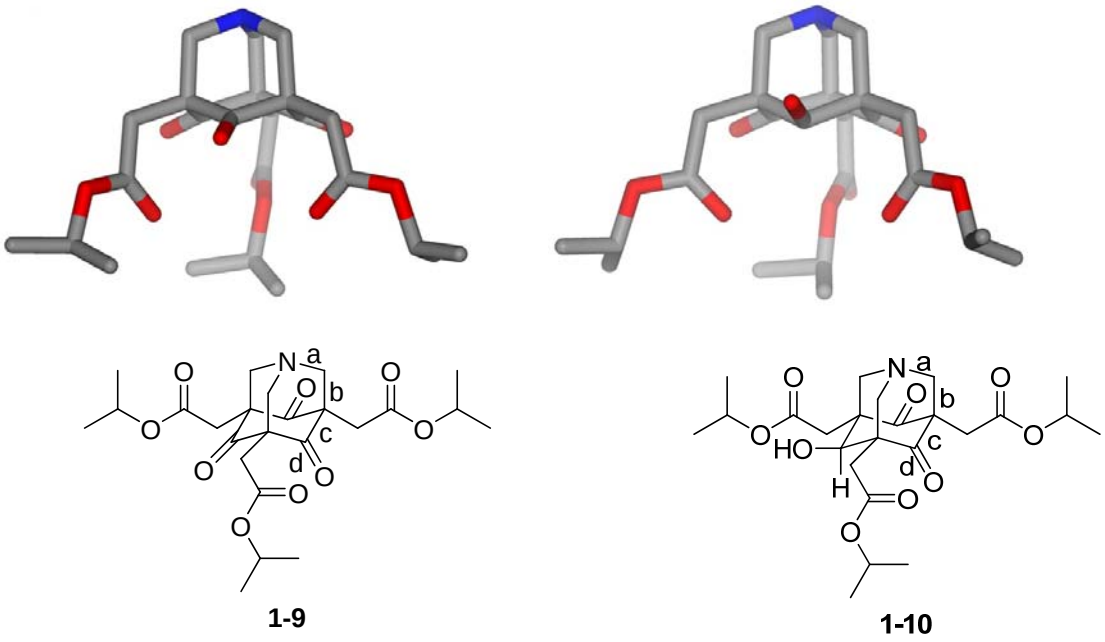

Figure 1-14. X-ray crystal structures of compounds **1-9** and **1-10**.[76]

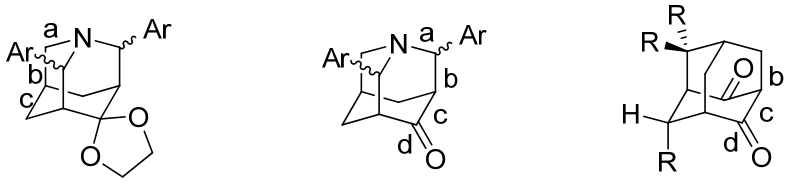

1-11 **1-12** **1-13**

Figure 1-15. The chemical structure of compound **1-11** (Ar = *p*-chlorophenyl), **1-12** (Ar = *p*-nitrophenyl, and **1-13**.[76]

Table 1-1. Comparison of average bond lengths (reported in) from the X-ray crystal structures of **1-9**, **1-10**, and related tricyclic molecules from Figure 1-15.[76]

Bond	**1-11**	**1-12**	**1-10**	**1-9**	**1-13**
a	1.49	1.48	1.44	1.45	–
b	1.53	1.55	1.59	1.59	1.55
c	1.53	1.51	1.52	1.51	1.51
d	–	1.21	1.21	1.22	1.22

Given such readily measured consequences of strong through-bond interactions in the AATs, this platform has been used to draw structure-property relationships at the macromolecular and supramolecular level.

Self-Assembly of AATs

The Castellano group has been exploring donor–acceptor through-bond interactions at the macromolecular/supramolecular level where they can complement traditional forces (e.g., hydrogen bonding, π-stacking, etc.) in controlling molecular architecture and emergent properties.[55, 56, 89, 90] For initial studies the AAT framework has been employed, the through-bond interactions of which (i.e., between N and C=O) were found to be unusually assessable and addressable in the ground state.[76]

AATs Bearing Simple Aromatic Side Chains

The first generation of functionalized AATs found to readily self-assemble in solution are shown in Figure 1-16; the molecules are decorated with simple aromatic side chains and represent a new class of organogelators.[56] Optically clear gels form upon heating and cooling

compounds like **1-14** (Ar = Ph) in DMSO. The critical gelation concentration (CGC) is 0.5% by weight and the gel exhibits a sol-gel temperature (T_{gel}) of 45 °C.[56] SEM and TEM techniques were used to explore the morphologies of the xerogels, formed from either critical point drying or conventional freeze drying techniques. Extended fibrillar structures appear that are consistent with the on-average 1-D self-assembly of the molecules.

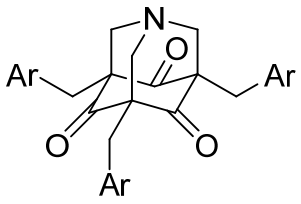

1-14

Figure 1-16. Generic structure of AATs bearing aromatic side chains.

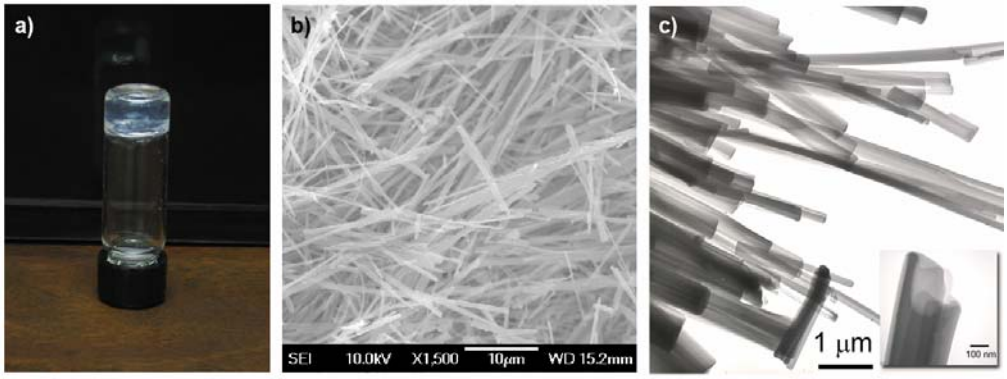

Figure 1-17. (a) Organogel of the tribenzyl AAT derivative **1-14** (Ar = Ph) in DMSO. (b) SEM image of the xerogel formed from critical point drying of an 0.5 wt % DMSO gel. (c) TEM image of the xerogel formed from critical point drying of an 0.5 wt % DMSO gel.[56]

Subsequent DFT-LDA/cc-pVDZ calculations identified the lowest energy conformation as the "all arms up" structure shown in Figure 1-18a, a conformation also present in solution based on NMR experiments (NOEs are observed between hydrogens H^c on the aromatic ring and H^a on the core; Figure 1-18b). Further molecular dynamics simulations by Sumpter and coworkers[90] revealed the tendency of these donor-σ-acceptor molecule to self-assemble (in the gas phase) in a

head-to-tail fashion to create polar columns. The predicted (homochiral) stacked dimer (Figure 1-18c) is stabilized by dipole-dipole interactions and π-π stacking to the tune of ~ 13 kcal mol^{-1} (the intercore spacing in the optimized dimer is ~ 5.1 Å).

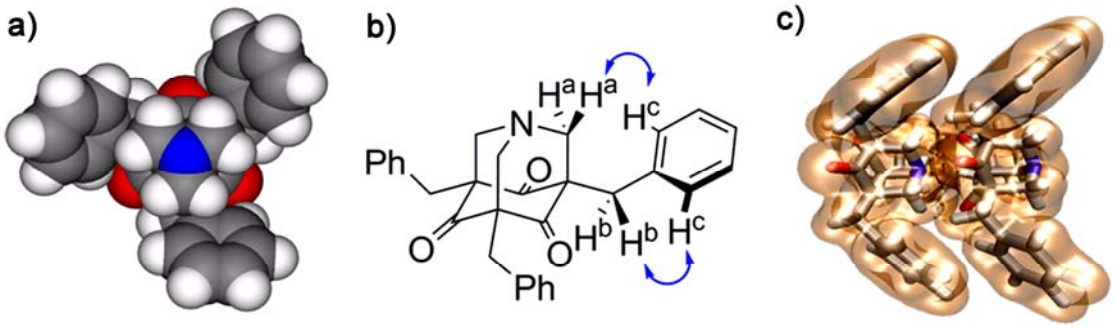

Figure 1-18. (a) Energy-minimized lowest energy "all-arms-up" conformation. (b) The NOE contacts identified from a NOESY experiment for **1-14** (Ar = Ph). (c) Total charge density isosurface for the gas-phase optimized dimer, (**1-14**)$_2$, obtained from DFT(LDA)/cc-pVDZ calculations.[55, 56, 89-92]

Amides in the Periphery

Triamide derivatives of the 1-aza-adamantanetriones (Figure 1-19)[55] were next studied to show how polar functional groups on the outside might interact in specific ways with the donor-σ-acceptor core and affect macromolecular behavior. Triamides **1-15** show enhanced aggregation properties and significantly more order in solution, the gel phase, and the bulk (compared with **1-14**). This comes, in part, from conformational stabilization (preorganization) of the arms by intramolecular H-bonding and favorable intramolecular dipolar interactions. Robust gels form from chloroform solutions of **1-15** (R = $C_{12}H_{25}$) quickly at low monomer concentration (~ 0.5 wt %); the sol–gel transition temperature (T_{gel}) is 57 ^{o}C.[55] A representative SEM image (Figure 1-20a) shows rope-like fibers upon evaporation of **1-15** (R = H) from a toluene/pyridine (3:1) solution. X-ray diffraction (XRD) studies (Figure 1-20b) then reveal long-range periodic order for the neat (solid) samples of **1-15**. Final evidence for the C_3-symmetric

conformation proposed for **1-15** comes through solid-state NMR studies performed with ^{15}N-enriched **1-15** (Figure 1-20c).

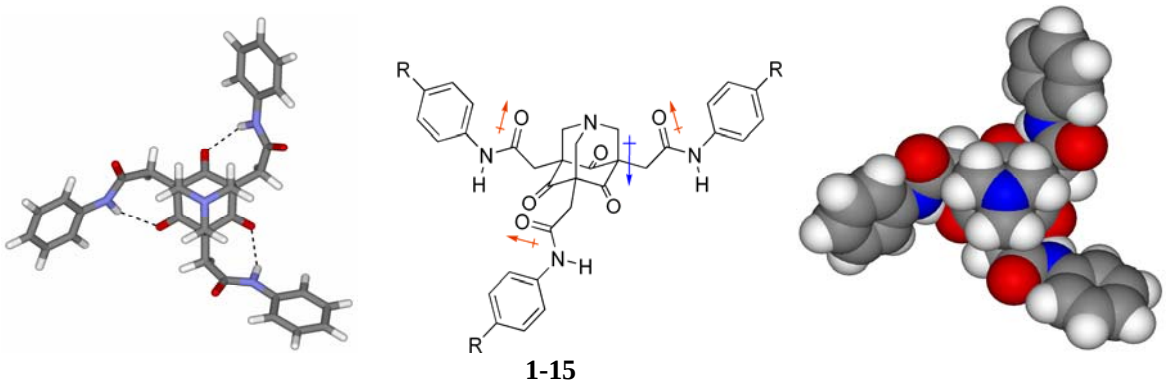

Figure 1-19. Amide functions on the periphery of the tricyclic core stabilize a C_3-symmetric monomer conformation by intramolecular hydrogen bonding and dipole–dipole interactions.[55, 91]

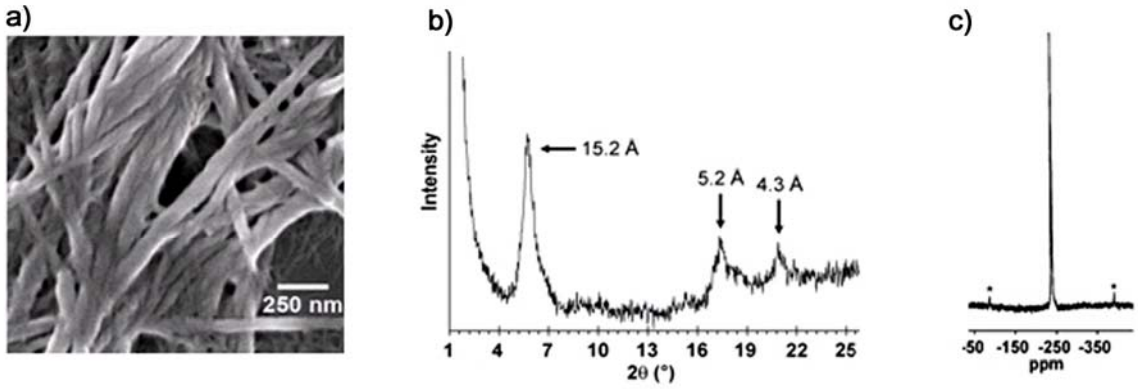

Figure 1-20. (a) SEM image of rope-like fibers of **1-15** (R = H) formed upon solvent evaporation. (b) X-ray diffraction pattern of neat **1-15** (R = H). (c) Solid-state NMR data using an ^{15}N-labeled derivative of **1-15** (where R = H).[55, 91]

Emergent Electronic Structure

Computational analysis has shown that an unprecedented electronic structure could result from assembly of AAT **1-14** (Ar = Ph), first into a homochiral dimer, and then into linear 1-D stacks (Figure 1-21).[89-91] Notable reduction of the HOMO-LUMO gap is predicted upon dimerization and oligomerization; ultimately a band structure develops akin to what is described for π-conjugated molecular systems. Formation of molecular wires through the self-assembly of

novel non-aromatic architectures is an important development toward organic electronic devices.[92]

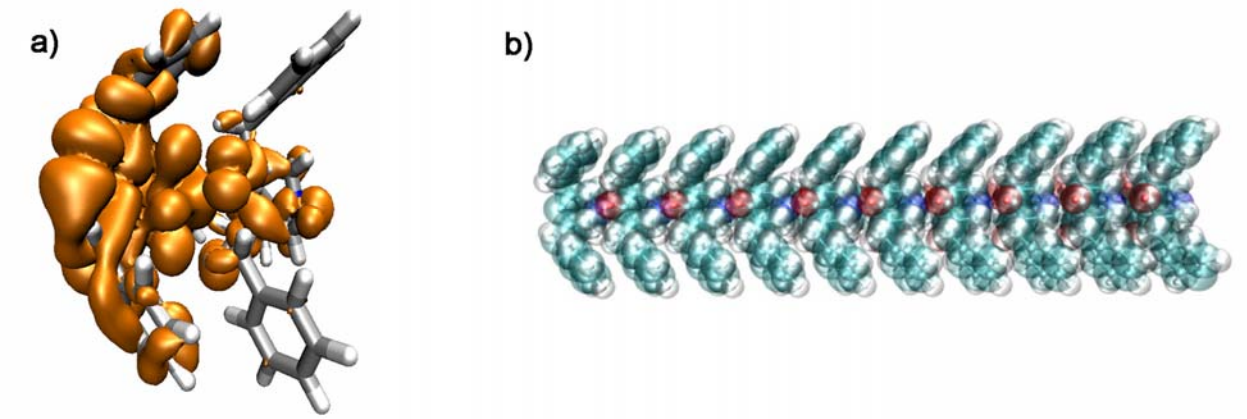

Figure 1-21. Calculated (DFT(LDA)/cc-pVDZ) dimer and stacking arrangement for **1-14** (Ar = Ph): (a) the HOMO charge density isosurface for the dimer showing delocalization over both AAT cores; (b) 1-D periodic stacking of **1-14** (Ar = Ph) monomers into wire-like assemblies.[89, 90, 92]

High-level computation has shown that the peripheral amides can also tune the electronic structure of these 1-AAT systems. The HOMO-LUMO gap for **1-15** is calculated to be substantially lower than that of its aryl isostere **1-14**. This reduction is largely due to lowering of the LUMO energy (by ≈ 0.7 eV, as compared to the tribenzyl system), which originates from the three hydrogen bonds between the amide –NHs and the core ketones.[89-93] The amide functional group provides a tunable element of electronic control over the resulting self-assembled structures.[91]

Scope of Dissertation

Extensive experimental and computational studies have been performed to understand how through-bond donor-acceptor interactions might complement traditional noncovalent forces, such as H-bonding and π–π stacking, in molecular self-assembly. One unique class of σ-coupled donor-acceptor molecules, the AATs, has been developed for the studies. Several challenges remain. First, theoretical studies suggest that exciting electronic properties should accompany

assembly of the AATs into 1-D arrangements. This level of order in solution and the solid state has yet to be achieved. Second, many of the more exciting AAT targets are those that are less symmetrical and even chiral; currently these are not readily accessible. Lastly, much work remains to understand the dynamic self-assembly behavior of the AATs in solution, and how macromolecular behavior emerges from this process.

This dissertation is focused on the design, rational synthesis, and self-assembly properties of new 1-aza-adamantanetrione derivatives. Chapter 2 describes the synthesis and self-assembly studies of AATs bearing expanded aromatic arms. The work shows the role of the AAT periphery in controlling the macromolecular properties of the assemblies that result, where the most robust gelating species from the AAT class are now described. Numerous characterization methods are used to study the assemblies, and some, including fluorescence spectroscopy and dynamic light scattering, are used for the first time. The data shows how AAT self-assembly responds to temperature, solvent, concentration, and structure. Chapter 3 is focused on new synthetic methodology that has been developed to prepare desymmetrized and asymmetric AATs. Accessing AATs bearing multiple peripheral functional groups could afford new macromolecular properties that are uniquely tunable. Chapter 4 highlights efforts made to prepare the first hydrophilic and potentially hydrogelating AATs, using, in part, the strategies presented in Chapter 3. Conclusions and future directions for the "unconventional" donor-acceptor molecules are discussed in Chapter 5.

CHAPTER 2
DESIGN, SYNTHESIS, AND PROPERTIES OF 1-AZA-ADAMANTANETRIONES WITH EXPANDED AROMATIC ARMS

Introduction

Low molecular weight organogelators (LMWGs) constitute an important class of functional materials that have recently emerged.[24, 94-96] Interest in gels derived from LMWGs continues to grow because of their many potential applications in diverse areas including drug delivery,[97, 98] organic light emitting devices,[99] cosmetics,[100] and sensing.[101] Organogels result when small organic molecules form nanoscale, cross-linked fibrous aggregates by noncovalent self-assembly. H-bonding, π–π stacking, metal coordination, the hydrophobic effect, and van der Waals interactions are typical forces responsible for gel formation.[14, 24, 32] Gels are readily identified as jelly-like materials that feature large volumes of immobilized organic solvent (generally the number of solvent molecules exceeds the number of organogelator molecules by several orders of magnitude), are thermoreversible, and have interesting rheological properties.

It has recently been shown that "unconventional" donor-acceptor molecules, 1-aza-adamantanetriones (AATs), constitute a new class of organogelators.[55, 56] Extensive experimental[55, 56] and electronic structure calculations[89, 90] have been used to explore the mechanism of AAT self-assembly and the properties of the resultant supramolecular structures. Several important conclusions have emerged from the work. At the molecular level, recent comprehensive studies by X-ray crystallography, UV/Vis, and NMR[76] confirm that "strong" through-bond donor-acceptor interactions[58, 62, 63, 102] characterize the AAT core. These interactions create understandable changes in bond structure and molecular dipole, but also respond to substitution on the core. Both experimental and theoretical studies have then shown that self-assembly involves dipolar interactions (modulated by the intramolecular donor–acceptor interactions) and traditional intermolecular forces.[55, 56, 89, 90] Among the latter, for molecules like

1-14 (Ar = Ph) and **1-15** (R = $C_{12}H_{25}$), π-stacking is particularly important. In dimers of **1-14** (Ar = Ph) studied by computation in the gas phase, MP2 calculations predict that nearly half of the binding energy arises from slipped face-to-face stacking interactions between the phenyl substituents.[89] Further work has considered the interesting electronic structure that arises when the same molecules organize into periodic 1-D structures that feature close core-to-core interactions.[90]

Both dipolar and π-stacking interactions are important for self-assembly of the AAT molecules in solution. In a goal to create well-ordered assemblies of the AATs to better probe their supramolecular electronic properties and potentially create ordered phases like liquid crystals, one approach is to enhance the interactions between the peripheral substituents. This chapter describes the design, synthesis, and properties of a class of AAT molecules which have expanded aromatic arms to potentially strengthen π-π stacking interactions between the molecules. The structure-property relationships that emerge will help in better understanding the mechanism of AAT self-assembly, to create new materials, and to afford new macromolecular properties.

Design and Synthesis

Design of AATs with Expanded Aromatic Arms

In a recent theoretical study[90] of AAT self-assembly, a mechanism was proposed for organization of compound **1-14** (Ar = Ph) into 1-D stacks (Figure 1-20b). The emergent electronic structure of this assembly was then shown to be dependent on the interaction of the cores. Given this model, enhancing the aromatic interactions between the molecules by using expanded aromatic surfaces could significantly increase the interactions of the AAT units and potentially confer these systems long-range order and interesting supramolecular and electronic

behavior. Certainly aromatic interactions are important in materials design strategies and influence broad areas like crystal engineering,[103, 104] host-guest chemistry,[105] and molecular recognition.[106, 107]

The notion of using shape along with aromatic interactions to promote 1-D self-assembly has been explored in a variety of other systems.[45, 108-110] In a recent example, V-shaped salicylidene-aniline derivatives were shown to pack into polar 1-D columns (Figure 2-1) through strong π-π interactions.[111, 112] These compounds could gelate various organic solvents, such as 1-butanol, 1-octanol, butyl acetate, carbon tetrachloride, benzene, and toluene. Studies further explored the hierarchical self-assembly of the molecules. First, left-handed helical nanofibers formed through unimolecular layer packing; these further twisted into thicker fibers capable of forming 3-D interpenetrated networks (and gel phases) that exhibited strong fluorescence enhancement.[111]

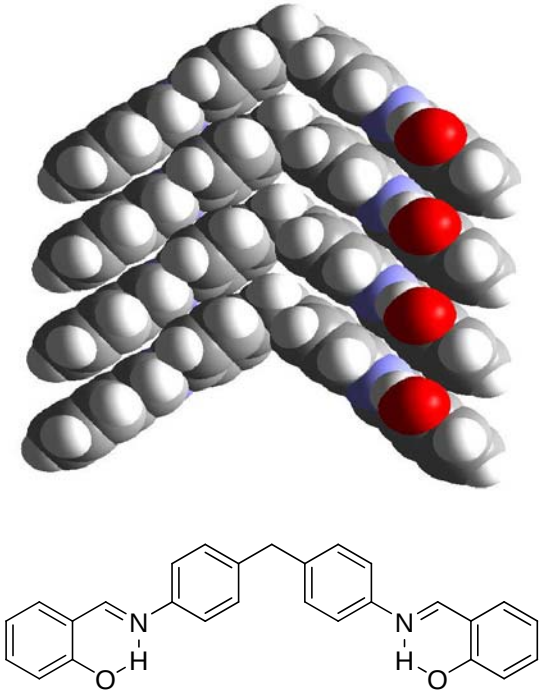

Figure 2-1. One-dimensional packing (J-aggregation) of salicylideneaniline derivative along the *b* axis in the crystal state.

Naphthalene, which is the simplest polycyclic aromatic compound,[113-120] has been chosen for incorporation into the AATs due to its availability and well understood electronic and optical properties. Furthermore, theoretical studies[121-123] predict that the stabilization energy of optimized parallel-displaced (PD) dimers of naphthalene is over three times that of benzene in the gas phase (2.60 kcal/mol for benzene versus 7.72 kcal/mol for naphthalene at the LMP2/6-31G* level). Additionally, naphthyl substituents offer useful absorption and emission properties that can be used to probe solution-phase assembly. The idea of using simple fluorescent aryl groups as reporter units in supramolecular systems has certainly been exploited before,[124, 125] and fluorescent signaling is one of the most sensitive techniques to monitor molecular association events. To this end, a small family of naphthyl-substituted AATs has been made and their gelation, solid-state and solution-phase assembly, and thermal properties have been studied.

Synthesis

Naphthylamines are the most important building blocks for the synthesis of naphthalene functionalized AAT molecules, based on general approaches that have been established previously to prepare amide-substituted AATs in the Castellano group. Napthylamine itself is commercially-available, however alkyl-substituted napthylamines are less common. We chose to install butyl and dodecyl substituents on the naphthyl ring to improve the solubility of the molecules[55, 76] and enhance the van der Waals interactions of the side chains. The synthesis of alkyl substituted naphthylamines is outlined in Figure 2-2. Important to note, naphthalene derivatives have wide industry and commercial applications but their toxic effects[126] are well-documented. Careful handling of these materials is required.

Commercially-available 6-bromo-2-naphthanol is first protected as its methyl ether using iodomethane and potassium carbonate to provide compound **2-2** in quantitative yield.[127] Alkyl groups are then introduced using Negishi cross-coupling[128-130] between the bromide and

appropriate organozinc reagent in the presence of $Pd(PPh_3)_4$. The organozinc reagent is formed through reaction of an alkyl Grignard reagent or alkyllithium reagent with anhydrous zinc bromide. Suzuki-Miyaura cross coupling can alternatively be used for this type of reaction as reported by Najera.[131] Deprotection of the methyl ether using BBr_3 affords 6-alkyl-naphthanol **2-4**; subsequent reaction with trifluoromethane-sulfonic anhydride converts the naphthanol to the corresponding triflate **2-5**.[132] Hydrobromic acid can alternatively be used for the demethylation.[133] Subsequent coupling[134, 135] of the naphthalene triflates **2-5** with $LiN(SiMe_3)_2$ in the presence of $Pd(dba)_2$ and $P(t\text{-}Bu)_3$, followed by deprotection of the silylamide using aqueous HCl, provides **2-6**. Toluene is the best solvent for the coupling reaction and room temperature is sufficient to consume all of the triflate starting materials. THF could also be used for this reaction but required heating (60–70 °C); starting material remained after stirring at room temperature overnight. As an alternative, naphthol **2-4** can be converted to naphthylamine **2-6** via the Bucherer reaction,[136] but this transformation requires harsh conditions.

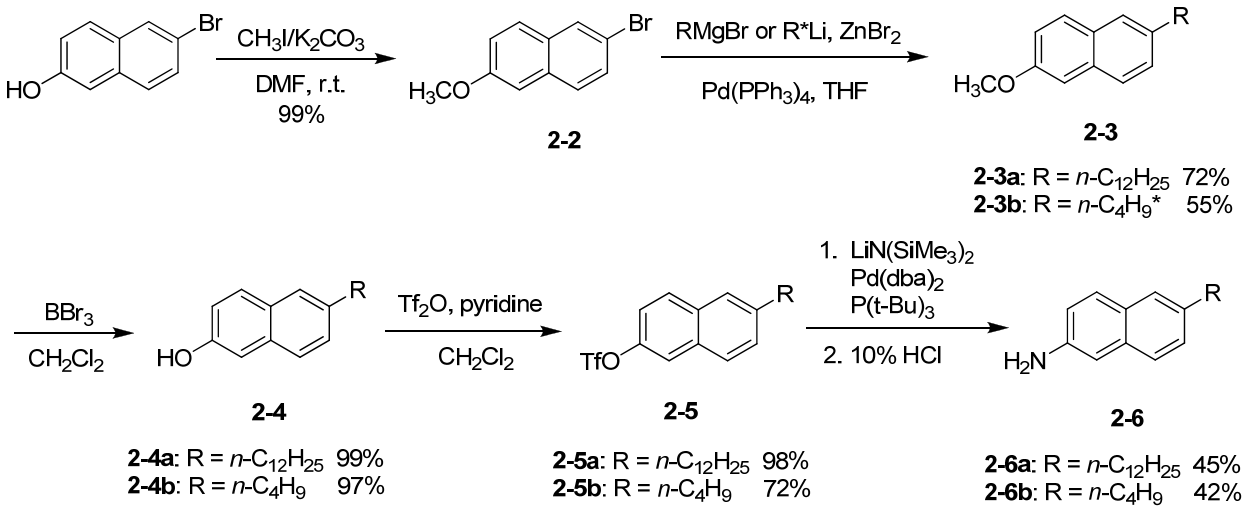

Figure 2-2. Synthesis of alkyl substituted naphthylamines.

Naphthylamine **2-6c**, that bears an electron-withdrawing group (EWG), was prepared as shown in Figure 2-3. This derivative could be the basis for a) exploring how electrostatics would

affect aromatic interactions in AAT assemblies (even mixed component assemblies), b) increasing the acidity of the amide proton that might also increase the intramolecular H-bonding between the amide –NH and core C=O (Figure 1-17), or c) providing a synthetic handle that could later be functionalized. Commercially-available 6-amino-2-naphthoic acid was simply converted to its *n*-butyl ester **2-6c** by treatment with the appropriate alcohol[137] and a catalytic amount of sulfuric acid.

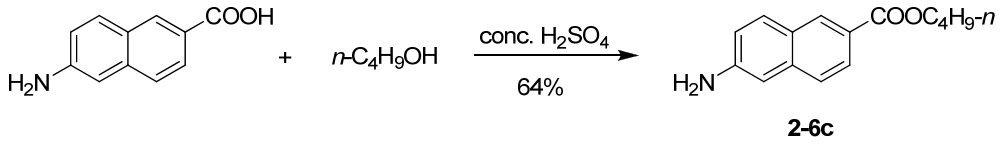

2-6c

Figure 2-3. Synthesis of a naphthylamine substituted with an electron-withdrawing group.

With the alkyl-substituted naphthylamine building blocks in hand, similar methods[55, 56, 91, 138] to those described previously for phenyl amide AATs were used to prepare the naphthyl derivatives (Figure 2-4). Coupling of triacid chloride compound **2-7b** with the more electron rich amines **2-6a** and **2-6b** provided **2-8a** and **2-8b** in moderate yield. Deactivated 6-amino-2-naphthoate **2-6c** unfortunately showed no appreciable reactivity with **2-7b**. The derivatives **2-8** could then be deprotected with BBr_3 as described above to provide the immediate AAT precursors, phloroglucinols **2-9a** and **2-9b**.

Subsequent cyclization of the naphthyl amide-functionalized phloroglucinol derivatives with hexamethylenetetramine (HMTA) to afford the AAT targets was particularly tricky. Either no product or complex mixtures were obtained in the initial runs, and attempts to change the amount of HMTA from one to three equivalents, solvent (from isopropanol to DMF to acetonitrile), and temperature (using a conventional oil bath or microwave irradiation) led to little improvement. The reason is probably the poor solubility of the amide phloroglucinol

derivatives. Fortunately, it was found that dilute solution (< 1 mM) and longer reaction times (heating to reflux for three days) could provide the target AATs in typical yields.

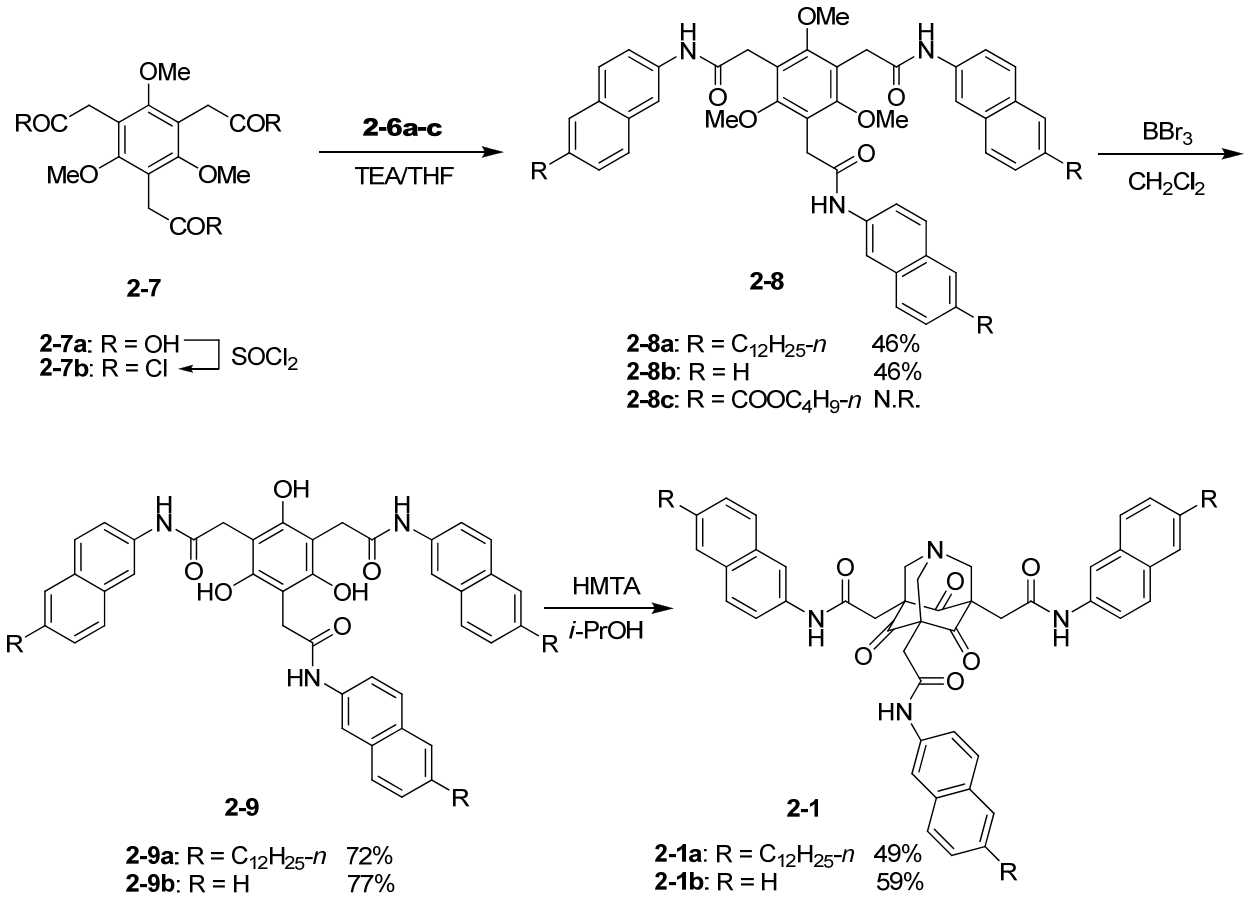

Figure 2-4. Synthesis of naphthyl amide-functionalized AATs.

Model compound **2-12** (Figure 2-5), which contains only one naphthyl arm in the AAT, and model compound **2-13** (Figure 2-6) were also prepared for control experiments (vide infra). Synthesis of **2-12** relies on the lactone-based desymmetrization chemistry[91] pioneered by Dr. Andy Lampkins in the Castellano group. Andy found that ester functionalized phloroglucinol derivatives can form the mono-, di-, and trilactones selectively under appropriate conditions.[91] We found that this approach can be expanded to amides (detailed information is provided in Chapter 3). Along these lines, dilactone **2-10** is available from naphthyl amide-functionalized phloroglucinol derivative **2-9b** by heating in a mixture of TFA and toluene. The C_2-symmetric

dilactone **2-10** is formed preferentially under these conditions. Nucleophilic attack with two equivalents of aniline in DMF at 120 °C opens both of the lactone rings to afford the new phloroglucinol **2-11**. The amount of the nucleophilic reagent and the reaction temperature are critical for this reaction. Compound **2-11** can then be converted to the corresponding desymmetrized AAT **2-12** by reaction with HMTA.

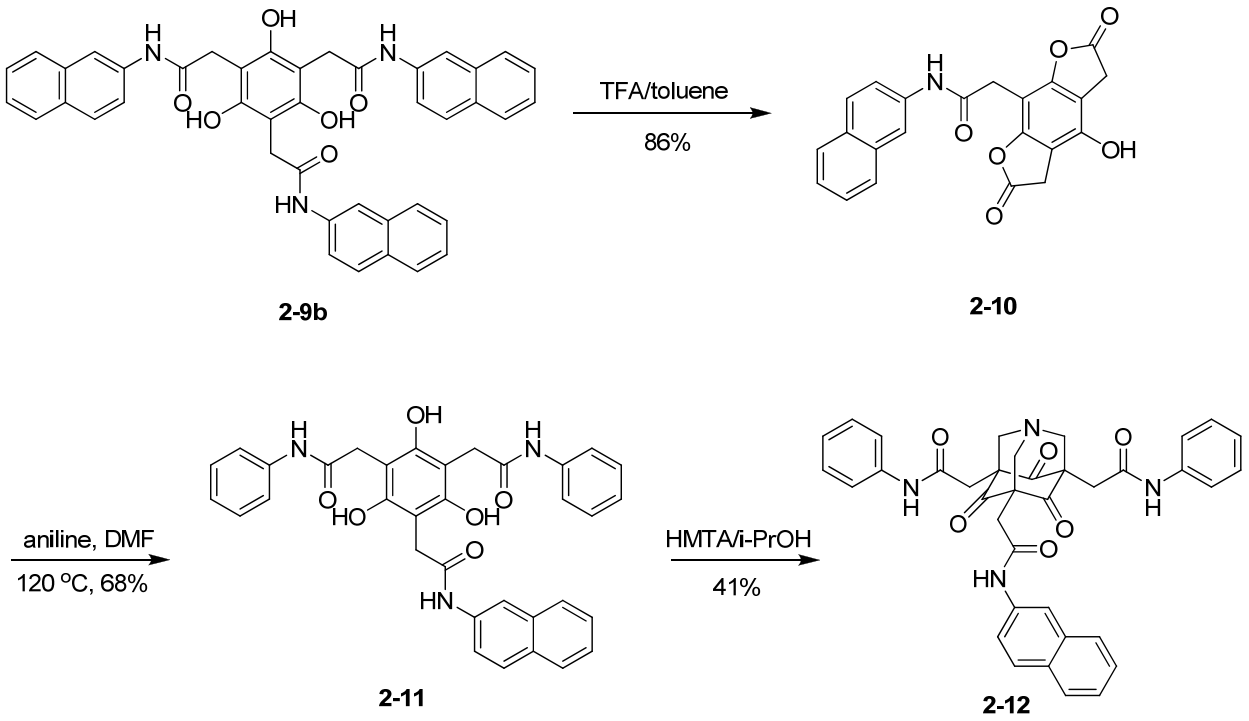

Figure 2-5. Synthesis of desymmetrized AAT using a lactone-based strategy.

Compound **2-13** (Figure 2-6) was also prepared as a control and contains the important functional groups of **2-1** and **2-12** but lacks the donor–acceptor core. The synthesis involves a simple coupling of 4-oxopentanoic acid with *β*-naphthylamine in the presence of DCC as a dehydrating agent. This naphthylamide will be useful for probing intramolecular seven-membered ring H-bond formation[139] between the amide –NH and ketone carbonyl oxygen, a structural feature potentially important to the conformation and self-assembly of the AAT

derivatives. It also will shed light on the mutual roles of the naphthyl substituents and donor-σ-acceptor core in the macromolecular behavior of **2-1** and **2-12**.

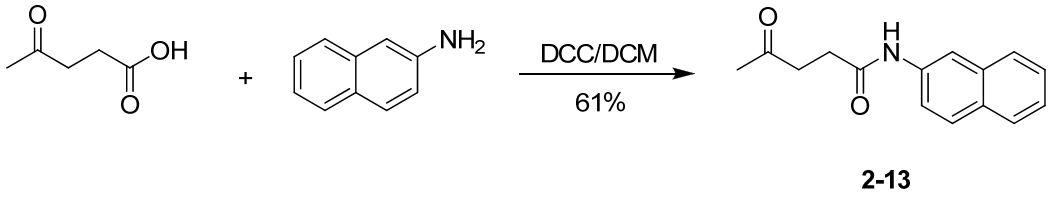

2-13

Figure 2-6. Synthesis of model compound **2-13**.

Gel Formation and Characterization

Organogels are broadly studied materials in terms of their structure-property relationships[140-143] due to their potential technological uses and unique macromolecular profiles. Most gelation processes involve H-bonding and π-π stacking interactions between gelator molecules. The consideration of through-bond donor–acceptor interactions as important components of these materials is new.

The solubility and gelation properties (Table 2-1) of compounds **2-1a** and **2-1b** were evaluated in various polar and apolar solvents. The model compound **2-12** was also studied for comparison. The triamides **2-1a** and **2-1b** are sparingly soluble in most organic solvents except for pyridine, DMF, and DMSO. Interestingly, compound **2-1a** forms optically clear gels (Figure 2-7) in aromatic solvents such as toluene and benzene. The gels are formed in the conventional way. First, a homogeneous solution of **2-1a** is obtained by heating the compound in the appropriate aromatic solvent (to the boiling point). The solution is then cooled to room temperature, and gel formation is evidenced by the complete immobilization of the solvent (the gel supports its weight upon inversion of a vial as shown in Figure 2-7). The gels are transparent and obtained immediately upon cooling. An ^{1}H NMR spectrum of the toluene gel shows broad resonances and weak signals characteristic of network formation, but confirms that the molecule

has not decomposed. Also characteristic of gel systems, the organogels of **2-1a** are thermally reversible. The mechanism of gel formation is presumably similar to other systems. The molecules of **2-1a** first self-assemble into elongated aggregates; when these structures are sufficiently long they become entangled and entrap solvent molecules in an infinite network.[144]

Gels are typically described using two parameters, the critical gelation concentration (CGC) and the sol-gel transition temperature (T_g). The former is determined by measuring the lowest amount of gelator required to completely immobilize the solvent. For **2-1a**, the CGC is 0.2% by weight (~ 1.4 mM). The T_g is measured using the "dropping ball" method[145] (see the Experimental Section) and is the temperature at which the gel begins to flow. This value is 72 °C for **2-1a**. The CGC is the lowest value and the T_g the highest value that we have observed to date for AAT gelators.[55, 56]

Figure 2-7. Organogel from trinaphthyl-1-aza-adamantanetrione **2-1a** (0.2 wt % in toluene after heating and cooling).

Compound **2-1a** forms gels in chloroform as well as toluene and benzene, but only at low temperature (–45 °C). Compounds **2-1b** and **2-12** do not form gels in any of the solvents tested, presumably due to their poor solubility. Neither compound is soluble in toluene or benzene even upon heating and sonication.[140, 146] This behavior parallels what was observed for phenylamides **1-15** ($R = C_{12}H_{25}$).

Table 2-1. Solubility and gelation properties of compound **2-1a**, **2-1b**, and **2-12**.

ORGANIC SOLVENT	**2-1A**	**2-1B**	**2-12**
hexanes	I	I	I
toluene	G	I	I
benzene	G	I	I
chloroform	G at –45 ºC	I	I
pyridine	S	S	S
THF	I	I	I
2-propanol	I	I	I
acetonitrile	P	P	P
DMF	S	S	S
DMSO	S	S	S

Key: I = insoluble, P = precipitate, G = gel, S = soluble.

Solid State Properties

The solid-state organization of the naphthyl-substituted AATs has been studied by scanning electron microscopy (SEM) and powder x-ray diffraction (XRD), and the thermal properties of the materials have been probed by differential scanning calorimetry (DSC) and thermal gravimetric analysis (TGA).

Morphology of Critical Point Dried Gels

Scanning electron microscopy (SEM) is widely used to explore the morphologies of nanoscale materials. To gain better insight into the molecular organization of the toluene gel of **2-1a**, SEM was used to observe dried gel samples. The solvent was removed from the gels (e.g., Figure 2-7) via critical point drying (CPD). The CPD technique involves removal of the solvent from the "wet gel" under supercritical conditions, where the bulk solvent is first exchanged for liquid CO_2. Simple evaporation of the liquid from a sample can result in the build-up of tensile stresses which cause the underlying supramolecular network to collapse as the vapor-liquid interface recedes.[147] CPD is conducted using liquid CO_2 which undergoes a phase change (from liquid to gas) at the critical point (critical temperature 304.2 K, critical pressure 72.8 bar), where the densities of the liquid and vapor are the same. The process reduces the interfacial (surface)

tension[148, 149] and therefore minimizes shrinkage of the gel and better preserves its structure. Drying gels by CPD is known to reveal structural features not found in air-dried blends.[150] Freeze drying is an alternative technique for drying gel samples, and we have used this approach as well in the past. In this method, the gel is quickly frozen in liquid nitrogen and then dried by sublimation to prevent the formation of a liquid-vapor meniscus. It is known, however, that the gel network may be destroyed by the nucleation and growth of solvent crystals in this process.[151]

In the CPD gel sample of **2-1a**, a lamellar sheet architecture is observed with layers of uniform thickness of about 5 μm (Figure 2-8). The surface of the sheets reveals ~3 μm entangled fibers. Smaller fibers are observed among the entangled fibers that comprise the self-assembled network. The three-dimensional networks are formed through molecular self-assembly of the gelator compound **2-1a** and the gel network is able to encapsulate a large volume of organic solvent upon heating and cooling. Freeze-dried gels were also investigated for comparison (not shown). These samples did show sheet-like packing but no finer features on the surfaces could be detected. Both fibrous and lamellar architectures have been observed before in the AAT systems,[55, 56] but this is the first case where both morphologies are visible in one sample.

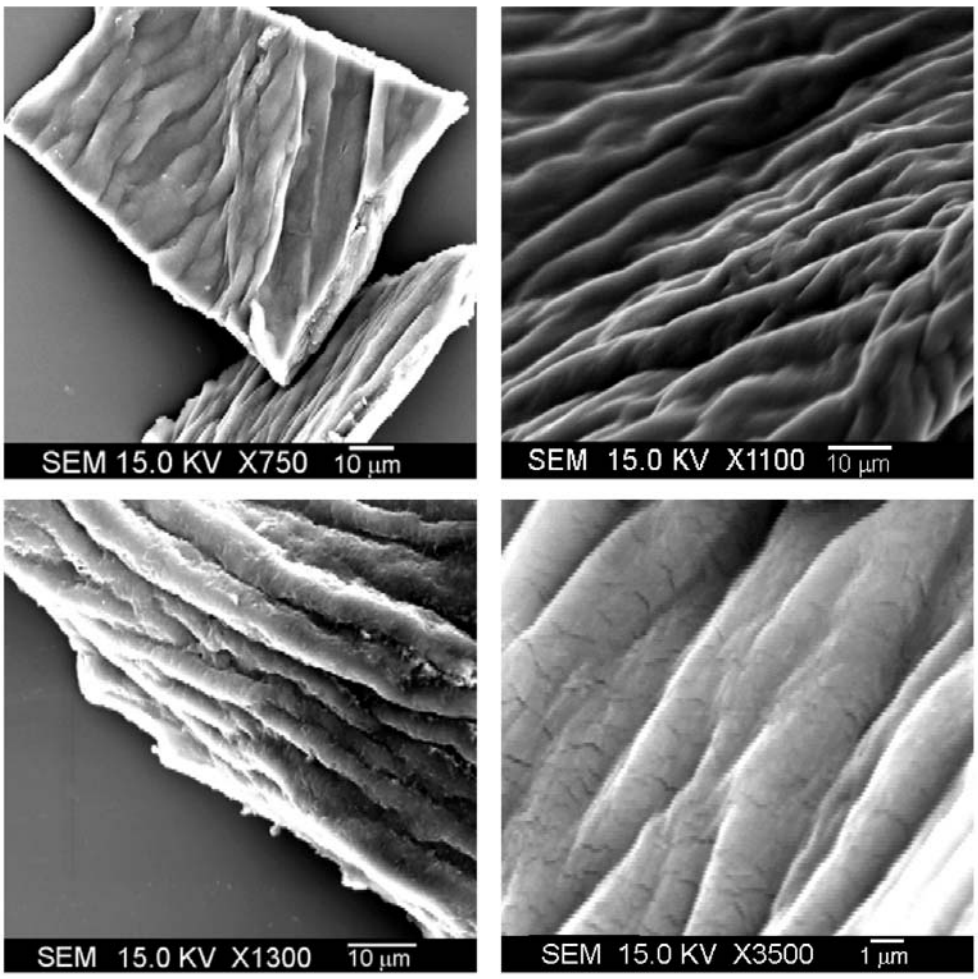

Figure 2-8. SEM images of a xerogel formed from critical point drying the 0.2 wt % toluene gel of compound **2-1a.**

X-Ray Diffraction (XRD)

In order to better understand the mechanism of self-assembly of the naphthyl-substituted AATs like **2-1a** and **2-1b**, numerous attempts were made to obtain single crystals suitable for X-ray crystallographic analysis. All attempts to date have failed using primarily the solvent diffusion technique (the AAT was dissolved in pyridine and exposed to hexane, ethyl acetate, ethyl ether, THF, or methanol). Particularly important for future attempts, it was recognized that the AATs gradually decompose in pyridine upon prolonged storage. It is possible that other solubilizing solvents could afford better results in the future.

Powder X-ray diffraction is frequently used in lieu of single crystal analysis for ascertaining the molecular packing of self-assemblies[152-154] and to shed light on assembly mechanism.[155] The data is reported for **2-1a** (Figure 2-9) and **2-1b** (Figure 2-10) as plots of 2θ versus intensity. The most intense peak is observed at a *d*-spacing of 4.1 Å for **2-1a** and 4.2 Å for **2-1b**. This is likely attributable to packing of the naphthalene groups at a slightly longer[140] than optimal π-π stacking distance due to steric constraints.[6, 156] The relatively small peak at *d*-spacing of 3.3 Å for **2-1a** and **2-1b** is very close to the typical π-π stacking[157] and may correspond to a different pattern of packing. The remaining peaks are less intense and at approximately the same positions for both compounds, despite the difference in their size. It appears therefore that the alkyl side chains of **2-1a**, the packing of which is identified by the broad peak at ~ 4 Å in Figure 2-9, do not significantly change the organization of the cores and naphthyl groups between the two systems. For example, the largest *d*-spacing for **2-1a**, 25.4 Å, is only ~ 1 Å longer than that of **2-1b** (24.4 Å). Molecular dynamics calculations are currently underway to help identify assembly modes of the molecules that might rationalize these distances.

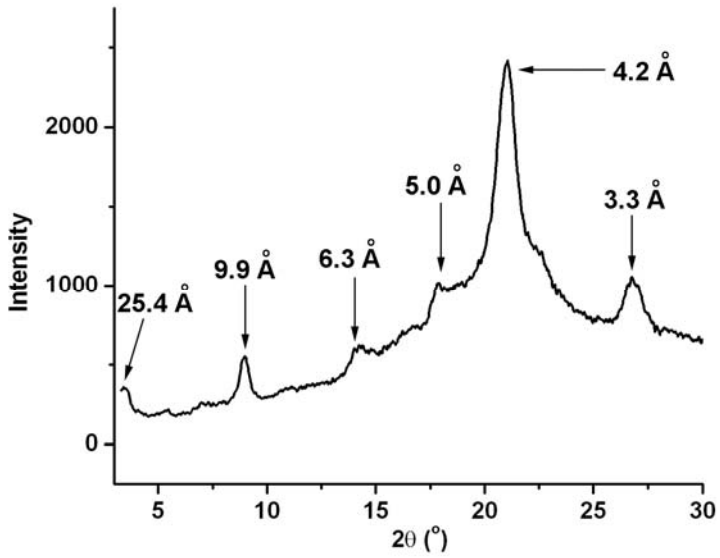

Figure 2-9. X-ray diffraction pattern of the neat powder **2-1a**.

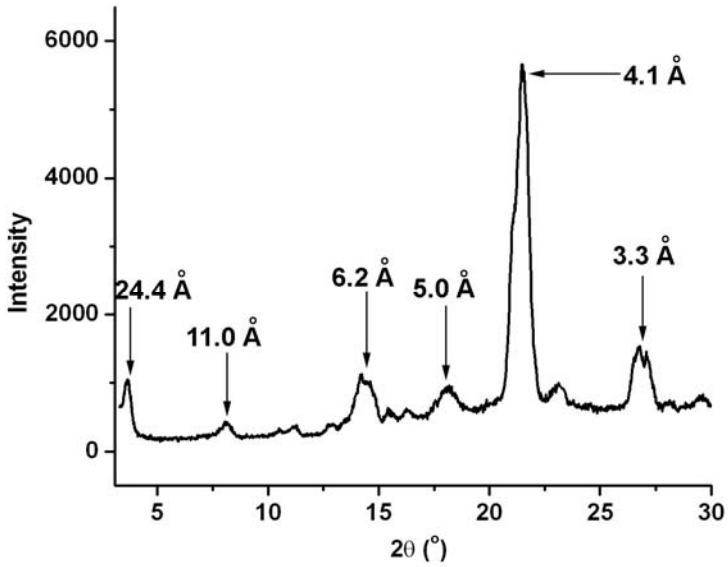

Figure 2-10. X-ray diffraction pattern of the neat powder **2-1b**.

Thermal Properties

Thermal transitions of compounds **2-1a** and **2-1b** were measured (Figure 2-11 and 2-12) using differential scanning calorimetry (DSC, TA instruments) and thermal stabilities were investigated (Figure 2-13 and 2-14) by thermal gravimetric analysis (TGA).

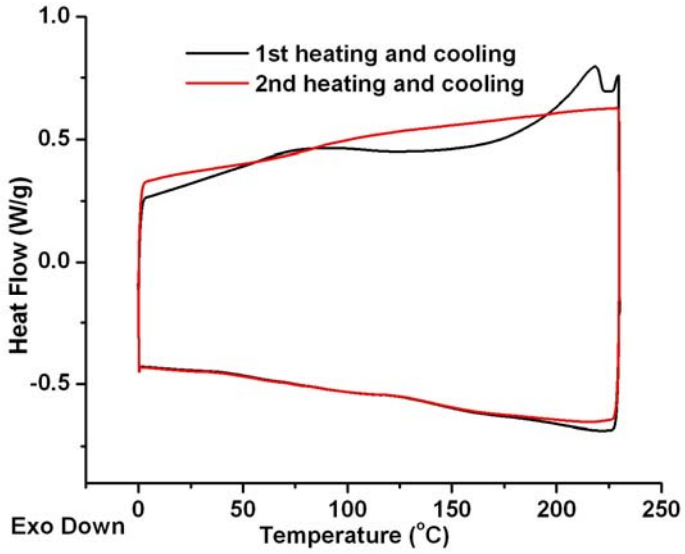

Figure 2-11. DSC traces for compound **2-1a**.

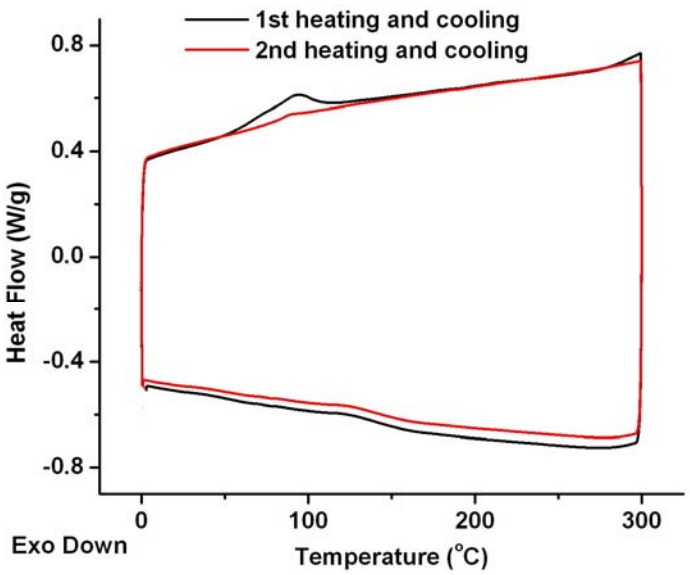

Figure 2-12. DSC traces for compound **2-1b**.

The DSC thermograms of **2-1a** and **2-1b** were recorded at a rate of 10 °C/min. Compound **2-1a** melts at 218 °C and then decomposes at 228 °C in the first heating cycle; consequently, no further transitions are observed upon cooling or upon a 2nd heating and cooling. Compound **2-1a** does show a broad transition prior to melting in the first heating cycle, possibly related to reorganization of the molecules upon heating (and the alkyl side chains). No ordered phases were observed by polarized optical microscopy (POM) upon a first heating of **2-1a**; the solid melts at ~ 218 °C with no subsequent change. The dried gel sample of **2-1a** (from toluene) behaves similarly. For AAT **2-1b**, only a broad transition is observed from 50–100 °C; no melting transition is found. It appears that the molecule decomposes before this temperature (vide infra).

The TGA data for both **2-1a** and **2-1b** show that the AAT molecules are thermally stable up to ~ 225 °C. Decomposition then ensues with significant molecular weight loss up until ~ 500 °C. Simple calculations suggest the fragments that may be lost. The molecular weight of **2-1a** (Figure 2-13) is 1233.7 g/mol. The remaining weight at 650 °C equals 18% of 1233.7, or 222 g/mol. Likewise, the molecular weight of **2-1b** (Figure 2-14) is 728.8 and the remaining weight

at high temperature equals 30% of 728.8 (= 219 g/mol). The average weight of the remaining fragment is therefore ~ 221 g/mol, the same mass as the trimethyl AAT core ($C_{12}H_{15}NO_3$ = 221 g/mol). This fragment would emerge from consecutive loss of the amide arms; such a stepwise decomposition is reflected in the TGA trace of **2-1b**.

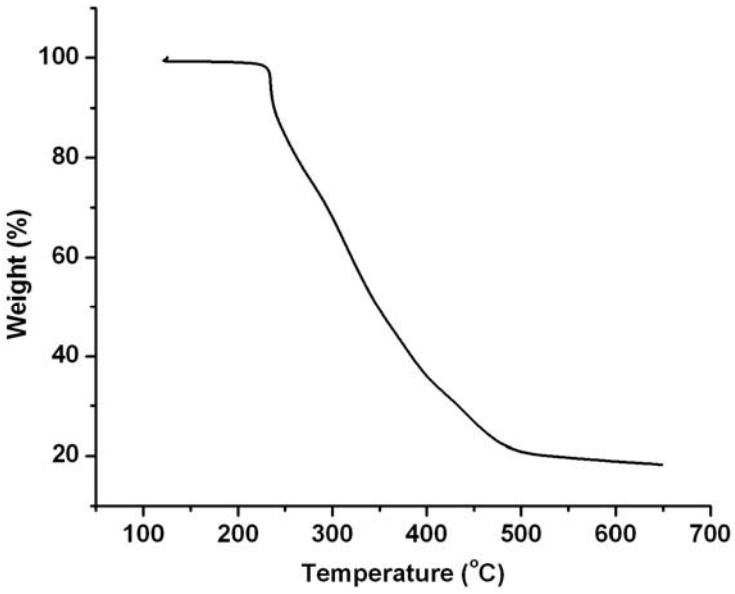

Figure 2-13. TGA measurements of solid **2-1a**.

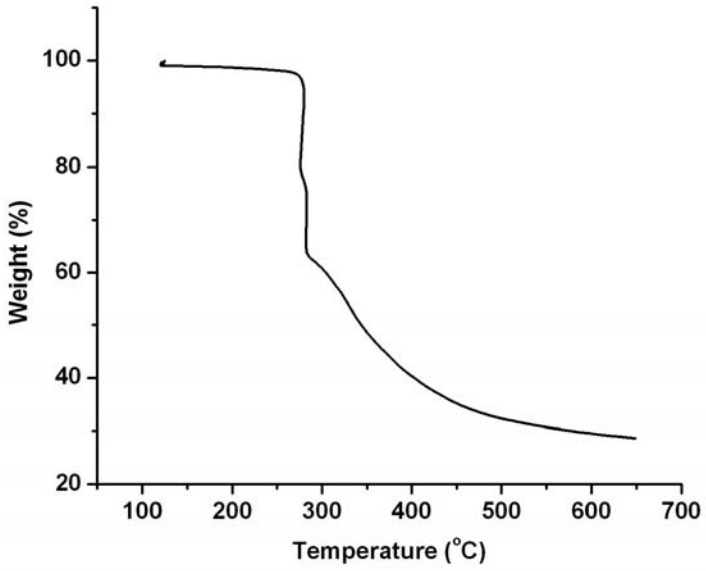

Figure 2-14. TGA measurements of solid **2-1b**.

Solution Phase Assembly

UV Absorption Spectra

UV/Vis measurements were performed for AAT compound **2-1a** and model compounds **2-12** and **2-13** in chloroform. Five absorption spectra at various concentrations in chloroform are shown for compound **2-1a** (Figure 2-15). There are two significant absorption bands that can be assigned to the naphthylamide chromophore. By analogy to naphthalene, the higher-energy absorption at 250 nm can be assigned to a non-emitting $^1(\pi\pi^* L_a)$ transition.[158] The lower energy absorption band at 285 nm is the emitting band and characterized as the $^1(\pi\pi^* L_b)$ transition;[159, 160] noteworthy also is the apparent vibronic structure within this band. This absorption is due principally to a longitudinally polarized transition with respect to the naphthalene chromophore and is therefore most sensitive to substitution in the 2, 3, 6, and 7 positions. Indeed, this band is red-shifted relative to unsubstituted naphthalene by about 10 nm.[161] Data from Figure 2-15 was then plotted to confirm that the optical density (at 285 nm) varies linearly with concentration (Figure 2-16). This is the case, and the molar extinction coefficient (ε) at 285 nm, calculated from the plot, is 44080 $M^{-1}cm^{-1}$.

The absorption spectra for model compounds **2-12** and **2-13** are shown in Figures 2-17 and 2-18, respectively. The molar extinction coefficient at 285 nm, calculated from plots of absorbance versus concentration, is 7570 $M^{-1}cm^{-1}$ for **2-12** and 8053 $M^{-1}cm^{-1}$for **2-13**. The absorbance of both compounds varies linearly with concentration. Somewhat surprising is that the molar extinction coefficient for **2-1a**, with its three naphthalene rings, is larger than three times the value for **2-12** (~ 5.8 times larger) and **2-13** (~ 5.5 times larger). The origin of this enhancement is not currently known.

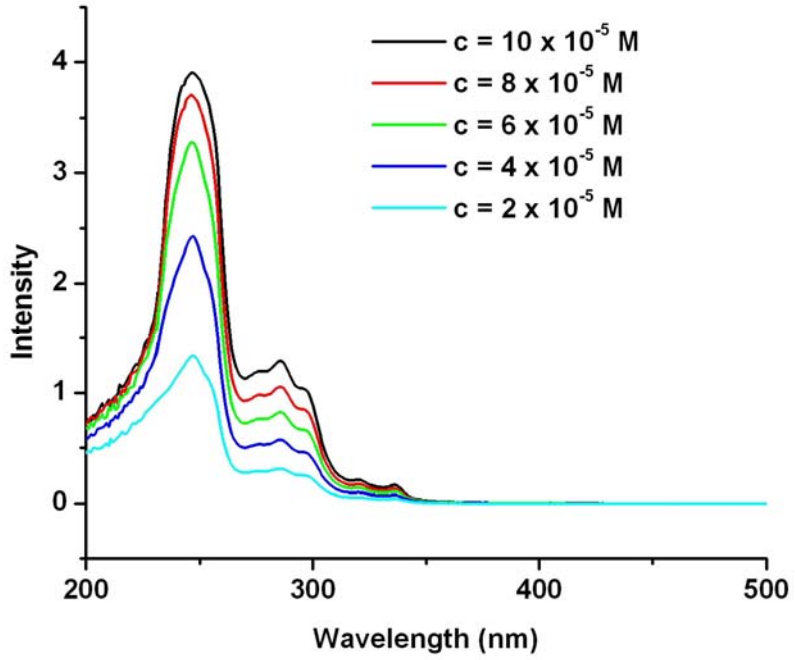

Figure 2-15. Absorption spectra for compound **2-1a** in chloroform (light path length: 3 mm).

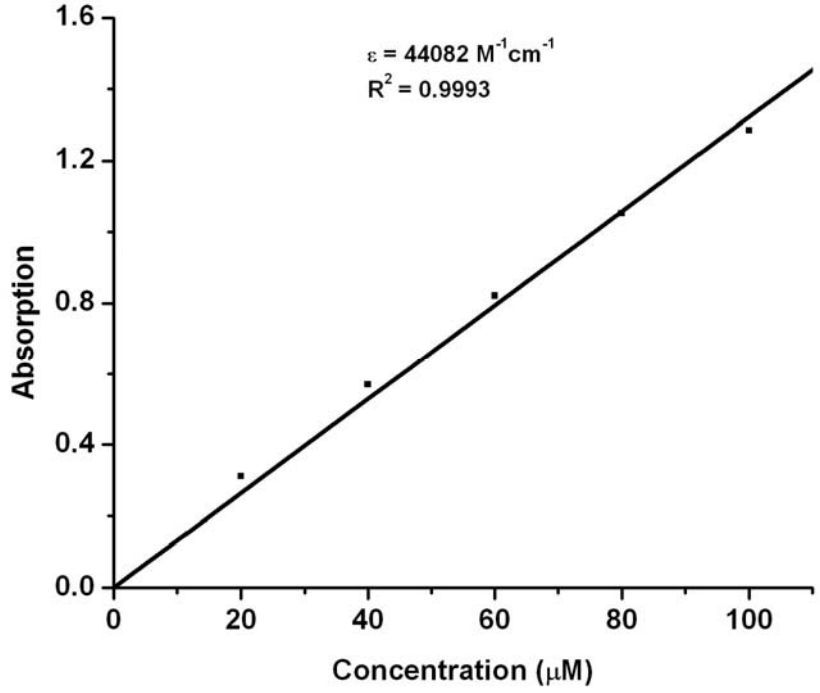

Figure 2-16. Absorption intensity at 285 nm vs. concentration for compound **2-1a**.

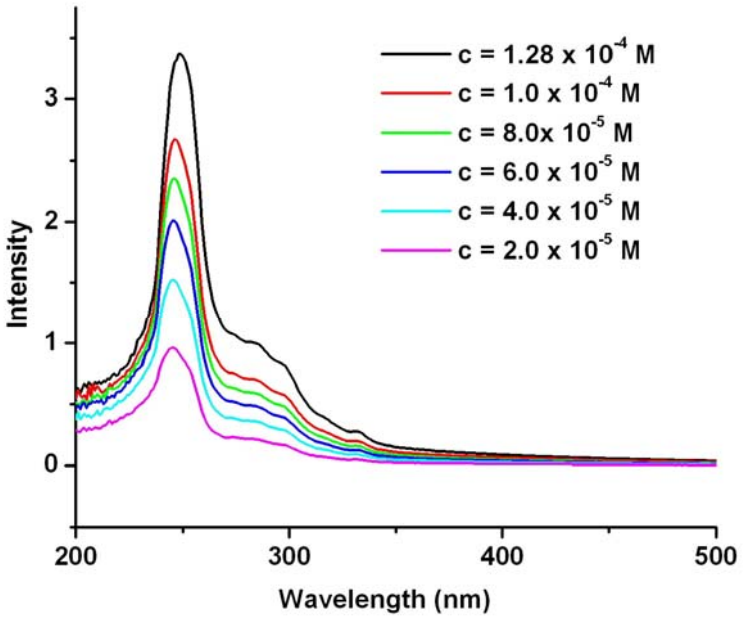

Figure 2-17. Absorption spectra for compound **2-12** in chloroform (light path length: 10 mm).

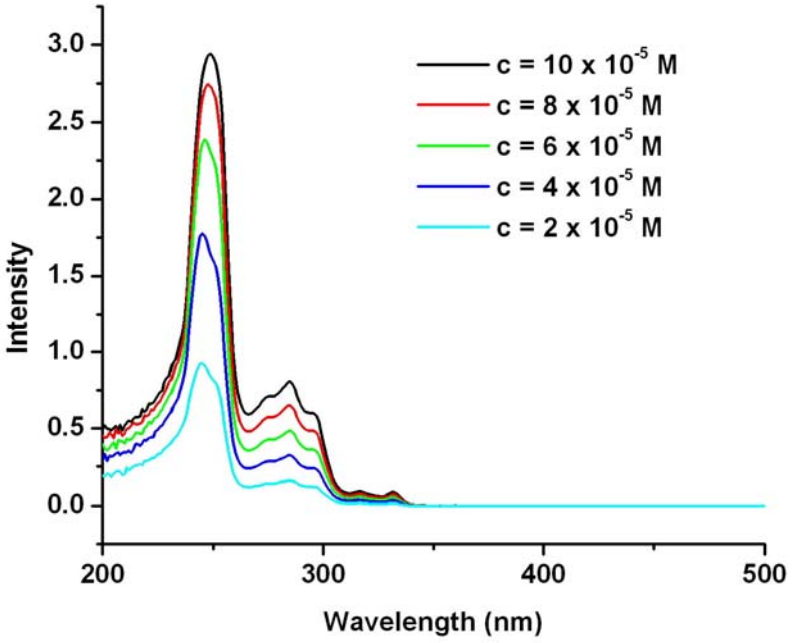

Figure 2-18. Absorption spectra for compound **2-13** in chloroform (light path length: 10 mm).

Fluorescence and Excimer Emission

Naphthalene groups are sensitive spectroscopic probes of self-assembly processes since they can fluoresce from either the singlet excited state (S1) or through excimer formation. The

latter is only possible when one ground state and one excited state molecule share a special geometric relationship and therefore the phenomenon reports on chromophore aggregation.[162] The fluorescence emission of compound **2-1a**, in chloroform at 25 °C, as a function of concentration is presented in Figure 2-19. Two emission bands can be observed upon excitation (λ_{exc} = 285 nm): one with a maximum emission at 355 nm (monomer) and an additional red-shifted emission band, centered at 433 nm, assigned to the excimer.[163-166] The emission spectra of model compound **2-13** versus concentration were measured as a control. Only observed is monomer emission at 355 nm (Figure 2-20).

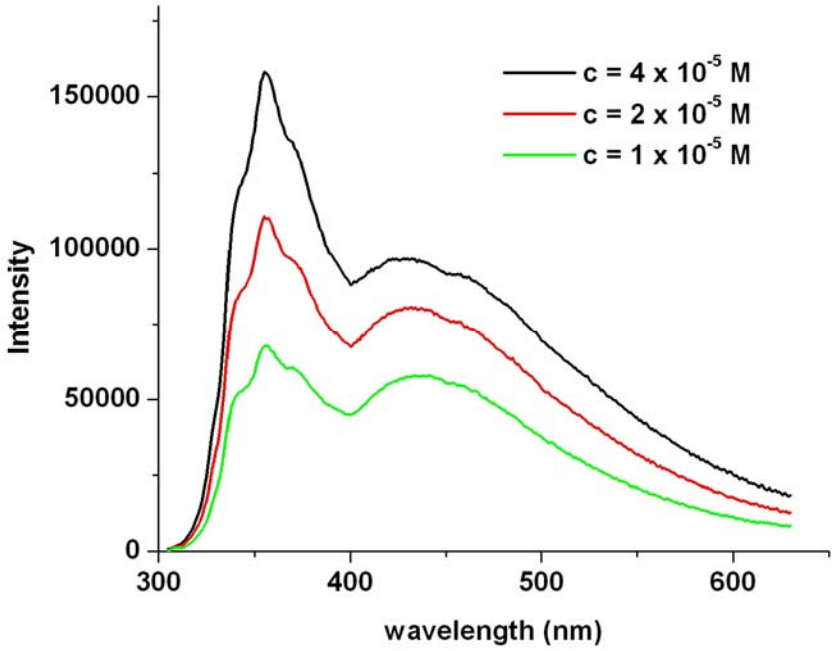

Figure 2-19. Emission spectrum of **2-1a** at λ_{exc} = 285 nm in chloroform.

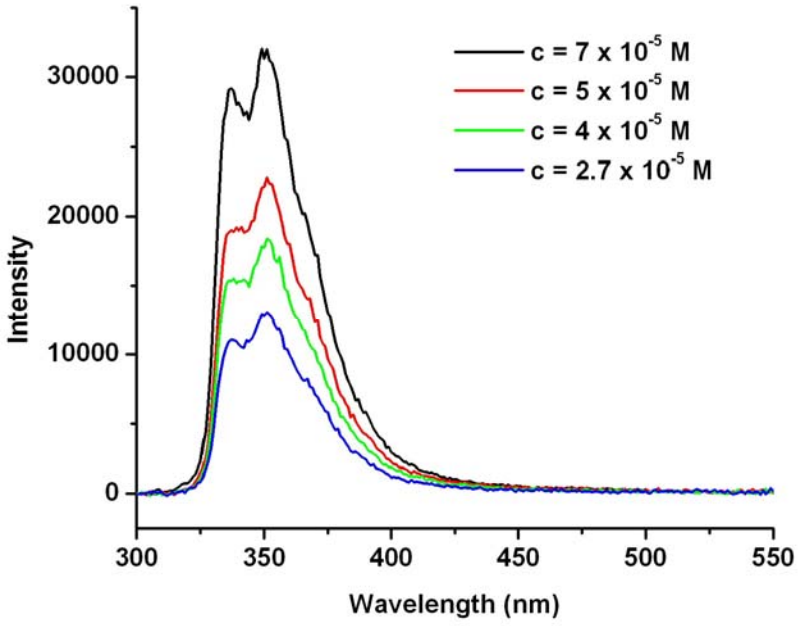

Figure 2-20. Emission spectrum of **2-13** at λ_{exc} = 285 nm in chloroform.

Excimer emission[167, 168] for **2-1a** suggests the π-π stacking of its naphthyl groups.[169] The emission can be interpreted as a consequence of the short-range approach of two naphthyl chromophores either in the same AAT molecule or within an assembly.[168, 170] Typical concentration- and temperature-dependent fluorescence experiments[171] have not been particularly conclusive with respect to distinguishing the scenarios. The λ_{max} of emission spectra for **2-1a** (in chloroform) is concentration independent (Figure 2-19) over a four-fold concentration range; the I_e/I_m (ratio of excimer emission intensity to monomer emission intensity) changes by ~ 1.4 in favor of the monomer emission over the same range. The poor solubility of **2-1a** in chloroform complicates these experiments.[172] Additionally, very little temperature dependence[171] of I_e/I_m was observed from 25 °C to 55 °C for a 2 x 10^{-5} M solution of **2-1a** (Figure 2-21). Certainly part of this behavior can be rationalized by intramolecular excimer formation, although it is possible that aggregation of the molecules also results in conformational changes that inhibit the close π-stacking required for this emission.

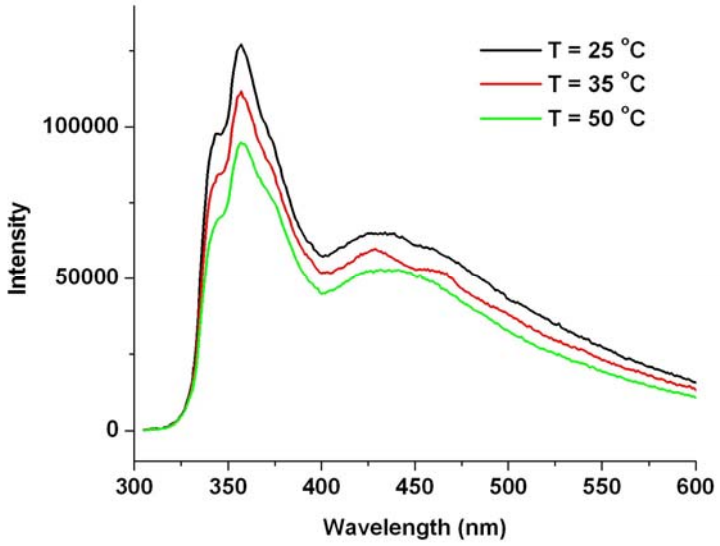

Figure 2-21. Emission spectrum of **2-1a** at λ_{exc} = 285 nm in chloroform with concentration 2 x 10^{-5} M.

Model compound **2-12** provides additional information since it contains only one naphthalene ring and eliminates the possibility of intramolecular excimer emission. The concentration-dependent fluorescence emission spectra of this compound, in chloroform at 25 ºC, are presented in Figure 2-22. Some excimer emission is noted which suggests that contribution from intermolecular aromatic interactions of the naphthalene groups is possible in these systems. Very little concentration dependence of I_e/I_m was observed for a chloroform solution of **2-12** over a nine-fold concentration range. Interestingly, excimer emission of the above compounds has not been observed in other organic solvents including toluene, acetonitrile, and DMSO. It is not completely clear why the solvent should have such a profound effect. The broad emission band from 300 nm to 450 nm of toluene may overlap with the excimer emission from AAT molecules. The poor solubility of **2-1a** and **2-12** in acetonitrile may compromise the excimer formation. Lastly, DMSO may disrupt the intramolecular H-bonding which might be important to the stacking in this solvent.

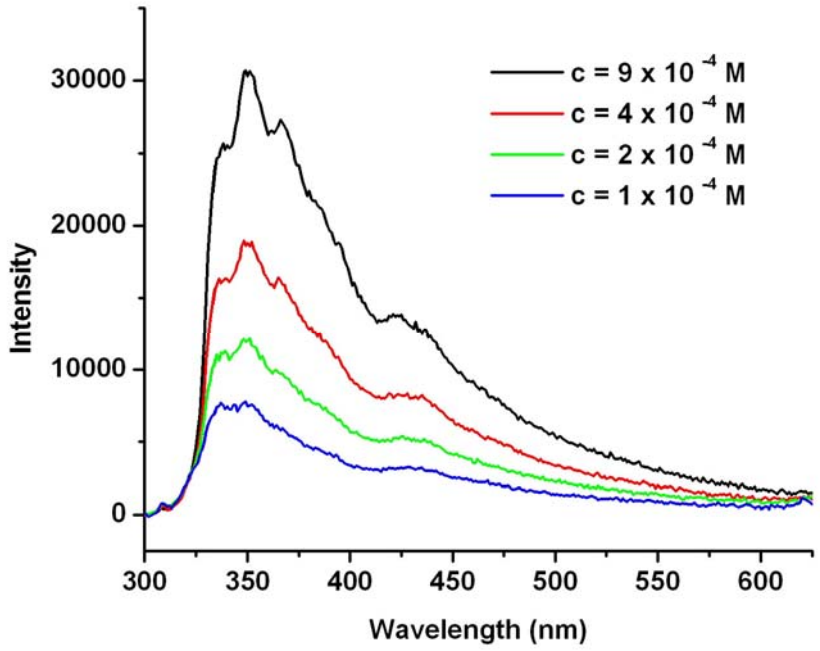

Figure 2-22. Emission spectrum of **2-12** at λ_{exc} = 285 nm in chloroform.

H-Bonding in Amide-Functionalized AATs

H-bonding interactions involving the amide side chains play an important role in the self-assembly of the AAT molecules. Observed in earlier systems, the amide protons can form intramolecular H-bonds with the carbonyl groups on the AAT core and stabilize the conformation of the molecules (preorganization). The amides also presumably provide conformational stability through the favorable and prefered alignment of their dipoles with respect to the dipolar AAT core.[55, 91]

Data from the N–H stretching region in IR spectra can provide insight into the degree of hydrogen bond formation in nonpolar solvents because the time scale of IR spectroscopic measurements is sufficiently short to distinguish clearly between the N–H stretchings of hydrogen-bonded and non-hydrogen-bonded states.[173]

Model compound **2-13** shows a single –NH absorption at 3309 cm^{-1} that presumably arises from intramolecular H-bonding in the solid state. This value is similar to the reported –NH

stretch (3325 cm^{-1}) for intramolecular H-bonding in γ-ketoamides in the solid state.[174] However this value is ~ 50 cm^{-1} red shifted compared to other intramolecularly H-bonded γ-ketoamides (ν N–H···O = 3360 cm^{-1})[55] in solution but still in the accepted hydrogen bonding range (3300–3500 cm^{-1}). The solid-state IR spectrum of **2-1a** shows an absorption at 3385 cm^{-1}, the free –NH stretch, while a second absorption is detected at 3287 cm^{-1} that possibly arises from intermolecular H-bonding. Both absorptions are ~ 40–50 cm^{-1} red shifted versus the free –NH stretch and the intermolecular H-bonding stretch in *N*-phenylacetamide[55] **2-14** in solution. Similar phenomena were reported by Banerjee in studies of synthetic peptides.[174] No band is visible at a wavenumber >3430 cm^{-1} for the reported peptides in the solid state while a band is observed at 3436 cm^{-1}, suggesting the occurrence of free –NH groups in solution.[174] Most of the free –NH stretches in the solid state for their peptides were observed around 3370 cm^{-1}. The bulk IR data overall suggests that AAT **2-1a** enjoys some intermolecular H-bonding in the solid state (Table 2-2).

In chloroform solution, the model compound **2-13** shows expected γ-ketoamide behavior (Figure 2-24) based on our previous work[55] and that of others:[139, 175] A sharp absorption is found at 3430 cm^{-1} and a broad absorption at 3360 cm^{-1} which represent the solvent-associated ("free") –NH stretch and intramolecularly H-bonded –NH stretch, respectively. Similar frequencies are reported for intramolecularly H-bonded γ-ketoamides (ν N–H···O = 3335–3380 cm^{-1} and ν $N–H_{free}$ = 3440 cm^{-1} (at 1 mM in CCl_4)).[173, 176] For **2-1a**, a sharp –NH absorption is found (Figure 2-23) at 3430 cm^{-1} while a broad absorption is detectable at 3383 cm^{-1} (with a shoulder at 3360 cm^{-1}). We tentatively assign the higher energy absorption to the "free" –NH stretch. Presumably then the 3383 cm^{-1} stretch comes from intramolecular H-bonding.[176, 177] The bands appear in the reported range of the IR spectral absorption bands of the non-hydrogen-bonded amide N-H

(3450-3400 cm^{-1}) and hydrogen bonded amide N–H (3300-3400 cm^{-1})[173, 176, 177] regions in solution. For comparison, phenylamide substituted aza-adamantane **2-15** was reported[178] as presenting a strong band at 3290 cm^{-1} indicating the presence of intermolecular H-bonding in the solid state while showing a free –NH stretch at 3446 cm^{-1} in $CDCl_3$.

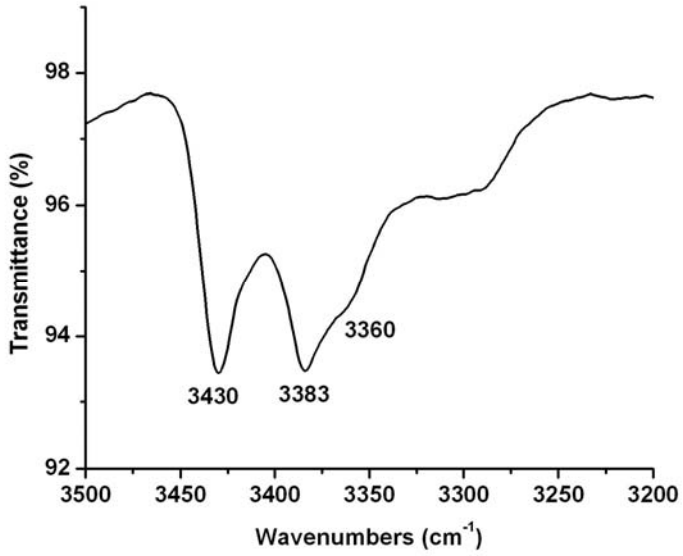

Figure 2-23. The IR spectrum of **2-1a** at 1.6 mM in chloroform.

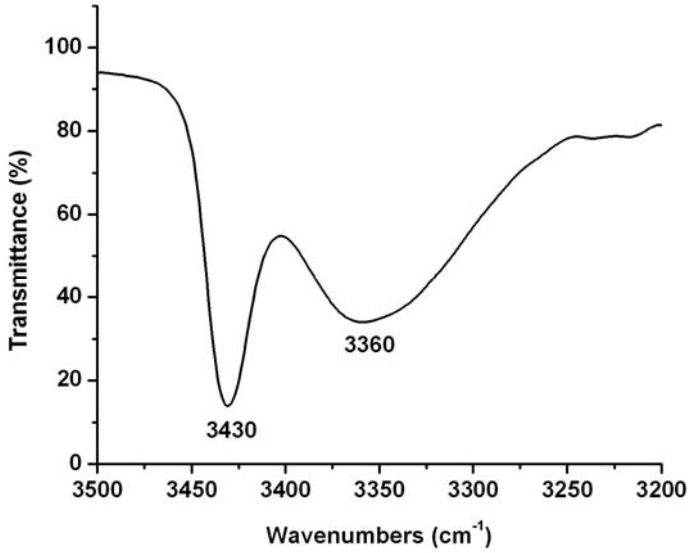

Figure 2-24. The IR spectrum of **2-13** at 0.13 M in chloroform.

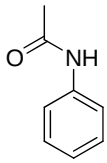

2-14

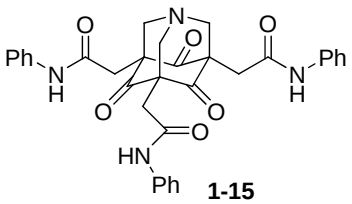

1-15

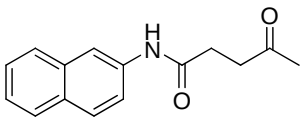

2-13

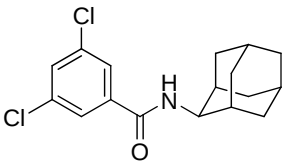

2-15

Table 2-2. Amide –NH IR frequency (cm^{-1}) for **2-1a** and representative molecules from the literature.

	Solid State (KBr)			Solution ($CHCl_3$)		
	Free –NH	Intermolecular H-bonding	Intramolecular H-bonding	Free –NH	Intermolecular H-bonding	Intramolecular H-bonding
1-15[55]						3360
2-14[55]				3440	3325	
2-1a	3385	3287		3430		3383 (3360)
2-13			3309	3430		3360
2-15[178]		3290		3446		

The IR studies in solution are supported by VT-NMR measurements[176, 177] of **2-1a** and model compound **2-13**. VT-NMR measurements of **2-1a** at 5.4 mM in the higher boiling $C_2D_2Cl_4$ confirm a very small temperature dependence (Figure 2-25) for the amide proton (7.86–7.65 ppm from 298–388 K; $\Delta\delta/\Delta T = -2.3$ ppb/K), consistent with intramolecular H-bonding.[176, 177] For comparison, the –NH shift (the assignment of the –NH proton was made by adding a drop of D_2O to the NMR tube) of model compound **2-13** at the same concentration (5.4 mM) in $C_2D_2Cl_4$ (Figure 2-26) shows a similarly small temperature dependence (7.62–7.42 ppm from 273–388K, $\Delta\delta/\Delta T = -1.6$ ppb/K).

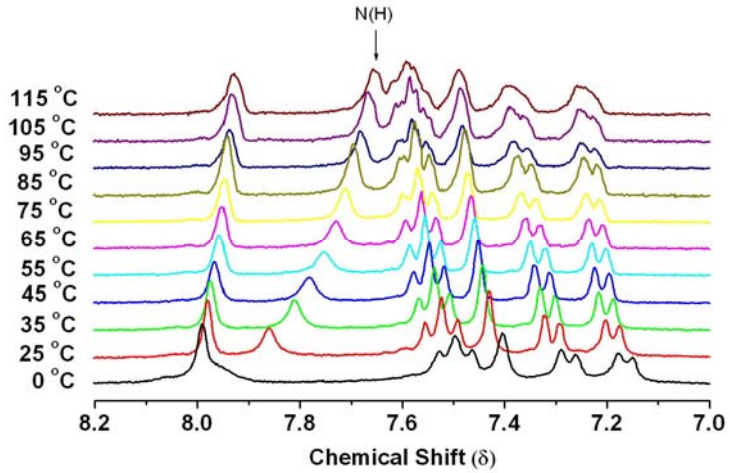

Figure 2-25. ^{1}H NMR spectra of **2-1a** in $C_2D_2Cl_4$ (5.4 mM) at different temperatures.

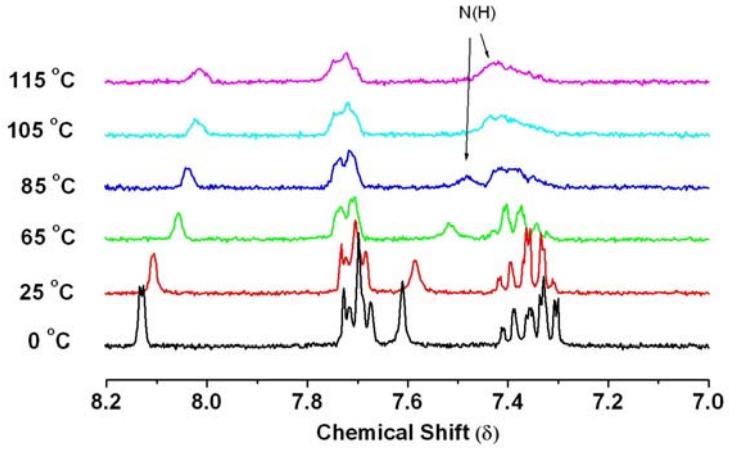

Figure 2-26. ^{1}H NMR spectra of **2-13** in $C_2D_2Cl_4$ (5.4 mM) at different temperatures.

The ^{1}H NMR spectra of compounds **2-1a** and **2-13** in $C_2D_2Cl_4$ (Figures 2-27 and 2-28, respectively) at different concentrations were also measured to further probe H-bonding effects. Relatively small chemical shift changes are observed with concentration for **2-1a** and **2-13**, ~ 0.1 ppm for **2-1a** (5.4 mM to 1.5 mM) and ~ 0.05 ppm for **2-13** (14.5 mM to 3.2 mM). Interestingly, the –NH chemical shift of **2-1a** is ~ 0.2 ppm further downfield than that of **2-13**, likely speaking to a difference in environment, H-bond acceptor (C=O electronic structure), and conformational equilibrium. Overall the solution-phase IR and NMR data show evidence of intramolecular H-bonding in the napthylamide AATs.

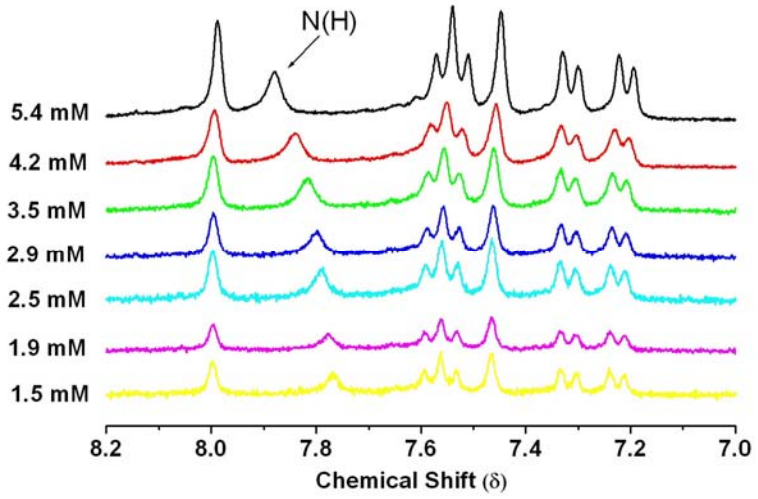

Figure 2-27. ^{1}H NMR spectra of **2-1a** in $C_2D_2Cl_4$ at different concentrations.

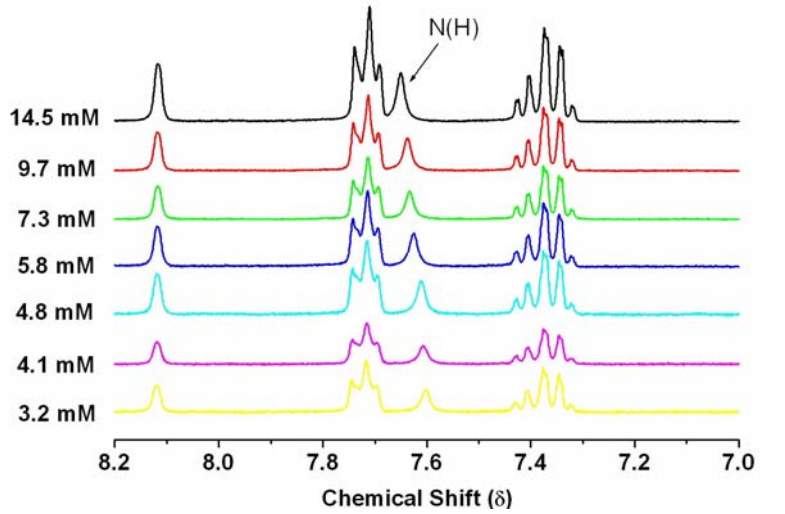

Figure 2-28. ^{1}H NMR spectra of **2-13** in $C_2D_2Cl_4$ at different concentrations.

Dynamic Light Scattering

Dynamic light scattering (DLS) is a powerful technique which can be used to determine the size distribution of particles in solution. The dynamic information of the particles is derived from an autocorrelation of the intensity trace recorded during the experiment. The scattered light signal decay is then related to the motion of the particles, the diffusion coefficient. CONTIN analysis is the ideal method for analyzing the autocorrelation function of heterodisperse systems.[179, 180]

With the help of collaborators at the Center for Nanophase Materials Sciences at Oak Ridge National Lab, DLS has been used to examine the self-assembly of various AATs that bear amides on their periphery (e.g., compound **1-15**, R = $C_{12}H_{25}$). Figure 2-29 shows the concentration-dependent size distribution of **1-15** in chloroform. Largely non-spherical aggregates are found, where the main distribution of the hydrodynamic radii is about 100 nm. The population of larger-sized aggregates, in the micrometer range, increases with concentration. Important to note, however, is that the actual percentage of the largest aggregates is quite small given a 10^6 dependence of intensity on size.

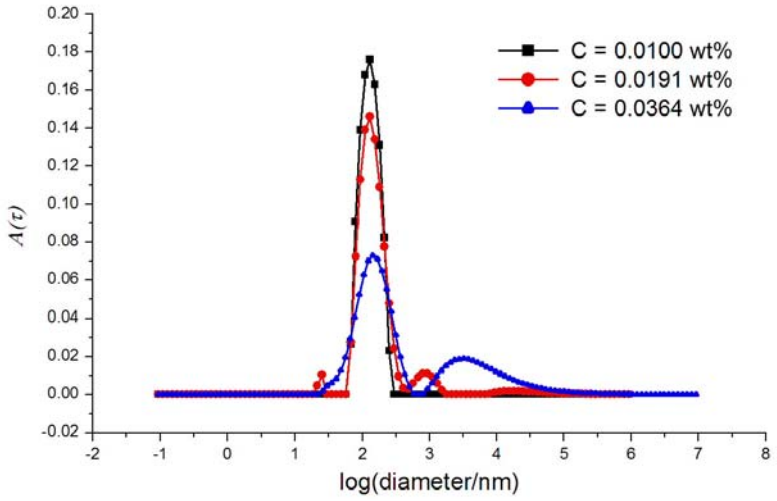

Figure 2-29. Size distribution of **1-15** (R = $C_{12}H_{25}$) at various concentration in chloroform (25 °C, θ (scattering angle) = 104°).

The temperature-dependent size distribution of **1-15** in chloroform (c = 0.0059 wt%) is shown in Figure 2-30. There is overall observed a shift to smaller-sized assemblies upon increasing the temperature, consistent with the effect of temperature on the self-assembly of molecules.

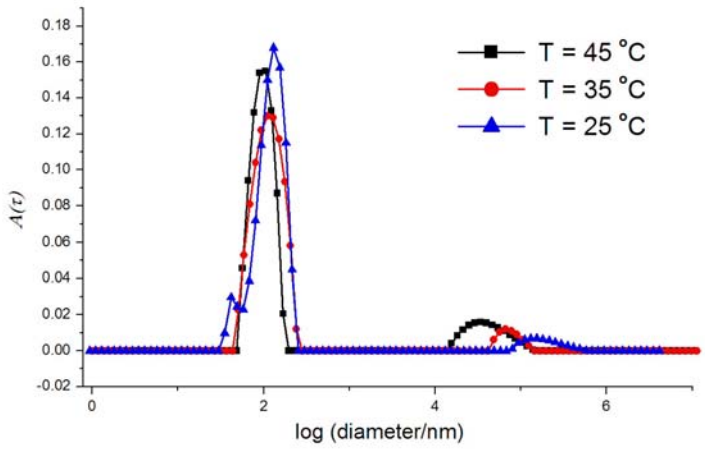

Figure 2-30. Size distribution of **1-15** chloroform solutions (c = 0.0059 %) at various temperatures (θ(scattering angle) = 104°).

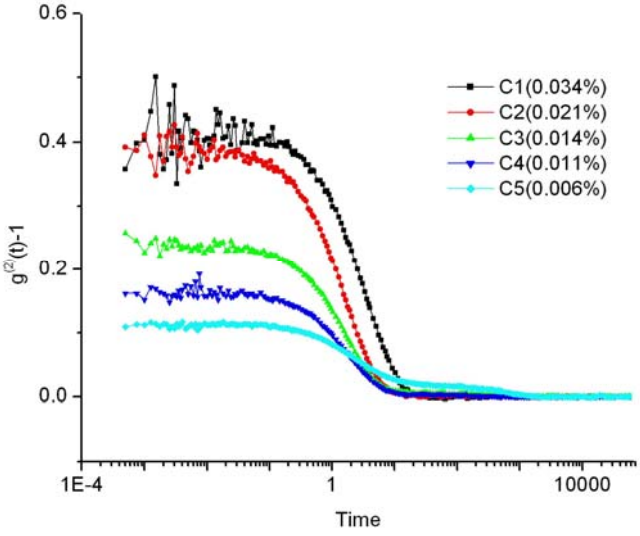

Figure 2-31. Time-intensity correlation functions ($g^{(2)}(\tau)-1$) for **2-1a** at various concentrations in toluene (25 °C, θ(scattering angle) = 88°).

DLS experiments were performed with **2-1a** in toluene and pyridine solution.[181] The autocorrelation functions obtained by collecting the scattered radiations as the function of decay time at five different concentrations (in toluene) are reported in Figure 2-31. The plots clearly show how the maximum value of the y-axis in the correlation function decreases with decreasing solution concentration. A single decay is observed and the relaxation becomes slower with increasing concentration.[182, 183] The time-intensity correlation function at various temperatures

(Figure 2-32) also shows interesting behavior. The shifting to shorter relaxation times with increasing temperature from 25–80 °C follows what is expected for reversible assembly.[184] However, the dynamic functions appear almost flat when the temperature is further decreased to 10 °C and –2 °C. It appears that at these temperatures the assemblies are essentially immobilized[185] as stationary clusters of gel networks;[186, 187] the consequence is a partially heterogeneous and strongly scattering mixture.

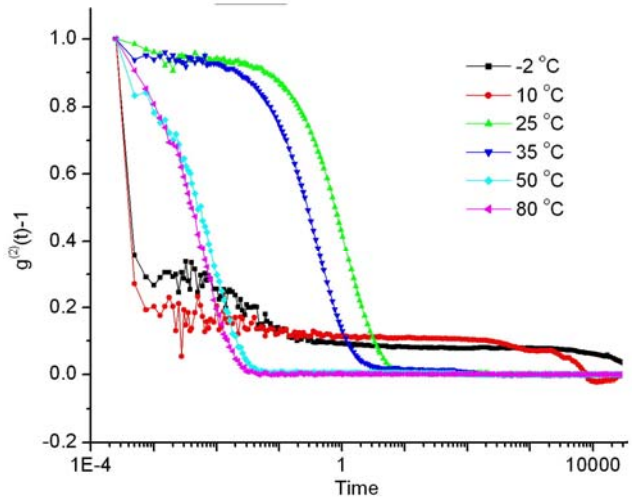

Figure 2-32. Time-intensity correlation functions ($g^{(2)}(\tau)-1$) for **2-1a** in toluene at various temperatures (c = 0.019 wt%).

Additional DLS studies show how the assembly process responds to solvent; essentially no aggregation is observed in pyridine consistent with the monomers' good solubility in this medium. Another reason for the extremely low scattering signal in pyridine is the solvent's low d*n*/d*c* value.

Final comparison of naphthylamide **2-1a** with phenylamide **1-15** (R = $C_{12}H_{25}$) at the same concentration in chloroform nicely shows the solution-phase consequence of introducing larger aromatic arms to the AAT core (Figure 2-33); compound **2-1a** forms significantly larger assemblies.

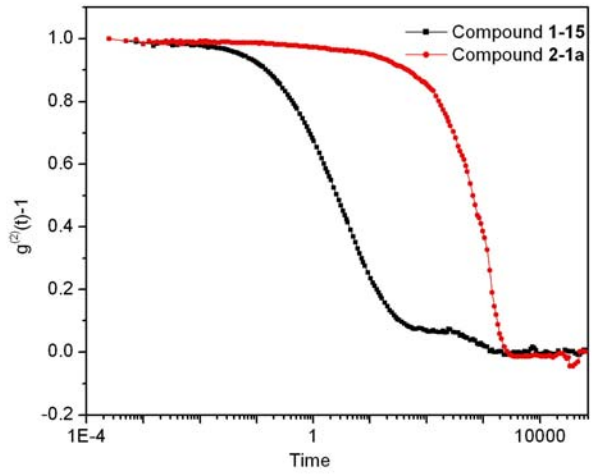

Figure 2-33. Time-intensity correlation functions ($g^{(2)}(\tau)-1$) for chloroform solutions of **2-1a** and **1-15** at c = 0.019 wt%.

Summary and Conclusions

A system of amide functionalized AATs with expanded aromatic arms has been synthesized and its properties have been fully characterized. These molecules show significantly enhanced self-assembly properties in both the bulk state and solution relative to derivatives with smaller aromatic appendages. In the solid state, SEM and powder XRD show well-organized structures.

In solution, UV/Vis absorption, fluorescence emission, IR, and NMR spectroscopies have confirmed the role of the aromatic side chains in self-assembly and shown that the conformation of the molecules is important. Excimer emission bands were observed that provide evidence for π-π stacking; a component of this emission was shown to be intermolecular by comparison of the target AAT molecules with model compounds. Concentration, solvent, temperature, and H-bonding effects on self-assembly were measured by NMR and IR. The data show the importance of intramolecular H-bonding to the amide functionalized AATs that presumably preorganizes the molecules and facilitates self-assembly.[55, 91] Dynamic light scattering studies provided

independent evidence for self-assembly and showed the dependence of assembly size on solvent, concentration, temperature, and AAT structure. In particular, the AATs bearing larger aromatic side chains appear to form larger assemblies in solution.

The expanded aromatic arms provide enhanced π-π stacking in the AAT assemblies and these interactions complement core-to-core dipolar interactions and hydrogen bonding. The supramolecular networks from these "unconventional" donor-σ-acceptor molecules are complex and additional studies are underway to continue drawing important structure-property relationships with the systems.

Experimental Section

Materials

Reagents and solvents were purchased from Acros, Aldrich, or Fluka and used without further purification. THF, ether, CH_2Cl_2, and DMF were degassed in 20 L drums and passed through two sequential purification columns (activated alumina; molecular sieves for DMF) under a positive argon atmosphere using the GlassContour solvent system (GlassContour, Inc.). Thin layer chromatography (TLC) was performed on DURASIL TLC aluminum sheets with visualization by UV light or staining.

Characterization Techniques

Melting points (m.p.) were determined on a MEL-TEMP melting apparatus and are uncorrected. ^1H (300) and ^{13}C NMR (75 MHz) spectra were recorded on a Varian Mercury 300 (300 MHz) and VXR 300 (300 MHz) spectrometers. Chemical shifts (δ) are given in parts per million (ppm) relative to TMS and referenced to residual protonated solvent ($CHCl_3$: δ_H 7.27 ppm, δ_C 77.00 ppm; DMSO: δ_H 2.50 ppm, δ_C 39.00 ppm; pyridine: δ_H 7.22 ppm, δ_C 123.90 ppm; $C_2H_2Cl_4$: δ_H 5.92 ppm). MS spectra (HRMS and LRMS) were recorded on a Finnigan MAT95Q Hybrid Sector spectrometer. Fluorescence emission spectra were recorded using a fluoromax

spectrophotometer. UV-Vis absorption spectra were measured on a Varian Cary 100 UV-Vis instrument. IR spectra were recorded using a Perkin Elmer 1600 Series spectrometer.

Scanning electron microscopy (SEM). For all scanning electron microscopy (SEM) experiments, a JEOL JSM 6400 scanning electron microscope was used. Samples were adhered to SEM stubs using conductive copper tape, then sputtered with Au/Pd to improve the resolution of the images. The sputtering current was 45 mA, the Ar pressure was 75 mTorr, and the sputtering time was 60 s. This yielded an Au/Pd film that was ~ 16 nm thick. The SEM measurements were operated at 15 kV.

X-ray diffraction (XRD). XRD data were collected on a Philips APD 3720 X-ray diffractometer with Cu Kα radiation (λ = 1.5406 Å). The pure solid was deposited onto a low-scattering quartz plate for the measurement. The step size of the scan was 0.02 degrees and the time per step was 1 second.

Critical point drying (CPD). Super critical fluid drying was performed in a 3000 psi rated vessel (Parr Instruments) to make the xerogels. Samples were placed into regenerated cellulose dialysis bags with a pore diameter of 12000 to 14000 MWCO (Fisher Scientific, USA). Samples were placed inside the drying chamber and liquid CO_2 was introduced. Toluene was exchanged with liquid CO_2 over 5–6 solvent exchange steps. After complete solvent removal, the vessel containing the liquid CO_2 was heated via a water jacket and water bath to 50 ºC and 1500 psi. At equilibrium the supercritical CO_2 was released from the vessel at a rate no greater than 4 L/min.

Dynamic light scattering (DLS). Dynamic light scattering measurements were performed with an ALV/CGS-5022F goniometer system equipped with a He-Ne laser (λ = 632 nm). The sample solutions were filtered through a 0.45 μm filter at room temperature. The samples for Figure 2-31 were filtered through 1.0 μm filters at 40 °C.

Differential scanning calorimetry (DSC) and thermal-gravimetric analysis (TGA). The DSC experiments were performed on a TA Instruments Q1000 equipped with a liquid nitrogen cooling accessory calibrated using sapphire and high-purity indium metal. All samples were prepared in hermetically sealed pans (2–4 mg/sample) and were referenced to an empty pan. The scan rate was 10 °C/min. Thermogravimetric analysis (TGA) was performed on a TA Instruments Q5000 IR using the dynamic high-resolution analysis mode and a two point Curie temperature calibration (alumel alloy and high purity nickel).

Gel formation and T_{gel} determination. Gels were formed by combining AAT **2-1a** (5 mg) and toluene or benzene in a sealed vial. The vial was then heated with a heat gun until a homogenous solution was formed. The vial was then allowed to gradually cool to room temperature on the bench top during which time the gel rapidly formed. To determine the T_{gel}, a steel ball with a diameter of 2 mm was placed on top of the gel and the vial was placed in an oil bath. The temperature was slowly increased (ca. 0.5 °C/min), and monitored using a thermometer submerged in a vial containing neat solvent also in the oil bath, while observing the position of the steel ball. The temperature at which the ball touched the bottom of the vial was taken as the T_{gel}.

Synthesis

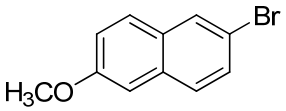

2-Bromo-6-methoxynaphthalene (2-2).[127] To a stirring solution of 6-bromonaphthalen-2-ol (8.9 g, 40 mmol) in DMF (40 mL) in a 100 mL round-bottomed flask was added potassium carbonate (8.3 g, 60 mmol) and methyl iodide (3.8 mL, 60 mmol) in one portion. The reaction mixture was stirred at room temperature overnight. Water was added and the mixture was extracted with ethyl acetate and the combined organic layers were dried with Na_2SO_4. The

solvent was removed on a rotary evaporator to afford a white solid (9.4 g, 99%). ^{1}H NMR (300 MHz, $CDCl_3$) δ 3.96 (s, 3H), 7.15 (m, 2H), 7.58 (m, 3H), 7.93 (m, 1H). ^{13}C NMR (75 MHz, $CDCl_3$) δ 55.73, 106.15, 117.43, 120.17, 128.78, 128.89, 130.01, 130.05, 130.41, 133.45, 158.28. The NMR data match the literature.[127]

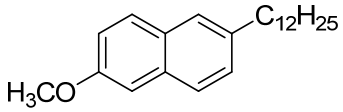

2-Dodecyl-6-methoxynaphthalene (2-3a).[133] To a stirred mixture of magnesium (0.60 g, 25 mmol) and dry THF (20 mL) in a 100 mL three-necked round-bottomed flask was slowly added 1-bromododecane (3.8 mL, 15 mmol) with heating. The reaction mixture was heated to reflux for 3 h under argon to prepare the Grignard reagent. In a separate reaction vessel, zinc bromide (5.0 g, 23 mmol) was added. The vessel was flame-dried, cooled, and then the zinc bromide was dissolved in dry THF (20 mL). The dodecyl-Grignard reagent was transferred to the zinc bromide solution and stirred for 10 min. To the stirred mixture was added 2-bromo-6-methoxynaphthalene (2.8 g, 10 mmol) and $Pd(PPh_3)_4$ (23 mg, 0.20 mmol). The reaction mixture was stirred at 60–70 ºC overnight. Water was added and the mixture was extracted with ethyl acetate and the combined organic layers were dried with Na_2SO_4. The solvent was removed on a rotary evaporator and the crude product was purified by column chromatography using hexane to afford a white solid (2.4 g, 72%). ^{1}H NMR (300 MHz, $CDCl_3$) δ 0.88 (t, 3H, J = 6.9 Hz), 1.27 (m, 18H), 1.69 (m, 2H), 2.74 (t, 2H, J = 7.5 Hz), 3.92 (s, 3H), 7.13 (m, 2H), 7.27 (m, 2H), 7.54 (s, 1H), 7.68 (m, 2H). ^{13}C NMR (75 MHz, $CDCl_3$) δ 14.11, 22.69, 29.36, 29.56, 29.62, 29.65, 29.68, 31.48, 31.93, 35.91, 55.24, 105.64, 118.54, 126.13, 126.57, 127.92, 128.56, 132.87, 138.13, 157.05.

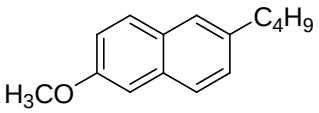

2-*n*-Butyl-6-methoxynaphthalene (2-3b).[131] Compound **2-3b** was synthesized from 2-bromo-6-methoxylnaphthalene (4.2 g, 18 mmol) and 1.6 M *n*-butyllithium in hexanes (16.6 mL, 26.6 mmol) according to the same procedure reported for **2-3a** to afford **2-3b** (2.1 g, 55%) as a white solid. ^{1}H NMR (300 MHz, $CDCl_3$) δ 0.92 (t, 3H, J = 7.5 Hz), 1.33 (m, 2H, J = 7.5 Hz), 1.64 (m, 2H, J = 7.5 Hz), 2.70 (t, 2H, J = 7.5 Hz), 3.85 (s, 3H), 7.09 (m, 2H), 7.25 (d, 1H, J = 8.4 Hz), 7.50 (s, 1H), 7.61 (m, 2H). ^{13}C NMR (75 MHz, $CDCl_3$) δ 13.97, 22.37, 33.61, 35.60, 55.21, 105.62, 118.53, 123.55, 126.13, 126.57, 127.63, 127.90, 128.85, 138.05, 157.04. The NMR data match the literature.[131]

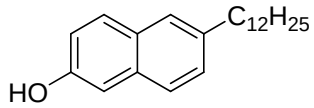

2-Dodecyl-6-naphthanol (2-4a). BBr_3 (4.5 mL, 48 mmol) was added dropwise to a solution of **3-3a** (7.9 g, 24 mmol) in 80 mL of CH_2Cl_2 at –78 °C. After 4 h the mixture was allowed to warm to room temperature, and stirring was continued overnight. The mixture was quenched with saturated $NaHCO_3$ at 0 ºC and then extracted with CH_2Cl_2. The organic layer was dried with anhydrous Na_2SO_4 and the solvent was removed under vacuum to provide a white solid (7.4 g, 99%). ^{1}H NMR (300 MHz, $CDCl_3$) δ 0.88 (t, 3H, J = 6.3 Hz), 1.25 (m, 18H), 1.67 (m, 2H), 2.72 (t, 2H, J = 7.2 Hz), 4.82 (s, 1H), 7.01 (m, 2H), 7.27 (m, 1H), 7.61 (m, 3H). ^{13}C NMR (75 MHz, $CDCl_3$) δ 14.12, 22.69, 29.35, 29.54, 29.60, 29.67, 31.45, 31.92, 35.91, 109.31, 117.56, 126.67, 128.16, 129.27, 137.50, 138.17, 152.67.

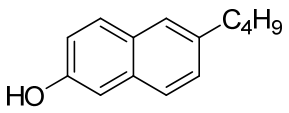

2-Butyl-6-naphthanol (2-4b).[133] Compound **2-4b** was synthesized from 2-*n*-butyl-6-methoxynaphthalene (1.6 g, 7.6 mmol) and BBr_3 (1.5 mL, 15 mmol) according to the same procedure reported for **2-4a** to afford **2-4b** (1.5 g, 97%) as a yellow solid. ^{1}H NMR (300 MHz, $CDCl_3$) δ 0.95 (t, 3H, J = 7.2 Hz), 1.41 (m, 2H), 1.68 (m, 2H), 2.74 (t, 2H, J = 7.5 Hz), 4.81 (s, 1H), 7.09 (m, 2H), 7.28 (m, 1H), 7.63 (m, 3H). ^{13}C NMR (75 MHz, $CDCl_3$) δ 14.21, 22.61, 33.82, 35.80, 109.55, 117.81, 126.43, 128.40, 129.51.

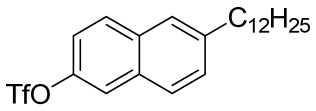

6-Dodecylnaphthalene-2-trifluoromethanesulfonate (2-5a). To a stirred solution of 2-dodecyl-6-naphthanol (7.2 g, 23 mmol), pyridine (4.5 mL, 55 mmol), and CH_2Cl_2 (60 mL) was added trifluoromethanesulfonic anhydride (4.6 mL, 28 mmol) slowly at 0 ºC. The reaction mixture was stirred at room temperature overnight. Water was added and the mixture was extracted with methylene chloride and the combined organic layers were dried with Na_2SO_4. The solvent was removed on a rotary evaporator and the crude product was purified by column chromatography using hexanes/ethyl actate (20:1) to afford a white solid (10.2 g, 98%). ^{1}H NMR (300 MHz, $CDCl_3$) δ 0.89 (t, 3H, J = 8.1 Hz), 1.31 (m, 18H), 1.71 (m, 2H), 2.79 (t, 2H, J = 8.1 Hz), 7.35 (m, 2H), 7.80 (m, 4H). ^{13}C NMR (75 MHz, $CDCl_3$) δ 14.10, 22.68, 29.28, 29.35, 29.50, 29.57, 29.65, 31.23, 31.92, 36.04, 118.94, 119.44, 126.29, 127.84, 129.23, 129.99, 131.71, 132.61, 142.17, 146.58. HRMS (ESI, $(M+Na)^+$) calcd for $C_{23}H_{31}F_3O_3S$: 467.1838; found: 467.1853.

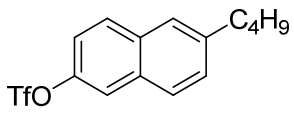

6-Butylnaphthalen-2-yl trifluoromethanesulfonate (2-5b). Compound **2-5b** was synthesized from 2-dodecyl-6-naphthanol (1.5 g, 7.5 mmol) and trifluoromethanesulfonic anhydride (2.5 mL, 15 mmol) according to the same procedure reported for **2-5a** to afford **2-5b** (1.8 g, 72%) as a colorless oil. ^{1}H NMR (300 MHz, $CDCl_3$) δ 0.96 (t, 3H, J = 8.1 Hz), 1.42 (m, 2H), 1.70 (m, 2H), 2.81 (t, 2H, J = 7.8 Hz), 7.35 (m, 1H), 7.45 (m, 1H), 7.79 (m, 4H). ^{13}C NMR (75 MHz, $CDCl_3$) δ 13.92, 22.33, 33.36, 35.73, 118.94, 119.46, 126.31, 127.85, 129.24, 129.98, 131.71, 142.13. HRMS (ESI, $(M+Na)^+$) calcd for $C_{15}H_{15}F_3O_3S$: 355.0586; found: 355.0642.

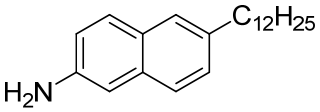

6-Dodecyl-2-naphthylamine (2-6a). To a flame-dried reaction tube containing $Pd(dba)_2$ (72 mg, 0.13 mmol) was added $P(t\text{-}Bu)_3$ (0.13 mmol from a 0.24 M stock solution in toluene) followed by THF (10 mL). The solution was stirred at room temperature for 10 min. 6-Dodecylnaphthalene-2-trifluoromethane-sulfonate (1.1 g, 2.5 mmol) and $LiN(SiMe_3)_2$ (5 mmol) were then added. The reaction mixture was stirred at 60–70 °C overnight. The silylamide was deprotected by adding aqueous 1N HCl. The mixture was transferred to a separatory funnel and washed with aqueous 1N NaOH. The organic layer was dried over Na_2SO_4, filtered, and concentrated at reduced pressure. The residue was purified by chromography (hexane/EtOAc 10:1) to afford a brown solid (0.36 g, 46%). ^{1}H NMR (300 MHz, DMSO-d_6) δ 0.84 (t, 3H, J = 6.6 Hz), 1.22 (m, 18H), 1.59 (m, 2H), 2.60 (t, 2H, J = 7.2 Hz), 5.23 (s, 2H), 6.77 (s, 1H), 6.88 (m, 1H), 7.12 (m, 1H), 7.47 (m, 3H). ^{13}C NMR (75 MHz, DMSO-d_6) δ 13.45, 21.59, 28.19, 28.38, 28.49, 30.51, 30.78, 34.54, 37.67, 38.17, 105.42, 117.87, 124.53, 125.36, 125.98,126.75,

127.44, 132.88, 134.11, 145.43. HRMS (ESI, $(M+H)^+$) calcd for $C_{22}H_{33}N$: 312.2686; found: 312.2689.

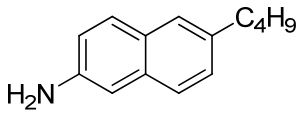

6-Butylnaphthalen-2-amine (2-6b).[136] Compound **2-6b** was synthesized from 6-butylnaphthalen-2-yl trifluoromethanesulfonate **2-5b** (1.5 g, 4.4 mmol) and $LiN(SiMe_3)_2$ (8.8 mmol), $P(t\text{-}Bu)_3$ (0.22 mmol from a 0.24 M stock solution in toluene) and $Pd(dba)_2$ (0.13 g, 0.22 mmol) according to the same procedure reported for **2-6a** to afford **2-6b** (0.36 g, 42%) as a yellow oil. ^{1}H NMR (300 MHz, DMSO) δ 0.90 (t, 3H, J = 7.2 Hz), 1.30 (m, 2H), 1.58 (m, 2H), 2.62 (t, 2H, J = 7.5 Hz), 5.22 (s, 2H), 6.77 (m, 1H), 6.88 (m, 1H), 7.14 (m, 1H), 7.45 (m, 3H). ^{13}C NMR (75 MHz, DMSO) δ 13.30, 21.24, 32.68, 34.19, 105.41, 117.85, 124.51, 125.33, 125.96, 126.72, 127.41, 132.84, 134.05, 145.35. HRMS (ESI, $(M+H)^+$) calcd for $C_{14}H_{17}N$: 200.1434; found: 200.1437.

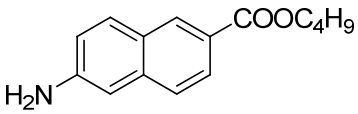

***n*-Butyl 6-amino-2-naphthoate (2-6c).** To a stirred solution of 6-amino-2-naphthoic acid (0.4 g, 2 mmol) in *n*-butyl alcohol (20 mL) was added concentrated sulfuric acid (2.0 mL) slowly at room temperature. The reaction mixture was stirred at reflux for 44 h. The mixture was cooled to room temperature. The solvent was removed on a rotary evaporator and the crude solid was suspended in water. Sodium hydroxide was added (2 M) to adjust the pH to 10. The mixture was filtered to afford a white solid (0.31 g, 64 %). ^{1}H NMR (300 MHz, DMSO-d_6) δ 0.95 (t, 3H, J =

7.2 Hz), 1.45 (m, 2H), 1.73 (m, 2H),4.29 (t, 2H, J = 6.6 Hz), 5.87 (br s, 2H), 7.08 (m, 2H), 7.78 (m, 3H), 8.38 (s, 1H). ^{13}C NMR (75 MHz, DMSO-d_6) δ 13.62, 18.77, 30.36, 64.12, 109.69, 119.99, 125.32, 126.03, 126.64, 130.46, 130.79, 136.81, 166.04.

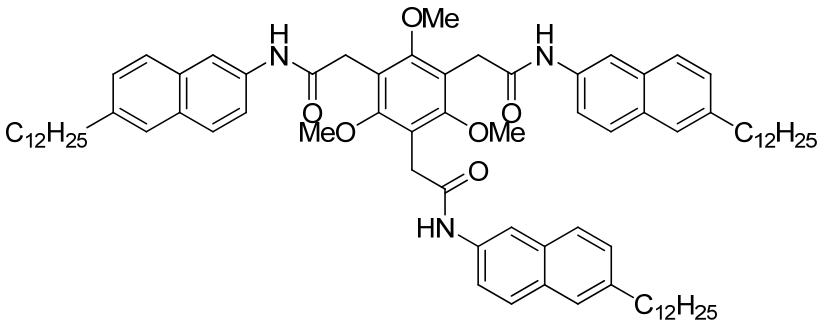

2-{3,5-Bis-[(6-dodecylnaphthylcarbamoyl)-methyl]-2,4,6-trimethoxynaphthyl}-*N*-(6-dodecylnaphthyl)-acetamide (2-8a). A solution of triacid **2-7a** (51 mg, 1.5 mmol) and thionyl chloride was heated to reflux for 2 h and the solvent was then removed in vacuo. The remaining crude brown oil (**2-7b**) was then dissolved in dry THF (20 mL) and slowly added to a solution of 6-dodecyl-2-naphthylamine (1.54 g, 4.95 mmol), TEA (2.1 mL, 15 mmol), and dry THF (20 mL) in a dry round-bottomed flask. The resulting solution was allowed to stir under a blanket of argon overnight. The reaction mixture was then diluted with methylene chloride (50 mL), washed with 10% aq HCl (25 mL), water (20 mL), and brine (20 mL). The solution was further dried over $MgSO_4$, evaporated in vacuo. The residue was purified by chromography (CH_2Cl_2/MeOH = 20/1) to afford **2-8a** (0.85 g, 46%) as a off-white solid: ^{1}H NMR (300 MHz, pyridine-d_5) δ 0.89 (t, 3H, J = 6Hz), 1.27 (m, 18H), 1.69 (m, 2H), 2.75 (t, 2H, J = 6.6 Hz), 4.03 (s, 3H), 4.11 (s, 2H), 7.38 (d, 1H, J = 7.8 Hz), 7.89 (m, 4H), 8.84 (s, 1H), 11.06 (s, 1H). ^{13}C NMR (75 MHz, pyridine-d_5) δ 14.99, 23.65, 30.32, 30.54, 30.61, 30.66, 32.42, 32.83, 34.46, 36.90, 62.72, 117.36, 121.20, 121.62, 127.26, 128.61, 129.08, 129.17, 131.82, 133.82, 138.19,

140.17, 159.41, 171.33. HRMS (ESI, $(M+Na+H)^+$) calcd for $C_{81}H_{111}N_3O_6$: 1246.7623; found: 1246.7619.

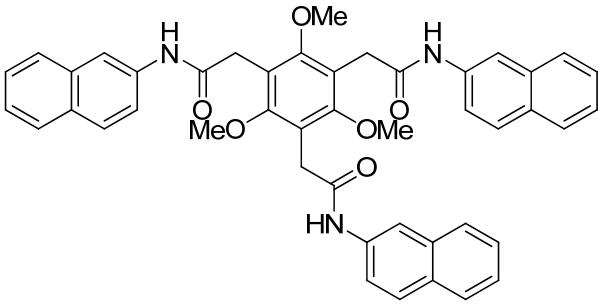

***N*-Naphthyl-2-(2,4,6-trimethoxy-3,5-bis-naphthylcarbamoylmethyl-naphthyl)-acetamide (2-8b).** This compound was synthesized from triacid chloride **2-7b** (504 mg, 1.47 mmol), 2-naphthylamine (695 mg, 4.86 mmol), and TEA (2.1 mL, 15 mmol) according to the same procedure reported for **2-8a** to afford **2-8b** (0.49 g, 46%) as an white solid: m.p. 198–200 °C. ^{1}H NMR (300 MHz, DMSO-d_6) δ 3.76 (s, 5H), 7.63 (m, 6H), 8.29 (s, 1H), 10.40 (s, 1H). ^{13}C NMR (75 MHz, DMSO-d_6) δ 33.12, 62.04, 115.70, 119.97, 120.64, 125.16, 127.07, 127.91, 128.12, 129.02, 130.36, 134.14, 137.68, 158.25, 170.56. HRMS (ESI, $(M+Na)^+$) calcd for $C_{45}H_{39}N_3O_6$: 740.2731; found: 740.2731.

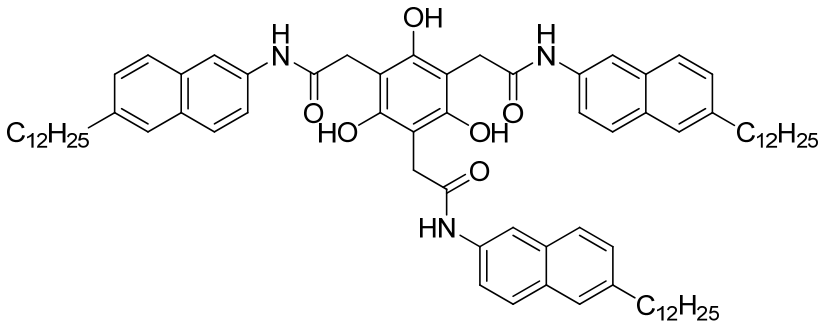

2-{3,5-Bis-[(6-dodecylnaphthylcarbamoyl)-methyl]-2,4,6-trihydroxy-naphthyl}-*N*-(6-dodecylnaphthyl)-acetamide (2-9a). To a solution of **2-8a** (0.37 g, 0.30 mmol) in dry

methylene chloride (15 mL) stirring at –78 ºC was added BBr_3 (0.17 mL, 1.8 mmol). The reaction was allowed to stir, under argon, at that temperature for 2 h before gradual warming to room temperature and stirring overnight. The solution was then cooled to 0 ºC, quenched via careful addition of saturated aq $NaHCO_3$, and filtered to remove all solid material. The filtrate was then extracted with methylene chloride (50 mL × 3). The organics were then combined, dried over $MgSO_4$, and evaporated in vacuo to afford **2-9a** (0.26 g, 72%) as a brown solid. ^{1}H NMR (300 MHz, pyridine-d_5) δ 0.88 (t, 3H, J = 6.6 Hz), 1.32 (m, 18H), 1.68 (m, 2H), 2.73 (t, 2H, J = 7.2 Hz), 4.38 (s, 2H), 7.39 (d, 1H, J = 8.7 Hz), 7.89 (m, 5H), 8.63 (s, 1H), 11.74 (s, 1H). ^{13}C NMR (75 MHz, pyridine-d_5) δ 14.61, 23.26, 29.93, 30.14, 30.22, 30.27, 32.00, 32.44, 36.52, 105.30, 118.31, 121.61, 123.12, 126.89, 128.33, 128.72, 128.77, 131.77, 133.15, 136.82, 140.25, 155.92, 174.34. HRMS (ESI, $(M+Na)^+$) calcd for $C_{78}H_{105}N_3O_6$: 1202.7901; found: 1202.7805.

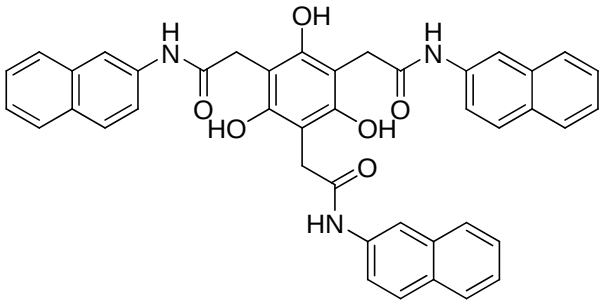

***N*-Naphthyl-2-(2,4,6-trihydroxy-3,5-bis-naphthylcarbamoylmethyl-naphthyl)-acetamide (2-9b).** This compound was synthesized from **2-8b** (0.92 g, 1.3 mmol) and BBr_3 (7.7 mmol) according to the same procedure used for **2-9a** to afford **2-9b** (0.68 g , 77%) as a brown solid. ^{1}H NMR (300 MHz, DMSO-d_6) δ 3.81 (s, 2H), 7.66 (m, 5H), 8.29 (s, 1H), 9.31 (s, 1H), 10.37 (s, 1H). ^{13}C NMR (75 MHz, DMSO-d_6) δ 116.13, 120.83, 125.23, 127.04, 127.98, 128.11, 128.99, 130.43, 134.10, 137.40, 172.76. HRMS (ESI, $(M+Na)^+$) calcd for $C_{42}H_{33}N_3O_6$: 698.2231; found: 698.2230.

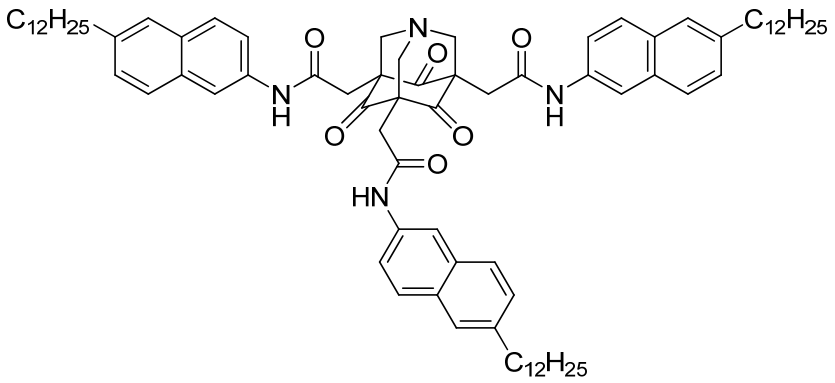

2-{5,7-Bis-[(6-dodecyl-naphthylcarbamoyl)-methyl]-4,6,10-trioxo-1-aza-tricyclo [3.3.1.1^{3,7}]dec-3-yl}-*N*-(6-dodecyl-naphthyl)-acetamide (2-1a). A solution of **2-9a** (120 mg, 0.10 mmol), HMTA (42 mg, 0.30 mmol) and isopropanol (5 mL) was heated to reflux for 72 h under a blanket of argon. After cooling the reaction to rt, the mixture was filtered to afford a brown solid then the solid was washed with 5% HCl and water. The solid was purified via recrystallization from ethyl acetate/dioxane to afford **13a** (78 mg, 49%) as a brown solid: m.p. 213–215 °C. ^{1}H NMR (300 MHz, pyridine-d_5) δ 0.88 (t, 3H, J = 7.2 Hz), 1.27 (m, 18H), 1.69 (m, 2H), 2.74 (t, 2H, J = 7.2 Hz), 3.40 (s, 2H), 4.36 (s, 2H), 7.37 (d, 1H, J = 8.7 Hz), 7.83 (m, 5H), 11.15 (s, 1H). ^{13}C NMR (75 MHz, pyridine-d_5) δ 14.98, 23.63, 26.75, 28.34, 30.30, 30.33, 30.53, 30.60, 30.65, 32.40, 32.81, 36.90, 72.11, 75.87, 117.39, 121.57, 127.24, 128.55, 129.02, 131.75, 133.74, 137.98, 140.11, 169.59, 200.21. HRMS (ESI, (M+Na)$^+$) calcd for $C_{81}H_{108}N_4O_6$: 1255.8167; found: 1255.8136. Anal. calcd for $C_{81}H_{108}N_4O_6 \cdot 2H_2O$: C, 76.62; H, 8.89; N, 4.41. Found: C, 76.74; H, 9.03; N, 4.67.

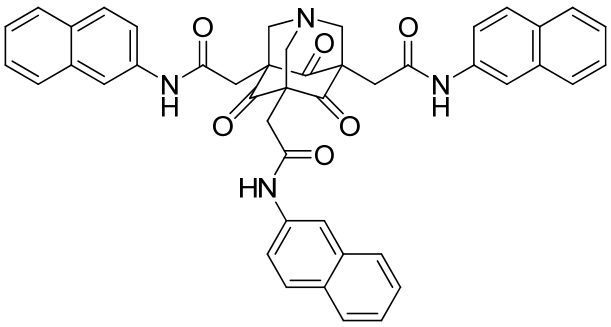

***N*-2-Naphthyl-2-(4,6,10-trioxo-5,7-bis-naphthylcarbamoylmethyl-1-aza-tricyclo [3.3.1.1^{3,7}]dec-3-yl)-acetamide (2-1b).** A solution of **2-9b** (0.30 g, 0.44 mmol), HMTA (188 mg, 1.33 mmol) and isopropanol (25 mL) was heated to reflux for 72 h under a blanket of argon. After cooling the reaction mixture to rt, the solvent was removed in vacuo and the residue was treated with ethyl acetate (10 mL). The solid was collected by suction filtration and purified via recrystallization from ethyl acetate/dioxane to afford **2-1b** (0.19 g, 59%) as a white solid: m.p. 277–279 °C. ^{1}H NMR (300 MHz, DMSO-d_6) δ 2.88 (s, 2H), 4.00 (s, 2H), 7.44 (m, 3H), 7.79 (m, 3H), 8.29 (s, 1H), 10.24 (s, 1H). ^{13}C NMR (75 MHz, DMSO-d_6) δ 31.75, 69.77, 108.64, 114.23, 119.30, 123.85, 125.80, 126.68, 126.86, 127.71, 129.03, 132.94, 136.34, 167.31, 176.37, 197.80. HRMS (ESI, (M+Na)$^+$) calcd for $C_{45}H_{36}N_4O_6$: 751.2517; found: 751.2517. Anal. calcd for $C_{45}H_{36}N_4O_6 \cdot 1.5H_2O$: C, 71.51; H, 5.20; N, 7.41. Found: C, 71.76; H, 5.20; N, 7.59.

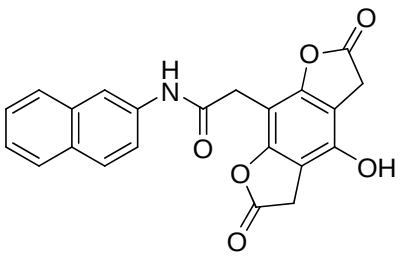

2-(4-Hydroxy-2,6-dioxo-2,3,5,6-tetrahydrobenzofuro[6,5-b]furan-8-yl)-N-(naphthalen-2-yl)acetamide (2-10). A solution of **2-9b** (0.2 g, 0.3 mmol), TFA (0.6 mL, 8 mmol) and toluene (20 mL) was heated at 80–90 ^{o}C for 2 h under a blanket of argon. After

cooling the reaction mixture to rt, the solvent was removed by filtration and the solid was washed with water to afford **2-10** (0.10 mg, 86%) as a peach-colored solid. ^{1}H NMR (300 MHz, DMSO-d_6) δ 3.72 (s, 2H), 3.83 (s, 4H), 7.43 (m, 2H), 7.59 (m, 1H), 7.82 (m, 3H), 8.28 (s, 1H), 10.25 (s, 1H), 10.38 (s, 1H). ^{13}C NMR (75 MHz, DMSO-d_6) δ 30.77, 94.43, 104.50, 114.63, 119.34, 123.99, 125.82, 126.68, 126.86, 127.78, 129.17, 132.84, 136.13, 147.26, 152.26, 166.97, 173.56. HRMS (ESI, $(M+Na)^+$) calcd for $C_{22}H_{15}NO_6$: 412.0792; found: 412.0788.

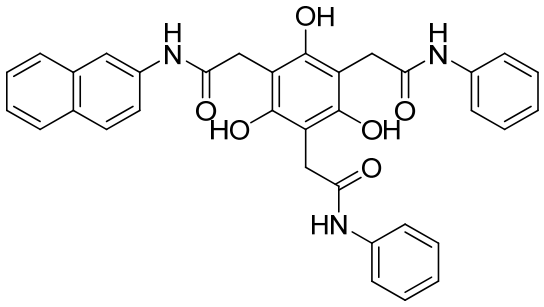

2,2'-(2,4,6-Trihydroxy-5-(2-(naphthalen-2-ylamino)-2-oxoethyl)-1,3-phenylene)bis(N-phenylacetamide) (2-11). A stirring solution of **2-10** (0.1 g, 0.3 mmol) in DMF (10 mL) was treated with aniline (0.1 mL, 1 mmol) and heated to 120 °C overnight. The solvent was removed in vacuo and the residue was dissolved in ethyl acetate. The organic layer was washed with 10% HCl and water. The combined organic layers were dried with Na_2SO_4. The solvent was removed on a rotary evaporator and the crude product was purified by column chromatography (hexane/EtOAc 1:1) to afford a yellow solid (0.10 g, 68%). ^{1}H NMR (300 MHz, DMSO-d_6) δ 3.73 (s, 4H), 3.78 (s, 2H), 7.05 (t, 2H, J = 7.5 Hz), 7.30 (t, 4H, J = 7.5 Hz), 7.43 (m, 2H), 7.62 (m, 5H), 7.85 (m, 3H), 8.28 (s, 1H), 9.31 (s, 2H), 9.32 (s, 1H), 10.19 (s, 2H), 10.37 (s, 1H). ^{13}C NMR (75 MHz, DMSO-d_6) δ 13.58, 20.26, 31.86, 59.25, 102.94, 105.26, 115.01, 117.88, 118.85, 119.55, 120.32, 122.91, 124.5, 125.33, 125.8, 125.9, 126.82, 126.95, 127.84, 127.96, 128.23,

129.29, 132.87, 134.49, 136.02, 138.41, 146.14, 153.15, 171.09, 171.26. HRMS (ESI, $(M+Na)^+$) calcd for $C_{34}H_{29}N_3O_6$: 598.1949; found: 598.1944.

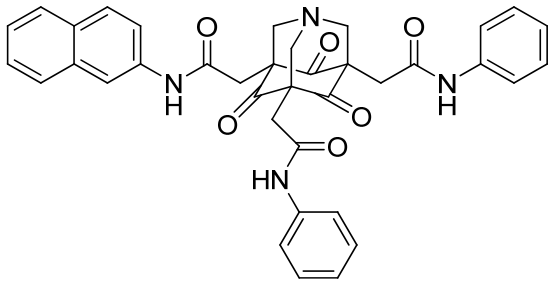

Mono-naphthylamine-di-phenylamine 1-aza-adamantantrione (2-12). This compound was synthesized from **2-11** (90 mg, 0.16 mmol) and HMTA (66 mg, 0.48 mmol) according to the same procedure used for **2-1a** to afford **2-12** (41 mg, 43%) as an off-white solid. ^{1}H NMR (300 MHz, DMSO-d_6) δ 2.79 (s, 4H), 2.85 (s, 2H), 3.95 (s, 6H), 6.99 (t, 2H, J = 7.5 Hz), 7.26 (t, 4H, J = 7.8 Hz), 7.45 (m, 8H), 7.81 (m, 3H), 8.27 (s, 1H), 10.01 (s, 2H), 10.23 (s, 1H). ^{13}C NMR (75 MHz, DMSO) δ 33.21, 69.71, 69.88, 114.19, 118.35, 119.28, 122.33, 123.85, 125.81, 126.69, 126.88, 127.72, 128.08, 129.03, 132.95, 136.36, 138.80, 167.03, 167.28, 197.79. HRMS (ESI, $(M+Na)^+$) calcd for $C_{37}H_{32}N_4O_6$: 651.2214; found: 651.2208.

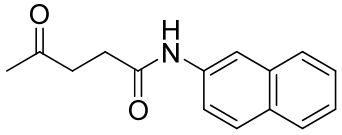

***N*-(Naphthalen-2-yl)-4-oxopentanamide (2-13).** To a mixture of levulinic acid (0.31 mL, 3.0 mmol) and β-naphthylamine (0.47 g, 3.3 mmol) in dichloromethane (10 mL) was added DCC (0.68 g, 3.3 mmol) at 0–5 °C. The mixture was stirred at 0–5 °C for 1 h and then at rt for 2 h. The solids were removed by filtration. The organic layer was then washed with 1 M HCl, 0.05 M NaOH, and water. The solvent was removed on a rotary evaporator and the crude product was

purified by column chromatography (hexane/EtOAc 1:1) to afford a white solid (0.44 g, 61%). ^{1}H NMR (300 MHz, $CDCl_3$) δ 2.22 (s, 3H), 2.67 (t, 2H, J = 6.6 Hz), 2.90 (t, 2H, J = 6.0 Hz), 7.43 (m, 3H), 7.74 (3H, d, J = 7.2 Hz), 8.15 (s, 1H), 8.18 (s, 1H). ^{13}C NMR (75 MHz, $CDCl_3$) δ 30.19, 31.48, 38.86, 116.67, 120.01, 125.16, 126.68, 127.75, 127.86, 128.94, 130.82, 134.06, 135.54, 170.62, 208.33. HRMS (ESI, $(M+Na)^+$) calcd for $C_{15}H_{15}NO_2$: 264.0995; found: 264.1003.

CHAPTER 3
DIFFERENTIALLY-FUNCTIONALIZED AND CHIRAL AATS FROM LACTONE PRECURSORS

Introduction

The 1-aza-adamantanetriones (AATs) are a new class of "unconventional" donor-σ-acceptor molecules which display interesting self-assembly and macromolecular properties upon proper functionalization of the adamantanoid core. Experiments have shown that the electronic structure of the molecules (defined by multiple through-bond donor–acceptor interactions) responds to appended substituents in unique ways, and dramatic changes have been observed between phenyl-substituted AAT **1-14** and phenylamide-substituted AAT **1-15** in terms of solution-phase behavior and solid-state organization. Likewise, the most robust AAT organogels to date have been prepared by converting the phenylamide group (of **1-15**) to a naphthylamide substituent (as in **2-1**). Peripheral functional groups are therefore the key to "fine tuning" the shape, dipole, solubility, and self-recognition capabilities of the AAT platforms.

This chapter first reviews the typical synthetic approaches to prepare C_3-symmetric but functionalized AATs and then introduces new, more versatile strategies based on lactone intermediates (derived from phloroglucinol) that afford access to differentially-functionalized and even chiral compounds. The synthetic scheme to access C_3-symmetric amide-based AATs is shown in Figure 3-1 and highlights two significant limitations. First, the protocol requires that a strong Brönsted or Lewis acid (HBr, HI, BBr_3, etc.) be used in the methyl-phenyl ether cleavage step for phloroglucinol synthon preparation. Milder conditions do not work efficiently for this multi-site deprotection. The procedure limits the functional groups that can be incorporated into the AAT periphery. While most amides, bulky esters, and alkyl/aryl groups survive, delicate (and chiral) biomonomers like amino acids, nucleosides, or glycosides, can't be introduced by this route. The latter functionalities are important for using the AATs as scaffolds to probe

interactions at biomolecular interfaces, for example, or as potential drug targets.[188] Alternative synthetic methods would ideally allow preparation of derivatives bearing a wide variety of functional groups in the AAT periphery.

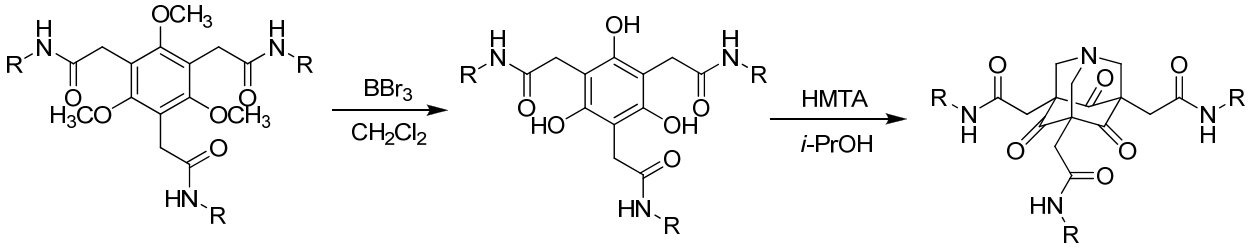

Figure 3-1. Current methodology used to construct the C_3-symmetric AATs. BBr_3 labile functionality is not tolerated in the current scheme.

The second limitation implied by Figure 3-1 is that only C_3-symmetric AAT derivatives are easily accessible. C_3-symmetric scaffolds are certainly widely used as supramolecular building blocks,[189] asymmetric catalysts, and in chiral recognition.[189-191] The last two applications generally require chiral compounds that are often prepared by introducing chiral centers to the otherwise symmetric objects. Developing synthetic methodology through which functionality can be differentially installed, selectively, into the arm units of the AAT core would greatly expand the potential applications of the molecules. That said, differentiating tripodal scaffolds is difficult and historically achieved statistically by unselective reactions; it therefore often involves tedious separation techniques to obtain mono-, di-, or trifunctionalized materials.[192] Interesting opportunities exist for the amide-based AATs if the peripheral groups can be independently addressed (Figure 3-2). The symmetry would be reduced from C_3 to C_s upon introduction of two different arms, and further to C_1 upon installation of three different appendages. In this last case, the bridgehead nitrogen appears as one of *four* chiral centers. Such molecules could then potentially share the properties of chiral tertiary amines (e.g., sparteine) that have enjoyed widespread application in chiral recognition and asymmetric catalysis.194-196

Similarly, the compounds could serve as building blocks for a variety of chiral self-assembled materials, present unusual chiroptical properties, and offer challenges and opportunities with respect to chiral separation.

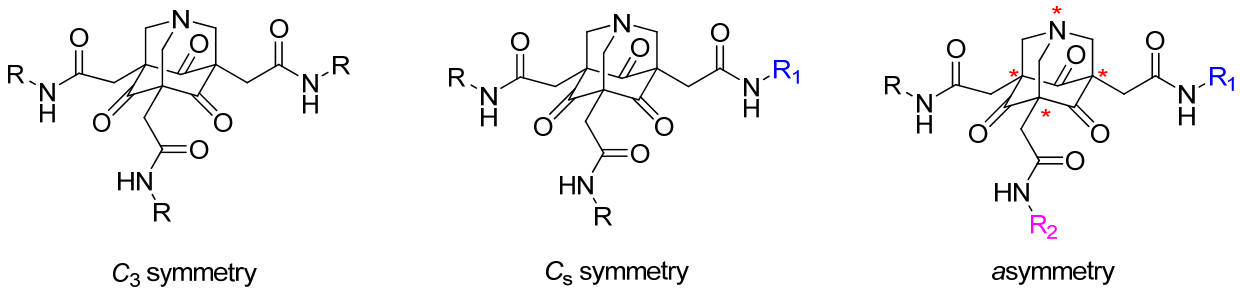

Figure 3-2. From symmetric to asymmetric triamide AATs.

A Lactone-Based Strategy

A strategy for preparing differentially substituted and even chiral AAT amides comes from the lactone chemistry[91] pioneered by Dr. Andy Lampkins in the Castellano group. Figures 3-3 and 3-4 revisit the discovery of these useful intermediates, initially the by-products of BBr_3 demethylation reactions.[91] With optimization, ester functionalized phloroglucinol derivatives can form the mono-, di-, and trilactones (Figure 3-3 and 3-4) selectively under appropriate conditions. Temperature is the key to controlling the lactone formation.[91]

Figure 3-3 shows the preparation of butenolides **3-1a** through **3-1c**. While the basic chemistry of coumaran-2-ones like **3-1a** has been described before,[193] **3-1b** and **3-1c** are novel scaffolds and ongoing work in the Castellano lab is exploring their properties and reactivity. For example, it is interesting that C_2-symmetric **3-1b** is formed quantitatively at the expense of its C_s-symmetric regioisomer (not shown). Shown schematically is how trilactone **3-1c** can be converted, in two steps (ring opening with an amine and then HMTA cyclization), to C_3-symmetric AATs like the ones that have been described thus far. The same two-step sequence can be applied to the mono- and dilactones to prepare differentially-functionalized AATs (vide

infra). The difference in each case versus Figure 3-1 is that the peripheral functional groups are introduced at a late synthetic stage and not subsequently subjected to the harsh BBr_3 conditions. The complementary preparation of pentenolides **3-2a–c** is shown in Figure 3-4; cyclization of these less strained six-membered ring lactones requires lower temperatures and is generally met with higher yields. Notably, C_s-symmetric **3-2b** is isolated as the major dilactone product here. Finally, as with the butenolides, the intermediates can be converted in two steps to various AAT derivatives.[194]

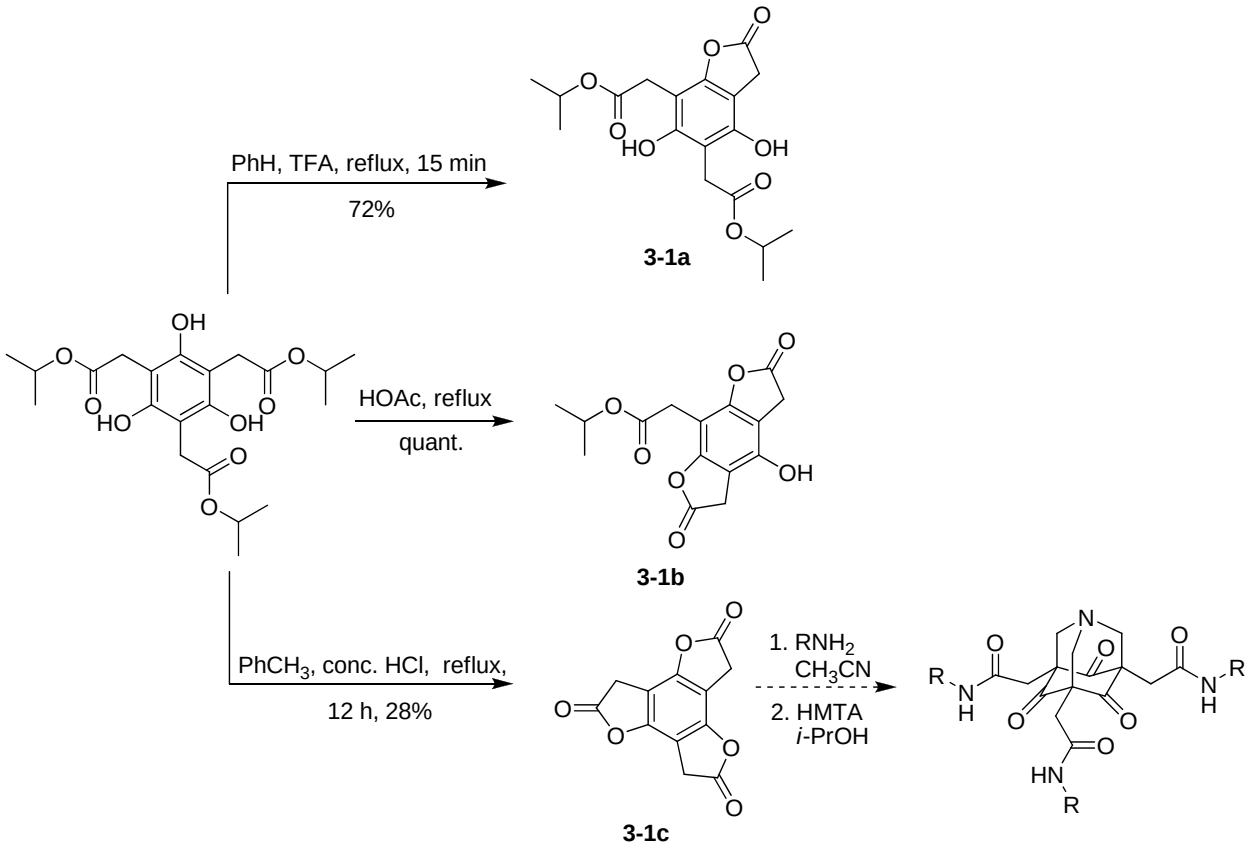

Figure 3-3. Synthetic methodology used to selectively annelate mono-, di-, and tributenolides from a common intermediate, an ester phloroglucinol derivative.[91]

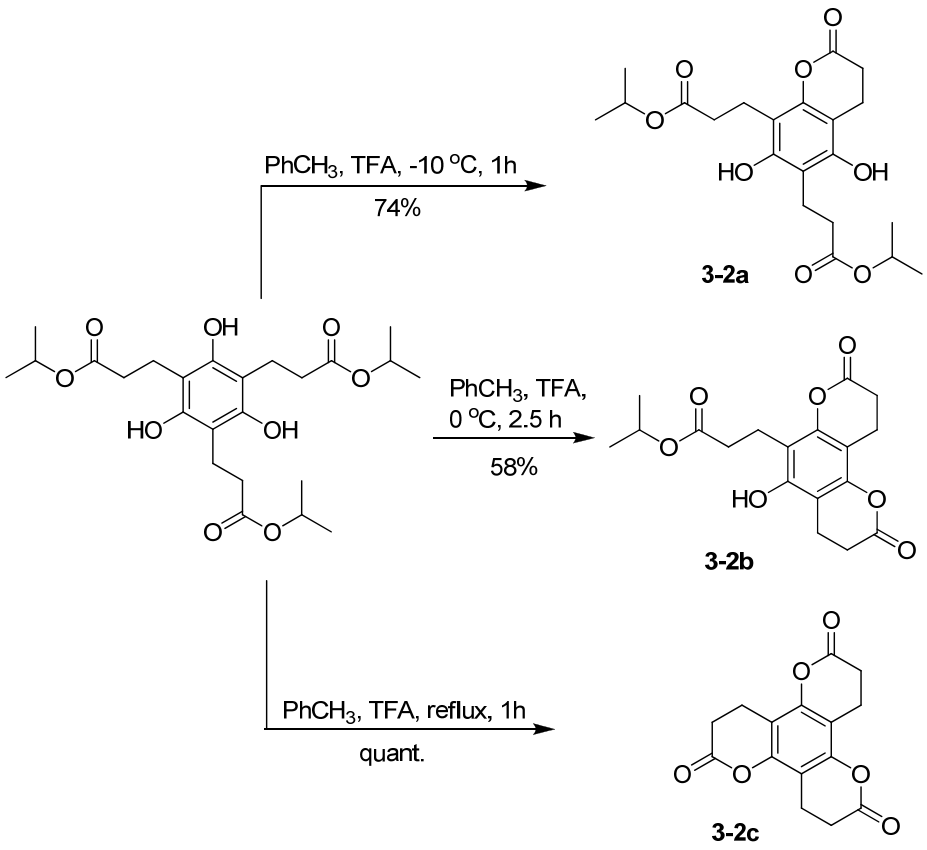

Figure 3-4. Synthetic methodology used to selectively annulate mono-, di-, and tripentenolides from a common intermediate, an ester phloroglucinol derivative.[91]

Toward triamide AAT targets like those presented in Figure 3-2, the lactone-based methodology has now been extended to phloroglucinol triamides. Amide functional groups play an important role in the self-assembly of AATs through structural preorganization that involves intramolecular H-bonding.[55, 91] Figure 3-5 shows the reasonably selective formation of the mono- and dilactones from amide-functionalized phloroglucinol **3-17** under various conditions. The initial synthetic approach was to use the conditions of Figure 3-3 and apply them to **3-17**. Treatment of the phloroglucinol derivatives with TFA at elevated temperature formed, instead of the monolactone as reported for the esters, the thermodynamic C_2-symmetric dilactone **3-3b** as the major product. The same conditions were used to prepare dilactone **2-10** (Figure 2-5) from naphthyl amide-functionalized phloroglucinol **2-9b**. Shorter heating times, as shown by Yan Li

in the Castellano group, can give the C_s-symmetric dilactone regioisomer, **3-3c**. The two regioisomers are readily distinguished by their ^{1}H NMR spectra; **3-3c** shows three singlets (in a 1:1:1 ratio) for the three sets of chemically unique α-CH_2 protons while only two singlets (in a 2:1 ratio) are observed for **3-3b**. Decreasing the temperature to room temperature yields mono-lactone **3-3a** in moderate yield. Comparing the conditions used in Figures 3-3 and 3-5, it is apparent that the amides generally cyclize at lower temperatures to provide the corresponding lactones. This rate discrepancy is presumably related to the difference in carbonyl electro-philicity between the bulky isopropyl esters and activated phenyl amides.

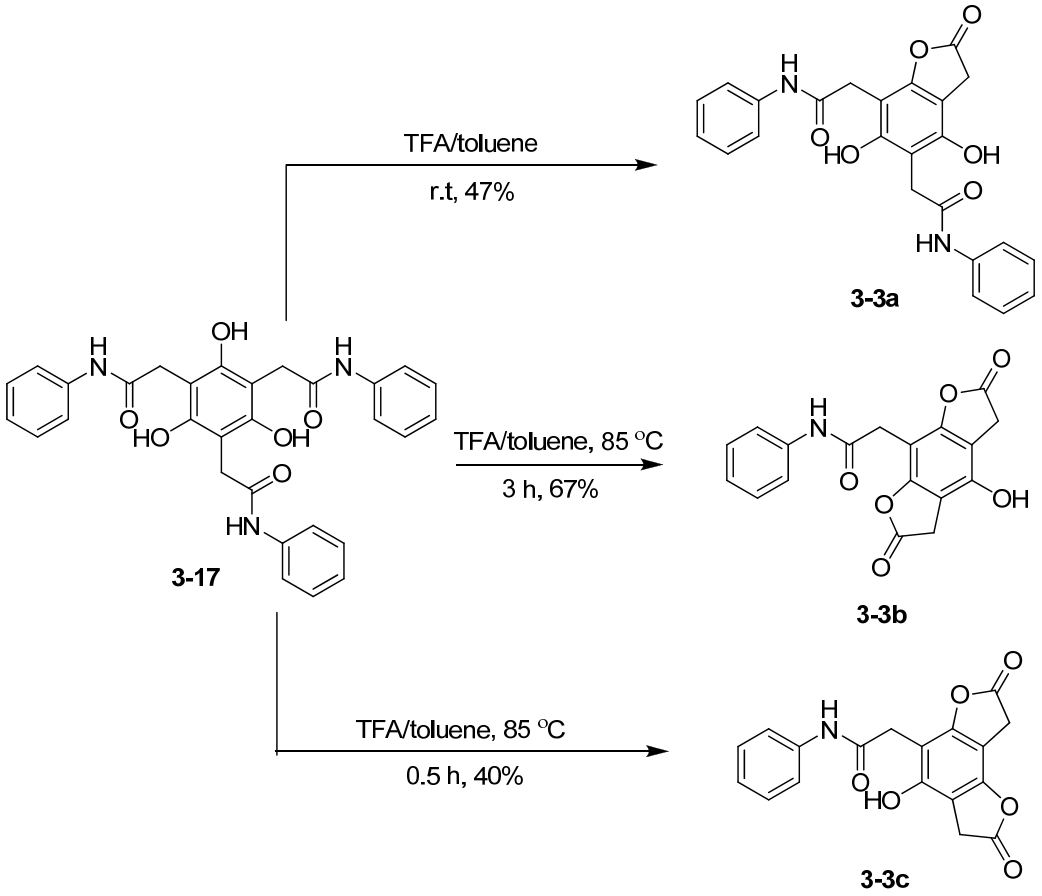

Figure 3-5. The synthetic approach of amide-functionalized lactones.

Approach to Differentially-Substituted AATs from Butenolide Precursors

The five-membered ring lactones should show good reactivity toward nucleophiles under mild conditions[195] due to relief of ring strain upon ring opening. To explore this reactivity and also prepare new desymmetrized AATs, ester intermediates **3-1a** and **3-1b** were treated with various aryl and alkyl amine nucleophiles (Figure 3-6 and Table 3-1). Under reflux conditions in DMF or acetonitrile, one or two equivalents of the amine are sufficient to afford the corresponding phloroglucinol derivatives **3-4** and **3-6**, respectively, in moderate to good yields. Subsequent cyclization with HMTA affords the corresponding differentially-substituted AATs **3-5** and **3-7**. Various aryl amines were selected to ultimately explore potential π-π stacking interactions in the context of self-assembly. Pyrene, for example,[113-120] was selected (with two different connectivities to the AAT core) due to its well understood electronic and optical properties that could be useful to study AAT self-assembly in solution.

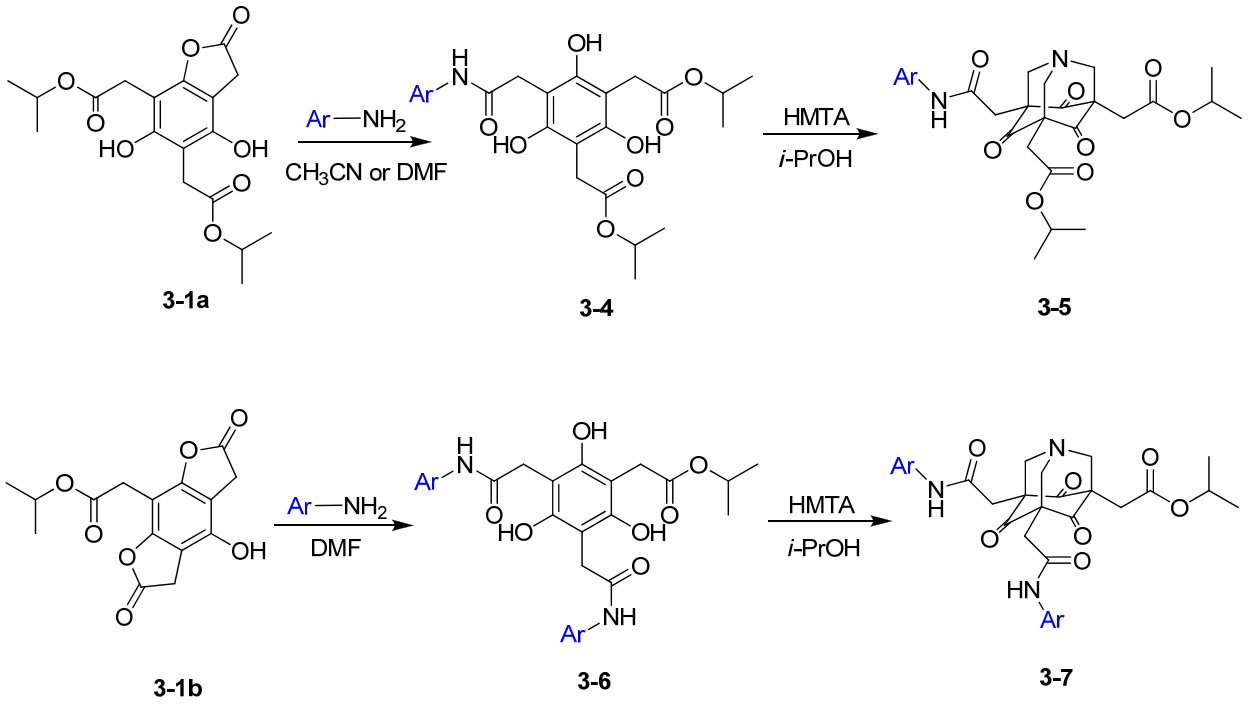

Figure 3-6. Preparation of mixed amide and ester AATs derived from the mono- and dibutenolides.

Table 3-1. Nucleophilic ring opening of mono- and dibutenolides with amines and subsequent cyclization with HMTA.

Ar group	entry	product	yield	product	yield
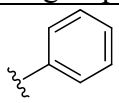	1	**3-4a**	84%	**3-5a**	42%
	2	**3-6a**	68%	**3-7a**	47%
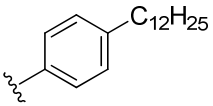	3	**3-4b**	73%	**3-5b**	49%
	4	**3-6b**	44%	**3-7b**	38%
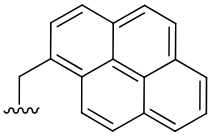	5	**3-4c**	70%	**3-5c**	45%
	6	**3-6c**	73%	**3-7c**	51%
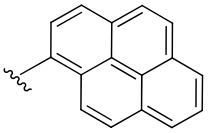	7	**3-4d**	52%	**3-5d**	41%
	8	**3-6d**	51%	**3-7d**	62%

The amide-functionalized butenolides show a similar reactivity toward amine nucleophilic attack. Monolactone **3-3a** reacts with both aryl and alkyl amines to form differentially-functionalized phloroglucinol and AAT triamides (Figure 3-7).

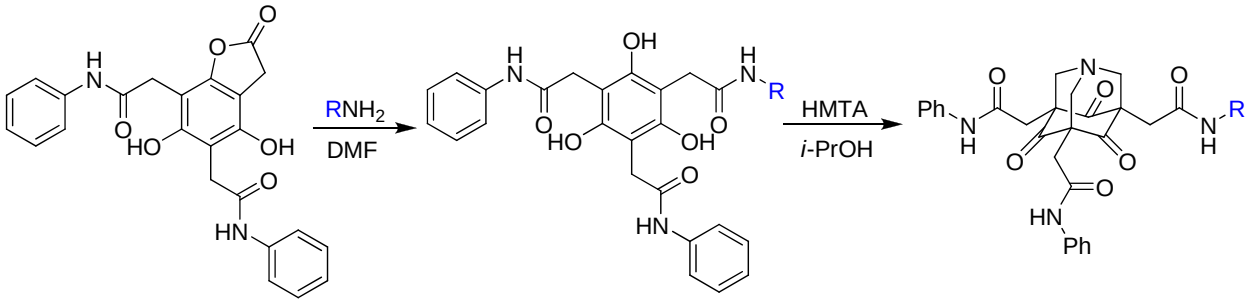

Figure 3-7. Synthesis of differential amide functionalized AATs from amide mono-lactone.

The β-naphthylamine requires heating at 120 °C in DMF overnight to consume all of the monolactone starting material while *n*-hexylamine reacts with **3-3a** at room temperature. The

differences are understandable given the primary alkyl amine and primary aryl amine. Dilactone **2-10** reacts with anilines in DMF at 120 °C to afford the phloroglucinol products where both of lactone rings have been opened (Figure 3-8).

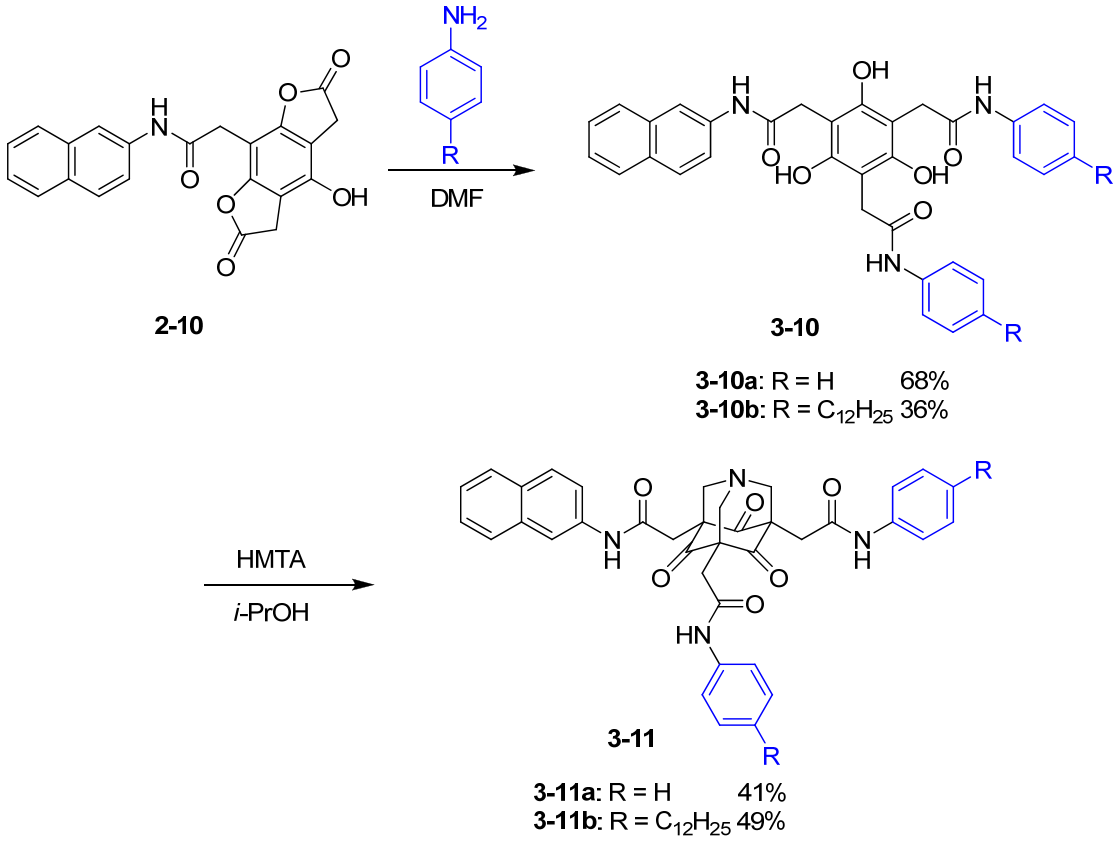

Figure 3-8. Synthesis of differentially-functionalized AATs from an amide dilactone.

Chiral AATs Derived from Lactone Methodology

An approach to synthesizing the first chiral AATs has emerged in the process of preparing the differentially-substituted AATs described above. One of the two lactone rings of the C_2-symmetric dilactones (e.g. **2-10**, **3-1b**, etc.) can be selectively opened upon addition of one equivalent of amine at 60–80 °C; the remaining lactone ring reacts at higher temperature (120 °C) in DMF (Figure 3-9). Figure 3-6 shows the temperature-dependent reactivity for **2-10**, where reasonable selectivity is observed for the single and double ring opening with aniline (to give **3-**

12 and **3-10a**, respectively). Further cyclization of **3-10a** with HMTA produces the AAT that is a hybrid of **1-15** and **2-1b**. The intermediate monolactone **3-12** of course then provides the opportunity to introduce a second amine (in this case *p*-dodecylamine) and produce the C_s-symmetric and prochiral phloroglucinol derivative **3-13**.

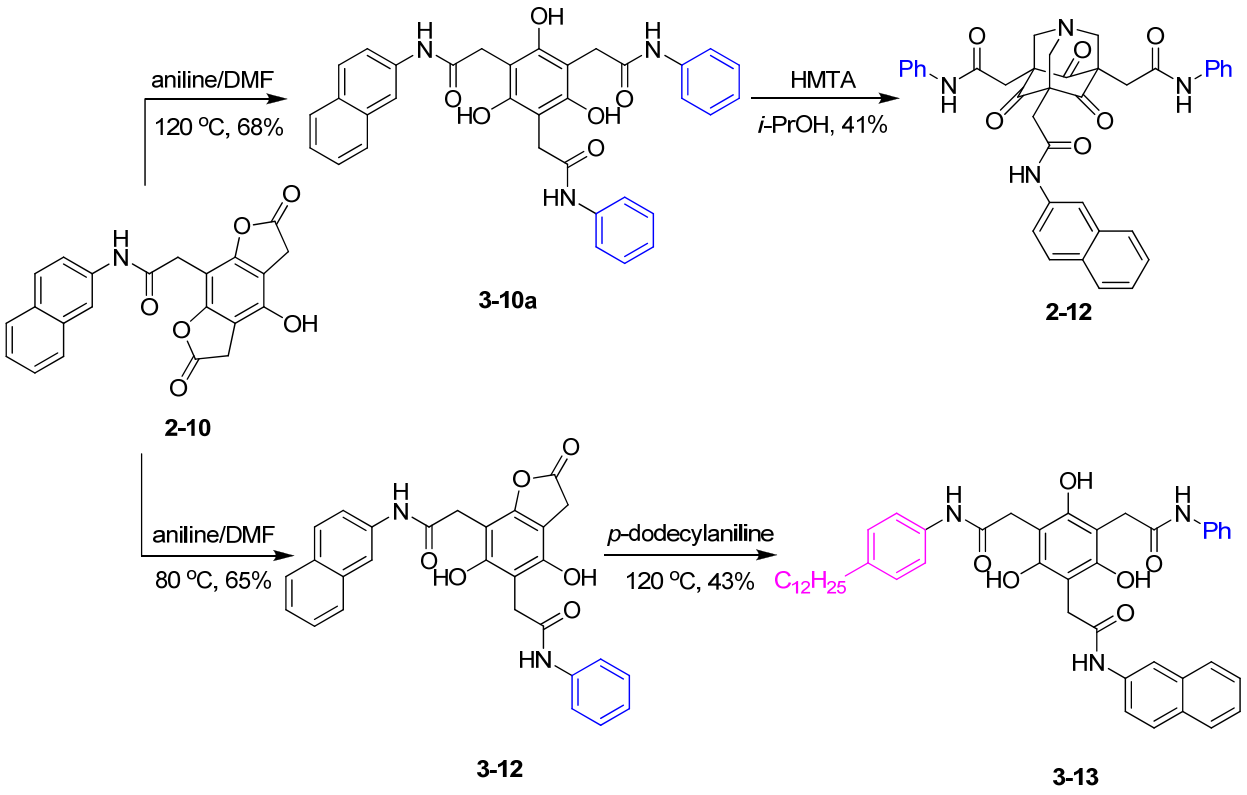

Figure 3-9. Different ring opening patterns of the dilactone **2-10** under different reaction conditions.

The ester-functionalized dilactone **3-1b** reacts similarly to **2-10** giving **3-14** (Figure 3-10). This reaction has yet to be optimized since the starting material and product have nearly the same R_f values by thin layer chromatography, making routine monitoring of the reaction difficult. Even so, the isolated **3-14** can be reacted with *n*-hexylamine to generate differentiated **3-15a**. Subsequent cyclization with HMTA affords asymmetric AAT **3-16** as a racemic mixture.

Initial attempts to visualize the mixture of stereoisomers were made. An ^{1}H NMR spectrum of **3-16a** recorded in the presence of a chiral shift reagent (1*R*)-(-)-10-camphorsulfonic

acid[196] did show doubling of the major peaks, but the spectrum was complex. Attempts to separate the enantiomers by chiral HPLC (columns used: (S,S) Whelk-01 10/100 kromasil FEC from Regis and chiral cel OB-H from Daicel chemical) failed due to poor peak resolution. Given these results, **3-15b** was prepared from reaction of **3-14** with L-(–)-α-methylbenzylamine with the intention of ultimately forming two separable diastereomers of **3-16b** upon cyclization with HMTA (Figure 3-10, see inset). Unfortunately, the cyclization product **3-16b** has been difficult to purify and clean NMR spectra have yet to be obtained.

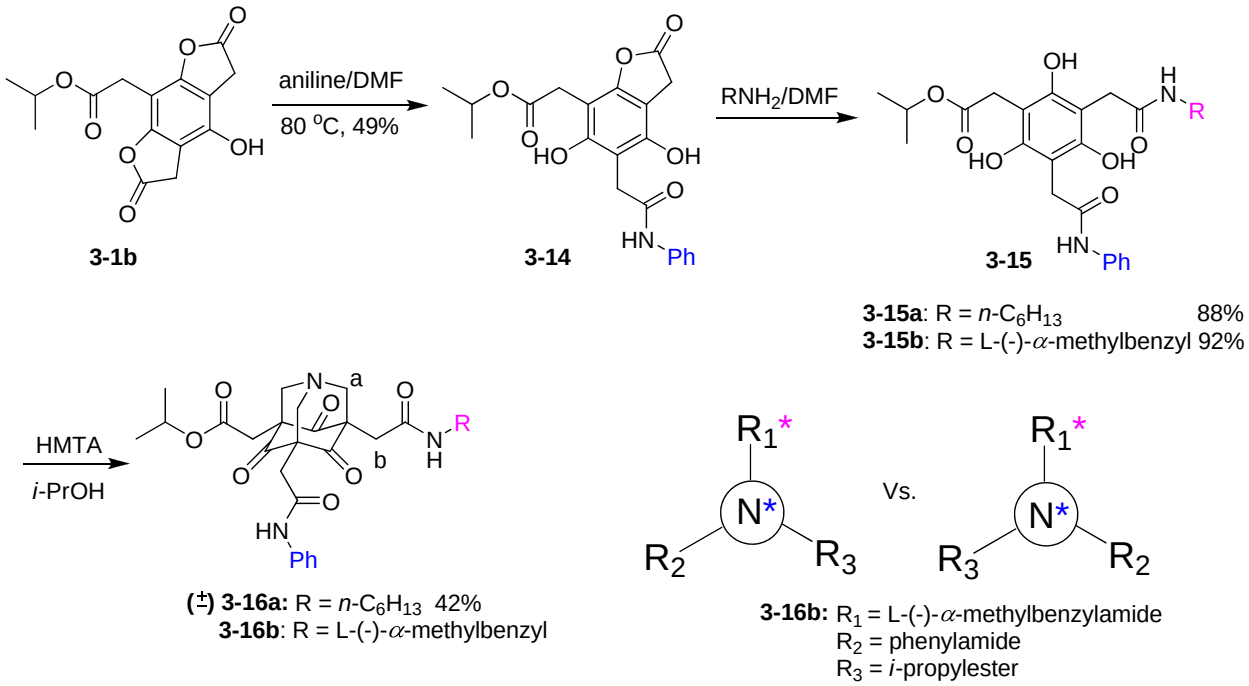

Figure 3-10. Chiral AAT derived from lactone methodology.

^{1}H NMR spectroscopy (Figure 3-11) nicely shows the result of reducing the symmetry in the AAT derivatives from C_3 (compound **1-15**), to C_s (compound **3-9b**), to C_1 (compound **3-16a**). The expected multiplicity for each set of protons **a** and **b** (Figure 3-11) across this series is one peak (singlet), five peaks (two doublets and a singlet), and 12 peaks (6 doublets). The AATs show this increase in complexity although the protons are not resolved at 300 MHz and have very similar chemical shifts.

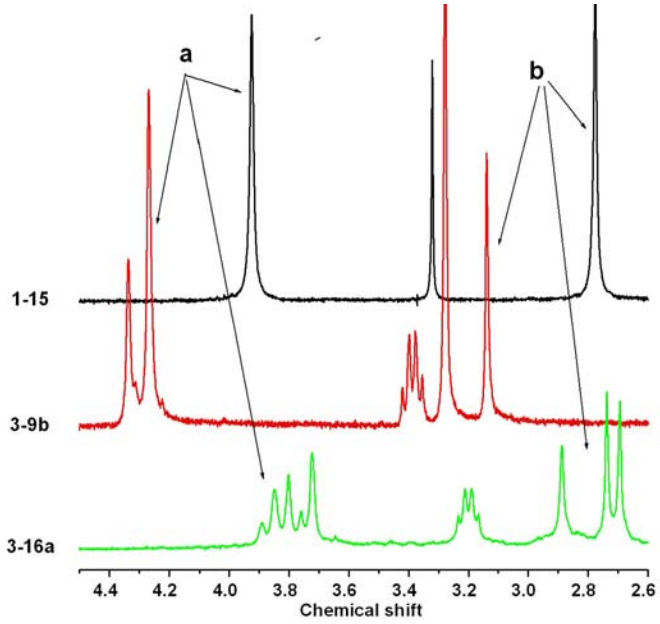

Figure 3-11. The ^{1}H NMR of compound **1-15** (in DMSO-d_6), **3-9b** (in pyridine-d_5), and **3-16b** (in $CDCl_3$). See Figure 3-10 for the proton assignments.

Interesting Thermal and Optical Properties of Differentially-Substituted AATs

With a small library of differentially-substituted AATs in hand, initial structure-property studies with respect to thermal and optical properties were pursued. The former come through differential calorimetry measurements (DSC) and the latter through thermal optical polarized microscopy (TOPM); both techniques probe bulk phase changes and possible liquid-crystalline behavior. In the DSC runs, two heating and cooling cycles were used with a rate of 10 °C/min. Most of the AAT molecules show normal endothermic transitions at their melting points and exothermic transitions upon cooling and crystallization. Compounds **3-5a** and **3-7a** show more complex thermal phase transition behavior (Figures 3-12 and 3-13, and Table 3-2).

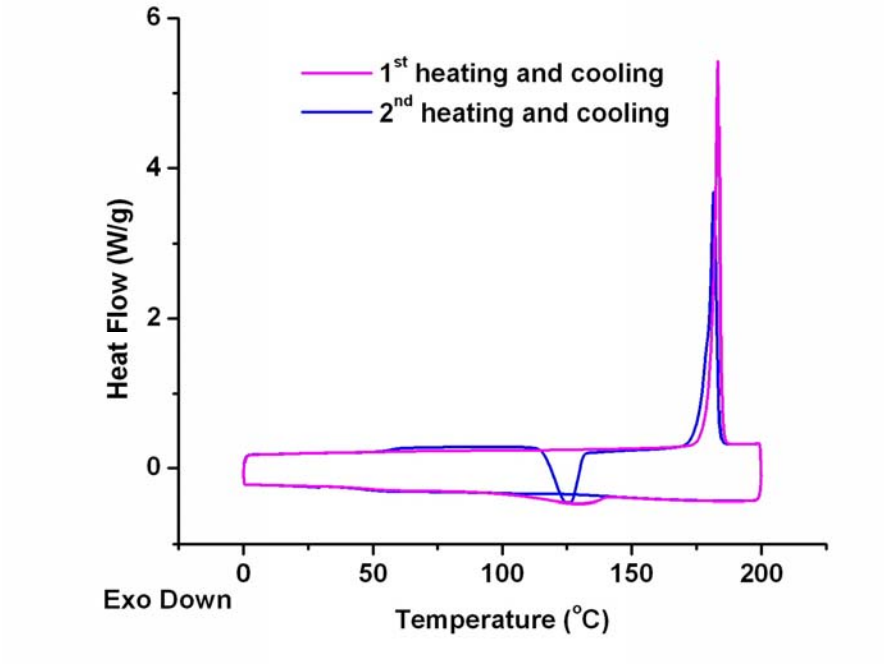

Figure 3-12. DSC curves obtained for **3-5a** for the first (red lines) and the second (blue lines) heating–cooling cycles. A cold-crystallization exotherm is identified in the second heating cycle (heating and cooling rate = 10 °C/min).

The DSC thermogram of **3-5a** (Figure 3-12) shows melting of the solid at 183 °C in the first heating cycle and then shows a broad exothermic transition upon cooling. A negative (exothermic) peak ("cold crystallization"[197-199]) is observed at 125 °C upon second heating. Apparently, the melting of the solid erases its organizational history and the compound reorganizes only upon a second heating. The DSC curves of **3-7a** (Figure 3-13) show two "cold crystallization" exotherms and one small endothermic transition prior to the melting transition in the first heating cycle. The phase transition temperatures and enthalpies for the transitions for **3-5a** and **3-7a** are summarized in Table 3-2.

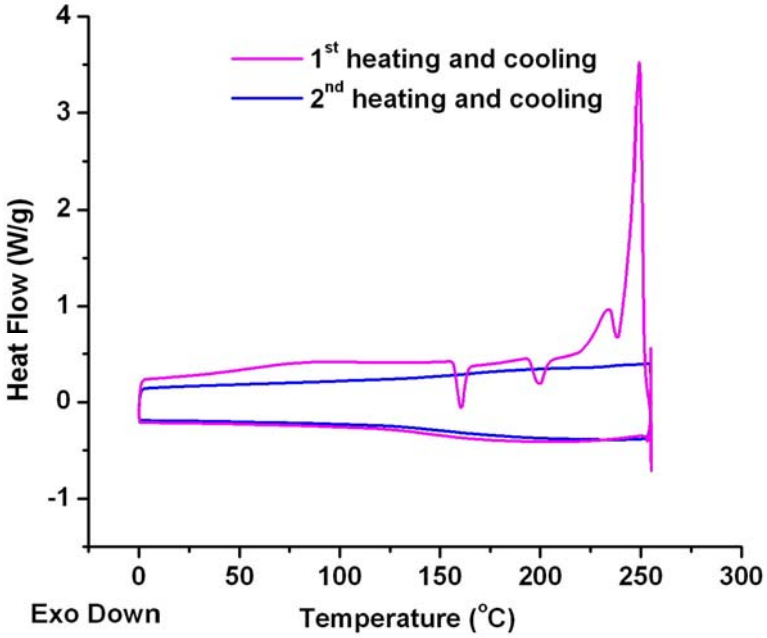

Figure 3-13. DSC curves obtained for **3-7a** for the first (red lines) and second (blue lines) heating–cooling cycles. Two cold-crystallization exotherms and one endothermic transition are identified in the first heating cycle (heating and cooling rate = 10 °C/min).

Table 3-2. Phase transition temperatures and enthalpies for **3-5a** and **3-7a**.

	3-5a			**3-7a**			
Transtion	K→I	K→K^1	K^1→I	K→K^1	K^1→K^2	K^2→K^3	K^3→I
T (°C)	183.3	125.0	181.7	160.3	199.8	232.8	249.1
ΔH (kJ/mol)	46.19	–22.82	42.15	–7.05	–5.64	11.55	54.52

K, K^1, K^2, K^3: crystalline phase; I: isotropic phase.

Thermal optical polarization microscopy (TOPM) was used to probe the phase changes optically for the two compounds upon heating and cooling. Compound **3-5a** shows needle-like crystals in the original solid state (Figure 3-14a). The first heating cycle accesses the isotropic state (not shown) upon melting. Upon a second heating, a birefringent crystal phase is formed at 124 °C that matches well the DSC transition. Crystallization into extended fibers or needles occurs from a central nucleation site (Figure 3-14b to 3-14i) upon second heating. A similar TOPM with **3-7a** did not show any remarkable features; no obvious morphology changes were observed at temperatures corresponding to the DSC transitions.

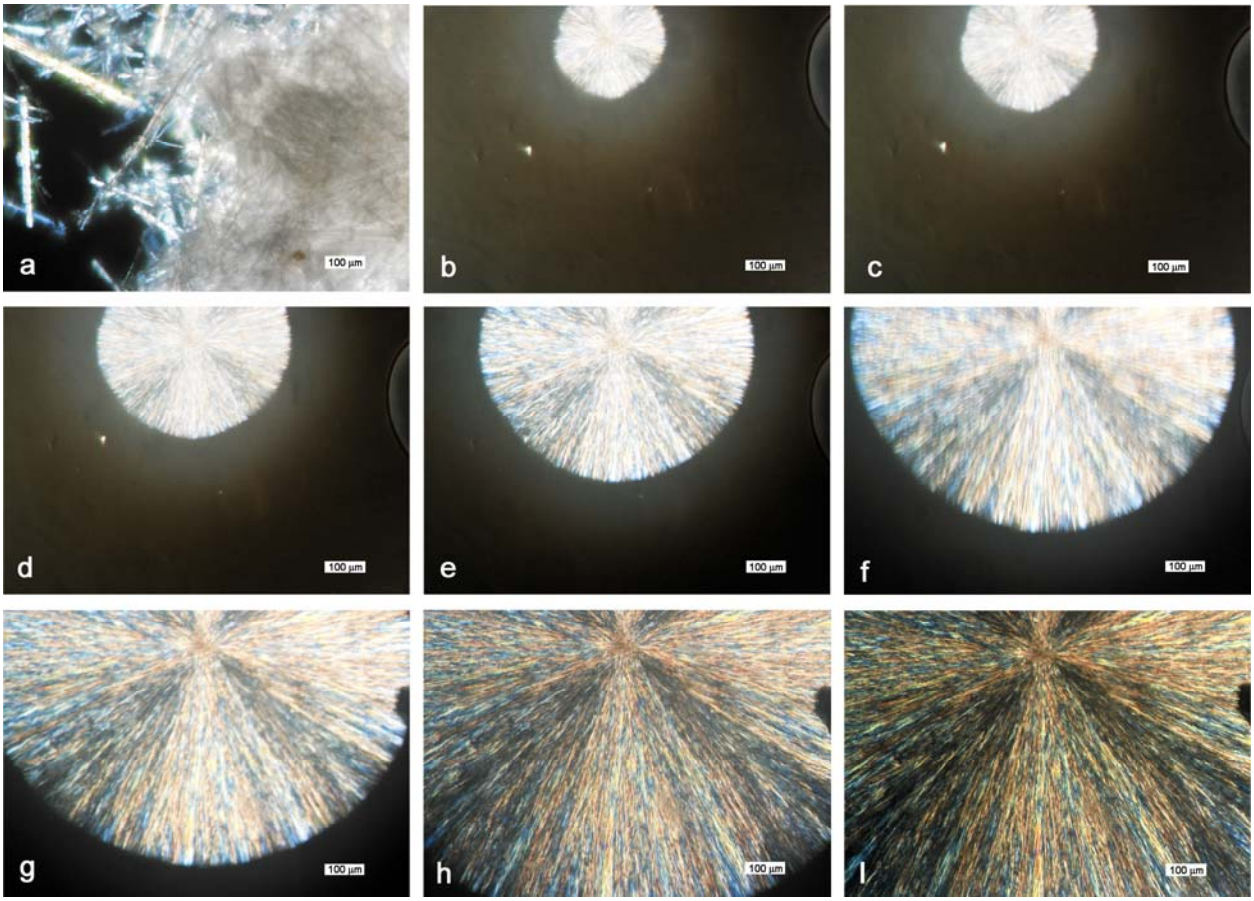

Figure 3-14. Cross-polarized optical microscopy images of compound **3-5a**: (a) The original solid sample shows needle-like crystals at room temperature. (b) to (h) Crystal growth in about 42 seconds in the second heating cycle (rate =10 °C/min). The temperature of (b) was 135 °C and the temperature of (h) was 142 °C. (I) Fully grown cold crystalline **3-5a**.

Summary

A library of differentially-substituted AATs has been prepared using a lactone-based strategy that allows for moderately selective functionalization of the phloroglucinol core. The approach allows, for the first time, a) the rational synthesis of chiral AATs and b) the introduction of sensitive functional groups to the periphery. Ongoing work seeks to use the synthetic methods to develop self-assembling AATs that can form chiral materials.

Experimental Section

Characterization Technique

Thermal optical polarized microscopy (TOPM). For all thermal optical polarized microscopy (TOPM) experiments, a Leica DMLP polarization microscope with a Linkam heating and cooling stage (temperature range of −196 to 350 °C) and a 35 mm automated camera system was used. The heating and cooling rates were 10 °C/min.

Synthesis

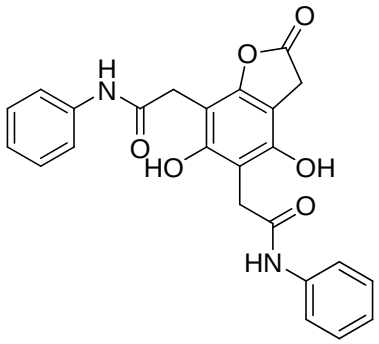

2,2'-(4,6-Dihydroxy-2-oxo-2,3-dihydrobenzofuran-5,7-diyl)bis(*N*-phenylacetamide) (3-3a). A mixture of *N*-phenyl-2-(2,4,6-trihydroxy-3,5-di-phenylcarbamoylmethylphenyl)-acetamide[55] (1.05 g, 2.00 mmol) and TFA (1.85 mL, 24.0 mmol) was stirred at room temperature for 3 h in toluene (40 mL). The solvent was then removed in vacuo and the remaining crude product was dissolved in ethyl acetate. The resulting solution was washed with 10 % NaOH solution, water, and brine. The organic layer was further dried over Na_2SO_4 and the solvent was removed on a rotary evaporator. The crude product was purified by column chromatography (hexanes/EtOAc = 3/2) to afford a white solid (0.41 g, 47%). ^{1}H NMR (300 MHz, DMSO-d_6) δ 3.68 (s, 2H), 3.69 (s, 2H), 3.75 (s, 2H), 7.05 (m, 2H), 7.29 (m, 4H), 7.59 (d, 4H, J = 8.1 Hz), 9.56 (s, 1H), 9.71 (s, 1H), 10.07 (s, 1H), 10.26 (s, 1H). ^{13}C NMR (75 MHz, DMSO-d_6) δ 31.14, 31.29, 31.43, 97.93, 100.04, 106.20, 118.51, 118.75, 122.51, 122.88, 128.17, 128.23, 138.45, 138.80,

149.97, 151.69, 154.53, 169.20, 169.82, 174.16. HRMS (ESI, $(M+H)^+$) calcd for $C_{24}H_{20}N_2O_6$: 433.1394; found: 433.1410.

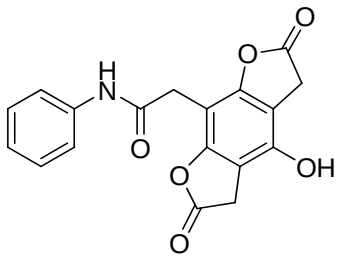

2-(4-Hydroxy-2,6-dioxo-2,3,5,6-tetrahydrobenzofuro[6,5-b]furan-8-yl)-*N*-phenylacetamide (3-3b). A solution of *N*-phenyl-2-(2,4,6-trihydroxy-3,5-di-phenylcarbamoyl-methylphenyl)-acetamide[55] (0.41 g, 0.78 mmol), TFA (0.80 mL, 9.4 mmol) and toluene (20 mL) was heated at 90–100 ^oC for 3 h under a blanket of argon. After cooling the reaction mixture to room temperature, the solvent was removed by filtration and the solid was washed with water to afford **3-3b** (0.17 g, 67%) as a off-white solid: m.p. 266–268 °C. ^1H NMR (300 MHz, DMSO-d_6) δ 3.65 (s, 2H), 3.82 (s, 4H), 7.04 (t, 1H, J = 7.2 Hz), 7.30 (t, 2H, J = 8.4 Hz), 7.58 (d, 2H, J = 7.8 Hz), 10.16 (s, 1H), 10.24 (s, 1H). ^{13}C NMR (75 MHz, DMSO-d_6) δ 31.91, 32.03, 95.71, 105.74, 119.74, 123.88, 129.41, 139.83, 148.48, 153.47, 167.94, 174.84. HRMS (ESI, $(M+H)^+$) calcd for $C_{18}H_{13}NO_6$: 340.0821; found: 340.0802.

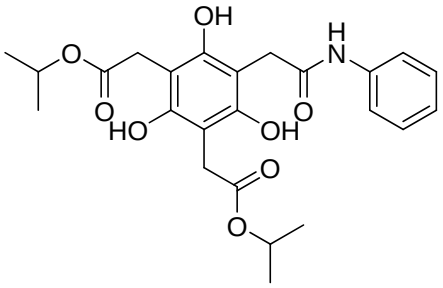

Isopropyl 2,2'-(2,4,6-trihydroxy-5-(2-oxo-2-(phenylamino)ethyl)-1,3-phenylene) diacetate (3-4a). A stirring solution of **3-1a** (0.37 g, 1.0 mmol) in CH_3CN (10 mL) was treated with aniline (0.10 mL, 1.0 mmol) and heated to reflux for 12 h. The solution was then concentrated to a crude oil and purified via column chromatography (hexanes/EtOAc = 2/1) to afford **3-4a** (0.38 g, 84%) as a yellow oil: ^{1}H NMR (300 MHz, $CDCl_3$) δ 1.28 (d, 12H), 3.77 (s, 4H), 3.81 (s, 2H), 5.01 (m, 2H, J = 6.3 Hz), 7.15 (m, 1H), 7.32 (m, 2H), 7.50 (m, 2H), 8.66 (s, 1H), 9.10 (s, 2H).

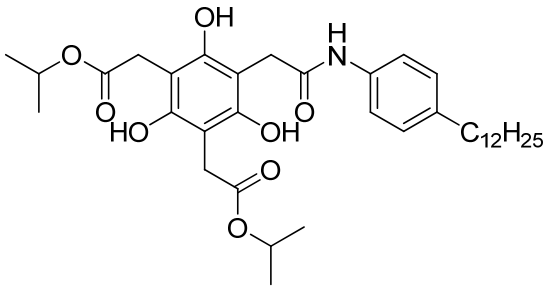

Isopropyl 2,2'-(5-(2-(4-dodecylphenylamino)-2-oxoethyl)-2,4,6-trihydroxy-1,3-phenylene)diacetate (3-4b). The compound was synthesized from **3-1a** (0.17 g, 0.46 mmol) and 4-dodecylaniline (0.12 g, 0.46 mmol) according to the same procedure used for **3-4a** to afford **3-4b** (0.21 mg, 73%) as a yellow oil. ^{1}H NMR (300 MHz, $CDCl_3$) δ 0.88 (t, 3H, J = 6.6 Hz), 1.26 (m, 30H), 1.55 (m, 2H), 2.54 (t, 2H, J = 7.5 Hz), 3.73 (s, 2H), 3.75 (s, 4H), 5.02 (m, 2H, J = 6.0 Hz), 7.08 (d, 2H, J = 8.7 Hz), 7.35 (d, 2H, J = 8.7 Hz), 8.58 (s, 1H), 9.13 (s, 2H). ^{13}C NMR (75 MHz, $CDCl_3$) δ 14.07, 21.61, 22.65, 29.17, 29.31, 29.62, 29.45, 29.55, 29.59, 30.53, 31.42,

31.88, 33.62, 35.32, 69.93, 102.79, 103.61, 120.44, 128.78, 134.63, 139.81, 153.85, 153.88, 172.54, 175.67. HRMS (ESI, $(M+Na)^+$) calcd for $C_{36}H_{53}NO_8$: 650.3663; found: 650.3649.

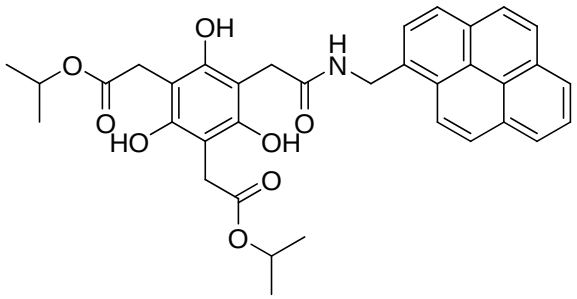

Isopropyl 2,2'-(2,4,6-trihydroxy-5-(2-oxo-2-(pyren-1-ylmethylamino)ethyl)-1,3-phenylene)diacetate (3-4c). A stirring solution of **3-1a** (0.55 g, 1.5 mmol) in CH_3CN (10 mL) was added with DMAP (238 mg, 1.95 mmol), and 1-pyrenmethylamine hydrochloride (0.40 g, 1.5 mmol) and heated to 60 °C for 12 h. The solution was concentrated to a crude oil and the remaining crude product was dissolved in CH_2Cl_2. The resulting solution was washed with 1N HCl, water, and brine. The organic layer was further dried over Na_2SO_4 and the solvent was removed on a rotary evaporator. The crude product was purified by column chromatography (CH_2Cl_2/MeOH = 100/1) to afford **3-4c** (0.66 g, 70%) as a yellow solid. ^{1}H NMR (300 MHz, $CDCl_3$) δ 1.27 (d, 12H, J = 6.6 Hz), 3.67 (s, 2H), 3.75 (s, 4H), 4.98 (m, 2H), 5.07 (d, 2H, J = 5.4 Hz), 6.48 (t, 1H, J = 5.4 Hz), 8.08 (m, 9H), 8.61 (s, 1H), 9.27 (s, 2H). ^{13}C NMR (75 MHz, $CDCl_3$) δ 21.62, 30.54, 32.51, 42.37, 69.91, 102.75, 103.74, 109.61, 122.44, 124.74, 125.39, 125.44, 126.10, 127.03, 127.27, 127.62, 128.29, 128.94, 129.91, 130.66, 131.18, 131.33, 153.86, 154.01, 174.05, 175.66. HRMS (ESI, $(M+Na)^+$) calcd for $C_{35}H_{35}NO_8$: 620.2260; found: 620.2243.

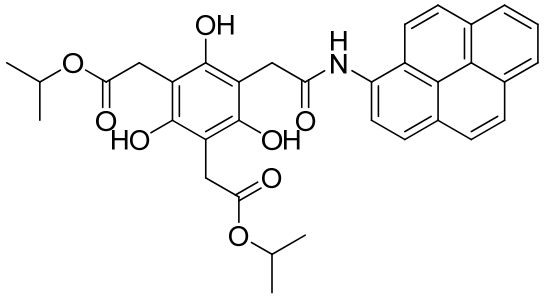

Isopropyl 2,2'-(2,4,6-trihydroxy-5-(2-oxo-2-(pyren-4-ylamino)ethyl)-1,3-phenylene)-diacetate (3-4d). A stirring solution of **3-1a** (0.42 g, 1.2 mmol) in DMF (10 mL) was added with 1-pyrenamine (0.25 g, 1.2 mmol) and heated to 120 °C for 2 days. The solution was concentrated to a crude oil and the remaining crude product was dissolved in CH_2Cl_2. The resulting solution was washed with 1N HCl, water, and brine. The organic layer was further dried over Na_2SO_4 and the solvent was removed on a rotary evaporator. The crude product was purified by column chromatography (CH_2Cl_2/MeOH = 100/3) to afford **3-4d** (0.35 g, 52%) as a yellow solid: ^{1}H NMR (300 MHz, DMSO-d_6) δ 1.20 (d, 12H, J = 6.6 Hz), 3.62 (s, 2H), 4.00 (s, 4H), 4.91 (m, 2H, J = 5.4 Hz), 8.13 (m, 9H), 9.09 (s, 1H), 9.55 (s, 1H), 10.47 (s, 2H). ^{13}C NMR (75 MHz, DMSO-d_6) δ 21.23, 31.79, 66.40, 76.31, 84.20, 102.93, 121.67, 122.77, 123.31, 123.80, 124.43, 124.76, 125.89, 126.73, 127.86, 129.91, 130.29, 130.92, 153.15, 153.27, 170.84, 171.94. HRMS (ESI, $(M+Na)^+$) calcd for $C_{34}H_{33}NO_8$: 606.2098; found: 606.2090.

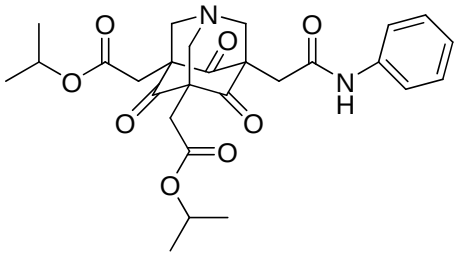

Mono-phenylamine-di-isopropyl ester 1-aza-adamantanetriones (3-5a). A solution of **3-4a** (0.38 g, 0.83 mmol), HMTA (234 mg, 1.66 mmol), and isopropanol (10 mL) was heated to

reflux overnight under a blanket of argon. After cooling the reaction mixture to room temperature, the solvent was removed in vacuo and the residue was dissolved in ethyl acetate. The organic layer was washed with 1N HCl and brine. The solution was then concentrated to a crude oil and purified via column chromatography (hexanes/EtOAc = 1/1) to afford **3-5a** (0.21 g, 42%) as a white solid: m.p. 180–182 °C. ^{1}H NMR (300 MHz, DMSO-d_6) δ 1.17 (d, 12H, J = 6.6 Hz), 2.62 (s, 4H), 2.75 (s, 2H), 3.70 (s, 4H), 3.88 (s, 4H), 4.81 (m, 2H), 7.01 (m, 1H), 7.26 (m, 2H), 7.56 (m, 2H), 10.00 (s, 1H). ^{13}C NMR (75 MHz, DMSO-d_6) δ 21.34, 31.79, 33.64, 63.68, 63.84, 67.25, 69.86, 70.02, 70.80, 118.76, 122,81, 128.59, 139.36, 167.32, 168.47, 197.74, 197.92. HRMS (ESI, $(M+Na)^+$) calcd for $C_{27}H_{32}N_2O_8$: 535.2051; found: 535.2047. Anal. calcd for $C_{27}H_{32}N_2O_8$: C, 63.27; H, 6.29; N, 5.47. Found: C, 63.24; H, 6.30; N, 5.37.

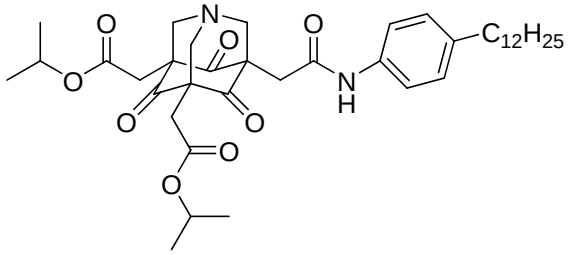

Mono-(4-dodecyl-phenylamine)-di-isopropyl ester 1-aza-adamantanetriones (3-5b). This compound was synthesized from **3-4b** (0.34 g, 0.54 mmol) and HMTA (229 mg, 1.62 mmol) according to the same procedure used for **3-5a** to afford **3-5b** (0.18 g, 49%) as an off-white solid: m.p. 133–135 °C. ^{1}H NMR (300 MHz, $CDCl_3$) δ 0.88 (t, 3H, J = 7.2 Hz), 1.23 (m, 30H), 1.56 (m, 2H), 2.53 (t, 2H, J = 7.2 Hz), 2.73 (s, 4H), 2.89 (s, 2H), 3.76 (m, 6H), 4.98 (m, 2H), 7.10 (d, 2H, J = 7.8 Hz), 7.38 (d, 2H, J = 7.8 Hz), 7.93 (s, 1H). ^{13}C NMR (75 MHz, $CDCl_3$) δ 14.34, 21.87, 22.91, 29.47, 29.58, 29.74, 29.86, 29.90, 31.78, 32.14, 32.43, 34.92, 35.60, 68.70,

70.51, 70.63, 70.74, 71.12, 120.20, 129.00, 135.55, 139.37, 167.59, 169.30, 197.24, 198.20. HRMS (ESI, $(M+Na)^+$) calcd for $C_{39}H_{56}N_2O_8$: 703.3929; found: 703.3937.

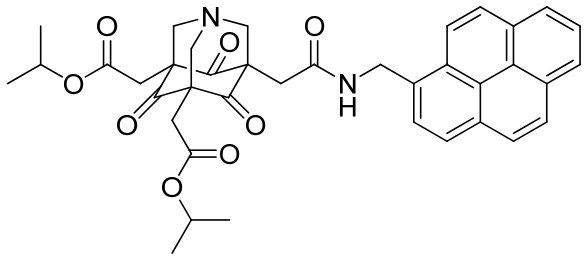

Mono-1-pyrenmethylamine-di-isopropyl ester 1-aza-adamantanetriones (3-5c). A solution of **3-4c** (0.56 g, 0.89 mmol), HMTA (374 mg, 2.66 mmol), and isopropanol (10 mL) was heated to reflux for 36 h under a blanket of argon. After cooling the reaction mixture to room temperature, the solvent was removed in vacuo and the residue was dissolved in ethyl acetate. The organic layer was washed with 1N HCl and brine. The solution was then concentrated to a crude oil and purified via column chromatography (CH2Cl2/MeOH = 100/2) to afford **3-5c** (0.29 g, 45%) as an off-white solid: m.p. 197–199 °C. ^{1}H NMR (300 MHz, DMSO-d_6) δ 1.55 (d, 12H, J = 6.6 Hz), 2.64 (s, 6H), 3.72 (s, 4H), 3.92 (s, 2H), 4.81 (m, 2H), 4.99 (d, 2H, J = 5.4 Hz). ^{13}C NMR (75 MHz, DMSO-d_6) δ 20.84, 31.31, 66.71, 69.33, 69.53, 70.13, 122.83, 124.13, 124.56, 124.64, 125.69, 126.03, 126.42, 126.86, 126.93, 129.50, 129.79, 130.27, 132.47, 168.03, 168.06, 197.19, 197.35. HRMS (ESI, $(M+Na)^+$) calcd for $C_{38}H_{38}N_2O_8$: 673.2520; found: 673.2537.

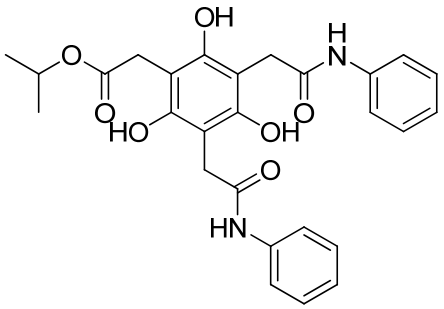

Isopropyl 2-(2,4,6-trihydroxy-3,5-bis(2-oxo-2-(phenylamino)ethyl)phenyl)acetate (3-6a). A stirring solution of **3-1b** (380 g, 1.24 mmol) in DMF (10 mL) was treated with aniline (220 mg, 2.36 mmol) and heated to 120 °C for 12 h. The solution was then concentrated to a crude oil and purified via column chromatography (hexanes/EtOAc = 1/1) to afford **3-6a** (0.41 g, 68%) as an off-white solid: m.p. 151–153 °C. ^{1}H NMR (300 MHz, DMSO-d_6) δ 1.19 (d, 6H, J = 6.3 Hz), 3.53 (s, 2H), 3.69 (s, 4H), 4.88 (m, 1H, J = 6.3 Hz), 7.05 (t, 2H, J = 8.1 Hz), 7.60 (d, 4H, J = 8.1 Hz), 8.92 (s, 2H), 9.22 (s, 1H), 10.18 (s, 2H). ^{13}C NMR (75 MHz, DMSO-d_6) δ 22.54, 30.60, 33.26, 67.66, 120.17, 124.28, 139.60, 140.05, 140.31, 154.15, 172.07, 172.45. HRMS (ESI, $(M+H)^+$) calcd for $C_{30}H_{31}N_3O_7$: 493.1969; found: 493.1953.

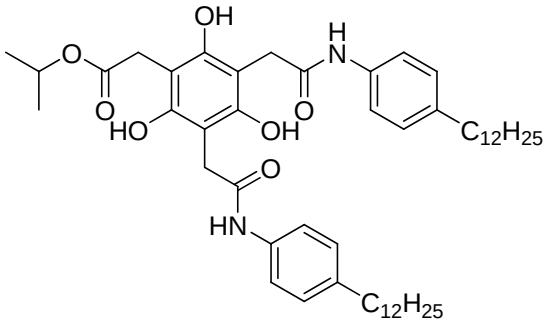

Isopropyl 2-(3,5-bis(2-(4-dodecylphenylamino)-2-oxoethyl)-2,4,6-trihydroxyphenyl)-acetate (3-6b). This compound was synthesized from **3-1b** (0.50 g, 1.7 mmol) and 4-dodecyl-aniline (0.30 g, 3.3 mmol) according to the same procedure used for **3-6a** to afford **3-6b** (0.33 g, 44%) as a yellow solid. ^{1}H NMR (300 MHz, DMSO-d_6) δ 0.85 (t, 6H, J = 6.0 Hz), 1.20 (m, 48

H), 1.52 (m, 4H), 3.52 (s, 2H), 3.67 (s, 4H), 4.87 (m, 1H, J = 6.3 Hz), 7.10 (d, 4H, J = 7.8 Hz), 7.47 (d, 4H, J = 7.8 Hz), 9.01 (s, 2H), 9.37 (s, 1H), 10.13 (s, 2H). ^{13}C NMR (75 MHz, DMSO-d_6) δ 13.95, 21.71, 22.10, 28.57, 28.70, 28.85, 29.00, 30.97, 31.28, 32.41, 34.53, 66.81, 103.19, 119.46, 128.39, 136.32, 137.52, 153.15, 171.27, 171.56. HRMS (ESI, $(M+H)^+$) calcd for $C_{54}H_{79}N_3O_7$: 829.5725; found: 829.5737.

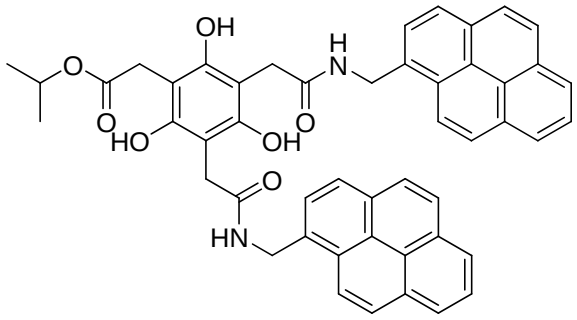

Isopropyl 2-(2,4,6-trihydroxy-3-(2-oxo-2-(pyren-1-ylmethylamino)ethyl)-5-(2-oxo-2-(pyren-2-ylmethylamino)ethyl)phenyl)acetate (3-6c). A stirring solution of **3-1b** (0.31 g, 1.0 mmol) in CH_3CN (10 mL) was treated with 1-pyrenmethylamine hydrochloride (0.54 g, 2.0 mmol) and DMAP (0.32 g, 2.6 mmol) then heated to reflux for 12 h. The solution was then concentrated to a crude oil and purified via column chromatography (CH_2Cl_2/MeOH = 100/1) to afford **3-6c** (0.56 mg, 73%) as a yellow solid. ^{1}H NMR (300 MHz, DMSO-d_6) δ 1.17 (d, 6H, J = 6.3 Hz), 3.50 (s, 2H), 3.60 (s, 4H), 4.87 (m, 1H), 5.02 (d, 4H, J = 5.4 Hz), 8.15 (m, 18H), 9.02 (s, 1H), 9.53 (s, 2H), 10.14 (s, 1H). HRMS (ESI, $(M+H)^+$) calcd for $C_{49}H_{40}N_2O_7$: 791.2728; found: 791.2704.

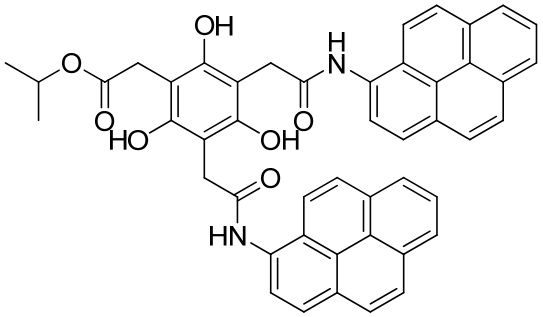

Isopropyl 2-(3-(2-dihydropyren-4-ylamino)-2-oxoethyl)-2,4,6-trihydroxy-5-(2-oxo-2-(pyren-4-ylamino)ethyl)phenyl)acetate (3-6d). This compound was synthesized from **3-1b** (0.31 g, 1.0 mmol) and 1-pyrenamine (0.43 g, 2.0 mmol) according to the same procedure used for **3-6a** to afford **3-6d** (0.38 g, 51%) as an off-white solid. ^{1}H NMR (300 MHz, DMSO-d_6) δ 1.17 (d, 6H, J = 6.3 Hz), 3.62 (s, 2H), 4.00(s, 4H), 4.91 (m, 1H), 8.15 (m, 18H), 9.09 (s, 2H), 9.55 (s, 1H), 10.46 (s, 2H). ^{13}C NMR (75 MHz, DMSO-d_6) δ 13.51, 20.18, 21.16, 29.36, 31.75, 59.17, 66.33, 102.93, 103.30, 121.56, 122.66, 123.27, 123.75, 124.35, 124.69, 125.80, 126.10, 126.65, 127.83, 129.85, 130.24, 130.85, 153.08, 153.24, 170.77, 171.90. HRMS (ESI, $(M+Na)^+$) calcd for $C_{47}H_{38}N_2O_7$: 763.2415; found: 763.2390.

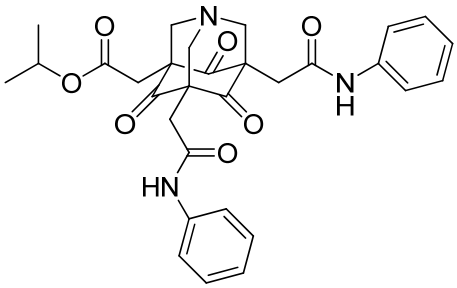

Di-phenylamine-mono-isopropyl ester 1-aza-adamantanetrione (3-7a). A solution of **3-6a** (0.41 g, 0.80 mmol), HMTA (0.22 g, 1.6 mmol) and isopropanol (5 mL) was heated to reflux overnight under a blanket of argon. After cooling the reaction mixture to room temperature, the solvent was removed in vacuo and the residue was dissolved in ethyl acetate. The organic layer

was washed with 1N HCl and brine. The solution was then concentrated to a crude oil and purified via column chromatography (CH_2Cl_2/MeOH = 20/1) to afford **3-7a** (0.21 g, 47%) as a white solid: m.p. 240–241 °C. ^{1}H NMR (300 MHz, DMSO-d_6) δ 1.13 (d, 6H, J = 6.0 Hz), 2.63 (s, 2H), 2.77 (s, 4H), 3.73 (s, 2H), 3.90 (s, 4H), 4.80 (m, 1H, J = 6.6 Hz), 7.00 (t, 2H, J = 7.2 Hz), 7.26 (t, 4H, J = 7.8 Hz), 7.53 (d, 4H, J = 7.5 Hz), 10.01 (s, 2H). ^{13}C NMR (75 MHz, DMSO-d_6) δ 11.75, 22.05, 34.40, 67.98, 70.64, 70.79, 71.26, 119.47, 123.53, 129.31, 140.05, 168.12, 169.29, 198.72, 198.96. HRMS (ESI, $(M+H)^+$) calcd for $C_{30}H_{31}N_3O_7$: 546.2235; found: 546.2271.

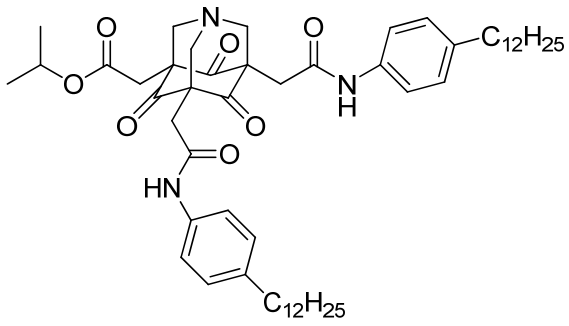

Di-(4-dodecyl-phenylamine)-mono-isopropyl ester 1-aza-adamantanetrione (3-7b). This compound was synthesized from **3-6b** (510 mg, 0.615 mmol) and HMTA (172 mg, 1.23 mmol) according to the same procedure used for **3-7a** to afford **3-7b** (0.21 g, 38%) as an off-white solid: m.p. 194–195 °C. ^{1}H NMR (300 MHz, DMSO-d_6) δ 0.85 (t, 6H, J = 6.3 Hz), 1.13 (d, 6H, J = 6.3 Hz), 1.22 (m, 36H), 1.51 (m, 4H), 2.46 (t, 4H, J = 6.6 Hz), 2.62 (s, 2H), 2.74 (s, 4H), 3.72 (s, 2H), 3.89 (s, 4H), 4.81 (m, 1H), 7.05 (d, 4H, J = 7.8 Hz), 7.42 (d, 4H, J = 8.4 Hz), 9.90 (s, 2H). ^{13}C NMR (75 MHz, DMSO-d_6) δ 13.95, 21.36, 22.10, 28.56, 28.71, 28.87, 29.02, 31.04, 31.29, 31.88, 34.52, 67.26, 70.04, 70.11, 70.54, 118.83, 128.23, 136.68, 137.11, 167.14,

168.55, 197.70, 197.92. HRMS (ESI, $(M+H)^+$) calcd for $C_{54}H_{79}N_3O_7$: 882.5991; found: 882.5976.

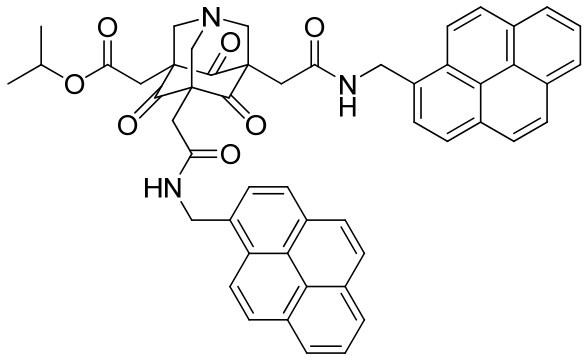

Di-1-pyrenmethylamine-mono-isopropyl ester 1-aza-adamantanetrione (3-7c). A solution of **3-6c** (0.12 g, 0.16 mmol), HMTA (66 mg, 0.47 mmol) and isopropanol (10 mL) was heated to reflux 2 days under a blanket of argon. After cooling the reaction mixture to room temperature, the solvent was removed in vacuo and the residue was dissolved in ethyl acetate. The organic layer was washed with 1N HCl and brine. The solution was then concentrated to a crude oil and purified via column chromatography (CH_2Cl_2/MeOH = 20/1) to afford **3-7c** (65 mg, 46%) as an off-white solid: m.p. 218–220 °C. ^{1}H NMR (300 MHz, DMSO-d_6) δ 1.15 (d, 6H, J = 6.0 Hz), 2.66 (s, 2H), 2.68 (s, 4H), 3.75 (s, 2H), 3.93 (s, 4H), 4.82 (m, 1H), 5.00 (d, 4H, J = 6.0 Hz), 8.21 (m, 18 H), 8.66 (t, 2H, J = 5.4 Hz). ^{13}C NMR (75 MHz, DMSO-d_6) δ 22.10, 33.29, 70.62, 70.80, 71.16, 124.00, 124.62, 124.68, 125.37, 125.78, 125.85, 126.89, 127.16, 127.62, 128.07, 128.16, 128.70, 130.69, 131.01, 131.48, 133.70, 169.39, 169.49, 198.68, 198.93. HRMS (MMI(APCI)–TOF, $(M+Na)^+$) calcd for $C_{52}H_{43}N_3O_7$: 844.2993; found: 844.3042.

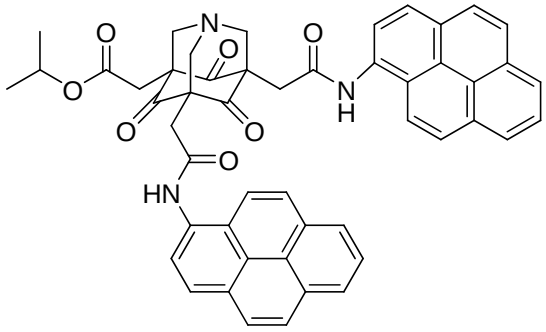

Di-1-pyrenamine-mono-isopropyl ester 1-aza-adamantanetrione (3-7d). This compound was synthesized from **3-6d** (0.33 g, 0.45 mmol) and HMTA (190 mg, 1.35 mmol) according to the same procedure used for **3-7c** to afford **3-7d** (0.22 g, 62%) as an off-white solid: m.p. 246– 248 °C. ^{1}H NMR (300 MHz, DMSO-d_6) δ 1.18 (d, 6H, J = 6.0 Hz), 2.72 (s, 2H), 3.09 (m, 4H), 3.82 (s, 2H), 4.09 (m, 4H), 4.85 (m, 1H), 8.19 (m, 18H), 10.44 (s, 2H). ^{13}C NMR (75 MHz, DMSO-d_6) δ 14.78, 21.46, 22.13, 32.69, 34.16, 60.45, 68.00, 70.81, 71.29, 123.32, 123.97, 124.58, 125.06, 125.43, 125.53, 125.78, 126.98, 127.14, 127.57, 127.93, 128.77, 131.16, 131.52, 132.73, 169.42, 169.49, 198.77, 199.22. HRMS (MMI(APCI)–TOF, $(M+Na)^{+}$) calcd for $C_{50}H_{38}N_3O_7$: 816.2680; found: 816.2728.

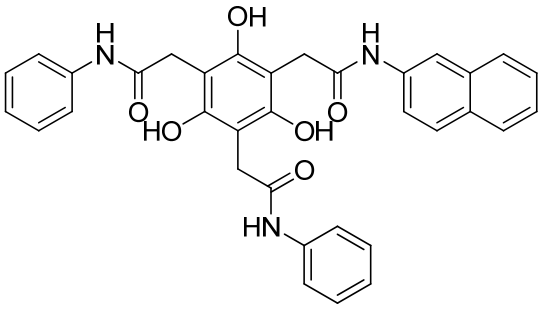

2,2'-(2,4,6-Trihydroxy-5-(2-(naphthalen-2-ylamino)-2-oxoethyl)-1,3-phenylene)bis(*N*-phenylacetamide) (3-8a). A stirring solution of **3-3a** (86 mg, 0.20 mmol) in DMF (5 mL) was treated with β-naphthylamine (34 mg, 0.24 mmol) and heated to 120 °C for 12 hours. The

solvent was removed in vacuo and the residue was dissolved in ethyl acetate. The organic layer was washed with 10% HCl and water. The combined organic layers were dried with Na_2SO_4. The solvent was removed on a rotary evaporator and the crude product was purified by column chromatography (hexane/EtOAc 1:1) to afford a yellow solid (80 mg, 70%). ^{1}H NMR (300 MHz, DMSO-d_6) δ 3.73 (s, 4H), 3.78 (s, 2H), 7.05 (t, 2H, J = 7.5 Hz), 7.30 (t, 4H, J = 7.5 Hz), 7.43 (m, 2H), 7.62 (m, 5H), 7.85 (m, 3H), 8.28 (s, 1H), 9.31 (s, 2H), 9.32 (s, 1H), 10.19 (s, 2H), 10.37 (s, 1H). ^{13}C NMR (75 MHz, DMSO-d_6) δ 13.58, 20.26, 31.86, 59.25, 102.94, 105.26, 115.01, 117.88, 118.85, 119.55, 120.32, 122.91, 124.5, 125.33, 125.8, 125.9, 126.82, 126.95, 127.84, 127.96, 128.23, 129.29, 132.87, 134.49, 136.02, 138.41, 146.14, 153.15, 171.09, 171.26. HRMS (ESI, $(M+Na)^+$) calcd for $C_{34}H_{29}N_3O_6$: 598.1949; found: 598.1944.

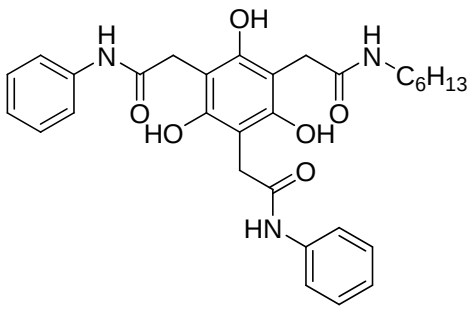

2,2'-(5-(2-(Hexylamino)-2-oxoethyl)-2,4,6-trihydroxy-1,3-phenylene)bis(N-phenylacetamide) (3-8b). A stirring solution of **3-3a** (90 mg, 0.21 mmol) in DMF (5 mL) was treated with *n*-hexylamine (0.030 mL, 0.25 mmol) and stirred at room temperature for 3 h. The solvent was removed in vacuo and the residue was dissolved in ethyl acetate (10 mL). The organic layer was washed with 10% HCl and water. The combined organic layers were dried with Na_2SO_4. The solvent was removed on a rotary evaporator and the crude product was purified by column chromatography (hexane/EtOAc 3:2) to afford **3-8b** as an off-white solid (89 mg, 80%). ^{1}H NMR (300 MHz, DMSO-d_6) δ 0.84 (t, 3H, J = 7.2 Hz), 1.30 (m, 8H), 3.05 (m,

2H), 3.50 (s, 2H), 3.69 (s, 4H), 7.05 (t, 2H, J = 7.2 Hz), 7.29 (t, 4H, J = 7.5 Hz), 7.59 (d, 4H, J = 8.4 Hz), 8.46 (br, 1H), 9.36 (s, 1H), 9.94 (s, 2H), 10.17 (s, 2H). ^{13}C NMR (75 MHz, DMSO-d_6) δ 13.39, 21.51, 25.53, 28.11, 30.39, 31.72, 102.26, 102.90, 118.82, 122.85, 128.19, 138.46, 153.11, 153.30, 171.05, 173.17. HRMS (ESI, $(M+H)^+$) calcd for $C_{30}H_{35}N_3O_6$: 534.2599; found: 534.2597.

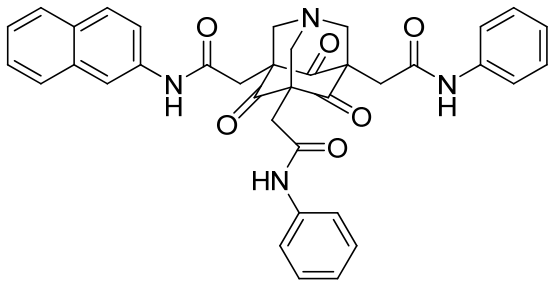

Mono-β-naphthylamine-di-phenylamine 1-aza-adamantanetrione (3-9a). A solution of **3-8a** (90 mg, 0.16 mmol), HMTA (66 mg, 0.48 mmol) and isopropanol (5 mL) was heated to reflux 2 days under a blanket of argon. After cooling the reaction mixture to room temperature, the mixture was filtered to afford an off-white solid. The solid was washed with 5% HCl and water to afford **3-9a** (41 mg, 43%) as an off-white solid. ^{1}H NMR (300 MHz, DMSO-d_6) δ 2.79 (s, 4H), 2.85 (s, 2H), 3.95 (s, 6H), 6.99 (t, 2H, J = 7.5 Hz), 7.26 (t, 4H, J = 7.8 Hz), 7.45 (m, 8H), 7.81 (m, 3H), 8.27 (s, 1H), 10.01 (s, 2H), 10.23 (s, 1H). ^{13}C NMR (75 MHz, DMSO) δ 33.21, 69.71, 69.88, 114.19, 118.35, 119.28, 122.33, 123.85, 125.81, 126.69, 126.88, 127.72, 128.08, 129.03, 132.95, 136.36, 138.80, 167.03, 167.28, 197.79. HRMS (ESI, $(M+Na)^+$) calcd for $C_{37}H_{32}N_4O_6$: 651.2214; found: 651.2208.

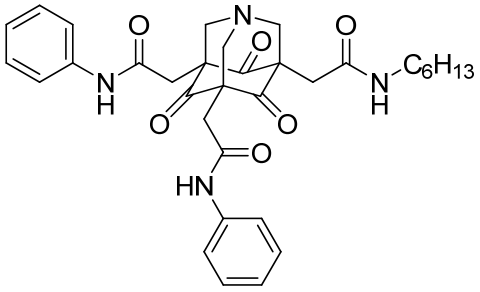

Mono-hexylamine-di-phenylamine 1-aza-adamantanetrione (3-9b). This compound was synthesized from **3-8b** (53 mg, 0.10 mmol) and HMTA (28 mg, 0.20 mmol) according to the same procedure used for **3-5a** to afford **3-9b** (32 mg, 48%) as a white solid. ^{1}H NMR (300 MHz, pyridine-d_5) δ 0.79 (t, 3H, J = 6.6 Hz), 1.13 (m, 6H), 1.53 (m, 2H, J = 7.2 Hz), 3.14 (s, 2H), 3.28 (s, 4H), 3.39 (m, 2H, J = 6.0 Hz), 4.27 (s, 4H), 4.34 (s, 2H), 7.08 (t, 2H, J = 7.5 Hz), 7.32 (t, 4H, J = 7.8 Hz), 7.95 (d, 2H, J = 7.8 Hz), 8.45 (t, 1H, J = 7.2 Hz), 10.96 (s, 2H). ^{13}C NMR (75 MHz, pyridine-d_5) δ 14.50, 23.15, 27.31, 30.30, 32.05, 34.27, 35.26, 40.19, 71.36, 71.53, 71.62, 120.49, 129.47, 140.85, 169.19, 169.99, 199.66, 199.69. HRMS (ESI, $(M+Na)^+$) calcd for $C_{33}H_{38}N_4O_6$: 609.2684; found: 609.2718.

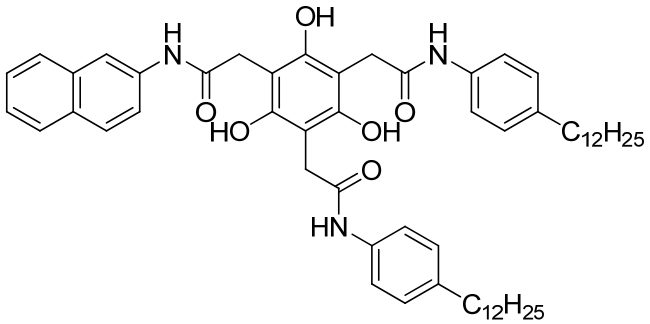

2,2'-(2,4,6-Trihydroxy-5-(2-(naphthalen-2-ylamino)-2-oxoethyl)-1,3-phenylene)bis(*N*-(4-dodecylphenyl)acetamide) (3-10b). This compound was synthesized from **2-10** (90 mg, 0.23 mmol) and *p*-dodecylaniline (0.29 g, 0.93 mmol) according to the same procedure used for **2-11** to afford **3-10b** (76 mg, 36%) as a yellow solid. ^{1}H NMR (300 MHz, DMSO-d_6) δ 0.84 (t, 6H, J

= 7.2 Hz), 1.20 (m, 36H), 1.51 (m, 4H), 2.50 (m, 4H), 3.71 (s, 4H), 3.77 (s, 2H), 7.09 (d, 4H, J = 8.7 Hz), 7.48 (m, 6H), 7.62 (m, 1H), 7.83 (m, 3H), 8.29 (s, 1H), 9.40 (s, 2H), 9.48 (s, 1H), 10.14 (2H), 10.38 (s, 1H). ^{13}C NMR (75 MHz, DMSO-d_6) δ 14.66, 22.79, 29.28, 29.41, 29.55, 29.69, 31.69, 31.98, 33.01, 35.23, 104.10, 104.20, 116.18, 120.17, 120.74, 127.09, 128.02, 128.13, 129.03, 129.12, 130.47, 134.07, 137.16, 137.24, 138.17, 154.37, 172.24, 172.45. HRMS (ESI, $(M+Na)^+$) calcd for $C_{58}H_{77}N_3O_6$: 912.5885; found: 912.5852.

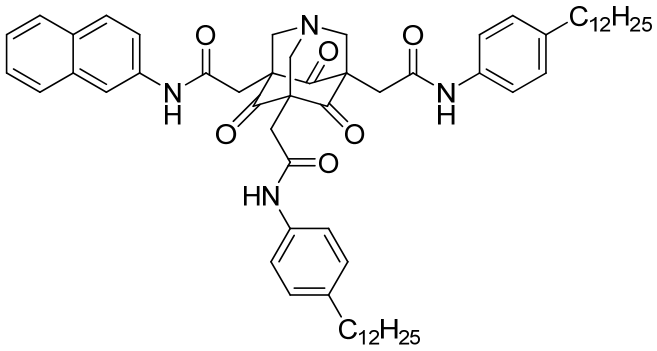

Mono-β-naphthylamine-di-*p*-dodecylphenylamine 1-aza-adamantantrione (3-11b).

This compound was synthesized from **3-10b** (0.08 g, 0.08 mmol) and HMTA (34 mg, 0.24 mmol) according to the same procedure used for **3-8a** to afford **3-11b** (38 mg, 49%) as a white solid. ^{1}H NMR (300 MHz, pyridine-d_5) δ 0.88 (t, 6H, J = 7.2 Hz), 1.27 (m, 34H), 1.61 (m, 4H), 2.57 (t, 4H, J = 7.2 Hz), 3.32 (s, 4H), 3.36 (s, 2H), 4.32 (s, 6H), 7.43 (m, 3H), 7.82 (m, 4H), 7.93 (m, 4H), 8.68 (m, 4H), 10.87 (s, 2H), 11.11 (s, 1H). ^{13}C NMR (75 MHz, pyridine-d_5) δ 14.65, 23.30, 29.87, 29.97, 30.18, 30.26, 30.32, 32.35, 32.47, 35.22, 35.92, 71.43, 71.69, 116.90, 120.59, 121.12, 123.16, 127.08, 128.23, 128.36, 129.13, 129.40, 131.08, 138.42, 138.55, 168.95, 169.26, 198.44, 199.74. HRMS (ESI, $(M+Na)^+$) calcd for $C_{61}H_{80}N_4O_6$: 987.5976; found: 987.6036.

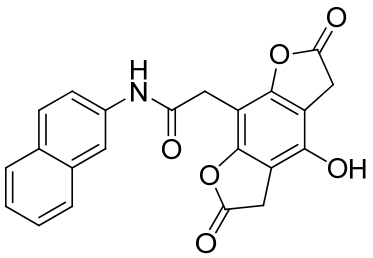

2-(4-Hydroxy-2,6-dioxo-2,3,5,6-tetrahydrobenzofuro[6,5-b]furan-8-yl)-*N*-(naphthalen-2-yl)acetamide (2-10). A solution of **2-9b** (0.2 g, 0.3 mmol), TFA (0.6 mL, 8 mmol) and toluene (10 mL) was heated at 80–90 °C for 2 h under a blanket of argon. After cooling the reaction mixture to room temperature, the solvent was removed by filtration and the resulting solid was washed with water to afford **2-10** (0.10 mg, 86%) as a peach-colored solid. ^{1}H NMR (300 MHz, DMSO-d_6) δ 3.72 (s, 2H), 3.83 (s, 4H), 7.43 (m, 2H), 7.59 (m, 1H), 7.82 (m, 3H), 8.28 (s, 1H), 10.25 (s, 1H), 10.38 (s, 1H). ^{13}C NMR (75 MHz, DMSO-d_6) δ 30.77, 94.43, 104.50, 114.63, 119.34, 123.99, 125.82, 126.68, 126.86, 127.78, 129.17, 132.84, 136.13, 147.26, 152.26, 166.97, 173.56. HRMS (ESI, $(M+Na)^+$) calcd for $C_{22}H_{15}NO_6$: 412.0792; found: 412.0788.

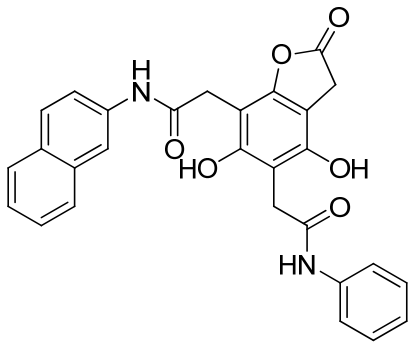

2-(4,6-Dihydroxy-2-oxo-5-(2-oxo-2-(phenylamino)ethyl)-2,3-dihydrobenzofuran-7-yl)-*N*-(naphthalen-2-yl)acetamide (3-12). A stirring solution of **2-10** (0.15 g, 0.46 mmol) in DMF (10 mL) was treated with aniline (0.17 mL, 1.9 mmol) and heated at 70−80 ºC for 12 h. The

solution was then concentrated to a crude oil and purified via column chromatography (hexanes/EtOAc = 1/1) to afford **3-12** (0.10 g, 65%) as a white solid: ^{1}H NMR (300 MHz, DMSO-d_6) δ 3.71 (s, 2H), 3.74 (s, 2H), 3.76 (s, 2H), 7.02 (t, 1H, J = 7.5 Hz), 7.29 (t, 2H, J = 7.8 Hz), 7.43 (m, 2H), 7.62 (m, 3H), 7.83 (m, 3H), 8.28 (s, 1H), 9.56 (s, 1H), 9.70 (s, 1H), 10.06 (s, 1H), 10.44 (s, 1H). ^{13}C NMR (75 MHz, DMSO-d_6) δ 13.54, 20.21, 31.15, 31.26, 59.20, 97.93, 100.06, 102.94, 106.20, 114.93, 118.53, 118.86, 119.46, 122.50, 124.10, 125.86, 126.77, 126.89, 127.82, 128.13, 129.27, 132.84, 136.00, 138.75, 149.96, 151.72, 153.13, 154.52, 169.39, 169.77, 169.82, 174.11. HRMS (ESI, $(M+Na)^+$) calcd for $C_{28}H_{22}N_2O_6$: 505.1370; found: 505.1369.

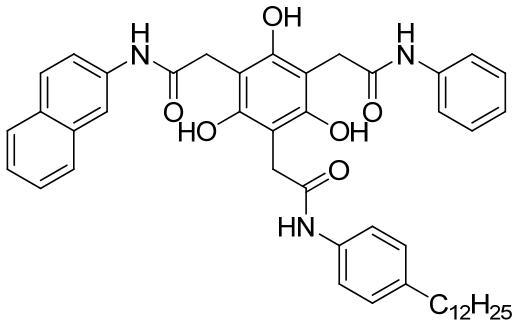

***N*-(4-Dodecylphenyl)-2-(2,4,6-trihydroxy-3-(2-(naphthalen-2-ylamino)-2-oxoethyl)-5-(2-oxo-2-(phenylamino)ethyl)phenyl)acetamide (3-13).** A stirring solution of **3-12** (60 mg, 0.13 mmol) in DMF (10 mL) was treated with 4-dodecylaniline (0.13 g, 0.50 mmol) and heated at 120 ºC for 12 h. The solution was then concentrated to a crude oil and purified via column chromatography (hexanes/EtOAc =3/1) to afford **3-13** (40 mg, 43%) as a brown solid: ^{1}H NMR (300 MHz, DMSO-d_6) δ 0.84 (t, 3H, J = 6.6 Hz), 1.22 (m, 18 H), 1.52 (m, 2H), 3.72 (s, 2H), 3.73 (s, 2H), 3.78 (s, 2H), 7.09 (m, 4H), 7.42 (m, 6H), 7.62 (m, 3H), 7.84 (m, 3H), 8.29 (s, 1H), 9.33 (s, 1H), 9.41 (s, 2H), 10.14 (s, 1H), 10.18 (s, 1H), 10.37 (s, 1H). ^{13}C NMR (75 MHz, DMSO-d_6) δ13.43, 21.57, 28.07, 28.18, 28.33, 28.48, 30.46, 30.77, 31.86, 34.03, 38.17, 102.90, 102.98, 115.03, 118.58, 118.87, 118.99, 119.56, 122.89, 124.12, 125.86, 126.80, 126.91, 127.90, 128.01,

128.13, 129.29, 132.86, 135.94, 136.01, 137.00, 138.40, 153.16, 171.06, 171.26. HRMS (ESI, $(M+Na)^+$) calcd for $C_{46}H_{53}N_3O_6$: 766.3827; found: 766.3867.

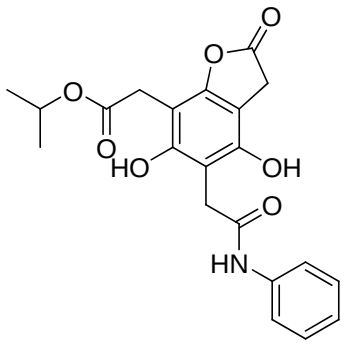

Isopropyl 2-(4,6-dihydroxy-2-oxo-5-(2-oxo-2-(phenylamino)ethyl)-2,3-dihydrobenzo-furan-7-yl)acetate (3-14). A stirring solution of **3-1b** (0.41 g, 1.3 mmol) in DMF (10 mL) was treated with aniline (0.13 mL, 1.3 mmol) and heated at 80 ºC overnight. The solution was then concentrated to a crude oil and purified via column chromatography (hexanes/EtOAc =2/1) to afford **3-14** (0.26 g, 49%) as a white solid: ^{1}H NMR (300 MHz, DMSO-d_6) δ 1.19 (d, 6H, J = 6.3 Hz), 3.51 (s, 2H), 3.69 (s, 2H), 3.74 (s, 2H), 4.89 (m, 1H, J = 6.3 Hz), 7.03 (t, 1H, J = 7.2 Hz), 7.29 (t, 2H, J = 7.2 Hz), 7.59 (d, 2H, J = 7.8 Hz), 9.30 (s, 1H), 9.56 (s, 1H), 10.11 (s, 1H). ^{13}C NMR (75 MHz, DMSO-d_6) δ 21.08, 28.96, 31.17, 66.93, 97.56, 100.02, 106.04, 118.57, 122.61, 128.16, 138.66, 149.87, 151.74, 154.10, 169.65, 170.02, 174.00. HRMS (ESI, $(M+Na)^+$) calcd for $C_{21}H_{21}NO_7$: 422.1210; found: 422.1212.

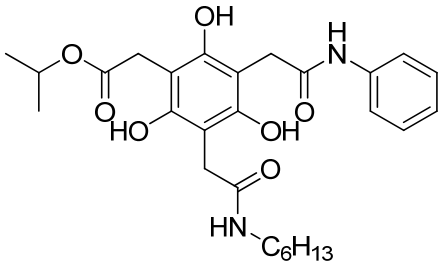

Isopropyl 2-(3-(2-(hexylamino)-2-oxoethyl)-2,4,6-trihydroxy-5-(2-oxo-2-(phenylamino)ethyl)phenyl)acetate (3-15a). A solution of **3-14** (0.10 g, 0.25 mmol) in DMF (5 mL) was treated with hexylamine (0.04 mL, 0.3 mmol) and stirred at room temperature for 1.5 h. The solution was then concentrated to a crude oil and purified via column chromatography (hexanes/EtOAc =2/1) to afford **3-15** (0.11 g, 88%) as a white solid: m.p. 64–65 °C. ^{1}H NMR (300 MHz, $CDCl_3$) δ 0.85 (t, 3H, J = 7.2 Hz), 1.26 (m, 12H), 1.45 (m, 2H, J = 6.9 Hz), 3.17 (q, 2H, J = 7.2 Hz), 3.60 (s, 1H), 3.76 (s, 2H), 3.77 (s, 2H), 5.02 (m, 1H, J = 6.3 Hz), 6.25 (t, 1H, J = 5.4 Hz), 7.12 (m, 1H), 7.26 (m, 2H), 7.46 (m, 2H), 8.13 (s, 1H), 9.21 (s, 1H), 9.49 (s, 1H), 9.73 (s, 1H). ^{13}C NMR (75 MHz, DMSO-d_6) δ 13.45, 21.19, 22.01, 25.99, 28.68, 30.10, 30.88, 32.09, 33.29, 39.66, 69.57, 102.06, 102.73, 103.17, 120.04, 124.52, 128.47, 136.72, 153.32, 153.39, 153.65, 172.42, 174.04, 175.59. HRMS (ESI, $(M+H)^+$) calcd for $C_{27}H_{36}N_2O_7$: 501.2595; found: 501.2634.

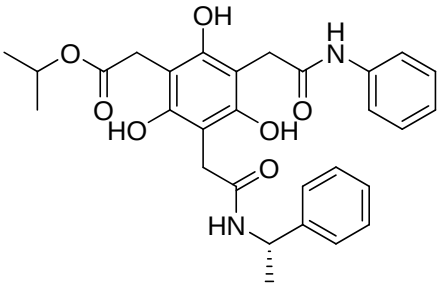

(*S*)-Isopropyl 2-(2,4,6-trihydroxy-3-(2-oxo-2-(1-phenylethylamino)ethyl)-5-(2-oxo-2-(phenylamino)ethyl)phenyl)acetate (3-15b). This compound was synthesized from **3-14** (0.2 g,

0.5 mmol) and L-(-)-α-methylbenzylamine (0.08 mL, 0.6 mmol) according to the same procedure used for **3-15a** to afford **3-15b** (0.24 g, 92%) as a yellow solid: $[\alpha]^{24}_{D} = -20.3$ (c 0.52, $CHCl_3$). ^{1}H NMR (300 MHz, $CDCl_3$) δ 1.29 (m, 6H), 1.49 (d, 3H, J = 6.6 Hz), 3.65 (m, 2H), 3.77 (d, 4H, J = 4.2 Hz), 5.04 (m, 1H), 6.35 (d, 1H, J = 7.2 Hz), 7.16 (m, 1H), 7.28 (m, 6H), 7.50 (d, 1H, J = 8.4 Hz), 7.92(s, 1H), 9.20 (s, 1H), 9.41 (s, 1H), 9.90 (s, 1H). ^{13}C NMR (75 MHz, $CDCl_3$) δ 21.63, 21.77, 30.53, 32.56, 33.70, 49.53, 70.07, 102.51, 103.21, 103.49, 120.42, 124.96, 125.98, 127.51, 128.74, 128.92, 137.13, 142.30, 153.75, 153.83, 154.02, 172.84, 173.72, 176.10. HRMS (MMI(APCI)–TOF, $(M+H)^+$) calcd for $C_{29}H_{32}N_2O_7$: 521.2282; found: 521.2306.

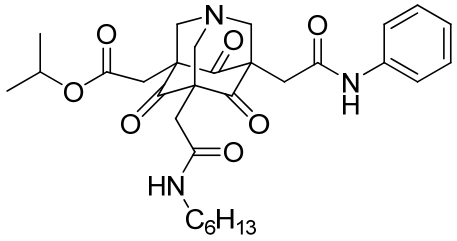

Mono-phenylamine-mono-hexylamine-mono-isopropyl ester 1-aza-adamantanetrione (3-16). A solution of **3-15a** (50 mg, 0.10 mmol), HMTA (28 mg, 0.20 mmol) and isopropanol (5 mL) was heated to reflux overnight under a blanket of argon. After cooling the reaction mixture to room temperature, the solvent was removed on a rotary evaporator and the residue was purified by column chromatography (ethyl acetate/triethylamine = 100/1) to afford **3-16** (16 mg, 42%) as a yellow solid. ^{1}H NMR (300 MHz, $CDCl_3$) δ 0.86 (t, 3H, J = 6.9 Hz), 1.26 (m, 18H), 2.69 (s, 2H), 2.74 (s, 2H), 2.89 (s, 2H), 3.20 (q, 2H, J = 6.6 Hz), 3.72 (s, 2H), 3.82 (q, 3H, J = 13.5 Hz), 4.97 (p, 1H, J = 6.3 Hz), 5.95 (t, 1H, J = 6.6 Hz), 7.09 (t, 1H, J = 7.5 Hz), 7.30 (t, 2H, J = 7.2 Hz), 7.49 (d, 2H, J = 7.8 Hz), 7.98 (s, 1H). ^{13}C NMR (75 MHz, $CDCl_3$) δ 14.00, 21.66, 22.54, 26.55, 29.39, 31.42, 32.25, 33.62, 34.86, 39.73, 68.54, 70.30, 70.44, 70.49, 70.55, 70.81,

119.89, 124.36, 128.92, 137.71, 167.30, 168.83, 169.17, 197.48, 197.82, 198.37. HRMS (ESI, $(M+Na)^+$) calcd for $C_{30}H_{39}N_3O_7$: 576.2680; found:576.2639.

CHAPTER 4
EFFORTS TOWARD HYDROPHILIC AND HYDROGELATING AATS

Introduction of Hydrogels and Their Broad Applications

Hydrogels are a class of biomaterials that have broad applications in drug delivery, three-dimensional cell cultures, screening biomolecules, wound healing, and tissue engineering.[200-202] Typically hydrogelation is a property of polymeric species of the right molecular composition, however the discovery and design of small organic molecules capable of gelling aqueous solvents is a rapidly expanding area of research.[95] Such gels are referred to as "supramolecular hydrogels", and the small molecules are referred to as "supramolecular hydrogelators" or "molecular hydrogelators".[200] Low-molecular weight hydrogelators offer several advantages over polymeric versions, but most notably they biodegrade more easily since they are generally derived from small, biocompatible components that are held together by noncovalent forces.[95]

Assembly of small organic molecules in aqueous solvents into fibrous structures poses interesting challenges in the field of self-assembly. To achieve gelation, there must be a balance between the tendency of the molecules to molecularly dissolve or to aggregate.[95] Hydrophobic forces become important for assembly in aqueous environments while hydrogen bonding (vide supra), a common driving force for aggregation, plays a secondary role.[95] Generally in hydrogelator design, functional groups are selected that are both hydrophilic and provide good solubility in water.[201] Among these, polyethylene glycol units are commonly used in supramolecular hydrogelator construction.[201, 202] Figure 4-1 shows one example of a monomer that forms hydrogels primarily by hydrophobic interactions, and secondarily through hydrogen bonding.[201] The center of the molecule features a bisurea motif that is well known to form strong hydrogen bonds in low polarity environments, in this case fostered, upon hydrophobic assembly,

by the nearby alkyl chain segments. The polyethylene glycol tails in the outer region are hydrophilic and directly interact with the solvent.

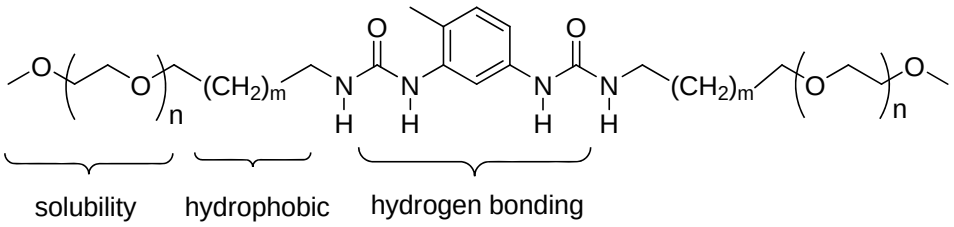

Figure 4-1. A bisurea based supramolecular polymer that forms hydrogels.[201]

The design of new hydrogelators is a rapid expanding area of research especially due to their possible practical applications.[95] The AATs are known to self-assemble in and gel organic solvents such as chloroform, DMSO, toluene, and benzene through hydrogen bonding, aromatic interactions, and dipolar interactions. The introduction of hydrophilic groups (side chains), such as polyethylene glycol units, to the AAT molecules should increase their hydrophilic character and possibly allow the formation of the first hydrogels from donor-σ-acceptor molecules.

Synthesis of Hydrophilic AATs

Discussed in Chapter 3, the lactone methodology allows incorporation of sensitive/labile functional groups into the AAT periphery at a late synthetic stage. Prior to the development of this methodology, polyethylene glycol units (the most commonly employed hydrophilic functional groups for hydrogelator design) were incompatible with the otherwise harsh BBr_3 demethylation chemistry (Figure 3-1). The lactone strategy overcomes this limitation and allows for the introduction polyethers into the AAT periphery where they can influence the self-assembly and hydrophilic properties of the molecules.

To test this methodology in the context of simple oligoethers, (aminomethoxy)methanol was selected as the peripheral functional group. The more reactive amino functionality should selectively ring open the lactone intermediates discussed in Chapter 3. Initial reactions between

the unprotected aminoalcohol and tripentenolides (shown in Figure 4-2) led to water soluble but intractable products.

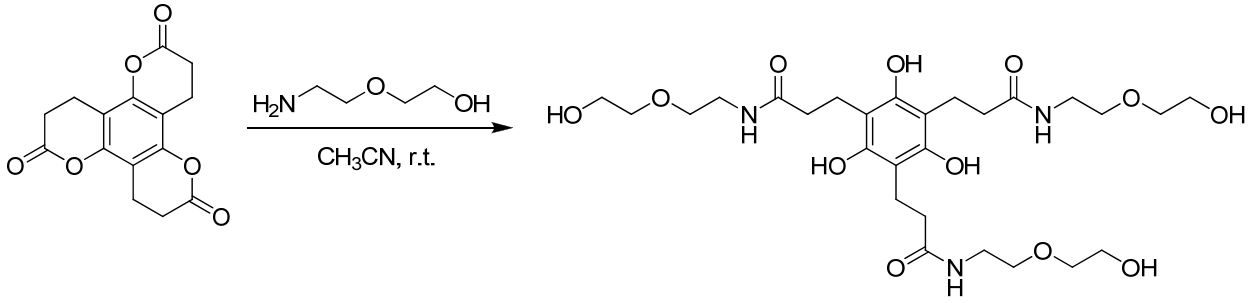

Figure 4-2. Initial reaction between the unprotected aminoalcohol and tripentenolides.

To help with purification and reduce side reactions, the (aminomethoxy)-methanol was alternatively first protected as its TBS ether (Figure 4-3).[203] Compound **4-1** was then used as the nucleophile in reactions with mono-, di-, and trilactones derived from the butenolides and pentenolides. Subsequent cyclization with HMTA affords intermediates en route to the first hydrophilic AATs (Figure 4-3).

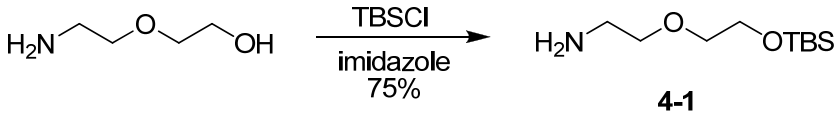

Figure 4-3. The synthesis of protected ethylene glycol building block.

Reaction of primary amine **4-1** with the butenolides occurs at room temperature in DMF to afford the corresponding substituted phloroglucinol derivatives in moderate yields (Figure 4-4). Subsequent AAT formation occurs using the same conditions as described previously, but the purification of the polar systems is challenging. Compounds **4-3a** and **4-3b** were successfully isolated after column chromatography using pure ethyl acetate; C_3-symmetric **4-3c**, observed by mass spectrometric analysis, could not be purified and isolated in this fashion. One reason is that the species is hard to visualize on silica gel even with UV light or staining ($KMnO_4$, *p*-

anisaldehyde, cerium molybdate, and phosphomolybdic acid were tried). $KMnO_4$ remains the most successful stain used to date that allows visualization at high product concentrations.

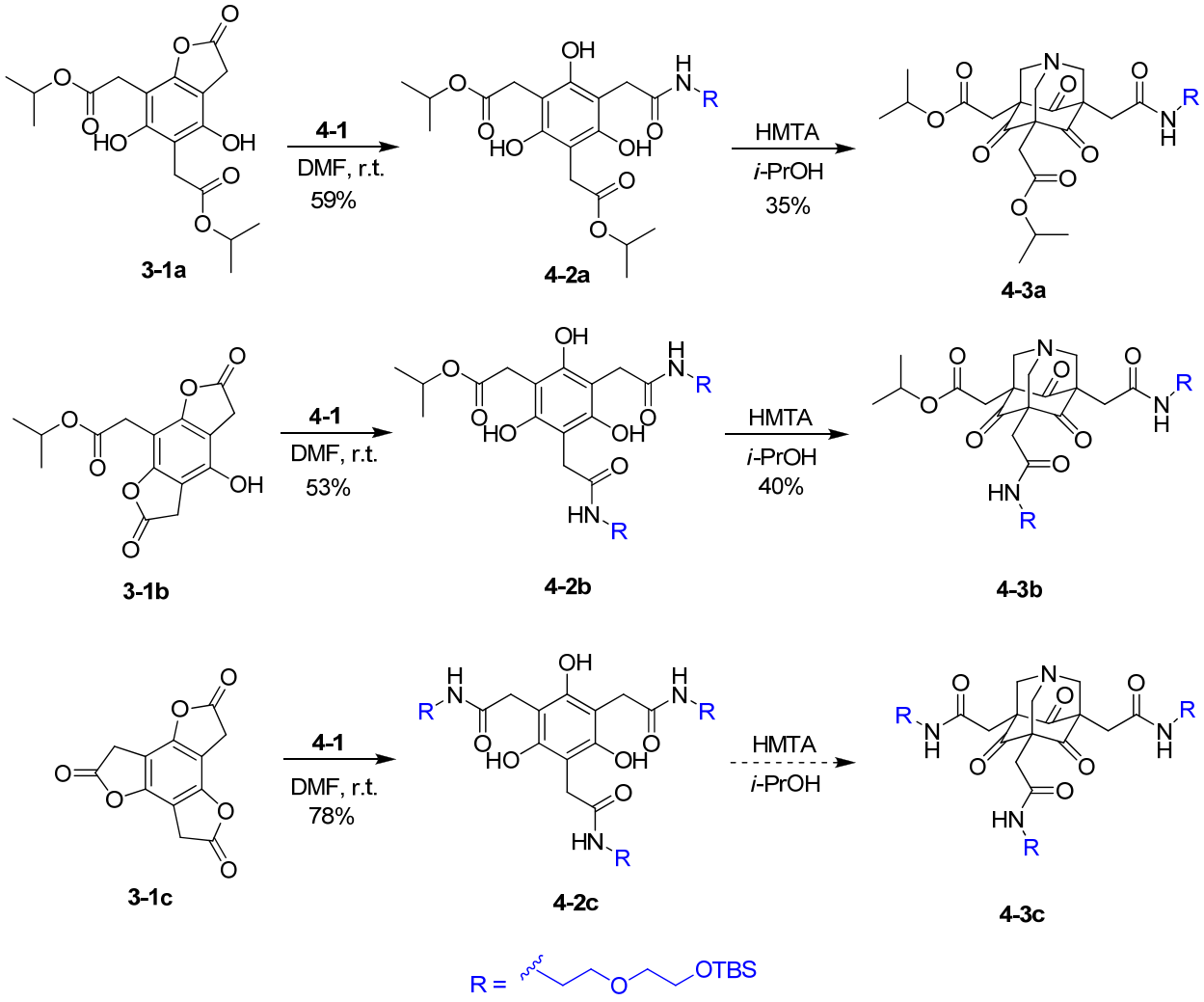

Figure 4-4. The synthesis of hydrophilic AATs derived from mono-, di-, and tributenolides.

The pentenolides react with 2-(2-(tert-butyldimethylsilyl)ethoxy)ethanamine **4-1** similarly to the butenolides, again at room temperature in DMF, to afford phloroglucinol derivatives **4-4a-c**. Figure 4-5 summarizes the results. Subsequent cyclization of **4-4a-c** with HMTA provides the desired AATs in typical yields for this reaction.[55, 56, 91] Like **4-3c**, the purification of **4-5c** is difficult. In this case, running the reaction in larger scale allowed TLC detection of the product upon concentration of the fractions during column chromatography.

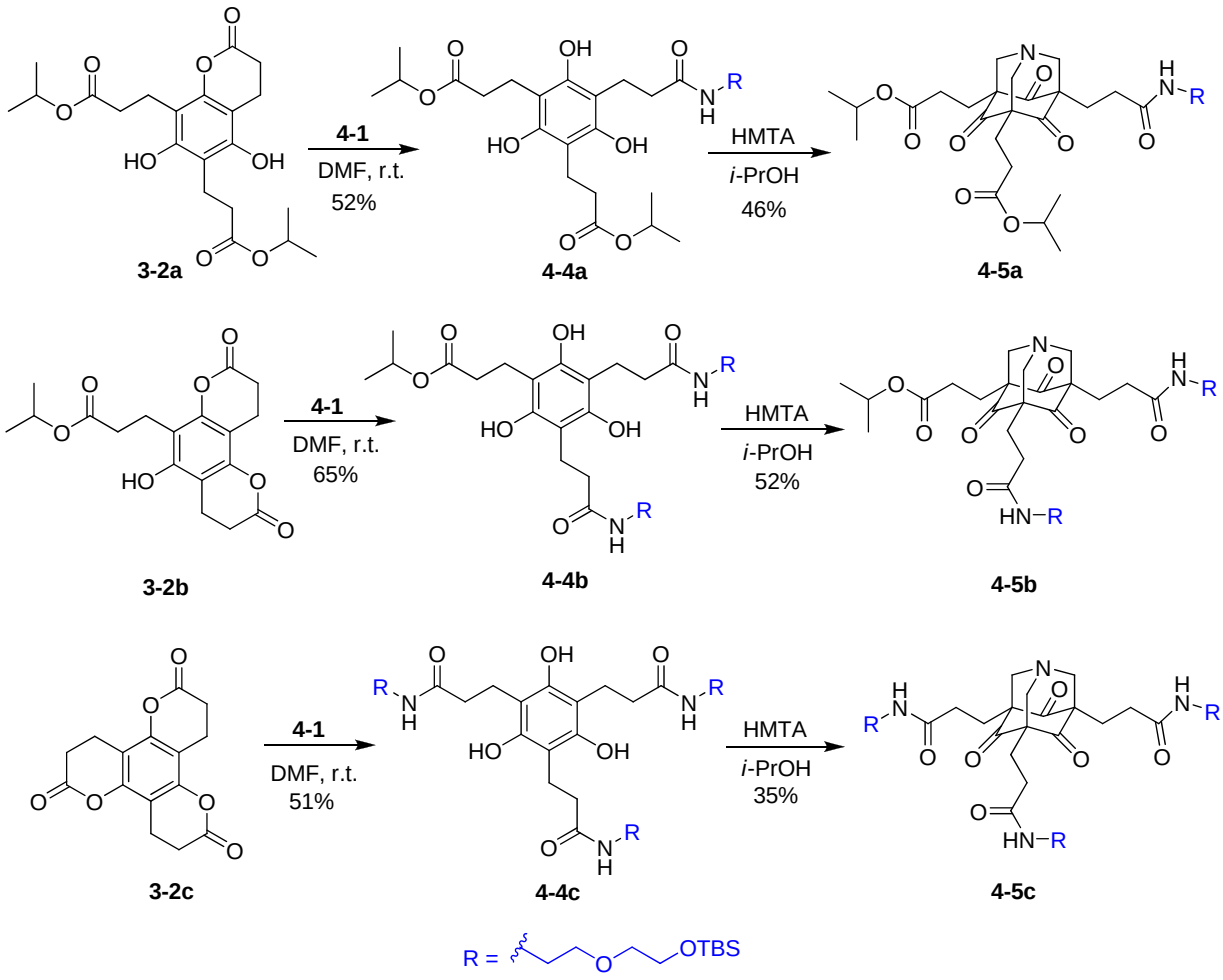

Figure 4-5. The synthesis of hydrophilic AATs derived from mono-, di-, and tripentenolides.

We have successfully introduced hydrophilic groups to the periphery of the AAT core, the first step toward creating hydrogelating AATs. The next step will be to deprotect the silyl groups of the compounds **4-3a,b** and **4-5a-c** and test their baseline aqueous assembly properties. The flexibility of the lactone-based synthetic methodology should allow fine-tuning of the solubility and hydrophilic/hydrophobic character of the molecules for future applications.

Experimental Section

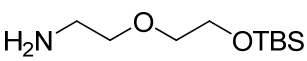

2-(2-(Tert-butyldimethylsilyloxy)ethoxy)ethanamine (4-1).[203] A stirring solution of 2-(2-aminoethoxy)ethanol (2.1 g, 20 mmol) in CH_2Cl_2 (10 mL) was treated with TBSCl (3.6 g, 24

mmol) and imidazole (2.7 g, 40 mmol) then stir at room temperature overnight. The solution was then diluted with CH_2Cl_2 and the organic layer was washed with water then dried with anhydrous Na_2SO_4. The solvent was removed on a rotary evaporator to afford **4-1** (3.8 g, 75%) as a colorless oil: ^{1}H NMR (300 MHz, $CDCl_3$) δ 0.06 (s, 6H), 0.82 (s, 9H), 2.47 (s, 2H), 2.78 (t, 2H, J = 6.0 Hz), 3.45 (m, 4H), 3.69 (t, 2H, J = 6.0 Hz). ^{13}C NMR (75 MHz, $CDCl_3$) δ –5.74, 17.89, 25.43, 41.31, 62.23, 71.96, 72.64. HRMS (ESI, $(M+H)^+$) calcd for $C_{10}H_{25}NO_2Si$: 220.1727; found: 220.1755.

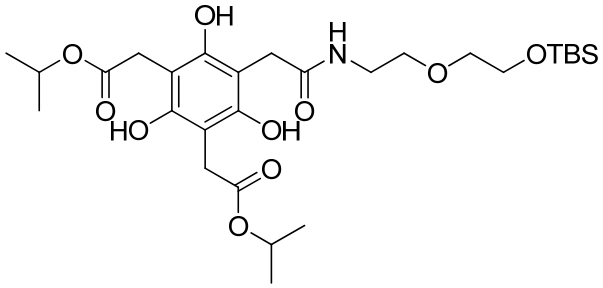

Isopropyl 2,2'-(2,4,6-trihydroxy-5-(2,2,3,3-tetramethyl-11-oxo-4,7-dioxa-10-aza-3-sila dodecan-12-yl)-1,3-phenylene)diacetate (4-2a). A stirring solution of **3-1a** (0.20 g, 0.55 mmol) in DMF (10 mL) was treated with **4-1** (0.12 g, 0.55 mmol) and stirred at room temperature for 2 hours. The solvent was removed on a rotary evaporator after which the residue was dissolved in ethyl acetate. The resulting organic layer was washed with 10% HCl and brine then dried with anhydrous Na_2SO_4. The solution was concentrated to a crude oil and purified via column chromatography (hexanes/EtOAc = 2/1) to afford **4-2a** (0.19 g, 59%) as a yellow oil: ^{1}H NMR (300 MHz, $CDCl_3$) δ 0.08 (s, 6H), 0.90 (s, 9H), 1.28 (m, 12H), 3.42 (q, 2H, J = 5.1 Hz), 3.54 (m, 4H), 3.66 (s, 2H), 3.77 (m, 6H), 5.02 (m, 2H), 6.62 (t, 1H, J = 5.1 Hz), 8.54 (s, 1H), 9.36 (s, 2H). ^{13}C NMR (75 MHz, $CDCl_3$) δ –4.90, 14.53, 18.74, 22.00, 26.28, 30.89, 32.75, 40.17, 60.75,

63.09, 69.67, 70.14, 72.90, 103.02, 104.15, 154.13, 154.41, 174.83, 175.93. HRMS (ESI, $(M+H)^+$) calcd for $C_{28}H_{47}NO_{10}Si$: 586.3042; found: 586.3126.

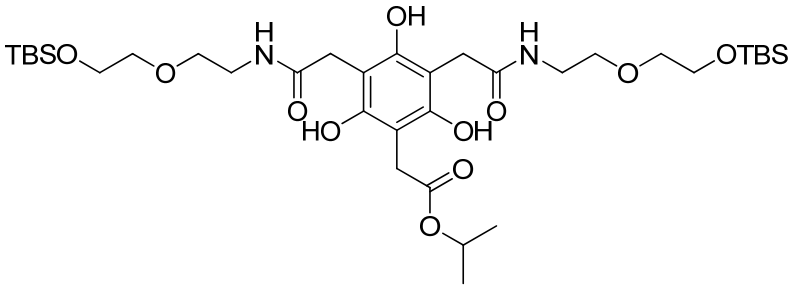

Isopropyl 2-(2,4,6-trihydroxy-3,5-bis(2,2,3,3-tetramethyl-11-oxo-4,7-dioxa-10-aza-3-siladodecan-12-yl)phenyl)acetate (4-2b). The compound was synthesized from **3-1b** (0.20 g, 0.65 mmol) and **4-1** (0.29 g, 1.3 mmol) according to the same procedure used for **4-2a** to afford **4-2b** (0.26 g, 53%) as a yellow oil: ^{1}H NMR (300 MHz, $CDCl_3$) δ 0.09 (s, 12H), 0.90 (s, 18H), 1.29 (d, 6H, J = 6.3 Hz), 3.43 (m, 4H), 3.56 (m, 8H), 3.61 (s, 4H), 3.77 (m, 6H), 5.01 (m, 1H), 6.63 (t, 2H, J = 5.1 Hz), 9.44 (s, 2H), 10.18 (s, 1H). ^{13}C NMR (75 MHz, $CDCl_3$) δ –5.28, 18.35, 21.61, 25.90, 30.49, 32.37, 39.78, 62.70, 69.26, 69.79, 72.50, 102.18, 103.35, 153.89, 154.12, 174.56, 175.88. HRMS (ESI, $(M+H)^+$) calcd for $C_{35}H_{64}N_2O_{11}Si_2$: 745.4121; found: 745.4210.

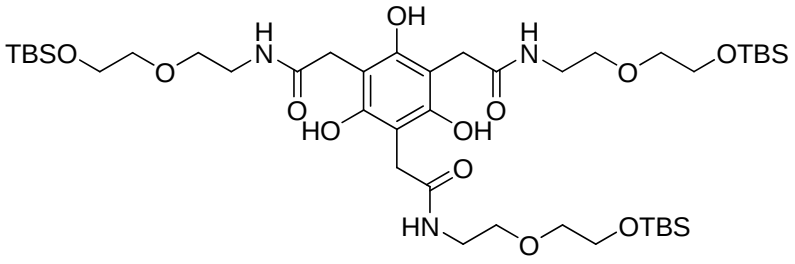

2,2',2''-(2,4,6-Trihydroxybenzene-1,3,5-triyl)tris(N-(2-(2-(tert-butyldimethylsilyloxy)-ethoxy)ethyl)acetamide) (4-2c). The compound was synthesized from **3-1c** (0.10 g, 0.41 mmol) and **4-1** (0.29 g, 1.3 mmol) according to the same procedure used for **4-2a** to afford **4-2c** (0.29 g,

78%) as a yellow oil.[1]H NMR (300 MHz, $CDCl_3$) δ 0.08 (s, 6H), 0.90 (s, 9H), 3.42 (q, 2H, J = 5.1 Hz), 3.54 (p, 4H, J = 4.8 Hz), 3.61 (s, 2H), 3.77 (t, 2H, J = 5.1 Hz), 6.70 (t, 1H, J = 5.1 Hz), 10.22 (s, 1H). ^{13}C NMR (75 MHz, $CDCl_3$) δ –5.29, 18.33, 25.88, 32.33, 39.77, 62.67, 69.25, 72.48, 102.94, 153.97, 174.69. HRMS (ESI, $(M+H)^+$) calcd for $C_{42}H_{81}N_3O_{12}Si_3$: 904.5206; found: 904.5200.

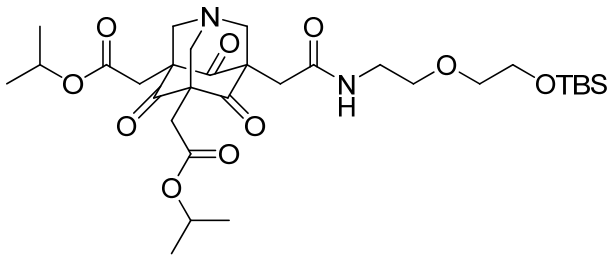

Mono-2-(2-(tert-butyldimethylsilyloxy)ethoxy)ethanamine-di-isopropyl ester 1-aza-adamantanetrione (4-3a). A solution of **4-2a** (0.18 g, 0.31 mmol), HMTA (0.13 g, 0.93 mmol), and isopropanol (5 mL) was heated to reflux for 2 days under a blanket of argon. After cooling the reaction mixture to room temperature, the solvent was removed in vacuo and the residue was dissolved in ethyl acetate. The organic layer was washed with 1N HCl and brine. The solution was then concentrated to a crude oil and purified via column chromatography (pure ethyl acetate) to afford **4-2b** (78 mg, 35%) as a yellow oil: ^{1}H NMR (300 MHz, $CDCl_3$) δ 0.08 (s, 6H), 0.88 (m, 12H), 2.33 (m, 2H), 2.76 (m, 4H), 3.24 (m, 4H), 3.60 (m, 4H), 3.76 (m, 6H), 4.98 (m, 2H), 6.10 (br, 1H). ^{13}C NMR (75 MHz, $CDCl_3$) δ -5.23, 14.10, 18.39, 21.76, 22.68, 25.92, 29.34, 29.68, 31.91, 33.60, 33.95, 35.37, 39.43, 44.58, 44.73, 57.97, 58.34, 59.43, 62.67, 66.77, 67.95, 68.31, 69.66, 72.48, 170.40, 171.02, 201.79, 202.70.

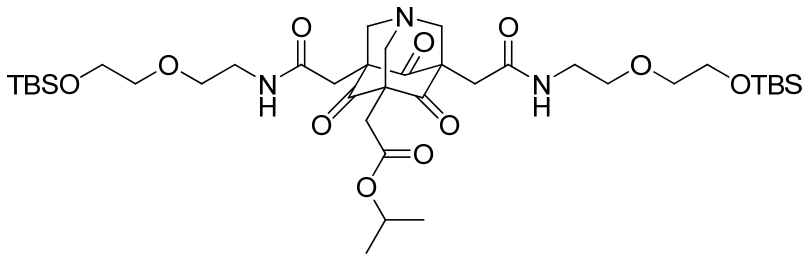

Mono-isopropyl ester di-2-(2-(tert-butyldimethylsilyloxy)ethoxy)ethanamine 1-aza-adamantanetrione (4-3b). A solution of **4-2b** (0.13 g, 0.17 mmol), HMTA (72 mg, 0.52 mmol), and isopropanol (5 mL) was heated to reflux overnight under a blanket of argon. After cooling the reaction mixture to room temperature, the solvent was removed in vacuo and the residue was dissolved in ethyl acetate. The organic layer was washed with 1N HCl and brine. The solution was then concentrated to a crude oil and purified via column chromatography (pure ethyl acetate) to afford **4-2b** (60 mg, 40%) as a yellow oil: ^{1}H NMR (300 MHz, $CDCl_3$) δ 0.08 (s, 12H), 0.90 (s, 18H), 1.24 (d, 6H, J = 6.0 Hz), 2.69 (s, 4H), 2.72 (s, 2H), 3.44 (m, 6H), 3.55 (m, 8H), 3.77 (m, 6H), 3.86 (s, 2H), 4.98 (m, 1H), 6.29 (t, 2H, J = 5.4 Hz). ^{13}C NMR (75 MHz, $CDCl_3$) δ –5.23, 18.38, 21.66, 25.92, 29.67, 32.17, 33.43, 39.38, 45.83, 62.67, 68.34, 69.67, 70.37, 70.63, 72.45, 169.07, 169.21, 197.53, 197.95. HRMS (ESI, $(M+Na)^+$) calcd for $C_{38}H_{67}N_3O_{11}Si_2$: 820.4206; found: 820.4227.

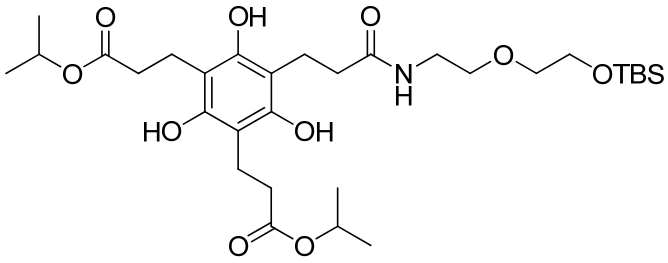

Isopropyl 3,3'-(2,4,6-trihydroxy-5-(2,2,3,3-tetramethyl-11-oxo-4,7-dioxa-10-aza-3-silatridecan-13-yl)-1,3-phenylene)dipropanoate (4-4a). The compound was synthesized from

3-2a (0.14 g, 0.33 mmol) and **4-1** (77 mg, 0.35 mmol) according to the same procedure used for **4-2a** to afford **4-4a** (0.11 g, 52%) as a yellow oil: ^{1}H NMR (300 MHz, $CDCl_3$) δ 0.07 (s, 6H), 0.90 (s, 9H), 1.21 (d, 12H, J = 6.3 Hz), 2.70 (m, 6H), 2.88 (m, 6H), 3.47 (m, 6H), 3.74 (t, 2H, J = 5.1 Hz), 4.98 (p, 5H, J = 6.3 Hz), 6.02 (t, 1H, J = 5.1 Hz), 8.21 (s, 1H), 8.72 (s, 2H). ^{13}C NMR (75 MHz, $CDCl_3$) δ –5.69, 17.98, 21.26, 25.47, 34.09, 35.04, 39.18, 62.21, 68.47, 68.96, 72.00, 107.98, 108.47, 152.30, 152.57, 174.91, 176.91.

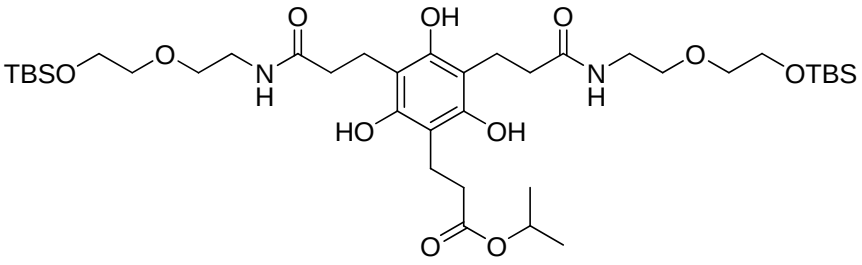

Isopropyl 3-(2,4,6-trihydroxy-3,5-bis(2,2,3,3-tetramethyl-11-oxo-4,7-dioxa-10-aza-3-silatridecan-13-yl)phenyl)propanoate (4-4b). The compound was synthesized from **3-2b** (0.10 g, 0.29 mmol) and **4-1** (0.13 g, 0.58 mmol) according to the same procedure used for **4-2a** to afford **4-4b** (0.15 g, 65%) as a yellow oil: ^{1}H NMR (300 MHz, $CDCl_3$) δ 0.06 (s, 12H), 0.89 (s, 18H), 1.20 (d, 6H, J = 6.3 Hz), 2.64 (m, 6H), 2.87 (m, 6H), 3.41 (m, 4H), 3.49 (m, 8H), 3.73 (t, 4H, J = 5.1 Hz), 4.97 (p, 1H, J = 6.3 Hz), 6.00 (t, 2H, J = 5.4 Hz), 8.69 (s, 2H), 9.19 (s, 1H). ^{13}C NMR (75 MHz, $CDCl_3$) δ –5.30, 18.24, 18.30, 18.35, 21.65, 25.85, 34.49, 35.44, 39.54, 62.58, 68.78, 69.33, 72.37, 108.19, 108.66, 152.90, 153.16, 175.36, 177.37. HRMS (ESI, $(M+H)^+$) calcd for $C_{38}H_{70}N_2O_{11}Si_2$: 787.4596; found: 787.4600.

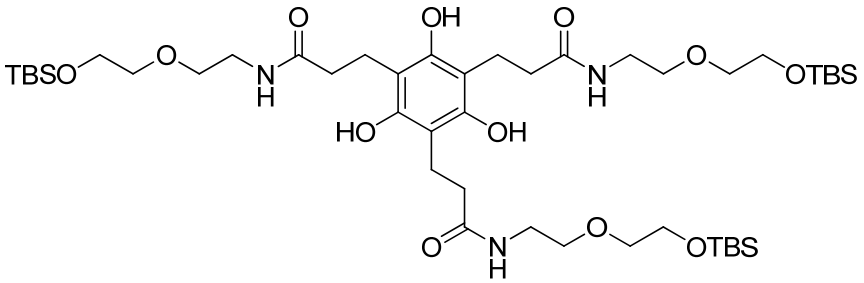

3,3',3''-(2,4,6-Trihydroxybenzene-1,3,5-triyl)tris(N-(2-(2-(tert-butyldimethylsilyloxy)-ethoxy)ethyl)propanamide) (4-4c). The compound was synthesized from **3-2c** (0.20 g, 0.69 mmol) and **4-1** (0.50 g, 2.3 mmol) according to the same procedure used for **4-2a** to afford **4-4b** (0.33 g, 51%) as a colorless oil: ^{1}H NMR (300 MHz, $CDCl_3$) δ 0.06 (s, 6H), 0.89 (s, 9H), 2,62 (m, 2H), 2.87 (m, 2H), 3.39 (m, 2H), 3.48 (m, 4H), 3.71 (t, 2H, J = 5.1 Hz), 6.06 (t, 1H, J = 5.4 Hz), 9.15 (s, 1H). ^{13}C NMR (75 MHz, $CDCl_3$) δ –5.28, 18.28, 18.33, 25.88, 35.47, 39.54, 62.60, 69.37, 72.39, 108.52, 153.08, 175.47. HRMS (ESI, $(M+Na)^+$) calcd for $C_{45}H_{87}N_3O_{12}Si_3$: 968.5490; found: 968.5614.

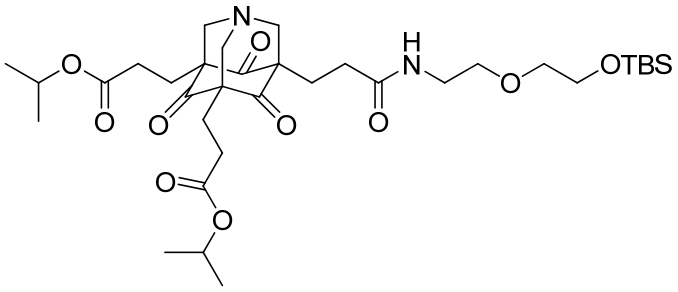

Mono-2-(2-(tert-butyldimethylsilyloxy)ethoxy)ethanamine-di-isopropylester 1-aza-adamantantrione (4-5a). A solution of **4-4a** (60 mg, 0.10 mmol), HMTA (42 mg, 0.30 mmol), and isopropanol (5 mL) was heated to reflux for 3 days under a blanket of argon. After cooling the reaction mixture to room temperature, the solvent was removed in vacuo and the residue was dissolved in ethyl acetate. The organic layer was washed with 1N HCl and brine. The solution

was then concentrated to a crude oil and purified via column chromatography (pure ethyl acetate) to afford **4-5a** (35 mg, 46%) as a yellow oil: ^{1}H NMR (300 MHz, $CDCl_3$) δ 0.08 (s, 6H), 0.89 (s, 9H), 1.23 (d, 12H, J = 6.3 Hz), 2.04 (m, 6H), 2.37 (m, 2H), 2.48(m, 4H), 2.78 (t, 2H, J = 7.8 Hz), 3.06 (t, 2H, J = 7.8 Hz), 3.38 (m, 8H), 3.55 (m, 4H), 3.77 (t, 2H, J = 6.0 Hz), 5.00 (q, 2H, J = 6.3 Hz), 6.01 (t, 1H, J = 5.4 Hz). ^{13}C NMR (75 MHz, $CDCl_3$) δ –5.24, 17.51, 21.84, 22.30, 22.90, 25,92, 28.17, 28.68, 30.04, 39.21, 62.65, 67.65, 69.82, 71.31, 72.43, 72.75, 72.83, 172.45, 172.86, 200.22, 200.24. HRMS (ESI, $(M+Na)^+$) calcd for $C_{34}H_{56}N_2O_{10}Si$: 703.3596; found: 703.3609.

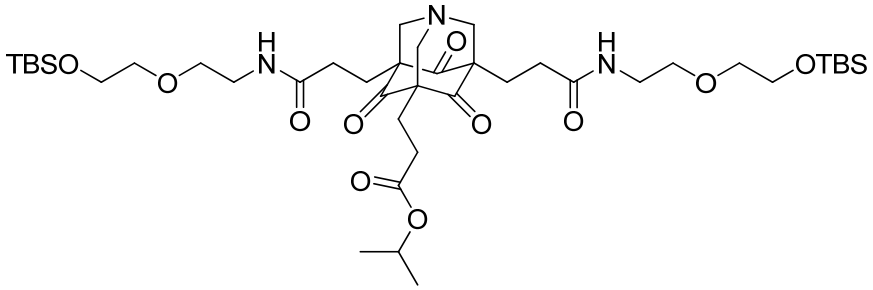

Mono-isopropylester-di-2-(2-(tert-butyldimethylsilyloxy)ethoxy)ethanamine 1-aza-adamantantrione (4-5b). The compound was synthesized from **4-4b** (90 mg, 0.11 mmol) and HMTA (48 mg, 0.34 mmol) according to the same procedure used for **4-5a** to afford **4-5b** (55 mg, 52%) as a yellow oil: ^{1}H NMR (300 MHz, $CDCl_3$) δ 0.08 (s, 12H), 0.90 (s, 18H), 1.22 (d, 6H, J = 5.7 Hz), 2.08 (m, 6H), 2.45 (m, 6H), 2.79 (t, 2H, J = 7.2 Hz), 3.06 (t, 2H, J = 6.6 Hz), 3.38 (m, 6H), 3.55 (m, 6H), 3.77 (s, 4H), 5.00 (m, 1H), 6.06 (t, 2H, J = 6.6 Hz). ^{13}C NMR (75 MHz, $CDCl_3$) δ –5.78, 16.43, 17.46, 21.11, 21.57, 22.22, 25.29, 27.08, 27.89, 28.73, 61.68, 66.34, 68.65, 69.17, 70.40, 71.12, 171.77, 172.05, 199.85. HRMS (ESI, $(M+Na)^+$) calcd for $C_{41}H_{73}N_3O_{11}Si_2$: 862.4681; found: 862.4803.

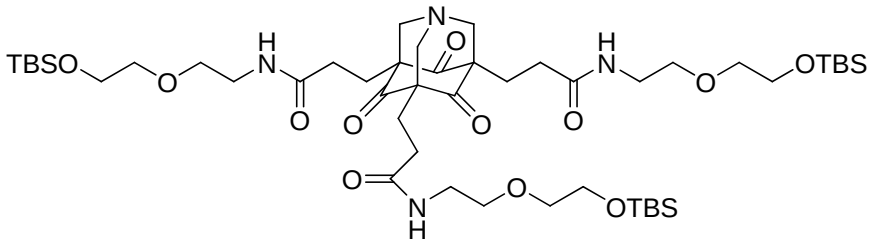

Tri-2-(2-(tert-butyldimethylsilyloxy)ethoxy)ethanamine 1-aza-adamantantrione (4-5c). The compound was synthesized from **4-4c** (0.75 g, 0.79 mmol) and HMTA (0.33 g, 2.4 mmol) according to the same procedure used for **4-5a** to afford **4-5c** (0.28 g, 35%) as a yellow oil: ^{1}H NMR (300 MHz, $CDCl_3$) δ 0.05 (s, 6H), 0.87 (s, 9H), 2.02 (t, 2H, J = 6.9 Hz), 2.35 (t, 2H, J = 6.9 Hz), 3.32 (s, 2H), 3.38 (q, 2H, J = 5.4 Hz), 3.50 (q, 4H, J = 5.4 Hz), 3.74 (t, 2H, J = 5.7 Hz), 6.05 (t, 1H, J = 5.7 Hz). ^{13}C NMR (75 MHz, $CDCl_3$) δ –4.84, 18.75, 23.40, 26.31, 30.65, 39.62, 63.01, 70.21, 71.53, 72.80, 73.12, 173.10, 200.97. HRMS (ESI, $(M+Na)^+$) calcd for $C_{48}H_{90}N_4O_{12}Si_3$: 1021.5755; found: 1021.5777.

CHAPTER 5
CONCLUSIONS AND OUTLOOK

Summary and Conclusions

The design, rational synthesis, and supramolecular properties of a series of highly functionalized amide-based AATs with expanded aromatic arms have been described. These molecules show significantly enhanced self-assembly properties in both the bulk state and solution relative to derivatives with smaller aromatic arms. Compound **2-1a** forms stable gels in aromatic solvents such as toluene and benzene with the lowest CGC and highest T_{gel} values that have been observed to date for AAT gelators. In the solid state, SEM of the dried gels shows well-organized structures and powder XRD shows evidence of π–π stacking. Thermal behavior of the AATs was studied by DSC and TGA for the first time; the latter shows that the core of the AAT molecules is stable up to 600 °C.

In solution, UV/Vis, fluorescence, IR, and NMR spectroscopies were used to study the role of the aromatic side chains in self-assembly and have revealed structure-property relationships for the molecules. Excimer emission bands were observed that provided evidence for π-π stacking; at least a component of this arises from intermolecular aromatic interactions of the naphthyl arms by comparison of the target AAT molecules with model compounds. The H-bonding effects of the peripheral amide functional groups of the AAT molecules were studied by concentration-dependent and temperature-dependent NMR and IR spectroscopy. The data shows the importance of intramolecular H-bonding to the amide-functionalized AATs that presumably preorganizes the molecules and facilitates self-assembly.[55, 91] The first ever dynamic light scattering studies of the AATs showed that the derivatives bearing larger aromatic side chains appear to form larger assemblies in solution than the AAT derivatives with smaller aromatic arms at similar concentrations. Light-scattering provides independent evidence for self-assembly

of the AATs and shows the dependence of assembly size on solvent, concentration, temperature, and molecular structure.

Differentially-functionalized and chiral AATs were prepared using a new lactone-based strategy from 5- and 6-membered ring ester and amide-functionalized lactones. The lactone strategy allows for late-stage synthetic introduction of sensitive or chemically labile functional groups and also provides a method for controlling the symmetry of an otherwise C_3-symmetric scaffold. Installation of three different arms on the AAT core gives a chiral molecule that should share the properties of chiral tertiary amines and therefore have potential applications in asymmetric catalysis and chiral recognition. The first application of this synthetic methodology was the synthesis of model compound **2-12**, which was used to explore inter- versus intramolecular π–π stacking effects in the naphthyl-substituted AATs. A small library of differentially-functionalized and chiral AATs was subsequently made and their thermal properties were studied by DSC and POM. Unexpected phase behavior (e.g., cold-crystalline phenomena) was found for compound **3-5a** that was identified by both DSC and POM.

The lactone synthetic methodology allows the synthesis of AATs bearing hydrophilic groups that are not available otherwise. The targets work toward the preparation of water soluble and hydrogelating AATs; hydrogels are an important class of biomaterials with numerous applications.

Outlook

AAT molecules constitute a unique class of donor-σ-acceptor molecules. Their self-assembly relies on both traditional noncovalent interactions as well as dipolar interactions of the donor-σ-acceptor cores. The supramolecular networks derived from these “unconventional”

molecules are complex and further functionalization of the cores could work toward further understanding their structure-property relationships and toward specific applications.

Arms Functionalized with H-bonding Recognition Groups

H-bonding is one of the most important and widely exploited noncovalent interactions in supramolecular chemistry. Columnar aggregation via hydrogen bonding and formation of liquid crystals and gels has been described for many C_3-symmetric molecules consisting of a single benzene ring. These notably include the 1,3,5-benzenetriamides that assemble through amide hydrogen bonding,[204, 205] benzenehexamine derivatives that assemble via 6-fold intermolecular hydrogen bonding,[206] and the tris(stearoylamino)triphenylamines that assembles via three-fold intermolecular hydrogen bonding.[207] Introducing functional groups which could form well-defined intermolecular H-bonds between AAT monomers, such as ureas, amides, and peptides, should facilitate long-range organization in the solid phase and liquid crystallinity in solution. The lactone strategy allows for the late-stage introduction of numerous functional groups to the AAT periphery. Improving the solubility of the AAT molecules would also help with single crystal growth in order to fully understand the packing patterns of the systems and their assembly mechanisms.

Hydrophilic and Hydrogelating AATs

The successful introduction of hydrophilic functional groups to the AAT periphery makes the formation of hydrogelating molecules worthwhile targets. The strategy could also be expanded to include installation of peptidic and polyethylene glycol units into the arms to investigate a variety of "smart" materials and biomedically interesting molecules.[208]

Differentially-Functionalized AATs

The lactone strategy provides a method for breaking the symmetry of otherwise C_3-symmetric phloroglucinol, and therefore AAT, scaffolds. Installation of three different arms on

the AATs offers a chiral molecule that should share the properties of chiral tertiary amines and therefore have potential applications in asymmetric catalysis and chiral recognition.[189-191] Meanwhile, installation of three different arms which have different functionalities may largely enhance the properties and functions of the molecules in particular applications. For example, two arm units can be functionalized with groups designed to recognize and bind a substrate, while the third arm unit could be equipped with a group that would improve the solubility or hydrophilic properties of the system.

APPENDIX A
NMR SPECTRA

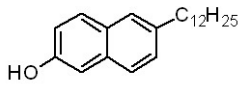

2-4a
^{1}H NMR $CDCl_3$

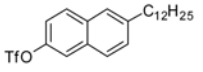

2-5a
^{1}H NMR $CDCl_3$

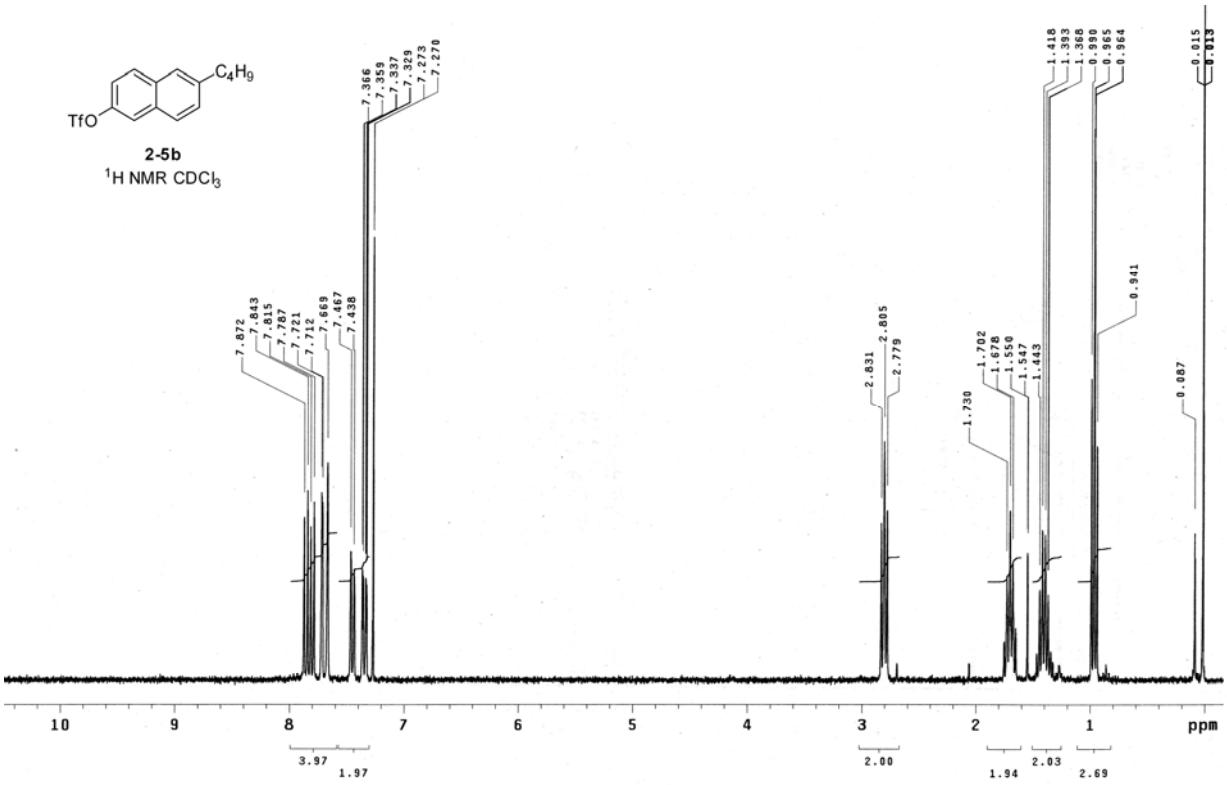
C4H9
TfO
2-5b
1H NMR CDCl3
7.872
7.843
7.815
7.787
7.721
7.712
7.669
7.467
7.438
7.366
7.359
7.337
7.329
7.273
7.270
2.831
2.805
2.779
1.730
1.702
1.678
1.550
1.547
1.443
1.418
1.393
1.368
0.990
0.965
0.964
0.941
0.087
0.015
0.013
10
9
8
7
6
5
4
3
2
1
ppm
3.97
1.97
2.00
1.94
2.03
2.69

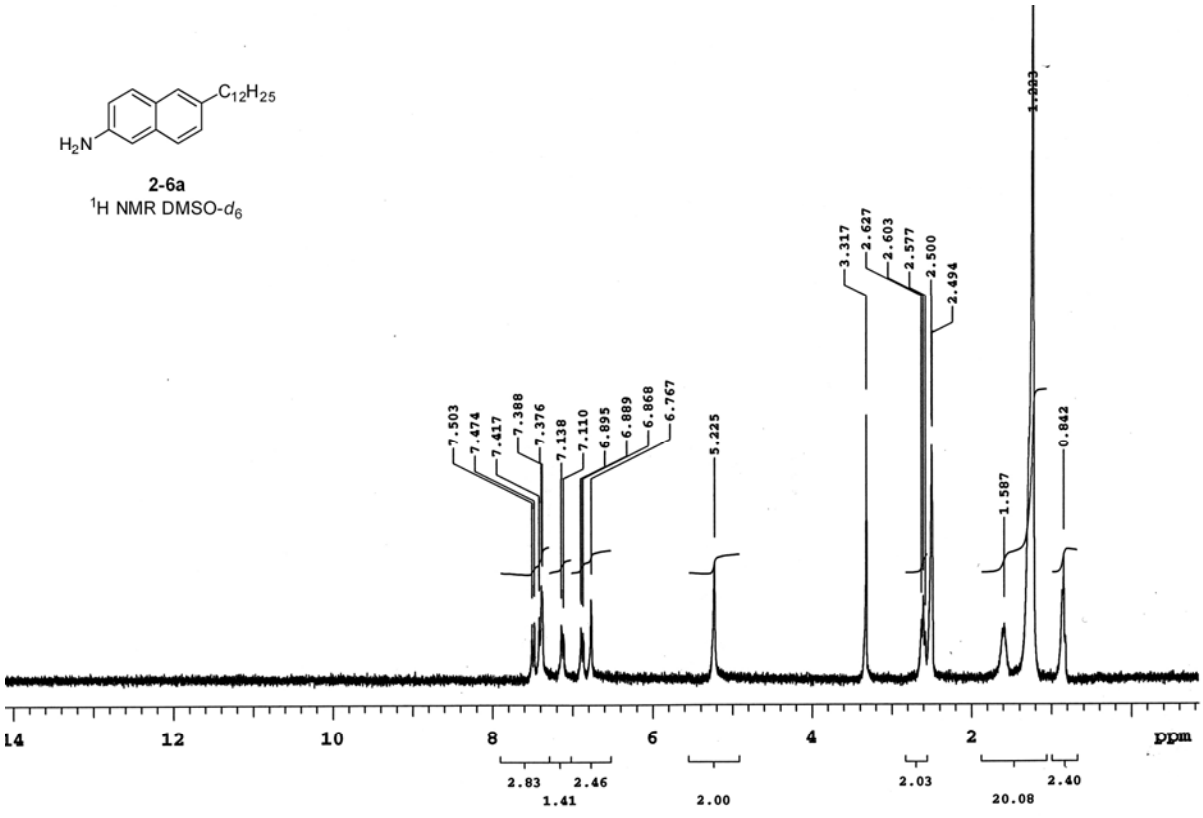
C12H25
H2N
2-6a
1H NMR DMSO-d6
7.503
7.474
7.417
7.388
7.376
7.138
7.110
6.895
6.889
6.868
6.767
5.225
3.317
2.627
2.603
2.577
2.500
2.494
1.587
0.842
14
12
10
8
6
4
2
ppm
2.83
2.46
1.41
2.00
2.03
20.08
2.40

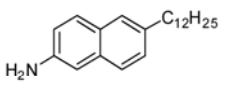

2-6c

^{1}H NMR DMSO-d_6

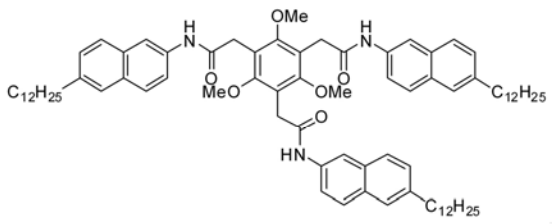

2-8a

^{1}H NMR pyridine-d_5

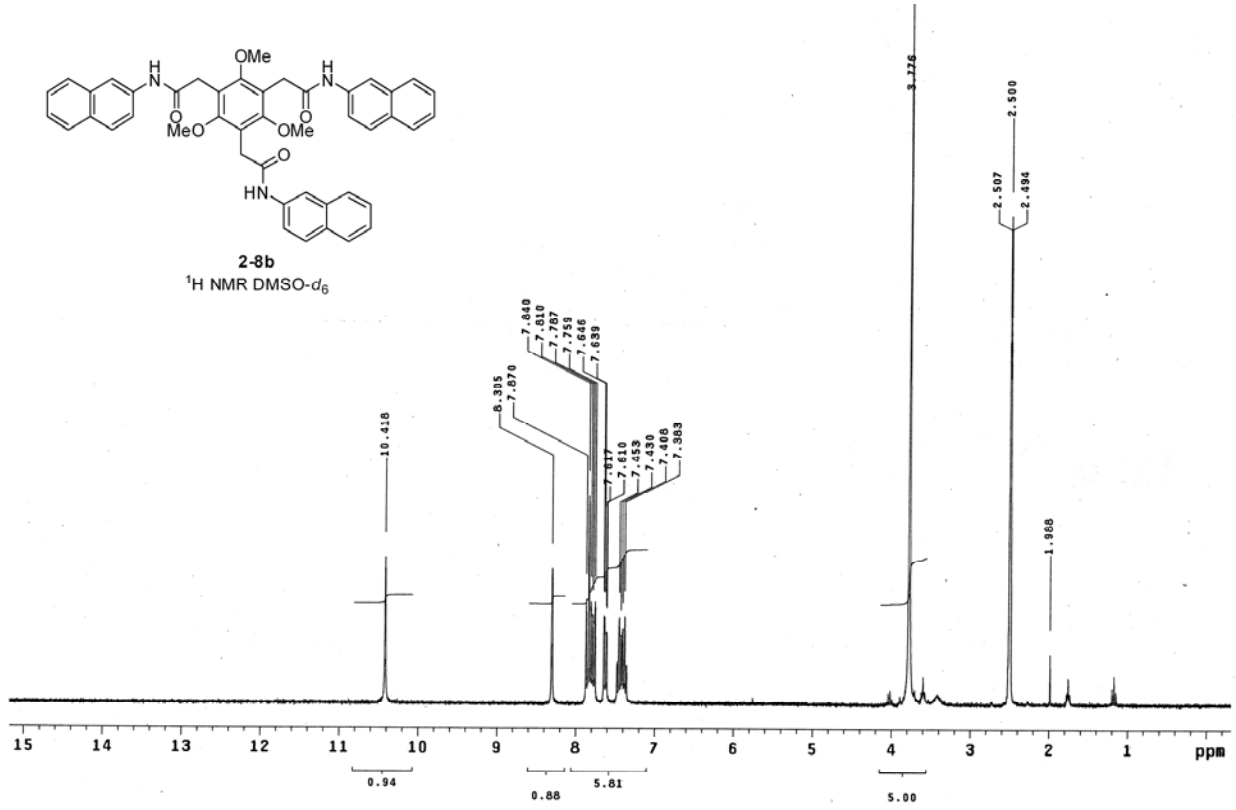
OMe
MeO
OMe
HN
2-8b
1H NMR DMSO-d6
10.418
8.305
7.870
7.840
7.810
7.787
7.753
7.646
7.639
7.617
7.610
7.453
7.430
7.406
7.383
3.776
2.507
2.500
2.494
1.868
15 14 13 12 11 10 9 8 7 6 5 4 3 2 1 ppm
0.94
0.88
5.81
5.00

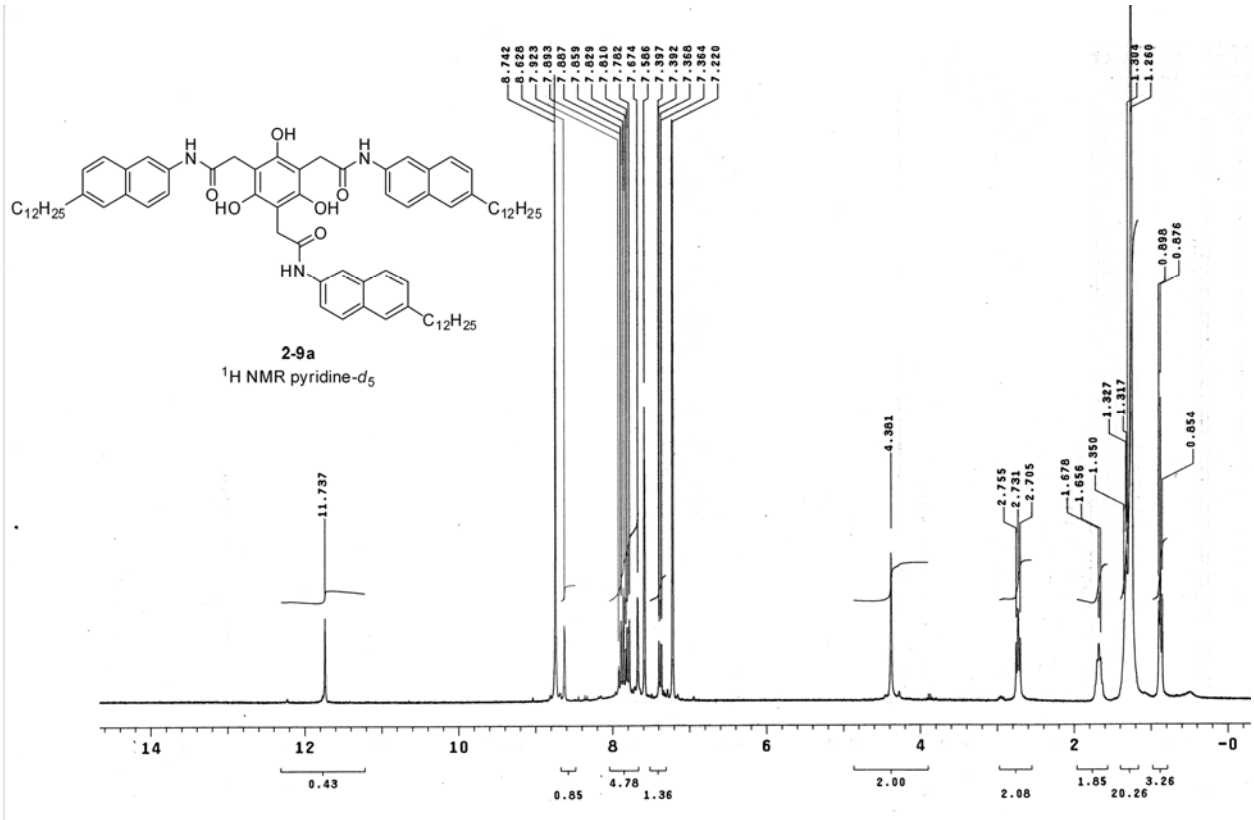
OH
HO
OH
HN
C12H25
2-9a
1H NMR pyridine-d5
11.737
8.742
8.626
7.923
7.893
7.887
7.859
7.829
7.810
7.782
7.674
7.586
7.397
7.392
7.366
7.364
7.220
4.381
2.755
2.731
2.705
1.678
1.656
1.350
1.327
1.317
1.304
1.260
0.898
0.876
0.654
14 12 10 8 6 4 2 -0
0.43
0.85
4.78
1.36
2.00
2.08
1.85
20.26
3.26

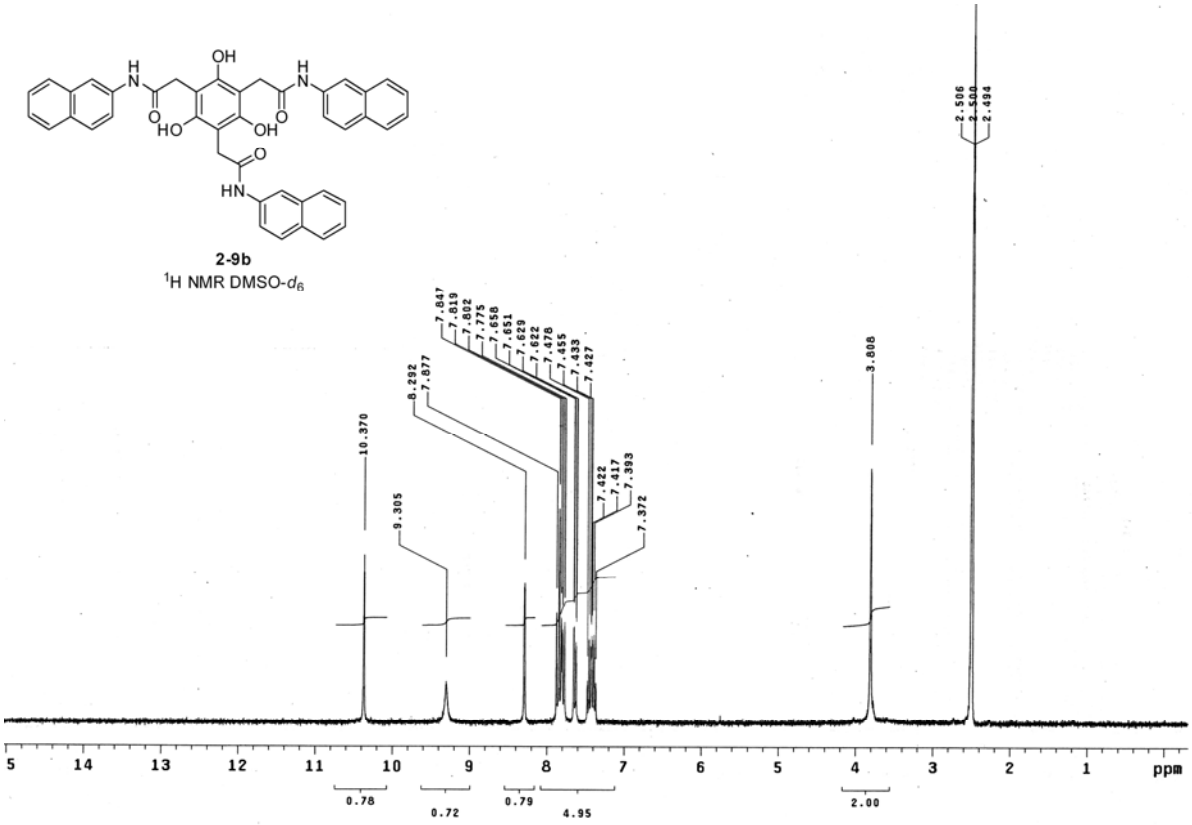
2-9b
1H NMR DMSO-d6
10.370
9.305
8.292
7.877
7.847
7.819
7.802
7.775
7.658
7.651
7.629
7.622
7.478
7.455
7.433
7.427
7.422
7.417
7.393
7.372
3.808
2.506
2.500
2.494
ppm
0.78
0.72
0.79
4.95
2.00

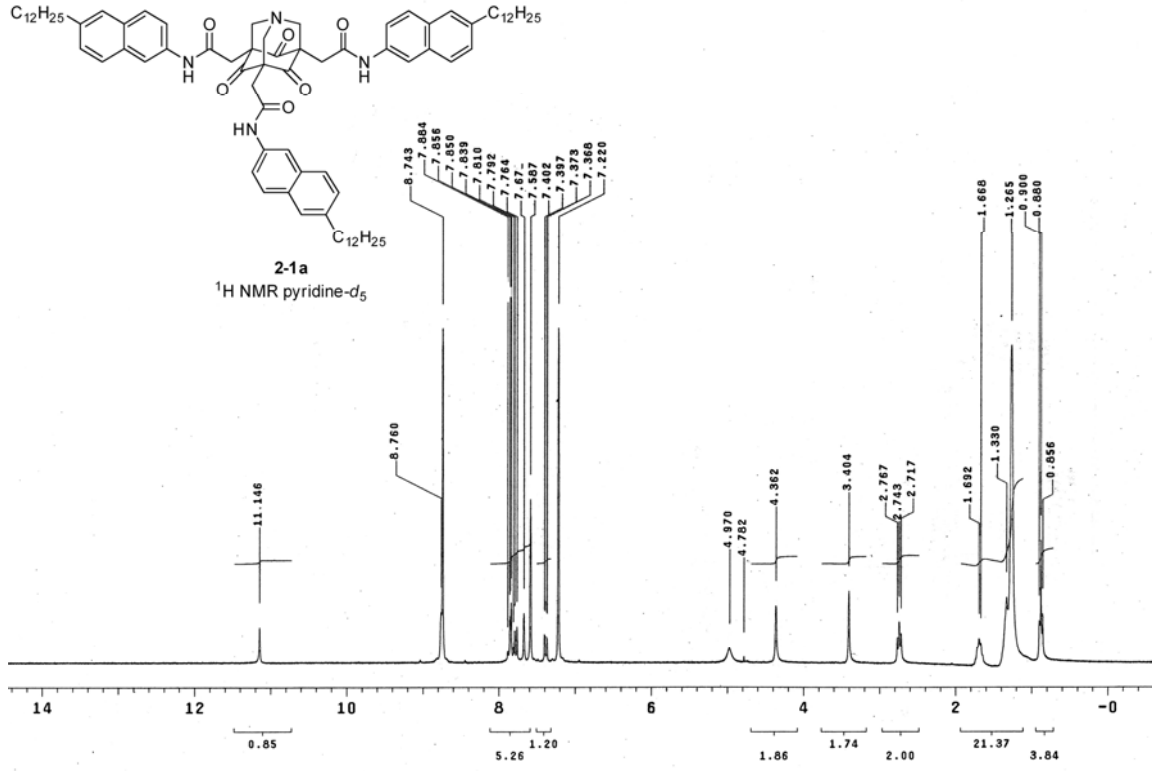
2-1a
1H NMR pyridine-d5
11.146
8.760
8.743
7.884
7.856
7.850
7.839
7.810
7.792
7.764
7.67
7.587
7.402
7.397
7.373
7.366
7.220
4.970
4.782
4.362
3.404
2.767
2.743
2.717
1.692
1.668
1.330
1.265
0.900
0.880
0.856
0.85
5.26
1.20
1.86
1.74
2.00
21.37
3.84

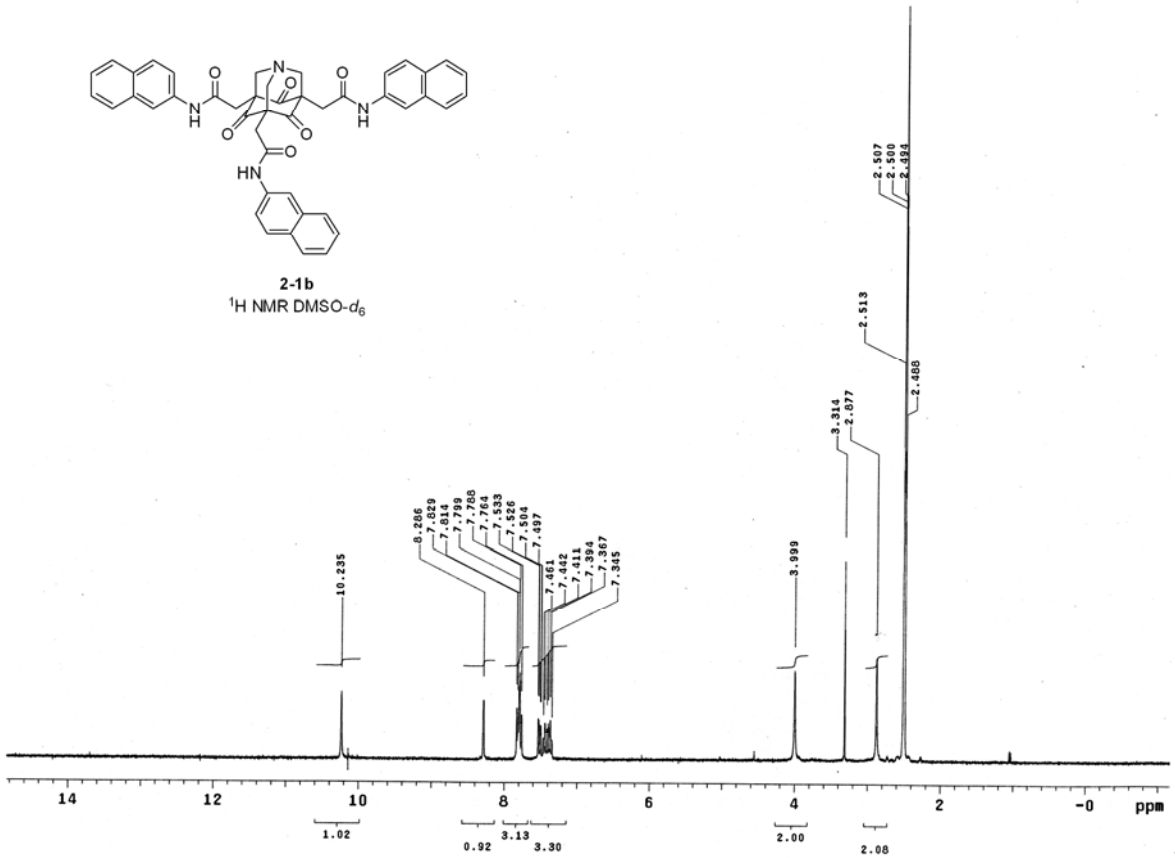

2-1b
^{1}H NMR DMSO-d_6

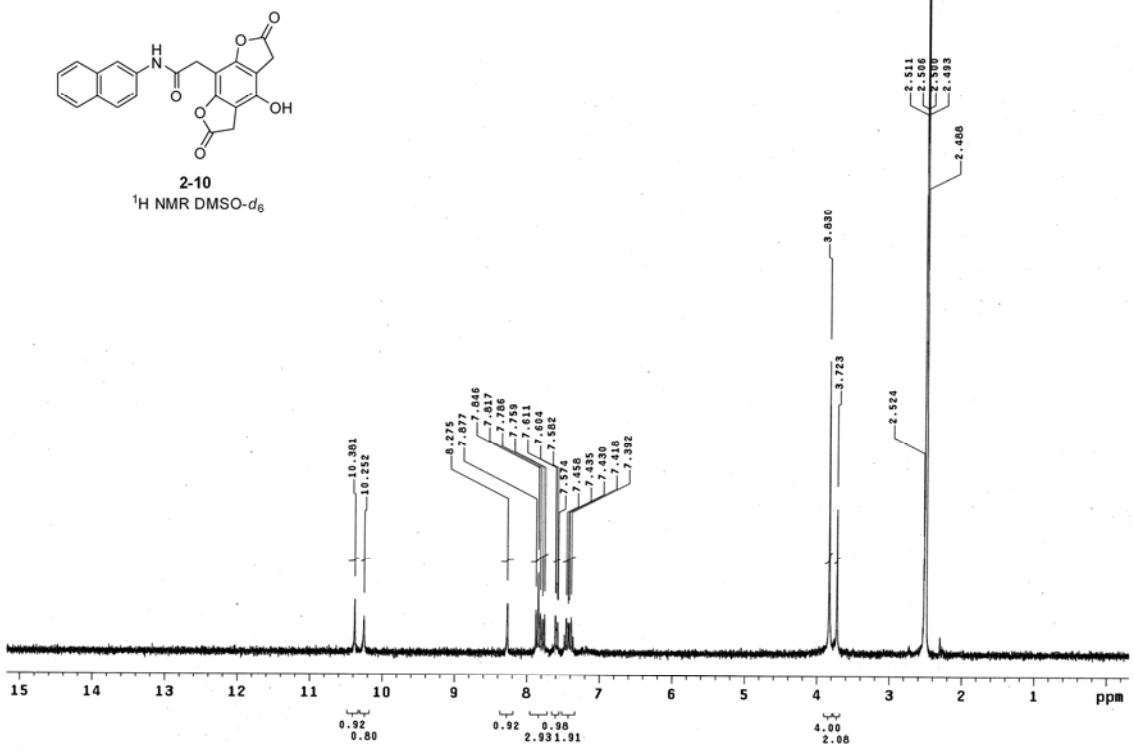

2-10
^{1}H NMR DMSO-d_6

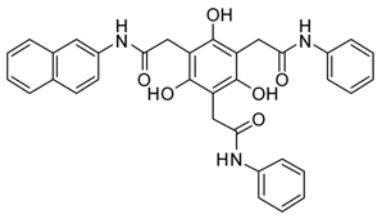

2-11

^{1}H NMR DMSO-d_6

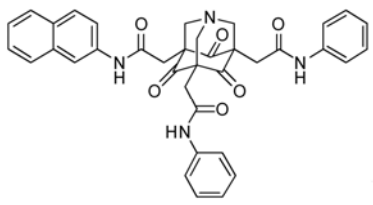

2-12

^{1}H NMR DMSO-d_6

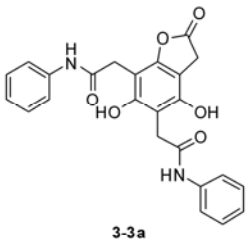

3-3a
^{1}H NMR DMSO-d_6

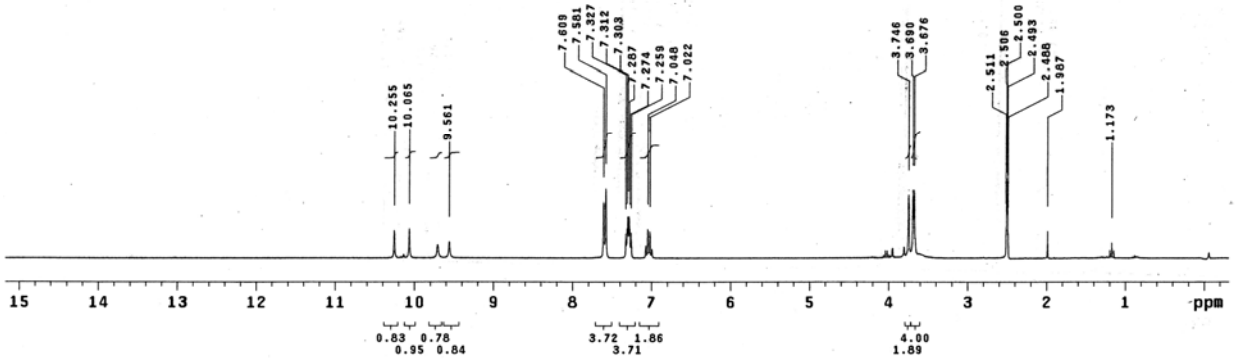

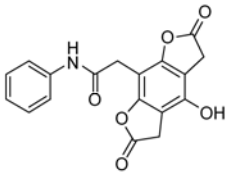

3-3b
^{1}H NMR DMSO-d_6

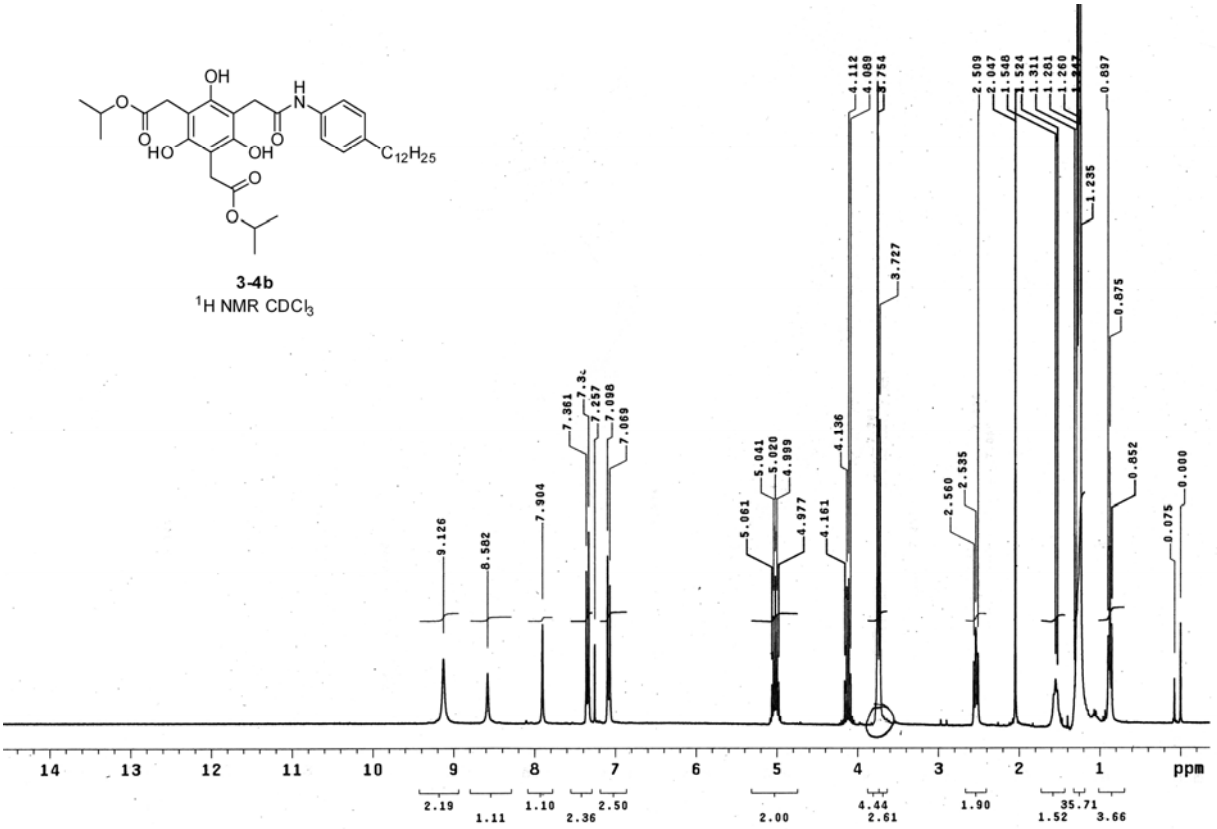

3-4b
^{1}H NMR $CDCl_3$

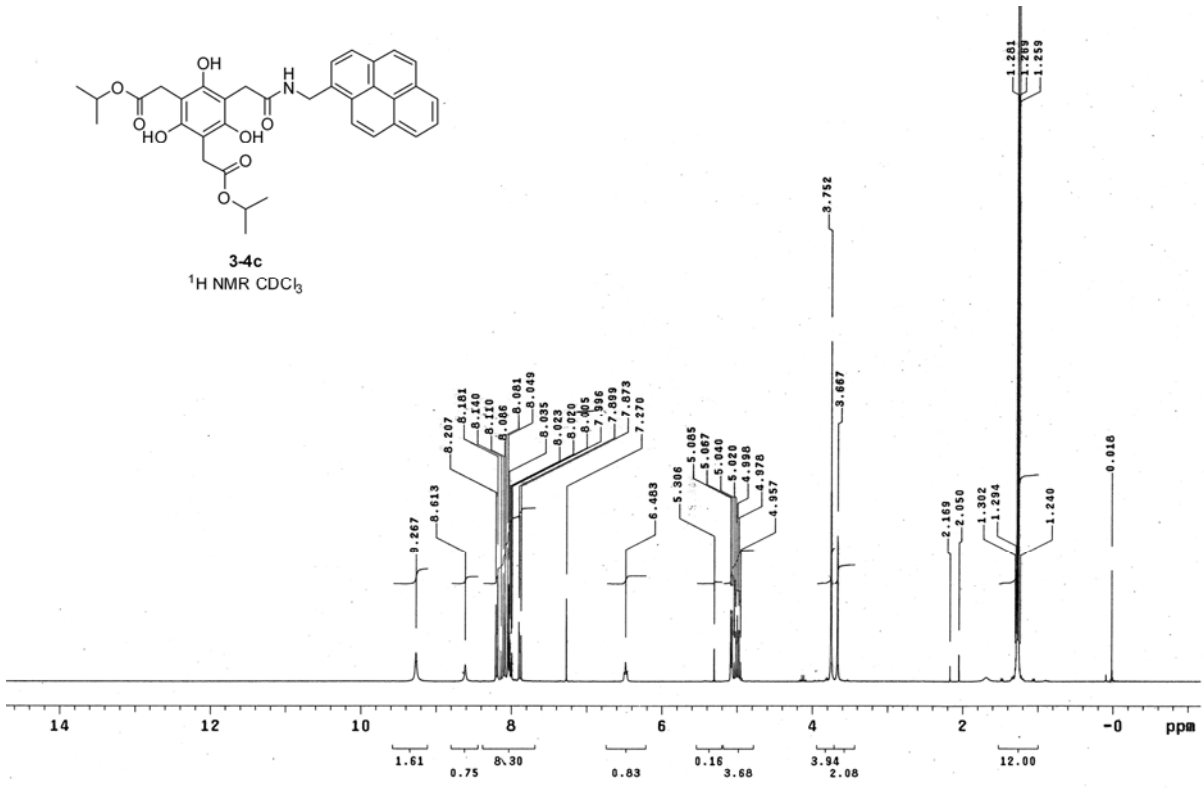

3-4c
^{1}H NMR $CDCl_3$

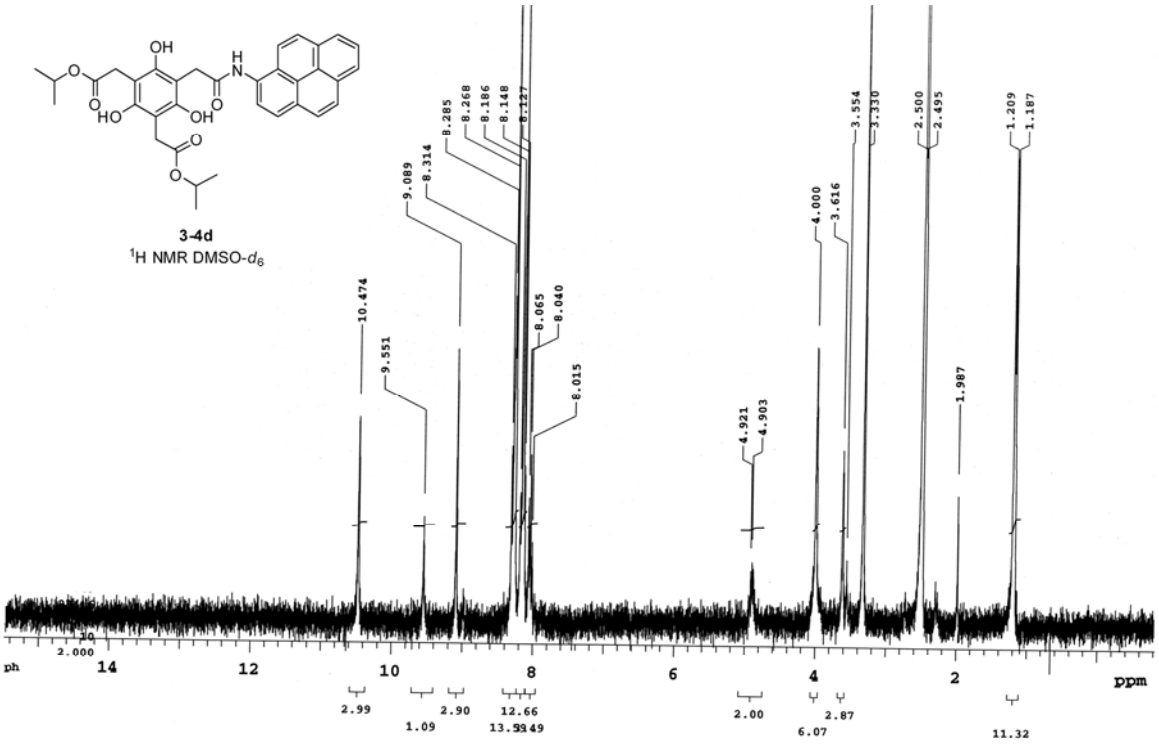
3-4d
1H NMR DMSO-d6
10.474
9.551
9.089
8.314
8.285
8.268
8.186
8.148
8.127
8.065
8.040
8.015
4.921
4.903
4.000
3.616
3.554
3.330
2.500
2.495
1.987
1.209
1.187
ppm

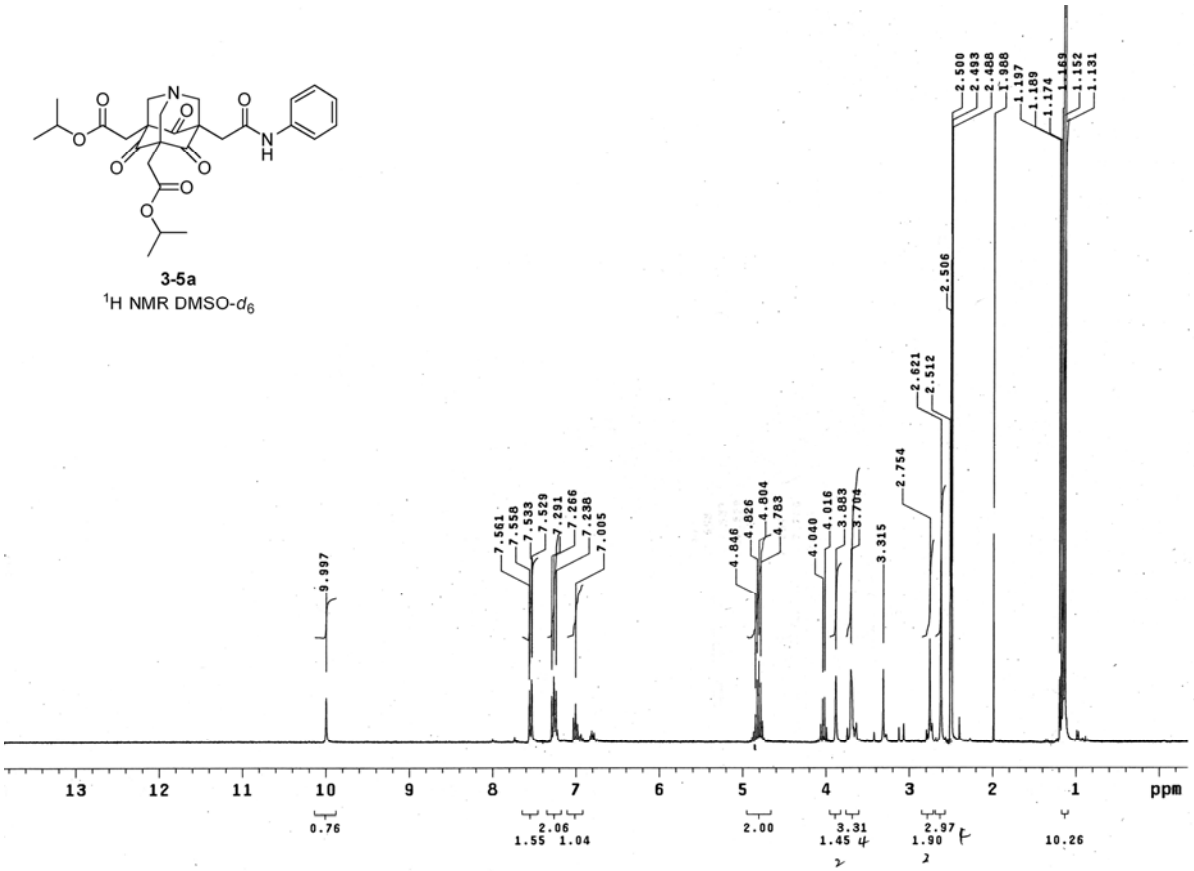
3-5a
1H NMR DMSO-d6
9.997
7.561
7.550
7.533
7.529
7.291
7.266
7.238
7.005
4.846
4.826
4.804
4.783
4.040
4.016
3.883
3.704
3.315
2.754
2.621
2.512
2.506
2.500
2.493
2.488
1.988
1.197
1.189
1.174
1.169
1.152
1.131
ppm

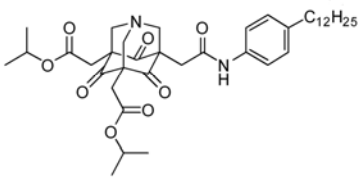

3-5b
^{1}H NMR $CDCl_3$

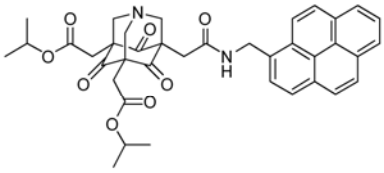

3-5c
^{1}H NMR DMSO-d_6

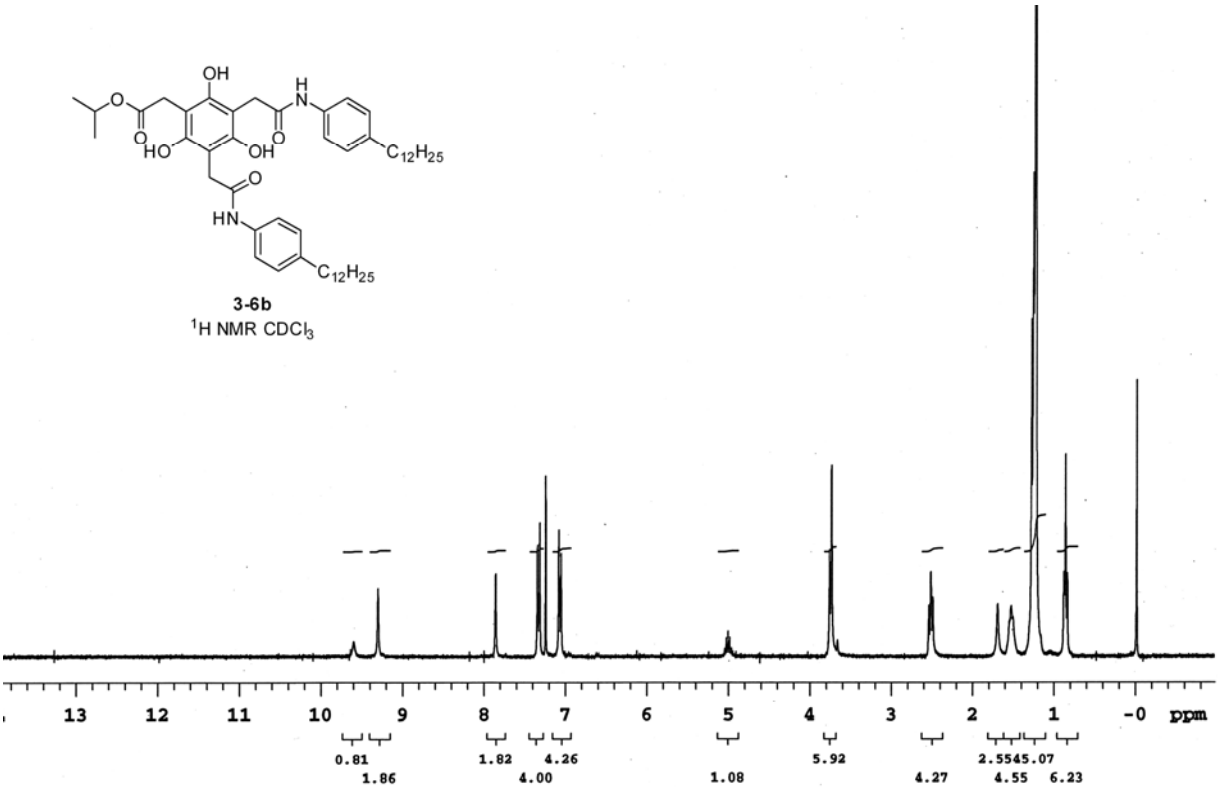

3-6b
^{1}H NMR $CDCl_3$

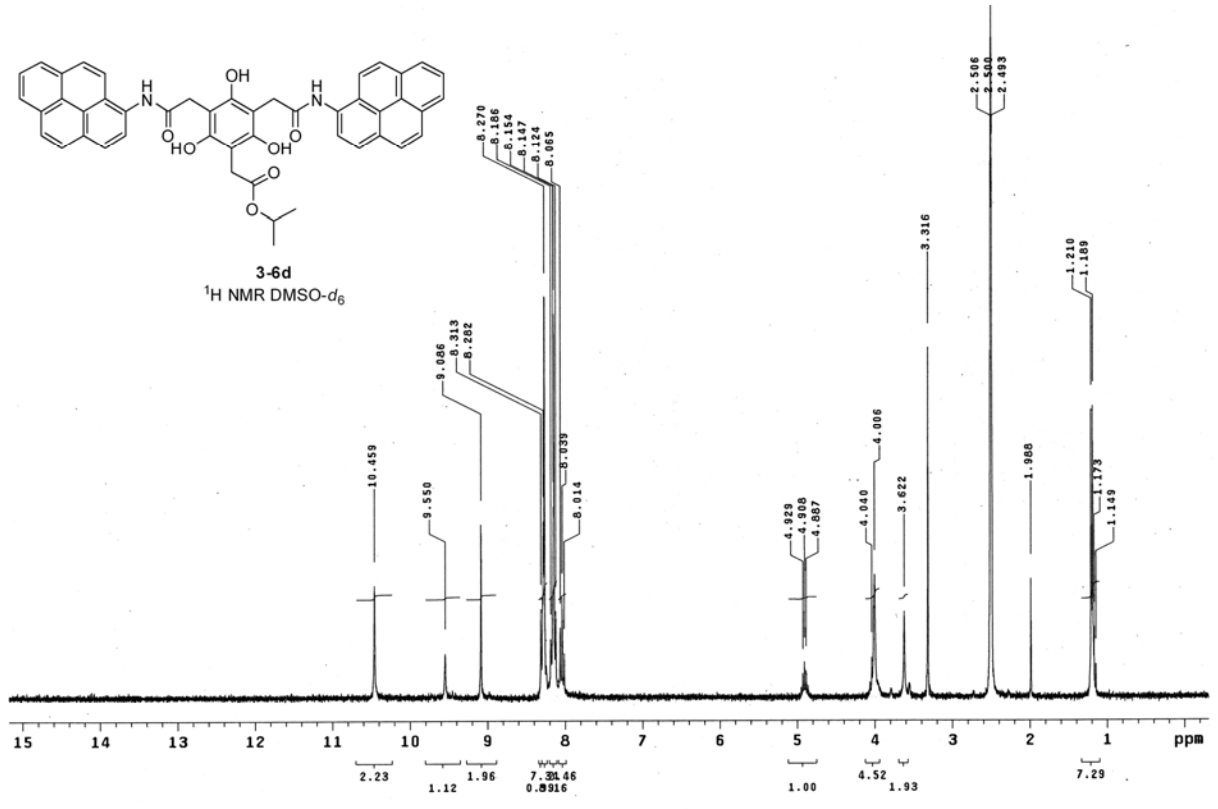

3-6d
^{1}H NMR DMSO-d_6

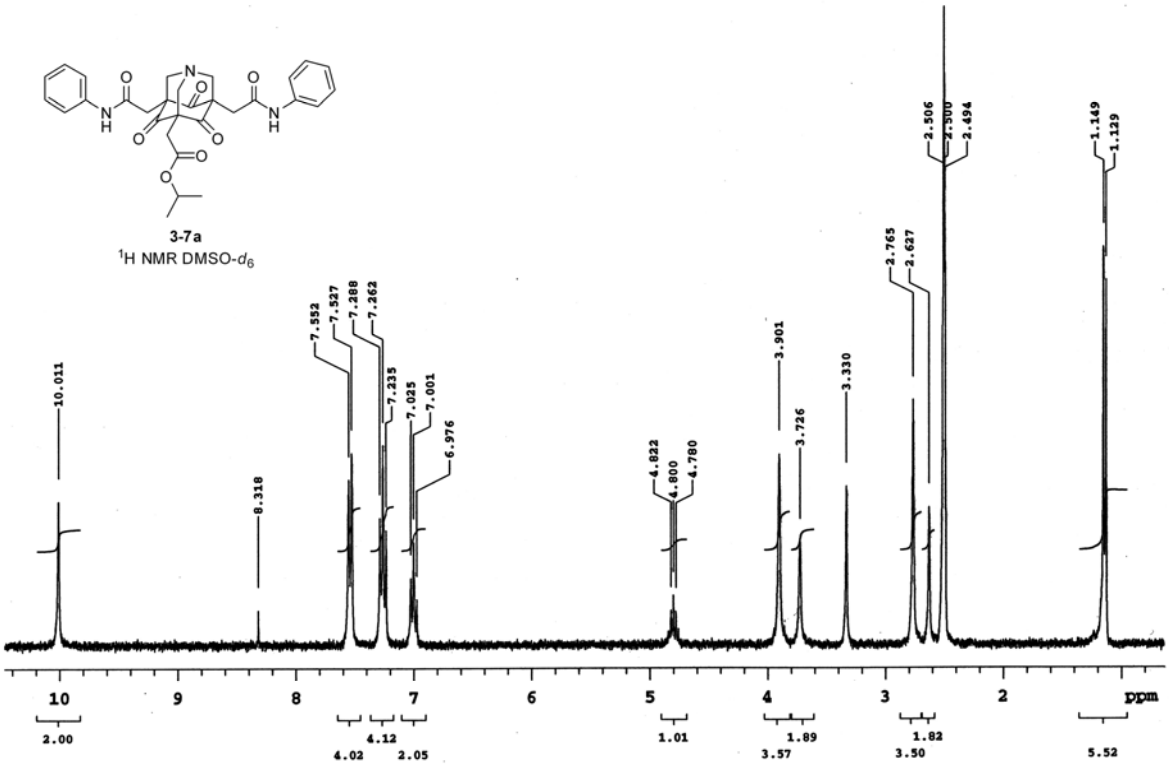

3-7a
^{1}H NMR DMSO-d_6

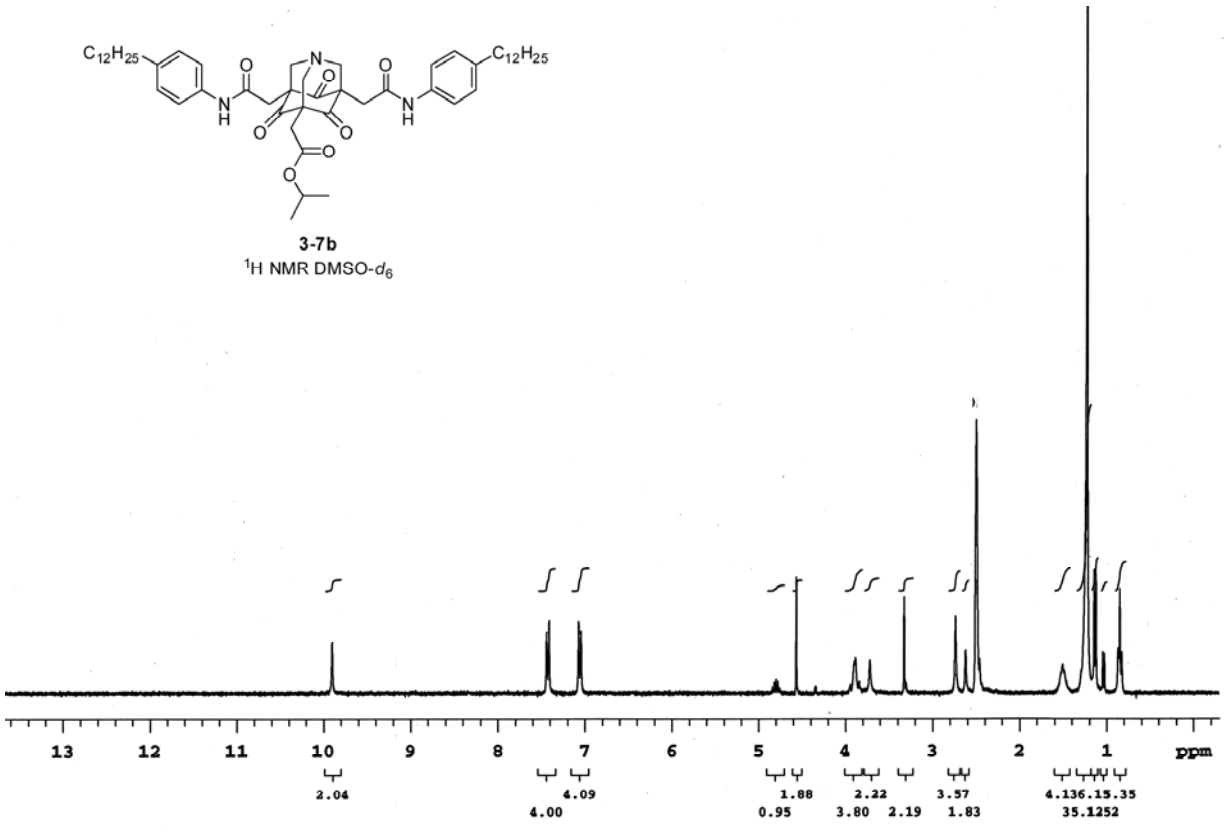

3-7b
^{1}H NMR DMSO-d_6

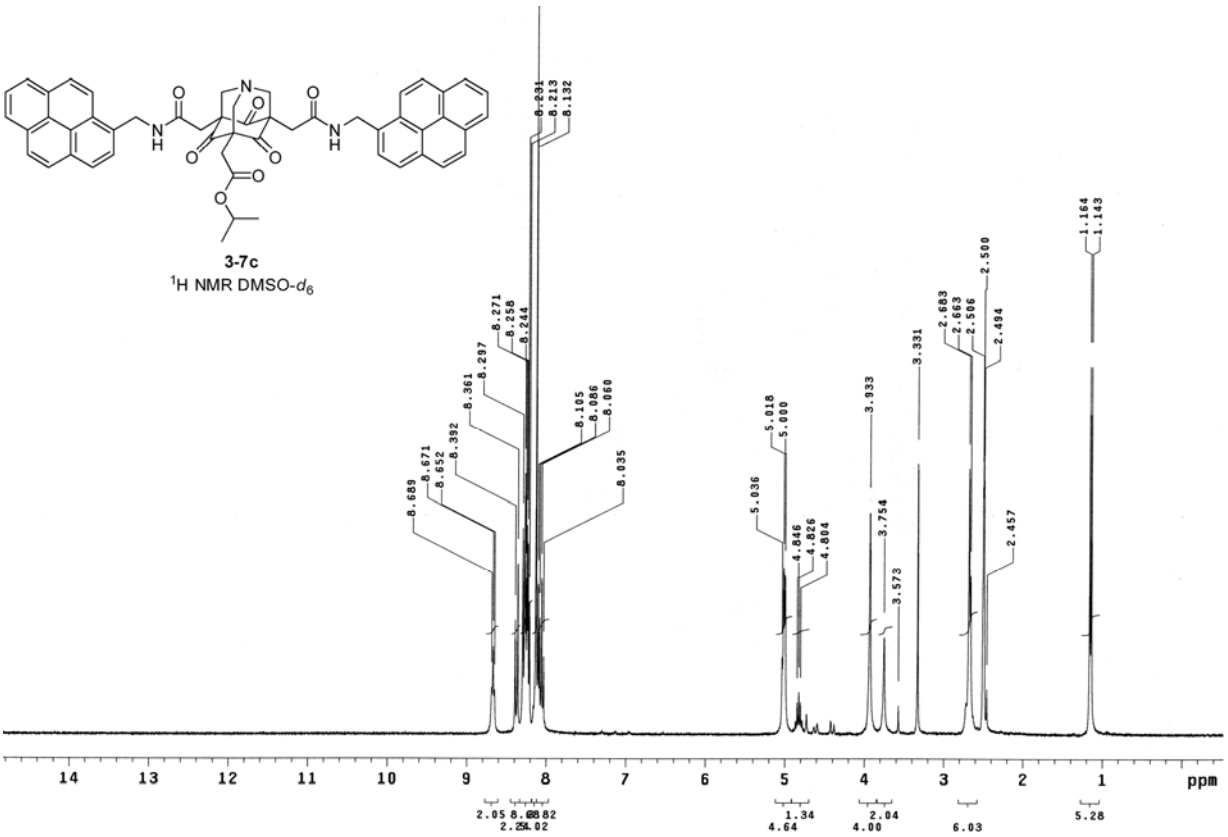

3-7c
^{1}H NMR DMSO-d_6

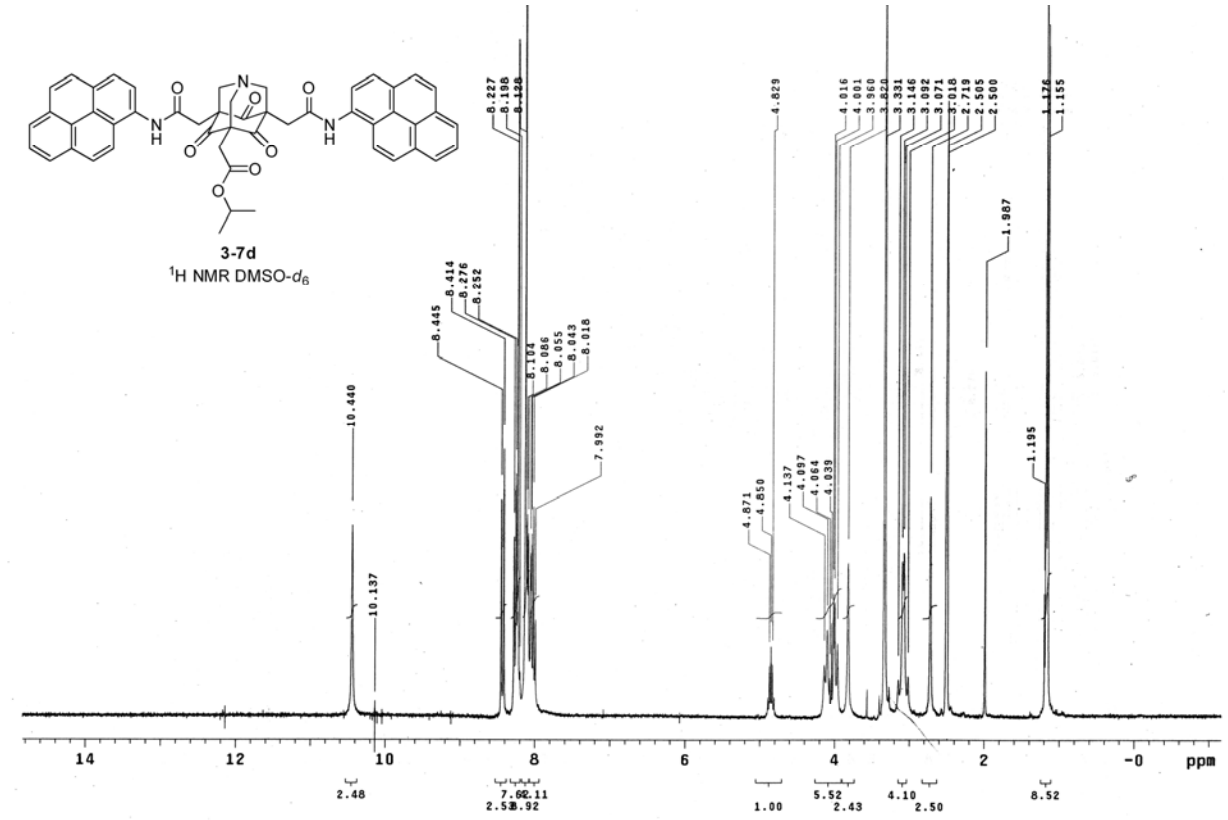

3-7d
^{1}H NMR DMSO-d_6

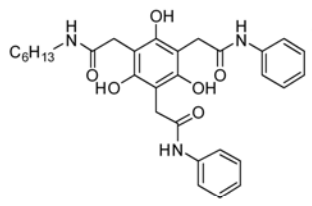

3-8b
^{1}H NMR DMSO-d_6

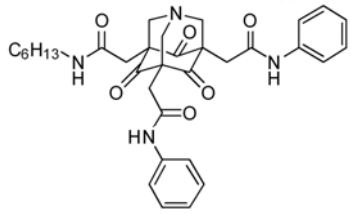

3-9b
^{1}H NMR pyridine-d_5

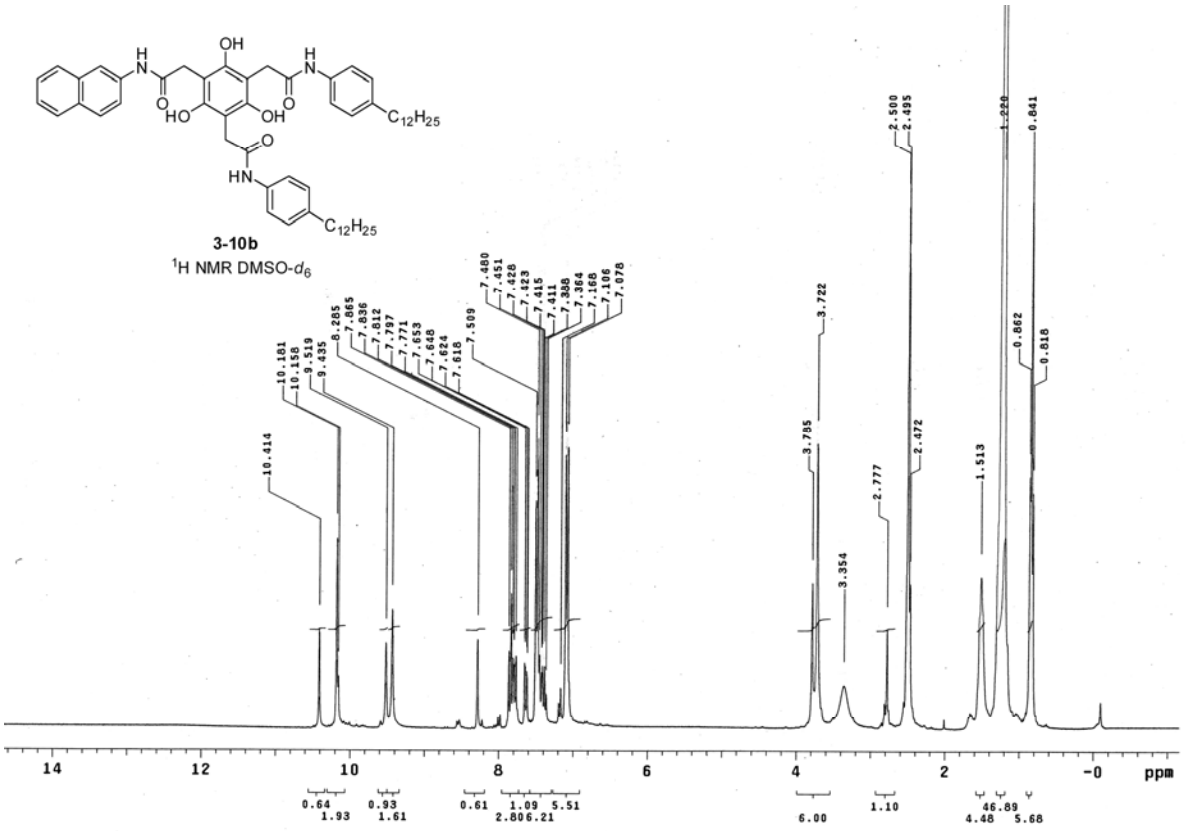
3-10b
^{1}H NMR DMSO-d_6
ppm

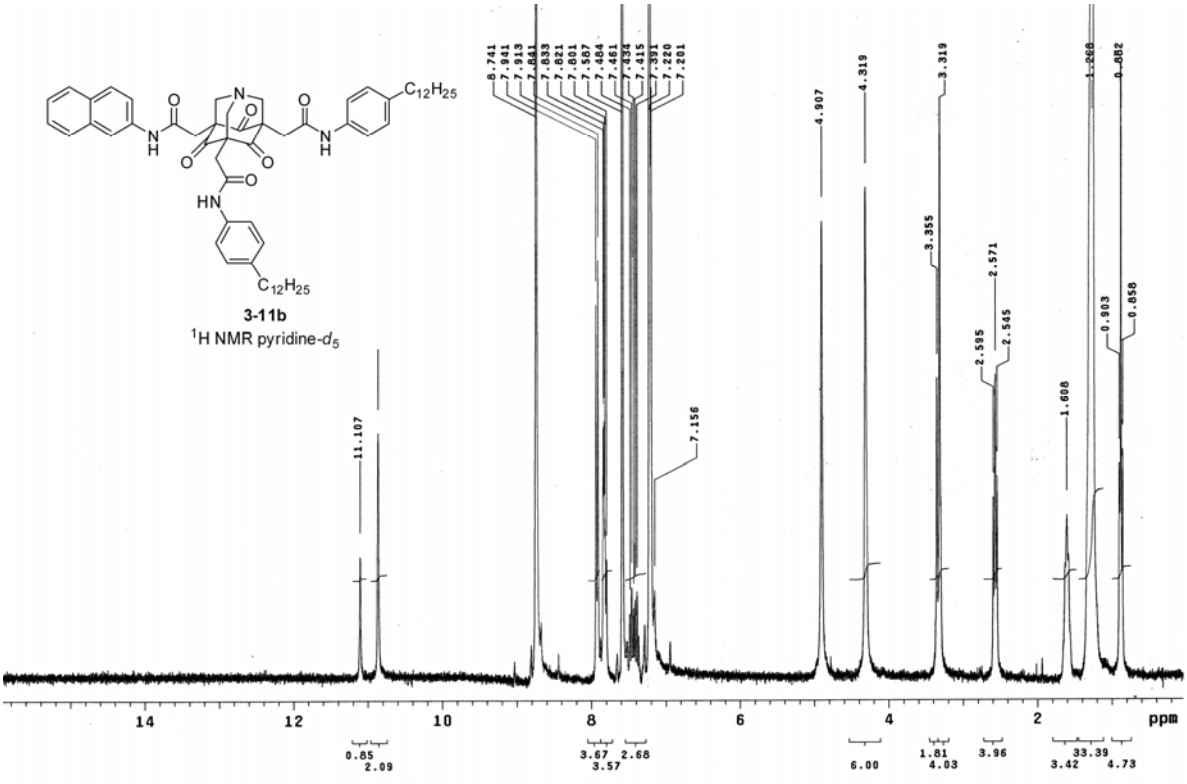
3-11b
^{1}H NMR pyridine-d_5
ppm

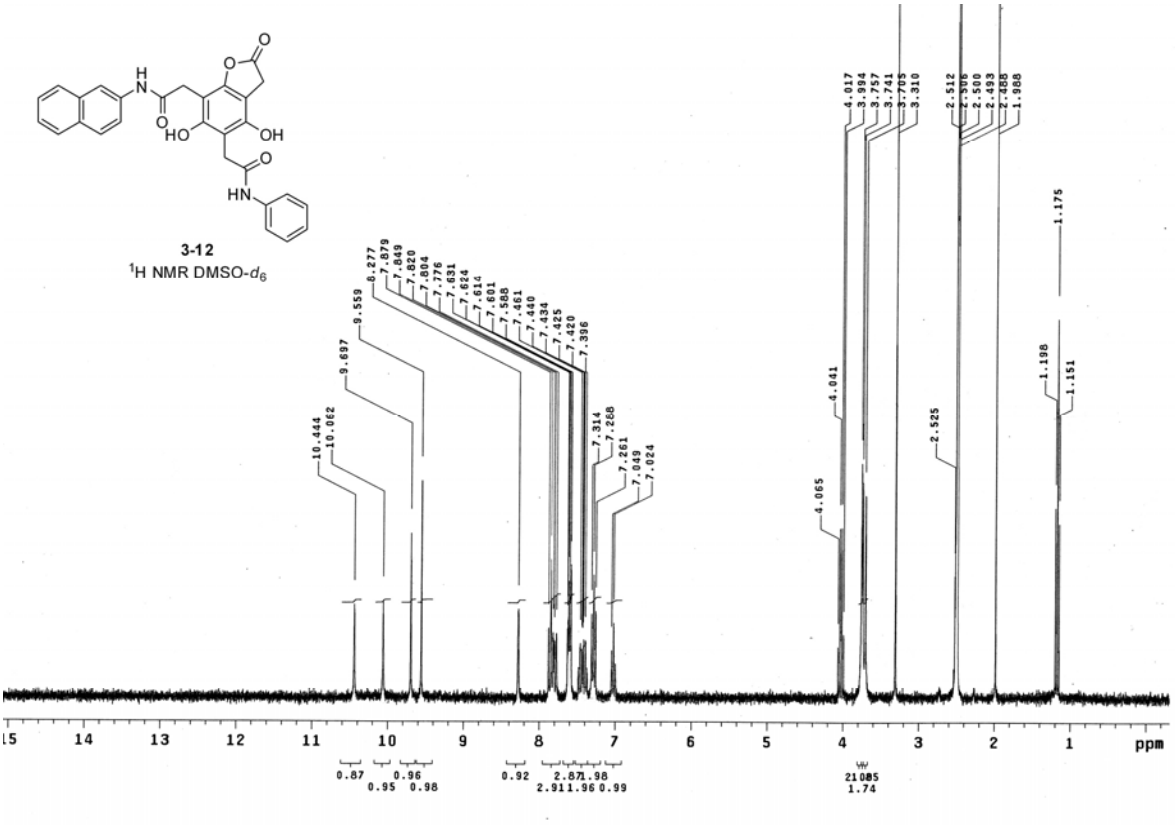

3-12
^{1}H NMR DMSO-d_6

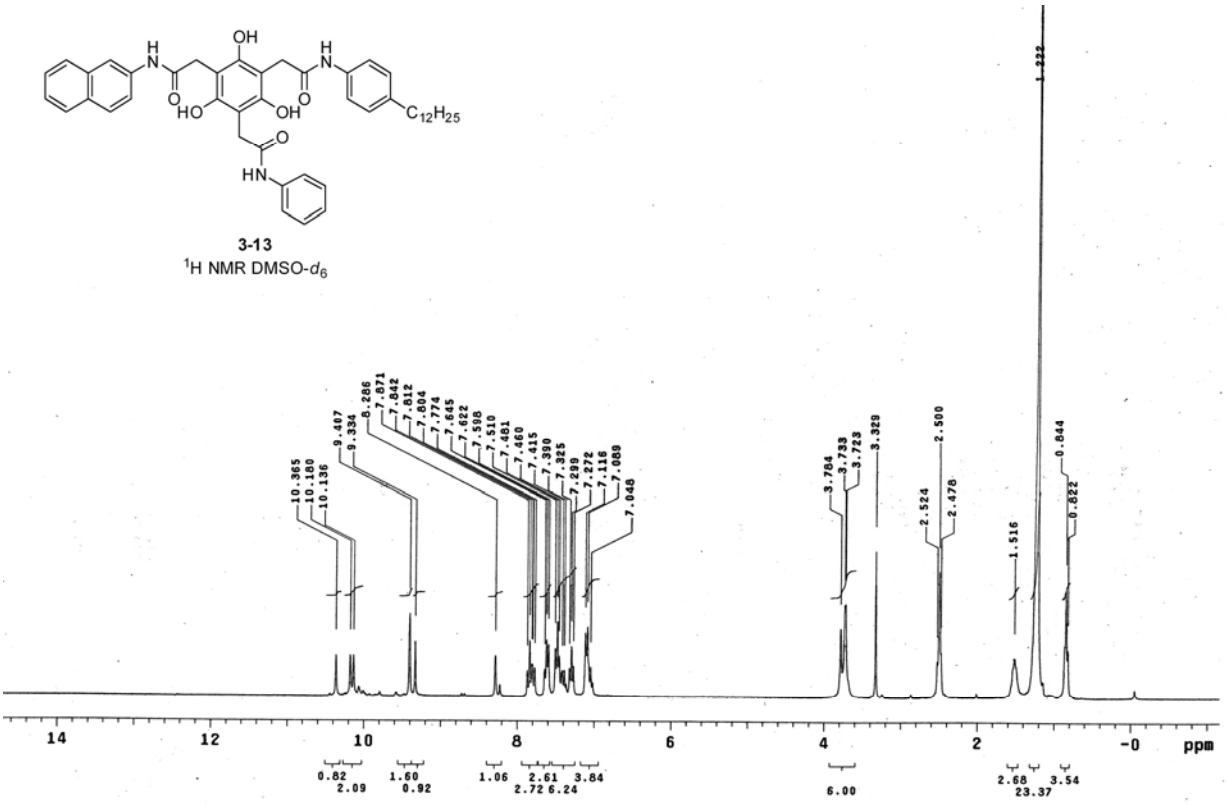

3-13
^{1}H NMR DMSO-d_6

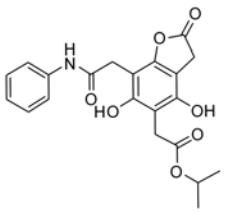

3-14
^{1}H NMR DMSO-d_6

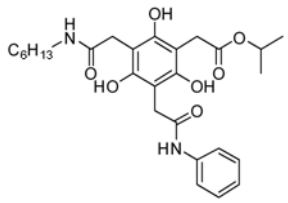

3-15a
^{1}H NMR $CDCl_3$

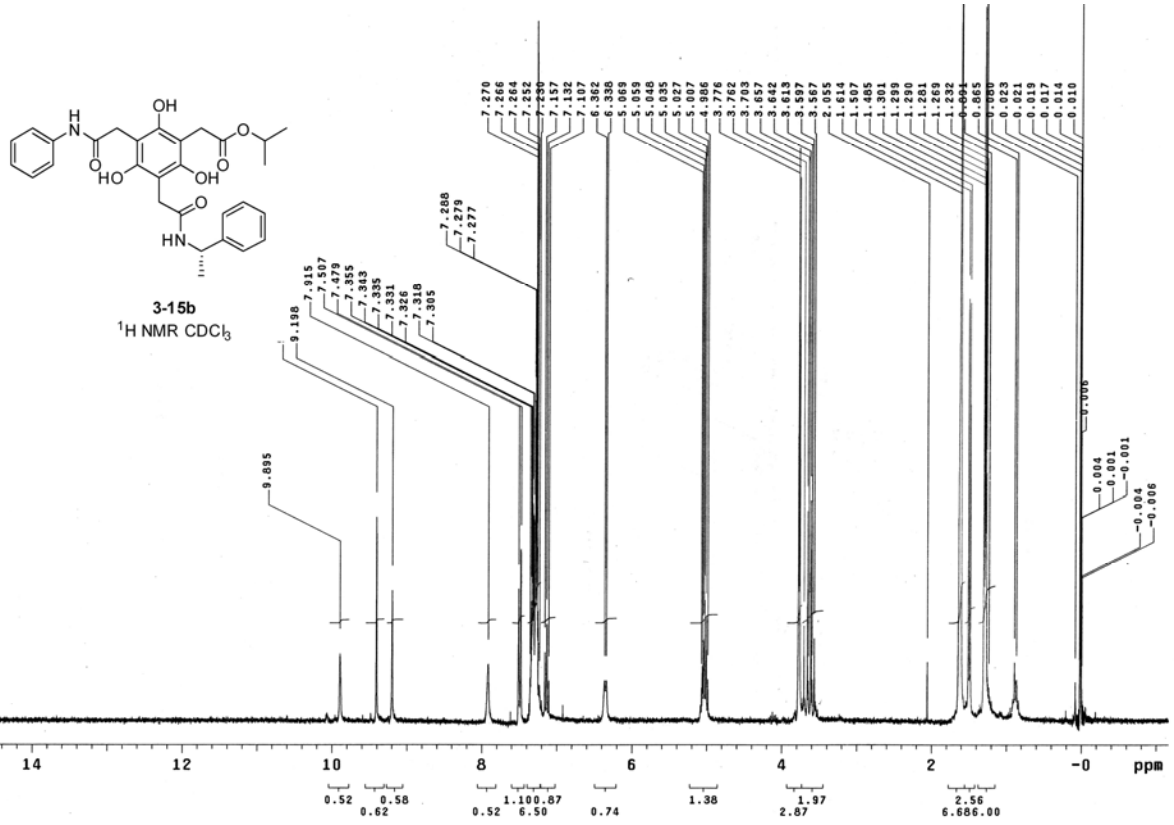
3-15b
^{1}H NMR $CDCl_3$

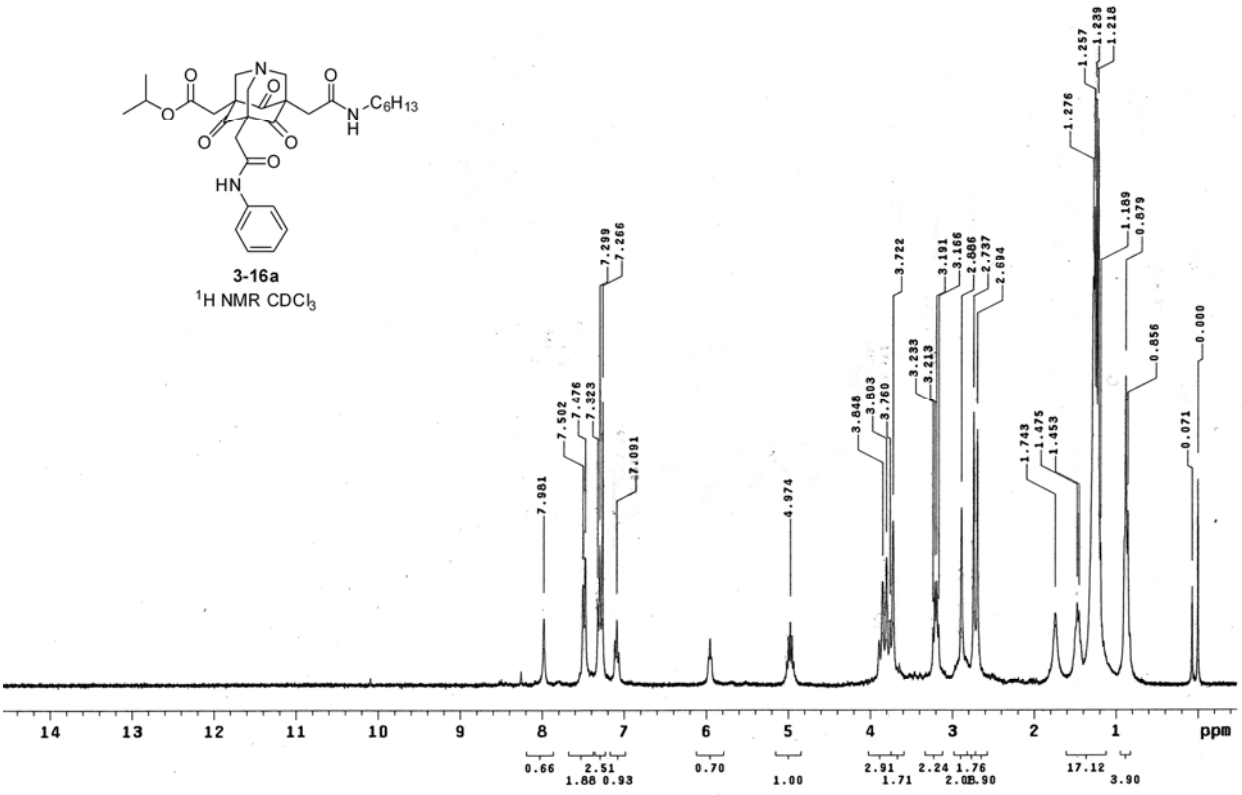
3-16a
^{1}H NMR $CDCl_3$

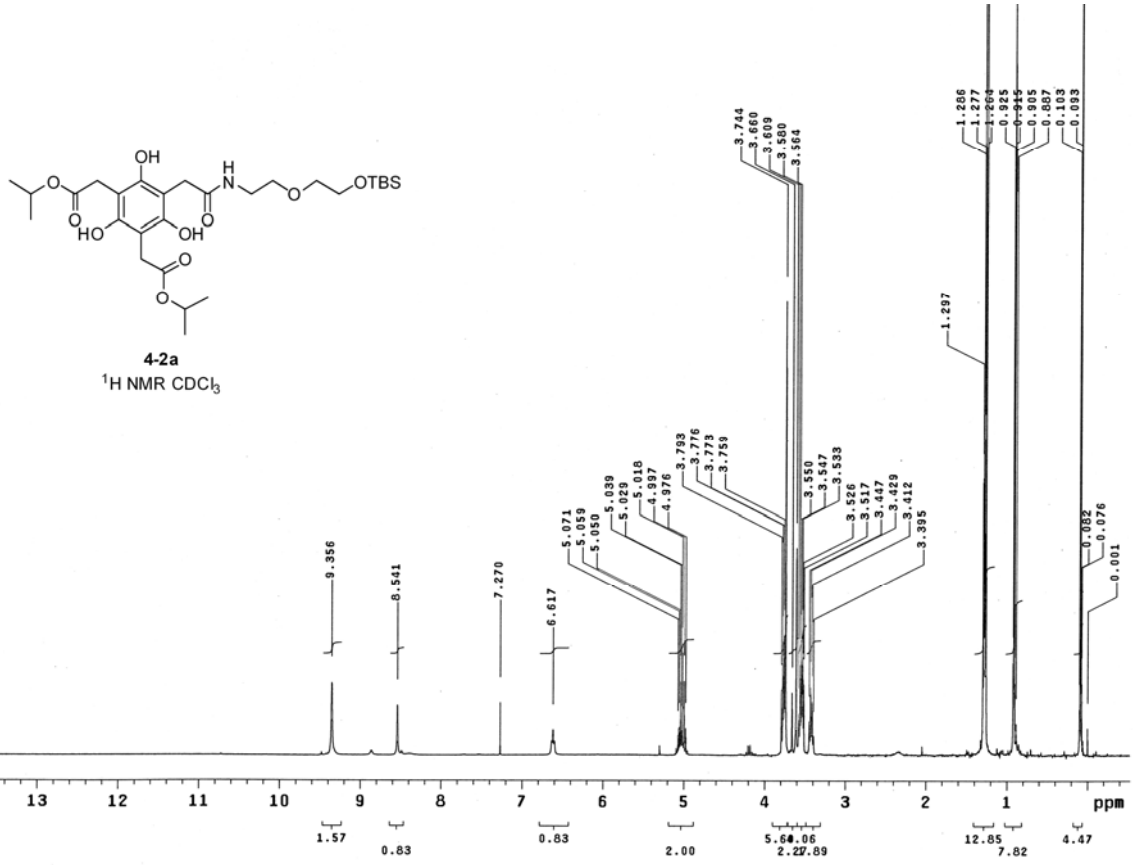

4-2a

^{1}H NMR $CDCl_3$

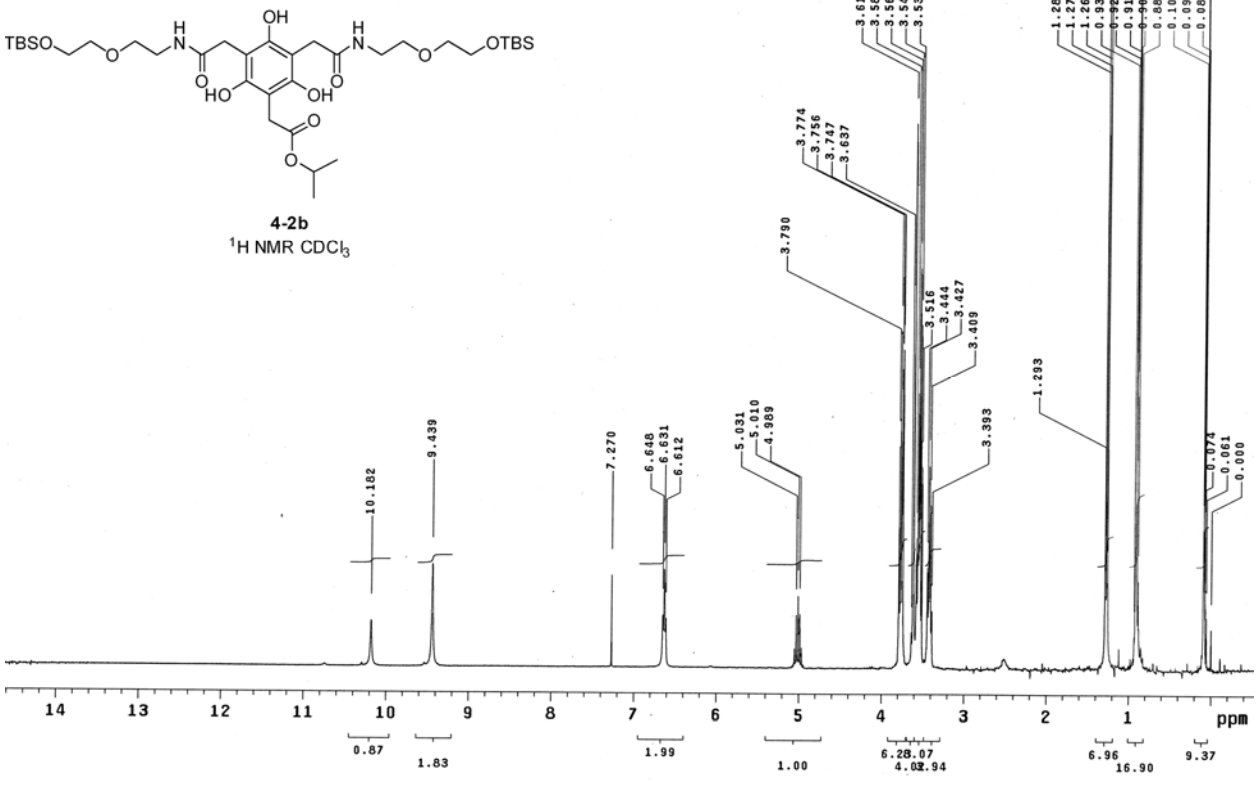

4-2b

^{1}H NMR $CDCl_3$

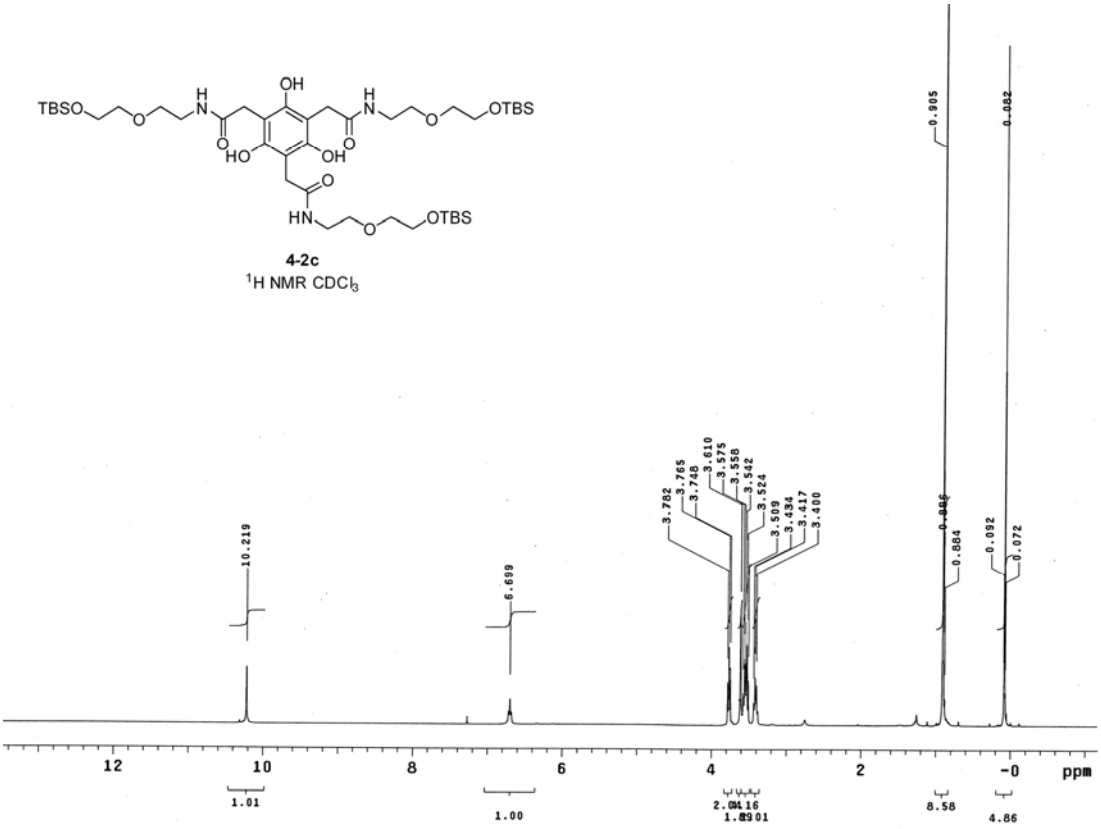
TBSO
OTBS
OH
HO
OH
HN
OTBS
4-2c
^{1}H NMR $CDCl_3$
10.219
6.699
3.782
3.765
3.748
3.610
3.575
3.558
3.542
3.524
3.509
3.434
3.417
3.400
0.905
0.884
0.092
0.072
12
10
8
6
4
2
-0
ppm
1.01
1.00
8.58
4.86

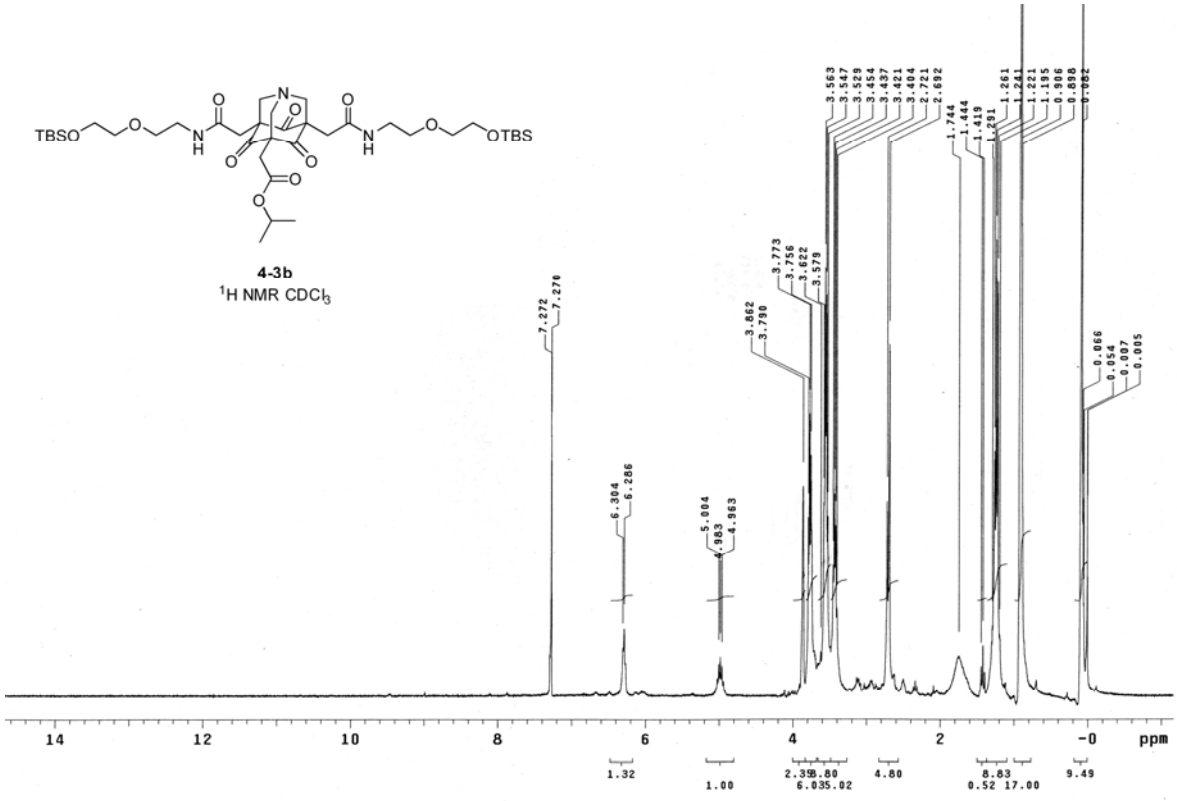
TBSO
OTBS
4-3b
^{1}H NMR $CDCl_3$
7.272
7.270
6.304
6.286
5.004
4.983
4.963
3.862
3.780
3.773
3.756
3.622
3.579
3.563
3.547
3.529
3.454
3.437
3.421
3.404
3.387
3.371
2.692
1.744
1.444
1.419
1.291
1.261
1.241
1.221
1.195
0.906
0.898
0.082
0.066
0.054
0.007
0.005
14
12
10
8
6
4
2
-0
ppm
1.32
1.00
6.03
5.02
4.80
0.52
17.00
9.49

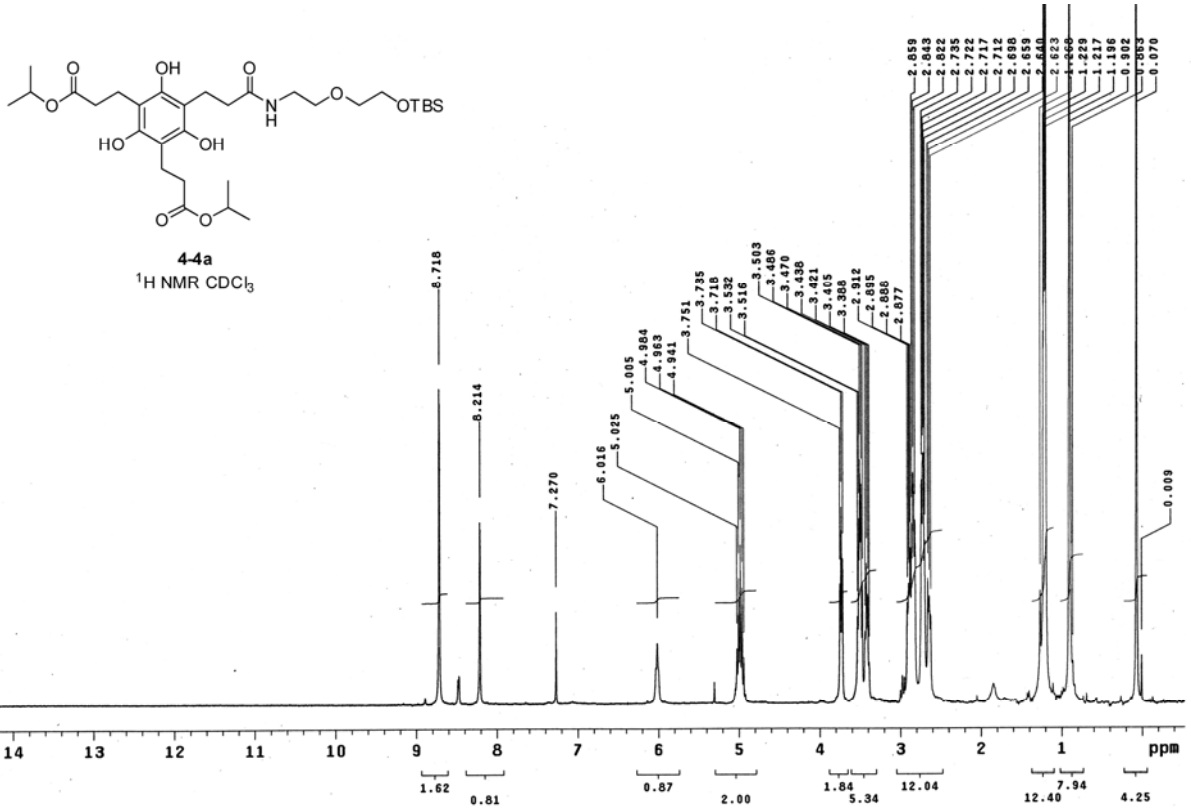

4-4a

^{1}H NMR $CDCl_3$

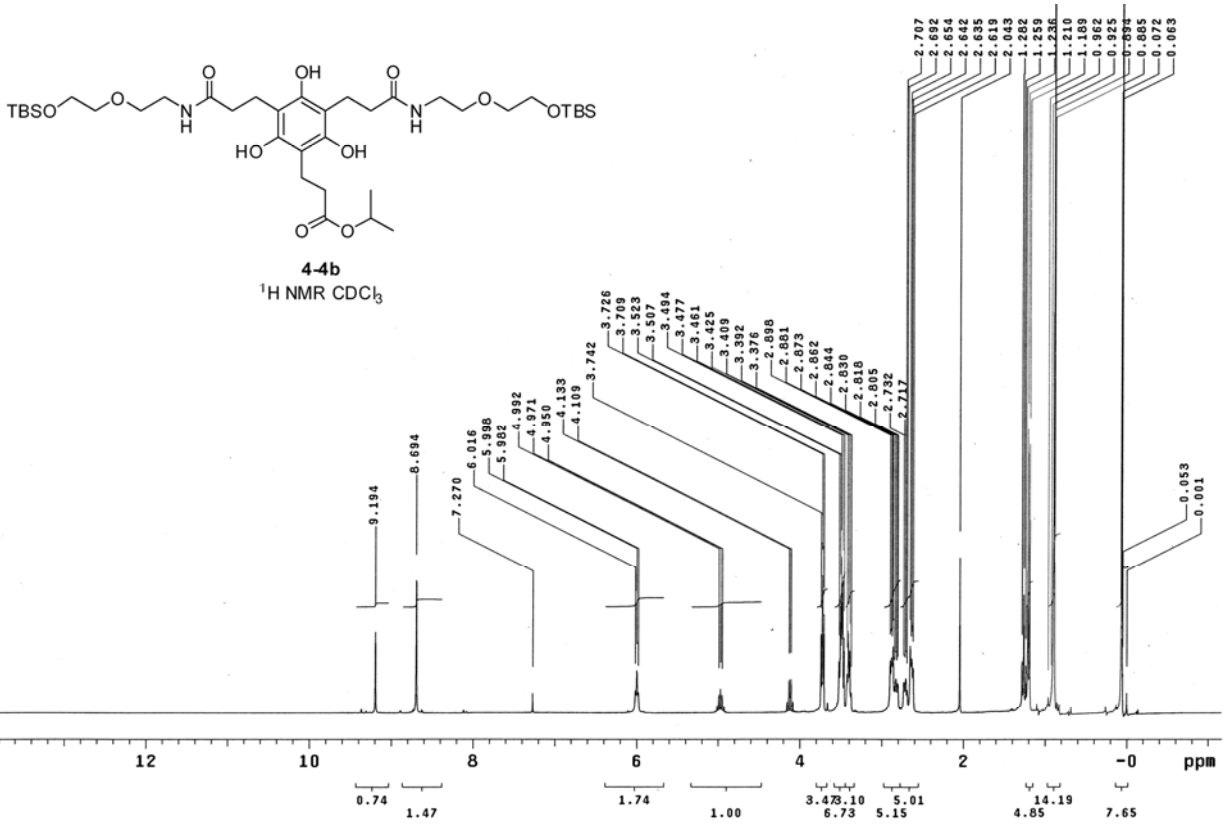

4-4b

^{1}H NMR $CDCl_3$

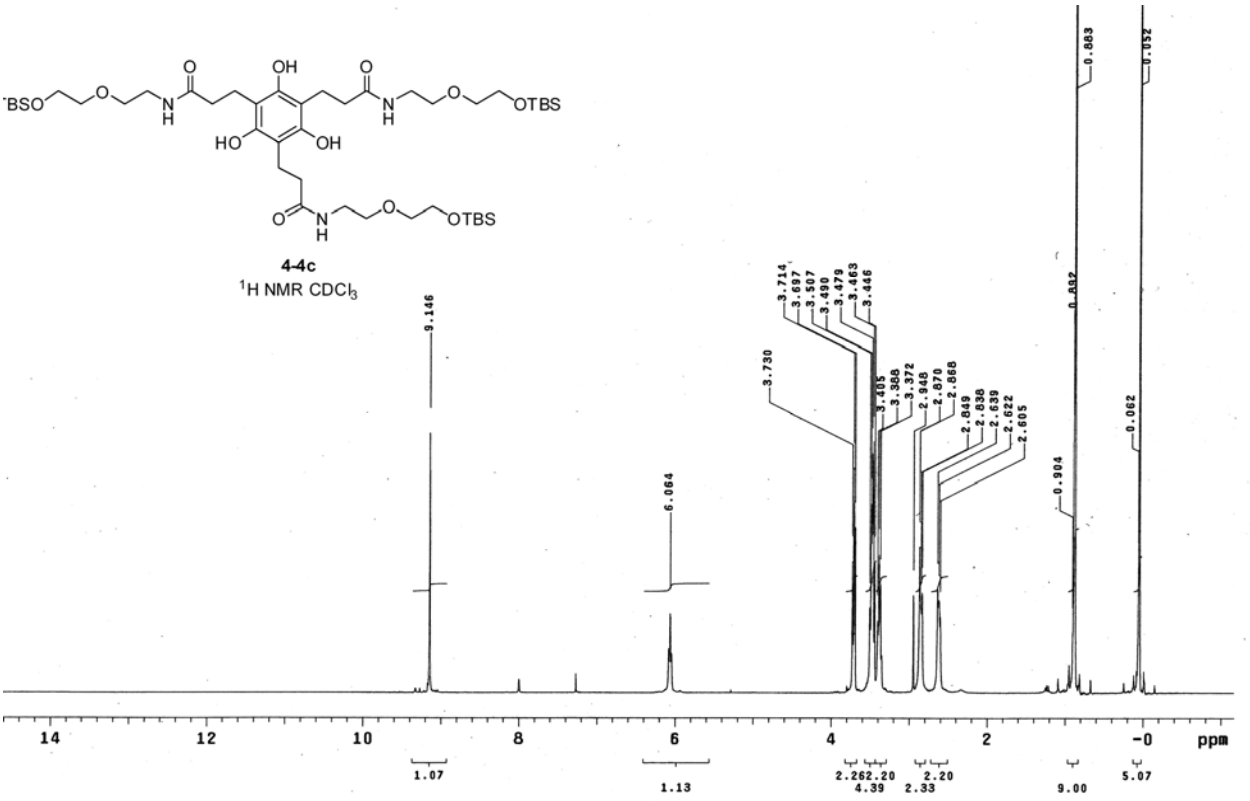
OH
O
N
H
HO
OTBS
4-4c
^{1}H NMR $CDCl_3$
9.146
6.064
3.730
3.714
3.697
3.507
3.490
3.479
3.463
3.446
3.405
3.388
3.372
2.948
2.870
2.868
2.849
2.830
2.639
2.622
2.605
0.883
0.882
0.904
0.062
14
12
10
8
6
4
2
-0
ppm
1.07
1.13
2.26
2.20
4.39
2.33
9.00
5.07

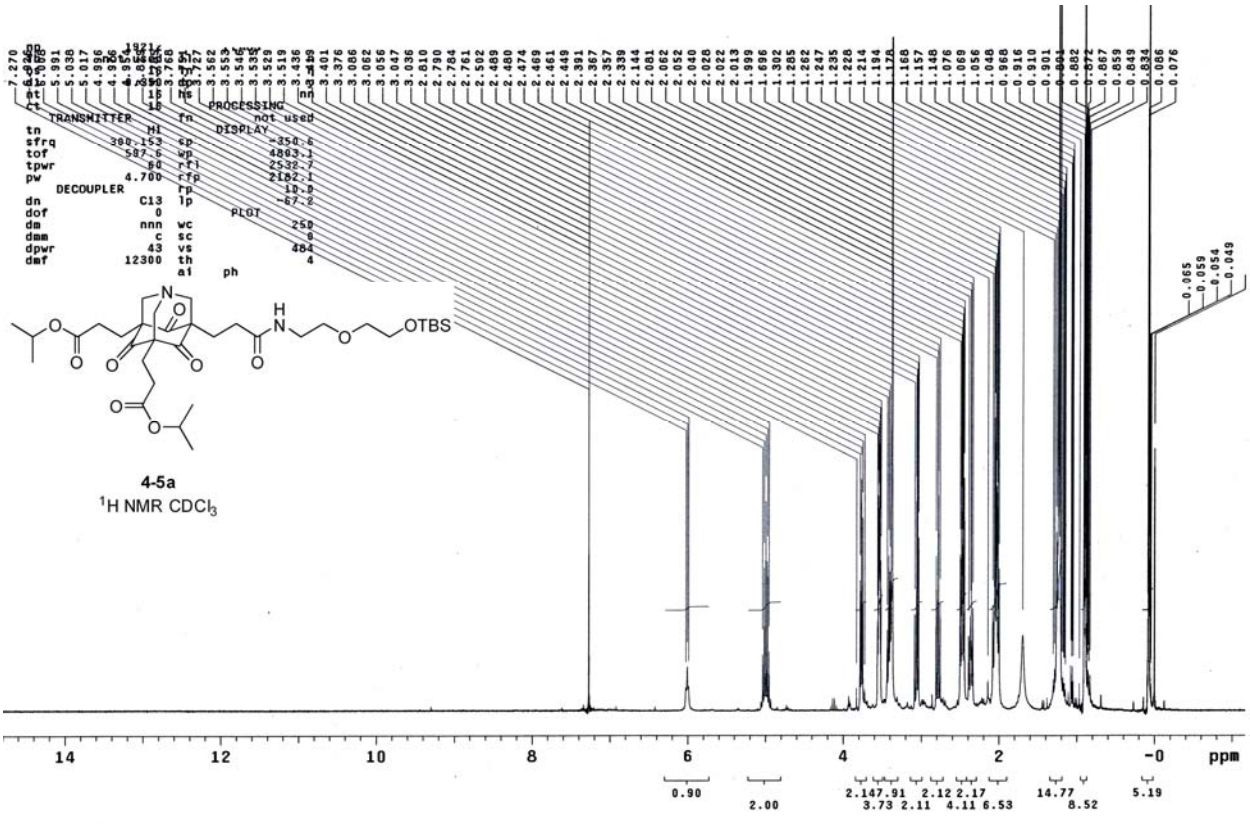
OTBS
4-5a
^{1}H NMR $CDCl_3$
0.065
0.059
0.054
0.049
14
12
10
8
6
4
2
-0
ppm
0.90
2.00
2.14
7.91
2.12
2.17
3.73
2.11
4.11
6.53
14.77
8.52
5.19

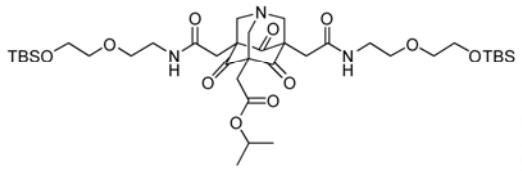

4-3b

^{1}H NMR $CDCl_3$

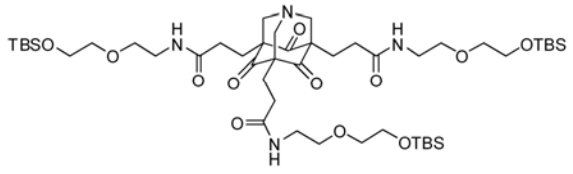

4-5c

^{1}H NMR $CDCl_3$

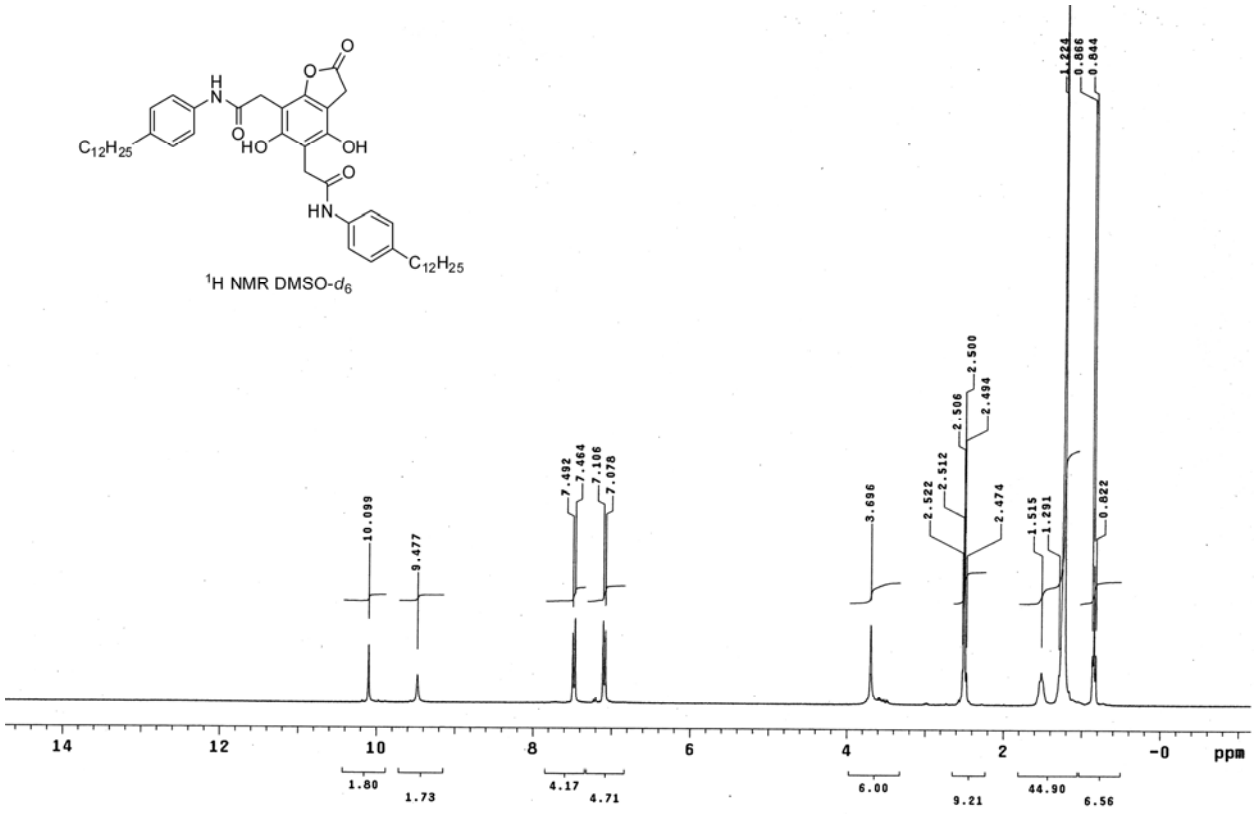
$C_{12}H_{25}$
H
N
O
O
HO
OH
O
HN
$C_{12}H_{25}$
^{1}H NMR DMSO-d_6
10.099
9.477
7.492
7.464
7.106
7.078
3.696
2.522
2.512
2.506
2.500
2.494
2.474
1.515
1.291
1.224
0.866
0.844
0.822
14
12
10
8
6
4
2
-0
ppm
1.80
1.73
4.17
4.71
6.00
9.21
44.90
6.56

LIST OF REFERENCES

1. Lehn, J. M., *Angew. Chem., Int. Ed.*, **1990,** *29*, 1304.

2. Lehn, J. M., *Science*, **1993,** *260*, 1762.

3. Steed, J. W.; Atwood, J. L., *Supramolecular Chemistry*, Wiley, Chichester, 2000.

4. Schneider, H.-J.; Yatsimirsky, A., *Principles and Methods of Supramolecular Chemistry*, Wiley, Chichester, 2000.

5. Lehn, J.-M., *Supramolecular Chemistry: Concepts and Perspectives*, VCH, New York, 1995.

6. Meyer, E. A.; Castellano, R. K.; Diederich, F., *Angew. Chem., Int. Ed.,* **2003,** *42*, 1210.

7. Lindoy, L. F.; Atkinson, I. M., *Self-assembly in Supramolecular Systems*, The Royal Society of Chemistry, Cambridge, UK, 2000.

8. Dodziuk, H., *Introduction to Supramolecular Chemistry*, Kluwer Academic Publishers, Netherlands, 2001.

9. Whitesides, G. M.; Grzybowski, B., *Science*, **2002,** *295*, 2418.

10. Fiammengo, R.; Crego-Calama, M.; Reinhoudt, D. N., *Curr. Opin. Chem. Biol.*, **2001,** *5*, 660.

11. Ghadiri, M. R.; Granja, J. R.; Buehler, L. K., *Nature*, **1994,** *369*, 301.

12. Vogtle, F., *Supramolecular Chemistry*, Wiley, Chichester, 1993.

13. Balzani, V.; Credi, A.; Venturi, M., *Chem. Eur. J.*, **2002,** *8*, 5524.

14. Hoeben, F. J. M.; Jonkheijm, P.; Meijer, E. W.; Schenning, A. P. H. J., *Chem. Rev.*, **2005,** *105*, 1491.

15. Messmore, B. W.; Hulvat, J. F.; Sone, E. D.; Stupp, S. I., *J. Am. Chem. Soc.*, **2004,** *126*, 14452.

16. Bushey, M. L.; Nguyen, T. Q.; Zhang, W.; Horoszewski, D.; Nuckolls, C., *Angew. Chem., Int. Ed.*, **2004,** *43*, 5446.

17. Allen, G., *Chemistry & Industry*, Uk-Research-Plc, 1984.

18. Crissey, J. T.; Fergason, J. L.; Bettenha.Jm, *J. Invest. Dermatol.*, **1965,** *45*, 329.

19. Meiboom, S.; Snyder, L. C., *Science*, **1968,** *162*, 1337-&.

20. Hoffmann, H.; Ebert, G., *Angew. Chem., Int. Ed.*, **1988,** *27*, 902.

21. Tour, J. M.; Wu, R. L.; Schumm, J. S., *J. Am. Chem. Soc.*, **1990,** *112*, 5662.

22. Aviram, A.; Ratner, M. A., *Chem. Phys. Lett.*, **1974,** *29*, 277.

23. Vintiloiu, A.; Leroux, J.-C., *J. Controlled Release*, **2008,** *125*, 179.

24. Sangeetha, N. M.; Maitra, U., *Chem. Soc. Rev.*, **2005,** *34*, 821.

25. Meister, A.; Bastrop, M.; Koschoreck, S.; Garamus, V. M.; Sinemus, T.; Hempel, G.; Drescher, S.; Dobner, B.; Richtering, W.; Huber, K.; Blume, A., *Langmuir*, **2007,** *23*, 7715.

26. Bissell, R.; Boden, N., *Chem. Ber.*, **1995,** *31*, 38.

27. Desiraju, G. R., *The Crystal as a Supramolecular Entity*, Wiley, Chichester, UK, 1996.

28. Jones, C. J., *Chem. Soc. Rev.*, **1998,** *27*, 289.

29. Knowles, P. F.; Stockley, P. G., *Chem. Ber.*, **1995,** *31*, 27.

30. Whitesides, G. M.; Mathias, J. P.; Seto, C. T., *Science*, **1991,** *254*, 1312.

31. Lawrence, D. S.; Jiang, T.; Levett, M., *Chem. Rev.*, **1995,** *95*, 2229.

32. Hof, F.; Craig, S. L.; Nuckolls, C.; Rebek, J., *Angew. Chem., Int. Ed.*, **2002,** *41*, 1488.

33. Risch, N., *J. Chem. Soc., Chem. Commun.*, **1983**, 532.

34. Kumar, S., *Liq. Cryst.*, **2004,** *31*, 1037.

35. Brand, J. D.; Kubel, C.; Ito, S.; Mullen, K., *Chem. Mater.*, **2000,** *12*, 1638.

36. Muller, M.; Kubel, C.; Mullen, K., *Chem. Eur. J.*, **1998,** *4*, 2099.

37. Andrienko, D.; Marcon, V.; Kremer, K., *J. Chem. Phys.*, **2006,** *125*, 124902.

38. Schmidt-Mende, L.; Fechtenkotter, A.; Mullen, K.; Moons, E.; Friend, R. H.; MacKenzie, J. D., *Science*, **2001,** *293*, 1119.

39. Halls, J. J. M.; Arias, A. C.; MacKenzie, J. D.; Wu, W. S.; Inbasekaran, M.; Woo, E. P.; Friend, R. H., *Adv. Mater.*, **2000,** *12*, 498.

40. Arias, A. C.; MacKenzie, J. D.; Stevenson, R.; Halls, J. J. M.; Inbasekaran, M.; Woo, E. P.; Richards, D.; Friend, R. H., *Macromolecules*, **2001,** *34*, 6005.

41. Hartgerink, J. D.; Beniash, E.; Stupp, S. I., *Science*, **2001,** *294*, 1684.

42. Jancy, B.; Asha, S. K., *Chem. Mater.*, **2008,** *20*, 169.

43. Yao, S.; Beginn, U.; Gress, T.; Lysetska, M.; Wurthner, F., *J. Am. Chem. Soc.*, **2004,** *126*, 8336.

44. Wurthner, F.; Yao, S.; Heise, B.; Tschierske, C., *Chem. Commun.*, **2001**, 2260-2261.

45. Serrette, A.; Carroll, P. J.; Swager, T. M., *J. Am. Chem. Soc.*, **1992,** *114*, 1887.

46. Yoshio, M.; Mukai, T.; Ohno, H.; Kato, T., *J. Am. Chem. Soc.*, **2004,** *126*, 994.

47. Kato, T.; Mizoshita, N., *Curr. Opin. Solid State Mater. Sci.*, **2002,** *6*, 579.

48. Kato, T.; Mizoshita, N.; Kishimoto, K., *Angew. Chem., Int. Ed.*, **2006,** *45*, 38.

49. Kato, T.; Mizoshita, N.; Moriyama, M.; Kitamura, T., *Low Molecular Mass Gelators: Design, Self-Assembly, Function*, **2005,** *256*, 219.

50. Canceill, J.; Lacombe, L.; Collet, A., *J. Am. Chem. Soc.*, **1986,** *108*, 4230.

51. Rapenne, G.; Crassous, J.; Collet, A.; Echegoyen, L.; Diederich, F., *Chem. Commun.*, **1999**, 1121.

52. Kirchhoff, P. D.; Dutasta, J. P.; Collet, A.; McCammon, J. A., *J. Am. Chem. Soc.*, **1999,** *121*, 381.

53. Tschierske, C., *Chem. Soc. Rev.*, **2007,** *36*, 1930.

54. Reddy, R. A.; Tschierske, C., *J. Mater. Chem.*, **2006,** *16*, 907.

55. Lampkins, A. J.; Abdul-Rahim, O.; Li, H. F.; Castellano, R. K., *Org. Lett.*, **2005,** *7*, 4471.

56. Li, H. F.; Homan, E. A.; Lampkins, A. J.; Ghiviriga, I.; Castellano, R. K., *Org. Lett.*, **2005,** *7*, 443.

57. Hoffmann, R.; Imamura, A.; Hehre, W. J., *J. Am. Chem. Soc.*, **1968,** *90*, 1499.

58. Hoffmann, R., *Acc. Chem. Res.*, **1971,** *4*, 1.

59. Haselbac.E; Hashmall, J. A.; Heilbron.E; Hornung, V., *Angew. Chem., Int. Ed.*, **1969,** *8*, 878.

60. Dewar, M. J. S.; Wasson, J. S., *J. Am. Chem. Soc.*, **1970,** *92*, 3506.

61. Paddon-Row, M. N., *Acc. Chem. Res.*, **1982,** *15*, 245.

62. Gleiter, R., *Angew. Chem., Int. Ed.*, **1974,** *13*, 696.

63. Cookson, R. C.; Henstock, J.; Hudec, J., *J. Am. Chem. Soc.*, **1966,** *88*, 1060.

64. Hudec, J., *J. Chem. Soc., Chem. Commun.*, **1970**, 829.

65. Dekkers, A. W. J.; Verhoeve.Jw; Speckamp, W. N., *Tetrahedron*, **1973,** *29*, 1691.

66. Pasman, P.; Rob, F.; Verhoeven, J. W., *J. Am. Chem. Soc.*, **1982,** *104*, 5127.

67. Pasman, P.; Verhoeven, J. W.; Deboer, T. J., *Tetrahedron Lett.*, **1977**, 207.

68. Krijnen, B.; Beverloo, H. B.; Verhoeven, J. W.; Reiss, C. A.; Goubitz, K.; Heijdenrijk, D., *J. Am. Chem. Soc.*, **1989,** *111*, 4433.

69. Heitele, H.; Finckh, P.; Michelbeyerle, M. E., *Angew. Chem., Int. Ed.*, **1989,** *28*, 619.

70. Metzger, R. M., *Chem. Rev.*, **2003,** *103*, 3803.

71. Schuddeboom, W.; Krijnen, B.; Verhoeven, J. W.; Staring, E. G. J.; Rikken, G. L. J. A.; Oevering, H., *Chem. Phys. Lett.*, **1991,** *179*, 73.

72. Verhoeven, J. W.; Goes, M.; Hofstraat, J. W., *Patent WO0065881*, 2000.

73. Oosterbaan, W. D.; van Gerven, P. C. M.; van Walree, C. A.; Koeberg, M.; Piet, J. J.; Havenith, R. W. A.; Zwikker, J. W.; Jenneskens, L. W.; Gleiter, R., *Eur. J. Org. Chem.*, **2003**, 3117.

74. Oosterbaan, W. D.; Kaats-Richters, V. E. M.; Jenneskens, L. W.; Van Walree, C. A., *J. Polym. Sci., Part A: Polym. Chem.*, **2004,** *42*, 4775.

75. Kawashima, N.; Kameyama, A.; Nishikubo, T.; Nagai, T., *J. Polym. Sci., Part A: Polym. Chem.*, **2001,** *39*, 1764.

76. Lampkins, A. J.; Li, Y.; Abbas, A. A.; Abboud, K. A.; Ghiviriga, I.; Castellano, R. K., *Chem. Eur. J.*, **2008,** *14*, 1452.

77. De Ridder, D. J. A.; Goubitz, K.; Schenk, H.; Krijnen, B.; Verhoeven, J. W., *Helv. Chim. Acta.*, **2003,** *86*, 812.

78. Yuan, L., *Master Thesis*, Gainesville, FL, 2005.

79. Risch, N., *Chem. Ber.*, **1985,** *118*, 4849.

80. Risch, N., *Chem. Ber.*, **1985,** *118*, 4073.

81. Risch, N.; Langhals, M.; Hohberg, T., *Tetrahedron Lett.*, **1991,** *32*, 4465.

82. Risch, N.; Langhals, M.; Mikosch, W.; Bogge, H.; Muller, A., *J. Am. Chem. Soc.*, **1991,** *113*, 9411.

83. Kardel, D.; Knoche, W.; Risch, N., *J. Chem. Soc., Perkin Trans. 2*, **1993**, 1455.

84. Jimenez-Cruz, F.; Cetina-Rosado, R.; Hernandez-Ortega, S.; Toscano, R. A.; Rios-Olivares, H., *Acta Crystallodr., Sect. C: Cryst. Struct. Commun.*, **2001,** *57*, 868.

85. Jimenez-Cruz, F.; Rios-Olivares, H.; Hernandez-Ortega, S.; Cervantes-Nevarez, A., *J. Mol. Struct.*, **2003,** *655*, 23.

86. Hickmott, P. W.; Ahmed, M. G.; Ahmed, S. A.; Wood, S.; Kapon, M., *J. Chem. Soc., Perkin Trans. 1*, **1985**, 2559.

87. Alabugin, I. V.; Manoharan, M., *J. Org. Chem.*, **2004,** *69*, 9011.

88. Allinger, N. L.; Chen, K. S.; Katzenellenbogen, J. A.; Wilson, S. R.; Anstead, G. M., *J. Comput. Chem.*, **1996,** *17*, 747.

89. Sumpter, B. G.; Meunier, V.; Vazquez-Mayagoitia, A.; Castellano, R. K., *Int. J. Quantum Chem.*, **2007,** *107*, 2233.

90. Sumpter, B. G.; Meunier, V.; Valeev, E. F.; Lampkins, A. J.; Li, H.; Castellano, R. K., *J. Phys. Chem. C*, **2007,** *111*, 18912.

91. Lampinks, A. J., *Ph.D. Dissertation*, 2006.

92. Sumpter, B. G.; Kumar, P.; Mehta, A.; Barnes, M. D.; Shelton, W. A.; Harrison, R. J., *J. Phys. Chem. B*, **2005,** *109*, 7671.

93. Mallajosyula, S. S.; Datta, A.; Pati, S. K., *Synth. Met.*, **2005,** *155*, 398.

94. Terech, P.; Weiss, R. G., *Chem. Rev.*, **1997,** *97*, 3133.

95. Estroff, L. A.; Hamilton, A. D., *Chem. Rev.*, **2004,** *104*, 1201.

96. van Esch, J. H.; Feringa, B. L., *Angew. Chem., Int. Ed.*, **2000,** *39*, 2263.

97. Haering, G.; Luisi, P. L., *J. Phys. Chem.*, **1986,** *90*, 5892.

98. Ramanan, R. M. K.; Chellamuthu, P.; Tang, L. P.; Nguyen, K. T., *Biotechnol. Prog.*, **2006,** *22*, 118.

99. O'Neill, M.; Kelly, S. M., *Adv. Mater.*, **2003,** *15*, 1135.

100. Patel, H. K.; Rowe, R. C.; Mcmahon, J.; Stewart, R. F., *Int. J. Pharm.*, **1985,** *25*, 13.

101. Dickert, F. L.; Haunschild, A., *Adv. Mater.*, **1993,** *5*, 887.

102. Pasman, P.; Verhoeven, J. W.; Deboer, T. J., *Tetrahedron*, **1976,** *32*, 2827.

103. Hunter, C. A.; Sanders, J. K. M., *J. Am. Chem. Soc.*, **1990,** *112*, 5525.

104. Jorgensen, W. L.; Severance, D. L., *J. Am. Chem. Soc.*, **1990,** *112*, 4768.

105. Hunter, C. A., *Chem. Soc. Rev.*, **1994,** *23*, 101.

106. Quiocho, F. A.; Vyas, N. K., *Nature*, **1984,** *310*, 381.

107. Vyas, N. K.; Vyas, M. N.; Quiocho, F. A., *Science*, **1988,** *242*, 1290.

108. Haino, T.; Tanaka, M.; Fukazawa, Y., *Chem. Commun.*, **2008**, 468.

109. Mori, A.; Yokoo, M.; Hashimoto, M.; Ujiie, S.; Diele, S.; Baumeister, U.; Tschierske, C., *J. Am. Chem. Soc.*, **2003,** *125*, 6620.

110. Hegmann, T.; Kain, J.; Diele, S.; Schubert, B.; Bogel, H.; Tschierske, C., *J. Mater. Chem.*, **2003,** *13*, 991.

111. Xue, P.; Lu, R.; Chen, G.; Zhang, Y.; Nomoto, H.; Takafuji, M.; Ihara, H., *Chem. Eur. J.*, **2007,** *13*, 8231.

112. Birkedal, H.; Pattison, P., *Acta Crystallodr., Sect. C: Cryst. Struct. Commun.*, **2006,** *62*, O139.

113. Dimitrakopoulos, C. D.; Purushothaman, S.; Kymissis, J.; Callegari, A.; Shaw, J. M., *Science*, **1999,** *283*, 822.

114. Afzali, A.; Dimitrakopoulos, C. D.; Breen, T. L., *J. Am. Chem. Soc.*, **2002,** *124*, 8812.

115. Ruani, G.; Fontanini, C.; Murgia, M.; Taliani, C., *J. Chem. Phys.*, **2002,** *116*, 1713.

116. Kurmoo, M.; Graham, A. W.; Day, P.; Coles, S. J.; Hursthouse, M. B.; Caulfield, J. L.; Singleton, J.; Pratt, F. L.; Hayes, W.; Ducasse, L.; Guionneau, P., *J. Am. Chem. Soc.*, **1995,** *117*, 12209.

117. Horiuchi, S.; Yamochi, H.; Saito, G.; Sakaguchi, K.; Kusunoki, M., *J. Am. Chem. Soc.*, **1996,** *118*, 8604.

118. Jehoulet, C.; Obeng, Y. S.; Kim, Y. T.; Zhou, F. M.; Bard, A. J., *J. Am. Chem. Soc.*, **1992,** *114*, 4237.

119. Ami, S.; Joachim, C., *Nanotechnology*, **2001,** *12*, 44.

120. Bachtold, A.; Hadley, P.; Nakanishi, T.; Dekker, C., *Science*, **2001,** *294*, 1317.

121. Reyes, A.; Tlenkopatchev, M. A.; Fomina, L.; Guadarrama, P.; Fomine, S., *J. Phys. Chem. A*, **2003,** *107*, 7027.

122. Tsuzuki, S.; Honda, K.; Uchimaru, T.; Mikami, M., *J. Chem. Phys.*, **2004,** *120*, 647.

123. Sato, T.; Tsuneda, T.; Hirao, K., *J. Chem. Phys.*, **2005,** *123*.

124. Balzani, V.; Scandola, F., *Supramolecular Photochemistry*, **1991**, ch.12.

125. Bissell, R. A.; Desilva, A. P.; Gunaratne, H. Q. N.; Lynch, P. L. M.; Maguire, G. E. M.; Sandanayake, K. R. A. S., *Chem. Soc. Rev.*, **1992,** *21*, 187.

126. Stohs, S. J.; Ohia, S.; Bagchi, D., *Toxicology*, **2002,** *180*, 97.

127. ter Wiel, M. K. J.; Feringa, B. L., *Synthesis*, **2005**, 1789.

128. Negishi, E.; Baba, S., *J. Chem. Soc., Chem. Commun.*, **1976**, 596.

129. Negishi, E. I., *Acc. Chem. Res.*, **1982,** *15*, 340.

130. Zhou, J. R.; Fu, G. C., *J. Am. Chem. Soc.*, **2003,** *125*, 12527.

131. Najera, C.; Gil-Molto, J.; Karlstrom, S., *Adv. Synth. Catal.*, **2004,** *346*, 1798.

132. Lansbury, P. T.; Nickson, T. E.; Vacca, J. P.; Sindelar, R. D.; Messinger, J. M., *Tetrahedron*, **1987,** *43*, 5583.

133. Desai, R. D.; Waravdekar, W. S., *Proc. Indian. Academy Sci.*, **1946,** *24A*, 382.

134. Lee, D. Y.; Hartwig, J. F., *Org. Lett.*, **2005,** *7*, 1169.

135. Lee, S.; Jorgensen, M.; Hartwig, J. F., *Org. Lett.*, **2001,** *3*, 2729.

136. Rosowsky, A.; Papathan.N; Chen, K. K. N.; Modest, E. J.; Nadel, M. E., *J. Heterocycl. Chem.*, **1972,** *9*, 275.

137. Sellarajah, S.; Lekishvili, T.; Bowring, C.; Thompsett, A. R.; Rudyk, H.; Birkett, C. R.; Brown, D. R.; Gilbert, I. H., *J. Med. Chem.*, **2004,** *47*, 5515.

138. Lampinks, A. J., *Ph.D. dissertation*, **2006**.

139. Chiron, R.; Graff, Y., *Spectrochim. Acta, Part A*, **1976,** *32*, 1303.

140. Baddeley, C.; Yan, Z. Q.; King, G.; Woodward, P. M.; Badjic, J. D., *J. Org. Chem.*, **2007,** *72*, 7270.

141. Bao, C. Y.; Lu, R.; Jin, M.; Xue, P. C.; Tan, C. H.; Xu, T. H.; Liu, G. F.; Zhao, Y. Y., *Chem. Eur. J.*, **2006,** *12*, 3287.

142. Camerel, F.; Ziessel, R.; Donnio, B.; Bourgogne, C.; Guillon, D.; Schmutz, M.; Iacovita, C.; Bucher, J. P., *Angew. Chem., Int. Ed.*, **2007,** *46*, 2659.

143. Puigmarti-Luis, J.; Laukhin, V.; del Pino, A. P.; Vidal-Gancedo, J.; Rovira, C.; Laukhina, E.; Amabilino, D. B., *Angew. Chem., Int. Ed.*, **2007,** *46*, 238.

144. Fuhrhop, J.-H.; Helfrich, W., *Chem. Rev.*, **1993,** *93*, 1565.

145. Brinksma, J.; Feringa, B. L.; Kellogg, R. M.; Vreeker, R.; van Esch, J., *Langmuir*, **2000,** *16*, 9249.

146. Naota, T.; Koori, H., *J. Am. Chem. Soc.*, **2005,** *127*, 9324.

147. Land, V. D.; Harris, T. M.; Teeters, D. C., *J. Non-Cryst. Solids*, **2001,** *283*, 11.

148. Smith, D. M.; Scherer, G. W.; Anderson, J. M., *J. Non-Cryst. Solids*, **1995,** *188*, 191.

149. Cho, K.; Park, S. H., *Macromol. Symp.*, **2001,** *166*, 93.

150. Cauich-Rodriguez, J. V.; Deb, S.; Smith, R., *J. Appl. Polym. Sci.*, **2001,** *82*, 3578.

151. Pierre, A. C.; Pajonk, G. M., *Chem. Rev.*, **2002,** *102*, 4243.

152. Cozzi, F.; Bacchi, S.; Filippini, G.; Pilati, T.; Gavezzotti, A., *Chem. Eur. J.*, **2007,** *13*, 7177.

153. Alcalde, E.; Mesquida, N.; Vilaseca, M.; Alvarez-Rua, C.; Garcia-Granda, S., *Supramol. Chem.*, **2007,** *19*, 501.

154. Bacchi, S.; Benaglia, M.; Cozzi, F.; Demartin, F.; Filippini, G.; Gavezzotti, A., *Chem. Eur. J.,* **2006,** *12*, 3538.

155. Lee, S. J.; Kim, E.; Seo, M. L.; Do, Y.; Lee, Y.-A.; Lee, S. S.; Jung, J. H.; Kogiso, M.; Shimizu, T., *Tetrahedron*, **2008,** *64*, 1301.

156. Hunter, C. A.; Lawson, K. R.; Perkins, J.; Urch, C. J., *J. Chem. Soc., Perkin Trans. 2*, **2001**, 651.

157. Anderson, K. M.; Day, G. M.; Paterson, M. J.; Byrne, P.; Clarke, N.; Steed, J. W., *Angew. Chem., Int. Ed.*, **2008,** *47*, 1058.

158. Tanaka, T., *Experimental Methods in Polymer Science: Modern Methods in Polymer Research and Technology*, Academic press, San Diego, 2000.

159. Ohno, K., *Chem. Phys. Lett.*, **1978,** *53*, 571.

160. Platt, J. R., *J. Chem. Phys.*, **1949,** *17*, 484.

161. Berlman, I. B., *Handbook of Fluorescence Spectra of Aromatic Molecules*, Academic Press, 1971.

162. Beeby, A.; Parker, D.; Williams, J. A. G., *J. Chem. Soc., Perkin Trans. 2*, **1996**, 1565.

163. Albelda, M. T.; Bernardo, M. A.; Diaz, P.; Garcia-Espana, E.; de Melo, J. S.; Pina, F.; Soriano, C.; Santiago, V. L. E., *Chem. Commun.*, **2001**, 1520.

164. Bernardo, M. A.; Alves, S.; Pina, F.; De Melo, J. S.; Albelda, M. T.; Garcia-Espana, E.; Llinares, J. M.; Soriano, C.; Luis, S. V., *Supramol. Chem.*, **2001,** *13*, 435.

165. de Melo, J. S.; Albelda, M. T.; Diaz, P.; Garcia-Espana, E.; Lodeiro, C.; Alves, S.; Lima, J. C.; Pina, F.; Soriano, C., *J. Chem. Soc., Perkin Trans. 2*, **2002**, 991.

166. Ghaddar, T. H.; Whitesell, J. K.; Fox, M. A., *J. Phys. Chem. B*, **2001,** *105*, 8729.

167. Emert, J.; Behrens, C.; Goldenberg, M., *J. Am. Chem. Soc.*, **1979,** *101*, 771.

168. Nishio, Y.; Tani, Y.; Kimura, N.; Suzuki, H.; Ito, S.; Yamamoto, M.; Harkness, B. R.; Gray, D. G., *Macromolecules*, **1995,** *28*, 3818.

169. Aucejo, R.; Alarcon, J.; Garcia-Espana, E.; Llinares, J. M.; Marchin, K. L.; Soriano, C.; Lodeiro, C.; Bernardo, M. A.; Pina, F.; Pina, J.; de Melo, J. S., *Eur. J. Inorg. Chem.*, **2005**, 4301.

170. Picraux, L. B.; Weldon, B. T.; McCusker, J. K., *Inorg. Chem.*, **2003,** *42*, 273.

171. George, S. J.; Ajayaghosh, A., *Chem. Eur. J.*, **2005,** *11*, 3217.

172. Bichenkova, E. V.; Sardarian, A. R.; Wilton, A. N.; Bonnet, P.; Bryce, R. A.; Douglas, K. T., *Org. Biomol. Chem.*, **2006,** *4*, 367.

173. Chen, F.; Song, K.-S.; Wu, Y.-D.; Yang, D., *J. Am. Chem. Soc.*, **2008,** *130*, 743.

174. Maji, S. K.; Haldar, D.; Banerjee, A.; Banerjee, A., *Tetrahedron*, **2002,** *58*, 8695.

175. Chiron, R.; Maisonne.P; Graff, Y., *Comptes Rendus Hebdomadaires Des Seances De L Academie Des Sciences Serie C*, **1973,** *276*, 105.

176. Gellman, S. H.; Dado, G. P.; Liang, G. B.; Adams, B. R., *J. Am. Chem. Soc.*, **1991,** *113*, 1164.

177. Dado, G. P.; Gellman, S. H., *J. Am. Chem. Soc.*, **1993,** *115*, 4228.

178. Iriepa, I.; Villasante, F. J.; Galvez, E.; Bellanato, J., *J. Mol. Struct.*, **1999,** *509*, 105.

179. Provencher, S. W., *Comp. Phys. Commun.*, **1982,** *27*, 229.

180. Provencher, S. W., *Comp. Phys. Commun.*, **1982,** *27*, 213.

181. Gohy, J. F.; Lohmeijer, B. G. G.; Alexeev, A.; Wang, X. S.; Manners, I.; Winnik, M. A.; Schubert, U. S., *Chem. Eur. J.*, **2004,** *10*, 4315.

182. Shibayama, M.; Okamoto, M., *J. Chem. Phys*, **2001,** *115*, 4285.

183. Martin, J. E.; Wilcoxon, J.; Odinek, J., *Phys. Rev. A*, **1991,** *43*, 858.

184. Lang, P.; Burchard, W., *Macromolecules*, **1991,** *24*, 814.

185. Diaz-Leyva, P.; Perez, E.; Arauz-Lara, J. L., *J. Chem. Phys.*, **2004,** *121*, 9103.

186. Song, Y.; Im, S. S.; Han, Y. K.; Sohn, D., *Bull. Chem. Soc. Jpn.*, **2000,** *73*, 2379.

187. Richter, S.; Matzker, R.; Schroter, K., *Macromol. Rapid Commun.*, **2005,** *26*, 1626.

188. Fournel, S.; Wieckowski, S.; Sun, W. M.; Trouche, N.; Dumortier, H.; Bianco, A.; Chaloin, O.; Habib, M.; Peter, J. C.; Schneider, P.; Vray, B.; Toes, R. E.; Offringa, R.; Melief, C. J. M.; Hoebeke, J.; Guichard, G., *Nat. Chem. Biol.*, **2005,** *1*, 377-382.

189. Gibson, S. E.; Castaldi, M. P., *Chem. Commun.*, **2006**, 3045.

190. Moberg, C., *Angew. Chem., Int. Ed.*, **1998,** *37*, 248.

191. van Gestel, J.; Palmans, A. R. A.; Titulaer, B.; Vekemans, J. A. J. M.; Meijer, E. W., *J. Am. Chem. Soc.*, **2005,** *127*, 5490.

192. Plas, S. E. V. d.; Gea, A.; Figaroli, S.; Clercq, P. J. D.; Madder, A., *Eur. J. Inorg. Chem.*, **2008**, 1582.

193. Heathcote, D. M.; De Boos, G. A.; Atherton, J. H.; Page, M. I., *J. Chem. Soc., Perkin Trans. 2*, **1998**, 535.

194. Thomaides, J.; Maslak, P.; Breslow, R., *J. Am. Chem. Soc.*, **1988,** *110*, 3970.

195. Huisgen, R.; Ott, H., *Tetrahedron*, **1959,** *6*, 253.

196. Oh, K.; Ryu, J., *Tetrahedron Lett.*, **2008,** *49*, 1935.

197. Supaphol, P.; Apiwanthanakorn, N., *J. Polym. Sci., Part B: Polym. Phys.*, **2004,** *42*, 4151.

198. Martinelli, A.; D'Ilario, L.; Caminiti, R., *J. Polym. Sci., Part B: Polym. Phys.*, **2005,** *43*, 2725.

199. Dikshit, A. K.; Kaito, A., *J. Polym. Sci., Part B: Polym. Phys.*, **2003,** *41*, 1665.

200. Yang, Z.; Liang, G.; Xu, B., *Acc. Chem. Res.*, **2008,** *41*, 315.

201. Obert, E.; Bellot, M.; Bouteiller, L.; Andrioletti, F.; Lehen-Ferrenbach, C.; Boue, F., *J. Am. Chem. Soc.*, **2007,** *129*, 15601.

202. Okumura, Y.; Ito, K., *Adv. Mater.*, **2001,** *13*, 485.

203. Bevers, S.; O'Dea, T. P.; McLaughlin, L. W., *J. Am. Chem. Soc.*, **1998,** *120*, 11004.

BIOGRAPHICAL SKETCH

Ling Yuan was born in Jianyang, Sichuan Province, P. R. China. She received her B.S. in medicinal chemistry from West China University of Medical Sciences in July 1996. After working 7 years in West China University of Medical Sciences, Shanghai Institute of Organic Chemistry and then Wuxi Pharmatech company in China, she came to the University of Florida as a graduate student of organic chemistry in August 2003. She joined Prof. Ronald K. Castellano's group in September 2003 and she received her M.S. in organic chemistry from University of Florida in December 2005. Ling Yuan will receive her Ph.D. in April 2008. Beginning in May 2008, she will join the Dow chemical company in Shanghai, China.